UNIVERSITY OF CALIFORNIA
RIVERSIDE

Molecular Level Characterization of Heparin Structure

A Dissertation submitted in partial satisfaction
of the requirements for the degree of

Doctor of Philosophy

in

Chemistry

by

Consuelo Natalia Beecher

June 2015

Dissertation Committee:
Dr. Cynthia K. Larive, Chairperson
Dr. Quan Jason Cheng
Dr. Wenwan Zhong

The Dissertation of Consuelo Natalia Beecher is approved:

_____

_____

_____

Committee Chairperson

University of California, Riverside

Acknowledgements

Completing this academic journey would not have been possible without the support from my wonderful family and my amazing friends. I would like to begin by thinking my graduate advisor and mentor, Dr. Cindy Larive. She is full of knowledge and wisdom and taught me how to think more critically and scientifically. I am very thankful for her patience with me and for guiding me through this program. I also like to thank all those who helped me get to graduate school. I am not sure where I would be today without the support and encouragement of my undergraduate professors at CSUSB. I would also like to thank the friends I made at Watson Pharmaceuticals, Lauren Brandt, Margreta Baeva, and Freada Dallal, for encouraging me to go back to school.

I am certain that this program would have been much more difficult without the support and encouragement from my former labmates. I would like to thank Dr. Derek Langeslay for his guidance and his patience with me and all my questions. I would also like to thank Dr. Szabolcs Beni for his patience when working with me and for teaching me how to interpret two-dimensional NMR spectra. A sincere thank you also goes out to Dr. Greg Barding, Dr. Daryl Bullock, Dr. Chris Jones, and Dr. John Limtiaco for their support and for making each day more bearable.

I would also like to thank everyone I have had the pleasure of working with these past five years. I worked with five talented undergraduates, Amy Morris, Jenny Mao, Sophia Nael, Adanma Nwachuku, and Matt Manighalam, who helped me isolate heparin oligosaccharides. I would also like to thank my current and former labmates, Dr. Marti Kraszni, Dr. Karcsi Mazak, and Dr. Berenice Aguilar, Meredith Dinges, Andrew Green,

Melissa Morgan, Corey Griffith, Dr. Caroline Mathon, Dr. Xiumei Liu, Dr. Luzi Tinoco, and Hortensia Monteiro, for such a great work environment.

I have made many wonderful, supportive friends along the way. Ashley Swanson, Preston Williams, and Nicole Williams, thank you for all the friendly conversations and morning walks with Colby and Kipper. They helped me start every day on a good note. I would like to send a thank you to my movie buddy, Yoo-Jin Ghang, for always being a great friend and for your support whenever I needed someone to talk to. Thank you to Erin Brinton, as well, for all the weekend hikes and chats that helped us both get through the rough times. I would like to send a special thank you to my boyfriend, Chad Priest, for his continued support, for challenging me to think outside of the box, and for all the puppy play dates with Lily.

Last but certainly not least, I thank my family for their continued love and support. My mom and dad have always taught me to follow my dreams and have always been supportive and encouraging. I love them both very much, and I know I would not be where I am today without them. A big thank you goes out to my brother, Carlos Beecher. We may not talk very often, but I know he is always there for me whenever I need him. I would also like to thank my best friends – my cousins. They always show me much love and care, and are always so supportive of everything I do. I would also like to give a special thank you to my little dog, Betty, who helped keep me sane and focused. She is my loyal companion and always brings so much joy and love at the end of the day no matter what kind of a day it has been.

Acknowledgement of Copyright

ABSTRACT OF THE DISSERTATION

Molecular Level Characterization of Heparin Structure

by

Consuelo Natalia Beecher

Doctor of Philosophy, Graduate Program in Chemistry
University of California, Riverside, June 2015
Dr. Cynthia K. Larive, Chairperson

Heparin is unbranched anionic polysaccharide that is part of the glycosaminoglycan family. Although its structural microheterogeneity allows heparin to mediate a variety of biological processes by binding to over 400 different proteins, it also makes structural characterization challenging. This dissertation focuses on the separation and isolation of unique heparin oligosaccharides and their structure elucidation using nuclear magnetic resonance (NMR) and mass spectrometry. The impact of sequence on secondary structure is evaluated through detection of specific intramolecular hydrogen bonds.

Separation of the low-molecular-weight heparin enoxaparin was accomplished using size-exclusion chromatography (SEC) followed by strong anion-exchange high-performance liquid chromatography (SAX-HPLC). Typically, size-similar SEC fractions are combined prior to SAX-HPLC separation. However, screening individual SEC fractions using their sulfamate ^{1}H and ^{15}N chemical shifts allowed for SAX-HPLC

resolution of the SEC fractions containing 3-*O*-sulfated oligosaccharides and led to the isolation and characterization of a unique 3-*O*-sulfated heparin tetrasaccharide.

The effect of structure, particularly glucosamine 3-*O*-sulfation, on hydroxyl proton hydrogen bonding was explored. Experimental conditions were optimized for the NMR detection and identification of heparin hydroxyl protons. Solvent exchange rates were determined using exchange spectroscopy (EXSY). Structurally specific differences in the hydroxyl proton exchange rates of the hydroxyl protons were explored for Arixtra, a synthetic pentasaccharide that mimics the Antithrombin-III binding sequence, and for isolated oligosaccharides that do not contain a 3-*O*-sulfated glucosamine. Transverse relaxation rates (R_2) measured for the Arixtra hydroxyl protons using the Carr-Purcell-Meiboom-Gill experiment are compared with EXSY solvent exchange rates. Because R_2 values are sensitive to factors other than exchange, good correlations with the EXSY exchange rates were not uniformly obtained.

Experimental conditions are reported allowing the ^{1}H NMR observation of the amine protons of glucosamine. Exchange properties of amine protons in monosaccharides differing only by 3-*O*-sulfation are compared. Amine group acidity (pK_a) was measured to probe participation of the amine group in a salt bridge. Although no evidence of a salt bridge between the amine and sulfate groups was found in the 3-*O*-sulfated glucosamine (GlcN3S) monosaccharide, these experiments demonstrate the feasibility of probing for structurally important salt bridges in longer oligosaccharides.

Table of Contents

LIST OF FIGURES

gradient pulse dephases all the magnetization. The composite 180° pulse selectively inverts the phase of all the resonances except for the solvent resonance. As a result, application of the second gradient pulse further dephases the solvent resonance while refocusing the other resonances. (D) Excitation sculpting is based on a double gradient spin echo and is similar to WATERGATE except that in lieu of the composite pulse, a selective pulse at the water frequency is followed by a non-selective 180° pulse. Both WATERGATE and excitation sculpting repeat their respective 180° pulses a second time before acquisition using a different gradient G2 to avoid unwanted coherences.

Figure 1.6. 25
The pulse sequences used for structure elucidation of heparin and heparan sulfate oligosaccharides. (A) The COSY pulse sequence is made up of two 90° pulses separated by an evolution time, t_1. COSY cross peaks will reveal ^{1}H couplings usually through three bonds. (B) In the TOCSY pulse sequence, a 90° degree pulse is followed by an evolution time, t_1, and a spin-lock, τ_m. The spin-lock is made up of a series (or train) of 180° pulses separated by very small delays that cause the magnetization to evolve under the effects of the spinlock field (B_1) which is much smaller than the applied field (B_0). TOCSY cross peaks relate all the coupled protons within a spin system. (C) The ROESY pulse sequence is similar the TOCSY, except that the spin-lock is applied in the rotating frame to allow the observation of dipolar (through-space) couplings. (D) The [^{1}H, ^{13}C] multiplicity-edited HSQC pulse sequence utilizes 90° and 180°pulses and delays that depend on the coupling constant ($1/4J_{HC}$) to transfer coherence between ^{1}H and ^{13}C. Gradients are used to remove any unwanted coherence pathways.

Figure 1.7. 28
The ISIS (A) tetrasaccharide structure (ΔUA2S-GlcNS6S-IdoA2S-GlcNS6S) was elucidated using (B) COSY, (C) TOCSY, (D) ROESY, and (E) [^{1}H, ^{13}C] HSQC spectra. ISIS is the most common tetrasaccharide in heparin.

Figure 1.8. 32
(A) When a group of spins is in the presence of an external magnetic field (M_0), some spins will align with the field (α) and some will align against the field (β). There will be a larger population of α spins, creating a bulk magnetization aligned with the magnetic field (B). This magnetization is represented by the vector, M, in the xyz coordinate system, aligned with the applied magnetic field (B_0) along the +z axis. (C) When a radiofrequency (rf) pulse is applied, the magnetization is tipped towards the

LIST OF TABLES

CHAPTER ONE

Introduction

The research presented in this dissertation focuses on the development of new analytical techniques for the structural analysis of anionic polysaccharides. The specific focus is on heparin oligosaccharides including isolating oligosaccharides with important and unique structures, elucidating their primary structure, and analyzing the effect that elements of primary structure have on secondary structure. Heparin is well-known for its anticoagulant activity which is mediated by binding of a specific pentasaccharide sequence to the protease inhibitor antithrombin-III (AT-III). Although this AT-III binding sequence has been studied extensively, the structure-function relationships by which heparin binds to more than 400 other proteins are less well understood.

Heparin structural characterization is challenging because of the high degree of microheterogeneity introduced during its biosynthesis. A bottom-up analytical approach is typically utilized, first by depolymerization of heparin followed by chromatographic isolation of individual oligosaccharides by size and charge. Absolute structure elucidation is then completed using the results of nuclear magnetic resonance (NMR) spectroscopy and mass spectrometry (MS) experiments.

The goal of this work is to demonstrate improved analytical methods for heparin primary and secondary structure analysis, building on the work of former lab members. This includes detection of exchangeable protons, structural profiling using ^{1}H and ^{15}N chemical shifts, and hydrogen bond detection by Derek Langeslay, and heparin

oligosaccharide isolation and characterization by John Limtiaco. The specific goals of this dissertation are summarized in the following objectives:

Objective 1: Identify unique and biologically important heparin oligosaccharide structures by screening individual SEC fractions using their ^{1}H and ^{15}N chemical shifts to locate important 3-*O*-sulfated glucosamine residues. Separation of these individual SEC fractions by SAX-HPLC produces less complex chromatograms more amenable to isolation of low abundance oligosaccharides. (Chapter 2)

Objective 2: Determine optimum solution conditions for the detection and identification of heparin hydroxyl protons by NMR. Determine the exchange rates of the hydroxyl protons with aqueous solvent from their exchange spectroscopy (EXSY) cross peaks. Explore the effect of structure on hydroxyl proton hydrogen bonds, specifically how hydrogen bonding is affected by the biologically important glucosamine 3-*O*-sulfate group. This is accomplished by measuring spectra for Arixtra, a synthetic pentasaccharide which mimics the ATIII-binding sequence (Chapter 3), as well as structurally related oligosaccharides that do not contain the 3-*O*-sulfate group. (Chapter 4)

Objective 3: Investigate the detection of exchangeable amine protons in monosaccharides related to heparin and heparan sulfate. Differences in the exchange properties of amine protons in monosaccharides differing only by a 3-*O*-sulfate residue are evaluated, along

with their acidity (pK_a) to probe for possible participation in a hydrogen bond or salt bridge. (Chapter 5)

Objective 4: Compare the results of EXSY measurements of hydroxyl proton exchange rates with T_2 relaxation rates measured using the CPMG experiment. Examine how structural elements of heparin and heparan sulfate monosaccharides and larger oligosaccharides affect the rates of chemical exchange and T_2 relaxation. (Chapter 6)

1.1 Heparin and heparan sulfate structure and biosynthesis

Heparin and heparan sulfate (HS) are long chain, anionic polysaccharides that are members of the glycosaminoglycan (GAG) family.[1,2] The GAG family also includes chondroitin sulfate (CS), dermatan sulfate (DS), keratan sulfate (KS), and hyaluronic acid (HA).[3] Each of these polysaccharides is composed of a repeating disaccharide, differing largely in the uronic acid residue, the hexosamine residue, and the linkage between them. Like the other members of the GAG family, heparin and HS are synthesized primarily in the endoplasmic reticulum and Golgi apparatus of cells. Heparin synthesis begins by attachment of a specific tetrasaccharide, called the linkage region, to serglycin, a core protein found in mast cells. HS, on the other hand, is synthesized on protein cores which are modified with HS proteoglycans. The following is the sequence of the linkage region: β-GlcA(1→3)-β-Gal(1→3)-β-Gal(1→4)-β-Xyl-1→Ser.[1] A list of saccharide names and abbreviations is found in Table 1.1. A GlcNAc residue is then added to the linkage

Table 1.1. Full names of abbreviations used throughout this dissertation.

Abbreviation	Name
Gal	Galactose
GlcA	Glucuronic Acid
GlcA2S	2-*O*-sulfated Glucuronic Acid
GlcN	Glucosamine
GlcNAc	*N*-Acetylated Glucosamine
GlcN3S	*N*,3-*O*-sulfated Glucosamine
GlcNS	*N*-sulfated Glucosamine
GlcNS6S	*N*,6-*O*-sulfated Glucosamine
GlcNS3S6S	*N*,3,6-*O*-sulfated Glucosamine
IdoA	Iduronic Acid
IdoA2S	2-*O*-sulfated Iduronic Acid
Ser	Serine
ΔUA	Unsaturated uronic acid that contains a C4-C5 double bond
ΔUA2S	2-*O*-sulfated unsaturated uronic acid that contains a C4-C5 double bond
Xyl	Xylose

region, followed by the addition of a β(1→4)-linked GlcA residue. Elongation of the chain then continues with alternating GlcNAc and GlcA residues.[1,2]

Microheterogeneity is introduced into heparin and HS through various patterns of sulfation and epimerization of the -GlcNAc-(1→4)-β-GlcA- residues along the polysaccharide chain. In the first substitution step, the glucosamine residue can be either *N*-deacetylated or *N*-sulfated by the *N*-deacetylase and *N*-sulfotransferase enzymes, respectively. Otherwise, it may remain acetylated at the *N*- position. The glucuronic acid residue can then be converted to its C5 epimer, iduronic acid (IdoA), by a C5 epimerase enzyme. The GlcA and IdoA residues can then be sulfated at the 2-*O*-position by the glucuronosyl and iduronosyl 2-*O*-sulfotransferase enzymes, respectively, only if the GlcNS residue does not contain an *O*-sulfation at the C6 position. The GlcNAc and GlcNS residues can subsequently be sulfated at the 6-*O*-position by a glucosamine 6-*O*-sulfotransferase enzyme. Finally, the 3-*O*-sulfotransferase enzyme can sulfate GlcNS6S residues at the 3-*O*-position, which occurs in only one of every three heparin chains.[1] Heparin is then cleaved from the core protein and stored in the granules of mast cells while HS remains as a proteoglycan linked to the core protein it modifies. These processes are believed to occur sequentially although the factors that regulate these enzymes is still not very well known.[1]

The basic heparin and HS disaccharides comprised of 1→4 linked uronic acid and glucosamine residues, along with their possible substitution patterns is illustrated in Figure 1.1. The carbon atoms are labeled starting with C1 as the anomeric carbon continuing around the ring to C5 for the uronic acid and C6 for the glucosamine residues.

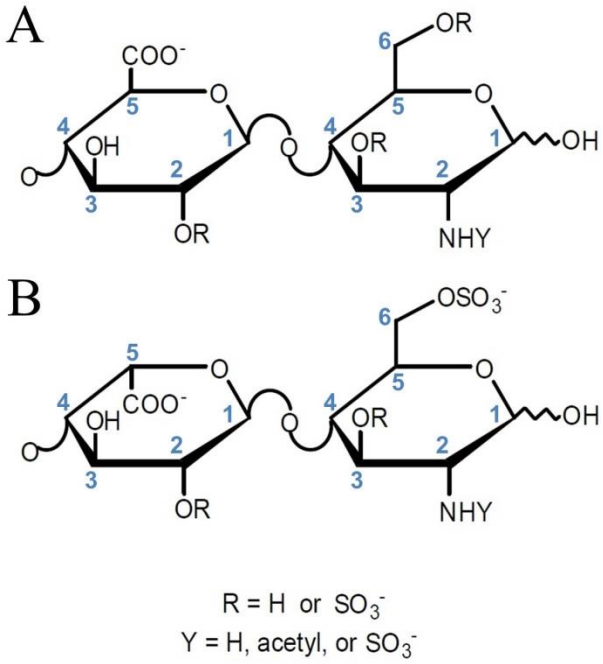

Figure 1.1. The structure of the basic heparin and heparan sulfate disaccharide, comprised of β(1→4)-linked uronic acid and glucosamine residues. The uronic acid residue can either be (A) glucuronic acid or (B) iduronic acid, which are epimers at the C5 position. The Y-group can be protonated, sulfated, or acetylated, and the R-groups can either be protonated or sulfated. The carbon atoms are labeled starting with the anomeric proton as C1 continuing around the ring to C5 for the uronic acid and C6 for the glucosamine residues.

The main difference between heparin and HS is in the pattern of sulfation. Although heparin is more highly sulfated, HS has regions of high and low sulfation along its chain.[4]

Long heparin chains form an α-helical secondary structure, with a few "kinks" observed along the chain.[1,5] IdoA2S is the most flexible residue and is capable of assuming three different conformations: two chair conformations, $^{4}C_{1}$ and $^{1}C_{4}$, and a skew-boat conformation, $^{2}S_{O}$. As a monosaccharide, the IdoA2S residue exists 90% of the time in the $^{1}C_{4}$ conformation and 10% of the time in the $^{2}S_{O}$ conformation, with little to no preference for the $^{4}C_{1}$ conformation. Within a heparin chain it is found 60% of the time in the $^{1}C_{4}$ conformation and 40% of the time in the $^{2}S_{O}$ conformation.[6] However, when IdoA2S is located within the AT-III binding heparin pentasaccharide in aqueous solution, it is found 40% of the time in the $^{1}C_{4}$ conformation and 60% of the time in the $^{2}S_{O}$ conformation.[6] Using NOE measurements and computational modeling for a heparin pentasaccharide, Hricovini et al. determined that the IdoA2S residue is exclusively in the $^{2}S_{O}$ conformation when the pentasaccharide is bound to AT-III.[5]

1.2 Pharmacological and biological significance of heparin and heparan sulfate

Heparin and HS exhibit a variety of biological activities including inhibition of angiogenesis and tumor growth through well-characterized interactions with fibroblast growth factors (FGF),[7-9] vascular endothelial growth factor (VEGF),[10-12] lipases[13-15] and cytokines.[16-18] Heparin is best known for its role as an anticoagulant and antithrombotic, acting by binding to the protease inhibitor AT-III.[19,20] The anticoagulant activity of heparin has been studied extensively, and the structure of the native pentasaccharide

sequence responsible for high affinity AT-III binding is known.[21] It is a commonly prescribed pharmaceutical, with the heparin market made up largely of low molecular weight heparin (LMWH). LMWH is heparin that has been depolymerized into smaller oligosaccharide chains either enzymatically or chemically. A synthetic pentasaccharide that mimics this binding sequence makes up a smaller fraction of the heparin market and is currently used clinically, marketed as Arixtra (fondaparinux sodium) (Figure 1.2).

Heparin protein binding occurs largely through non-specific electrostatic interactions of the negatively charged sulfate and carboxyl groups and the positively charged amino acids of proteins, such as lysine and arginine, making its microstructure very important for high affinity binding.[3,22,23] The 3-*O*-sulfate group of the internal GlcNS6S residue of the ATIII-binding pentasaccharide is also an important contributor to AT-III binding; without it, affinity to ATIII decreases 1000-fold.[24] The sulfamate ($NHSO_3^-$) proton on the internal GlcNS3S6S residue is found in a hydrogen bond with the adjacent 3-*O*-sulfate group, most likely causing the observed "kink" in heparin and pre-organizing it for protein binding.[25] Another important component of the pentasaccharide sequence is the flexible IdoA2S residue. As described in Chapter 3, hydroxyl proton hydrogen bond patterns in heparin oligosaccharides, specifically involving the IdoA2S residue, depend on the presence of the GlcNS 3-*O*-sulfate group, suggesting that the flexibility of the IdoA2S contributes to the stability of heparin secondary structure through intramolecular hydroxyl proton hydrogen bonds.[26] Although the pentasaccharide is the minimum binding sequence responsible for heparin's

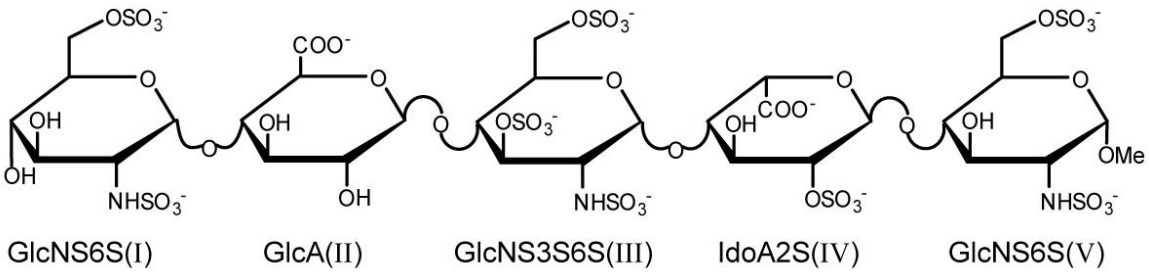

Figure 1.2. The structure of Arixtra with residues labeled. Arixtra is a synthetic pentasaccharide that mimics the heparin pentasaccharide that binds to AT-III.

anticoagulant activity, a heparin octasaccharide containing a second 3-*O*-sulfated GlcNS residue has been discovered to bind more strongly to AT-III than the pentasaccharide.[27]

The 3-*O*-sulfated GlcN residue is also important in other biological processes, such as in aiding the entry of herpes simplex virus 1 (HSV-1) into cells.[28] The specific HS sequence required for binding glycoprotein-D (gD) receptors that allows the entry of HSV-1 into cells has not been fully characterized, but it has been shown that expression of the enzyme 3-*O*-sulfotransferase 2 (3-OST-2) and 3-OST-3 facilitates the entry processes.[28,29] Studies have also shown that fibroblast growth factor 2 (FGF-2) prevents the HSV-1 entry into cells, most likely through competitive binding with HS.[30] Although the specific HS sequence required for binding proteins such as gD and FGF-2 has not been completely characterized, it is known that at least one of the two following disaccharides are a part of this mechanism: -IdoA2S-$GlcNH_2$3S6S- and -IdoA2S-$GlcNH_2$3S-.[28] These disaccharides differ from the AT-III binding heparin pentasaccharide in that the 3-*O*-sultated GlcN nitrogen is present as a free amine.

1.3 Heparin depolymerization

The inherent microheterogeneity of heparin and HS makes their structure elucidation challenging. Depolymerization methods are commonly used prior to structural analyses to decrease the length of the chains. Appropriate choice of reaction time and conditions permits partial digestion to produce oligosaccharides of varying lengths. Longer digestion times will produce shorter oligosaccharides, and exhaustive digestions reduce the biopolymers to their constituent disaccharides. The most common

disaccharide in heparin is L-IdoA2S-β(1→4)-D-GlcNS6S while that in HS is D-GlcA-β(1→4)-D-GlcNS6S.[31] Heparin contains 200-250 sulfate groups per 100 disaccharide units while HS contains 60-125 sulfate groups per 100 disaccharide units.[4]

1.3.1 Enzymatic depolymerization. Heparin and HS depolymerization can be accomplished through digestion by various heparinase enzymes. There are three different heparinase enzymes, each with different cleavage specificities, which are isolated from *Flavobacterium heparinum*.[32] Heparinase I cleaves along the GlcNS-(1→4)-IdoA2S linkage. The GlcNS residue can be either sulfated or protonated at the 6-*O*-position. This disaccharide is the most common disaccharide in the heparin chain, making heparin the more susceptible to cleavage by heparinase I than HS. Heparinase I is used in the commercial preparation of the LMWH, tinzaparin.[33] Heparinase II specificity is a little broader, cleaving between GlcN and UA residues. The GlcN residue can either be *N*-acetylated or *N*-sulfated, and the UA residue can either be IdoA2S, IdoA or GlcA. Heparinase III cleaves between GlcN-(1→4)-UA residues, with the GlcN residue being either *N*-sulfated or *N*-acetylated, and the UA residue being either IdoA or GlcA. HS is usually digested using heparinase III because its major sequence is GlcNAc(or NS)-(1→4)-GlcA. Digestion with any of the heparinase enzymes creates a double bond between C4 and C5 of the UA residue at the non-reducing end, allowing the digestion to be monitored by UV absorption at 232 nm.

1.3.2 Chemical depolymerization. Heparin depolymerization can also be accomplished chemically by means of β-elimination, reductive deamination, and oxidation reactions. Each digestion reaction introduces different structural modifications

in the oligosaccharide products. As with enzymatic reactions, chemical digestions can be exhaustive for constitutive analysis, or partial to produce a mixture of variously sized oligosaccharides. Chemical digestions are often used commercially to produce LMWH pharmaceuticals, for example enoxaparin and dalteparin.[33] β-Elimination occurs by formation of an ester at the non-reducing end uronic acid residue using a benzyl halide, followed by treatment with a strong base which hydrolyzes the benzyl ester. Similar to enzymatic degradation, products of β-elimination also produce oligosaccharides with a double bond between the uronic acid C4 and C5 atoms at the non-reducing end of the cleavage site. Reductive deamination occurs by treatment with nitrous acid with the products generated determined by the solution pH. Below pH 1.5, cleavage of GlcNS residues occurs, and at pH 4.0 cleavage occurs at GlcN residues that are unsubstituted at the *N*-position. This depolymerization method also produces 2,5-anhydro-D-mannose residues at the reducing end of the cleaved oligosaccharide. Oxidative depolymerization occurs by treatment of heparin with hydrogen peroxide and divalent copper or iron ions. This cleavage mechanism is specific for unsubstituted GlcA or IdoA residues and produces an oxidized fragment of the uronic acid residue at the reducing end of the cleavage site.[34]

1.4 Oligosaccharide isolation

Much of what is known about heparin and HS structure has been determined by structural characterization of oligosaccharides isolated from partial digestion reactions.

Because of the complexity of these digests, isolation of individual oligosaccharides is accomplished through chromatographic separations based on size and charge.

1.4.1 Size-exclusion chromatography. The first step in the resolution of digested oligosaccharides is separation by size using size exclusion chromatography (SEC).[35-39] Analytical scale high-pressure liquid chromatography (HPLC)-SEC separations coupled to MS are commonly used to screen the composition of digested GAGs.[35,40-42] More recently, profiling of a LMWH, enoxaparin, was accomplished by Shastri et al. using HPLC-SEC, with the oligosaccharides collected and subsequently analyzed by ion chromatography (IC).[43] The advantage of using HPLC-SEC compared to low-pressure preparative-scale SEC is the smaller amount of sample and shorter analysis time. HPLC-SEC requires μg-mg quantities separated over a period of a few hours while low-pressure preparative-scale SEC can accommodate mg-g quantities separated over a period of a few days. Preparative-scale low-pressure SEC is especially useful when isolating individual heparin oligosaccharides in sufficient quantities for structural characterization by NMR. Each size-uniform SEC peak is collected over multiple fractions, which are then typically combined.[37-39]

The nature and specificity of the enzymatic and chemical digestion processes described in section 1.3 generates predominantly oligosaccharides with an even number of residues. The SEC chromatogram of a chemically digested LMWH, enoxaparin, is shown in Figure 1.3. This separation was performed on a 3 x 200 cm column packed with Bio-Rad Bio-Gel P-10 fine resin. Elution was accomplished using a 0.5 M ammonium

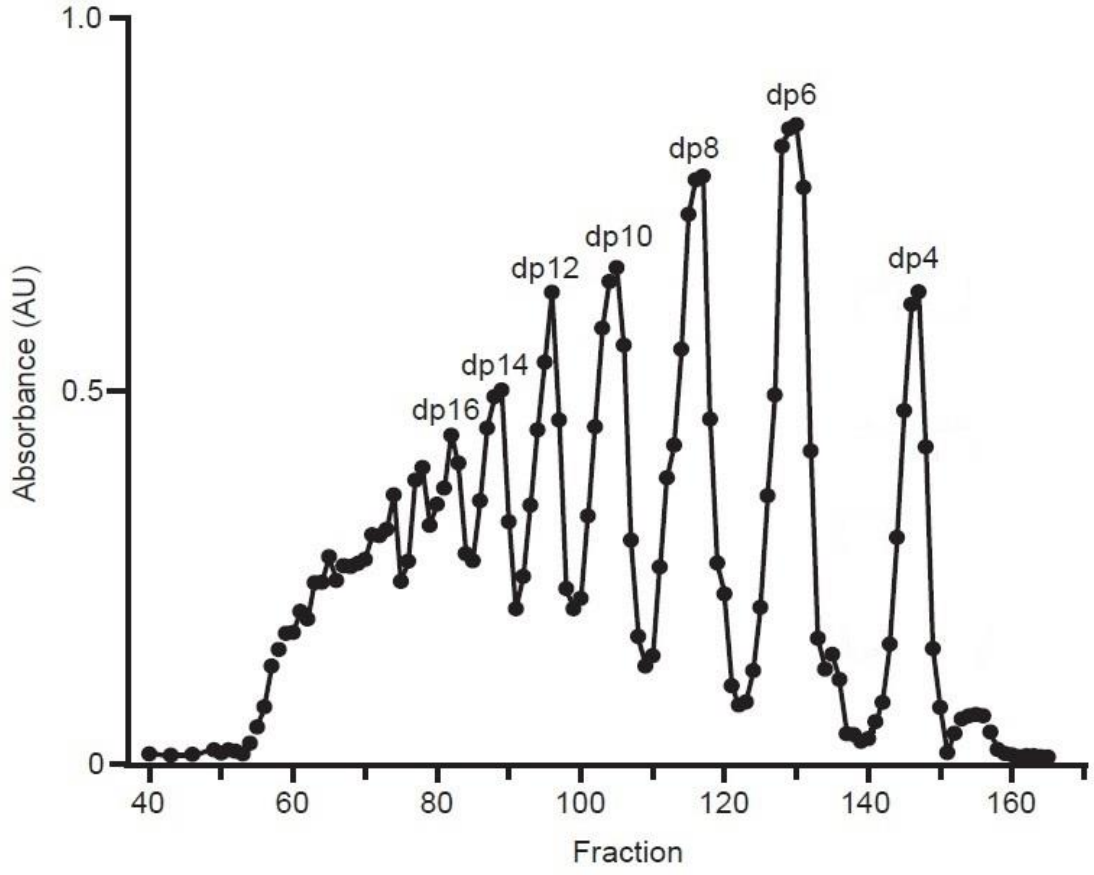

Figure 1.3. Enoxaparin SEC separation. Data points represent individual 4.5 mL size-uniform fractions. The peaks are labeled as digestion product (dp) followed by a number indicating the number of monosaccharide residues. For example, dp4 represents the tetrasaccharide fraction, dp6 the hexasaccharide fraction, and so forth.

bicarbonate solution at a flow rate of 0.076 mL/min. The eluent was collected in 4.5 mL fractions and the separation monitored offline using UV absorption at 232 nm.

Each data point in Figure 1.3 represents the UV absorbance of an individual 4.5 mL SEC fraction. The typical practice is to combine (or pool) all of the fractions that comprise each peak. The resulting solutions of size-uniform oligosaccharides (e.g., tetra-, hexa- or octasaccharides) are lyophilized to remove the ammonium bicarbonate and concentrate the oligosaccharides by dissolving the dried sample in a smaller volume. The component oligosaccharides from each SEC peak are subsequently separated by strong anion-exchange high-performance liquid chromatography (SAX-HPLC). Though each SEC peak contains oligosaccharides of the same length, the SEC fractions collected across each peak are not homogeneous in their composition.[44] Though it produces a more concentrated sample, pooling the SEC fractions for each peak increases the complexity of SAX-HPLC chromatograms, making it more challenging to isolate less abundant, yet important oligosaccharides.[44] As will be described in Chapter 2, SAX separation of individual 4.5 mL SEC fractions coupled with compositional monitoring by NMR can facilitate the isolation of low abundance oligosaccharides obscured by more abundant components in pooled samples.

1.4.2 Strong anion-exchange chromatography. The second step in heparin and HS oligosaccharide isolation typically relies on the separation of SEC fractions by charge using SAX-HPLC.[36,37,39] Figure 1.4 shows a SAX-HPLC chromatogram of a sample obtained by pooling the SEC tetrasaccharide fractions of enoxaparin. This separation used a CarboPac PA1 semi-preparative column having a stationary phase of a 10 μm

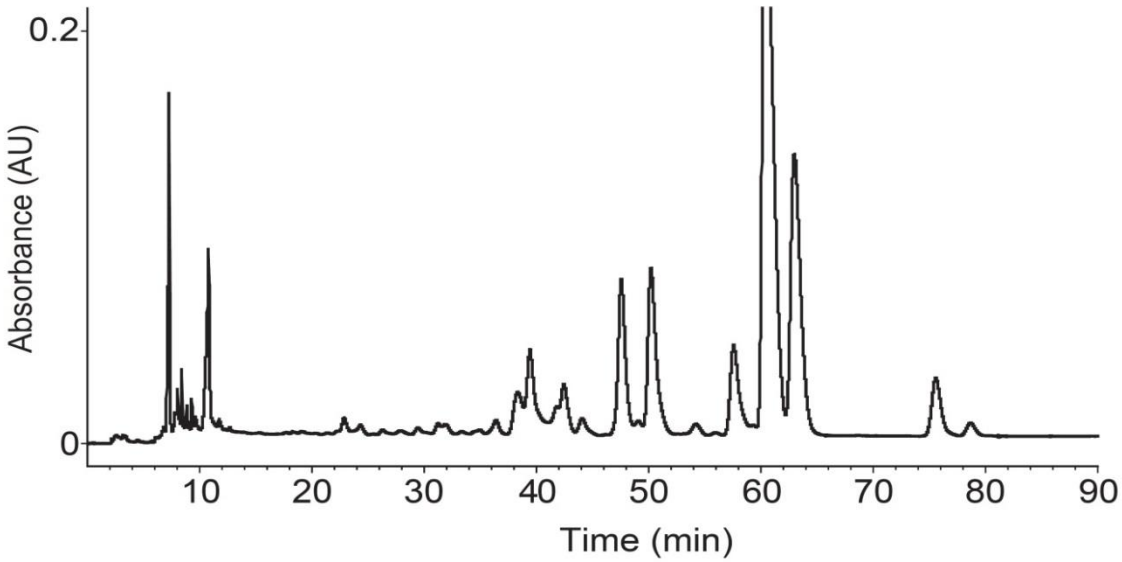

Figure 1.4. A SAX-HPLC chromatogram for the pooled Enoxaparin SEC tetrasaccharide fraction. Each peak is collected over multiple injections and analyzed by NMR and MS to elucidate the structure of the components in each peak, as explained in greater detail in Chapter 2.

substrate composed of 2% polystyrene cross-linked with divinylbenzene agglomerated with 500-nm MicroBead quaternary ammonium functionalized latex. Although this type of column typically provides lower resolution than an analytical scale column because of its larger diameter and particle size, it has a higher column capacity facilitating the isolation of oligosaccharides for subsequent characterization. The heparin oligosaccharides are eluted using a 2 M NaCl gradient and each peak is collected as a separate fraction.

Especially for minor components, it is necessary to combine the collected fractions from many SAX runs to obtain sufficient material for subsequent characterization experiments. To concentrate the oligosaccharides in these samples and reduce the NaCl content, the fraction collected for each peak is reinjected onto the SAX column and collected in a smaller volume. The remaining salt is removed from the oligosaccharide sample using a 1.6 x 70 cm desalting column containing Sephadex G-10 (superfine) and HPLC grade water as the eluent at a flow-rate of 0.15 mL/min.[37]

1.5 Oligosaccharide structural elucidation

The complete structural characterization of isolated heparin oligosaccharides is determined by mass spectrometry (MS) and both one-dimensional (1D) proton (^{1}H) and two-dimensional (2D) NMR experiments.

1.5.1 Reverse-phase ion-pairing high-performance liquid chromatography-mass spectrometry. To determine the purity of the peaks isolated by SAX-HPLC, reverse-phase ion-pairing- (RPIP-) HPLC is used as an orthogonal separation method. Coupled

with MS detection, this method also provides key structural information about the component oligosaccharides.

RPIP-HPLC utilizes a non-polar C_{18} stationary phase with an ion-pairing reagent (IPR) in the running buffer. This IPR is typically a lipophilic ion able to interact with the nonpolar stationary phase as well as the negatively charged heparin oligosaccharides. Therefore, the separation is based on a complex mechanism that depends on the strength of the interactions of each oligosaccharide with the IPR and the interactions of the IPR with the nonpolar stationary phase and polar organic mobile phase. For RPIP-HPLC-MS experiments, it is necessary to select a volatile IPR, for example alkylamines. Many IPRs have been utilized for heparin oligosaccharide separations including tributylamine (TrBA), dibutylamine (DBA), tripropylamine (TrPA), triethylamine (TrEA), tripentylamine (TrPA), tetrapropylamine (TPA), tetrabutylamine (TBA), and pentylamine (PTA).[45-53] The IPR chosen in this work for the structural analyses of heparin tetra and hexasaccharides was dibutylamine (DBA) because it provided a better separation than the commonly used tributylamine (TrBA).

Electrospray ionization (ESI), used in negative mode due to the natural negative charge of heparin oligosaccharides, provides information about the molecular ion and the number of sulfates and *N*-acetyl groups. However, it is difficult to obtain absolute structural information of the oligosaccharides because sulfate groups are easily lost during ionization. Methods such as electron detachment dissociation (EDD) and electron induced dissociation (EID) have been used to determine the identity of the GlcA and IdoA isomers by their fragmentation patterns. Methods such as MS/MS can be used to

distinguish structures of isomers but are difficult to use for highly sulfated GAG oligosaccharides such as those derived from heparin because one of the conditions for good ionization with minimal sulfate loss is that the charged state should be equal to or slightly more than the number of sulfate groups.[54] Although the addition of NaOH helps to prevent sulfate loss by stabilizing the charges, as the length of the chain increases, the increased presence of sulfate groups creates more negative charge repulsion, making the sulfate groups harder to stabilize. Furthermore, it becomes more difficult to determine the absolute structure of larger oligosaccharides because their MS fragmentation patterns become more complicated.[55,56] Statistical analyses such as PCA are currently being developed to overcome this problem.[57]

Methods to determine the absolute primary structure of GAGs by MS are rapidly improving and significant advances in this area are anticipated in the coming decade. Efficient MS analysis of complex samples will require a database of MS fragmentation patterns determined for oliogosaccharides of known structure. Advances underway in methods for the synthesis of heparin oligosaccharides should soon allow the creation of a library of standards for MS analysis, however, currently NMR analysis is still required for complete structure elucidation. An additional advantage of NMR is that it can also be used to investigate oligosaccharide secondary structure and dynamics, and protein-binding.

1.5.2 ^{1}H NMR spectroscopy. Inspection of 1D ^{1}H NMR spectra allows the identification of resonances of heparin oligosaccharides through their characteristic chemical shifts. In heparin samples digested using enzymatic or β-elimination reactions,

the unique chemical shift of H4 (Figure 1.1) ~ 6 ppm reflects the C4-C5 double bond of the uronic acid at the nonreducing end. The anomeric (H1) protons are fairly well resolved with chemical shifts between 4.6 and 5.6 ppm. Resonances characteristic of GlcNAc amide methyl groups are detected as singlets at around 2.0 ppm. The region of the spectrum between 3.2 and 4.4 ppm is more crowded containing the H2-H6 resonances, with the H5 proton of the IdoA residues having a chemical shift of ~4.8 ppm. Resonances due to protons adjacent to an *O*- or *N*-sulfo group will experience a downfield shift.

NMR experiments are typically performed in phosphate buffer at neutral pH to ensure all the carboxyl groups have been deprotonated and their chemical shifts are stable. Chemical shift stabilization can be achieved using EDTA-d_{16}, which is typically added to complex metal ions and minimize line broadening introduced by the interaction of trace paramagnetic ions with the heparin oligosaccharides.[58-61]

Solvent suppression techniques including presaturation,[62] WET,[63,64] WATERGATE,[65] and excitation sculpting[66] are often employed in the measurement of ^{1}H NMR spectra to reduce the intensity of the solvent resonance and better observe the analyte signals. Protic solvents such as water give rise to a very intense signal that limits the receiver gain that can be applied. Even with the 18 bit analog-to-digital converters (ADCs) typically used in modern spectrometers, in the absence of solvent suppression the low the receiver gain settings necessary to avoid overflowing the ADC make it difficult to detect low intensity analyte signals, especially in dilute aqueous solutions. Because of

the Lorentzian lineshape of NMR resonances, the intense solvent peak also obscures a significant region of the ^{1}H NMR spectrum.

The various solvent suppression techniques are based on different mechanisms, which are briefly summarized in this section. Presaturation reduces the intensity of the water signal by saturating the resonance transition with a long selective pulse prior to application of a non-selective excitation pulse and acquisition of the FID (Figure 1.5A). WET solvent suppression is carried out by applying four selective pulses each of which are followed by a gradient to dephase the water magnetization (Figure 1.5B). A particular disadvantage of presaturation, and to a lesser extent WET, is that these pulse sequences may also suppress the resonances of exchangeable protons of the analyte (see section 1.7).

The problem of saturation transfer from water to the analyte exchangeable protons is overcome using methods such as WATERGATE or excitation sculpting (Figures 1.5C and D). The WATERGATE pulse sequence utilizes a selective spin echo involving a pair of identical gradient pulses on either side of a selective 180º pulse (Figure 1.5C). The first gradient pulse dephases all the magnetization excited by the initial 90º pulse. The selective 180º pulse reverses the precession of all of the resonances except for the water resonance. As a result, application of the second gradient pulse refocuses the analyte resonances while further dephasing the water magnetization. In WATERGATE the selective 180º pulse is typically a composite pulse (e.g. 3-9-19) that produces additional nulls on either side of the water resonance at a spacing of 1/t, where t is the time between the pulses. The gradient pulse pairs in surrounding the first and second 180º pulses have

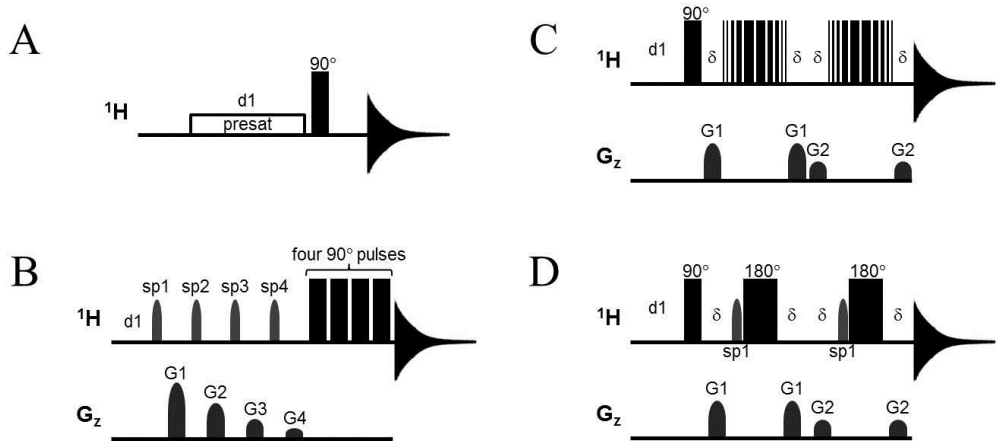

Figure 1.5. Bruker pulse sequences for various solvent suppression methods. (A) In presaturation, a weak rf pulse is applied at the frequency of the solvent for a specific length of time prior to pulse and acquisition, saturating its spins. (B) WET solvent suppression occurs by applying four selective pulse (sp1, sp2, sp3, and sp4) on the solvent, each followed by a different gradient to dephase the solvent (G1, G2, G3, and G4, respectively) making the solvent resonance unobservable while leaving all other signals in-phase. The selective pulses are then followed by four composite 90° pulses, which have been shown to produce a better baseline than one 90° pulse alone. (C) WATERGATE uses a composite 180^{o} pulse flanked by two gradients (G1 for the first 180^{o} pulse, and G2 for the second 180^{o} pulse). The first gradient pulse dephases all the magnetization. The composite 180° pulse selectively inverts the phase of all the resonances except for the solvent resonance. As a result, application of the second gradient pulse further dephases the solvent resonance while refocusing the other resonances. (D) Excitation sculpting is based on a double gradient spin echo and is similar to WATERGATE except that in lieu of the composite pulse, a selective pulse at

the water frequency is followed by a non-selective 180° pulse. Both WATERGATE and excitation sculpting repeat their respective 180° pulses a second time before acquisition using a different gradient G2 to avoid unwanted coherences.

different amplitudes. The excitation sculpting pulse sequence (Figure 1.5D) is a water-selective gradient double spin echo. It is in similar in concept to WATERGATE but uses a shaped 180º pulse (typically Sine.100) applied at the water frequency followed by a non-selective 180º pulse to refocus the magnetization of resonances outside the region containing the water signal. Excitation sculpting is preferred over WATERGATE in this work because it provides a more selective excitation profile reducing the attenuation of signals near the solvent frequency and, because excitation sculpting uses shaped selective pulses, it avoids the problem of nulls produced by the WATERGATE 3-9-19 composite pulse, giving a more uniform excitation profile over the entire ^{1}H spectrum.

1.5.3 Homonuclear two-dimensional NMR spectroscopy. It is difficult to assign the ^{1}H resonances of oligosaccharides using only 1D ^{1}H NMR spectra because of their limited chemical shift dispersion which produces resonance overlap, even for oligosaccharides of modest size. The homonuclear 2D ^{1}H NMR experiments typically used for oligosaccharide resonance assignment and structure elucidation include the correlation spectroscopy (COSY), total correlation spectroscopy (TOCSY), and rotating-frame nuclear Overhauser effect spectroscopy (ROESY) experiments (Figure 1.6). Either presaturation or excitation sculpting may be applied in these experiments to suppress the water resonance, depending on whether the focus is measurements of carbon-bound or exchangeable protons.

Heparin oligosaccharide structure elucidation typically begins with the COSY and TOCSY spectra. The COSY pulse sequence (Figure 1.6A) utilizes two $90°_{x}$ pulses separated by an evolution period, t_1, followed by an acquisition period. During the

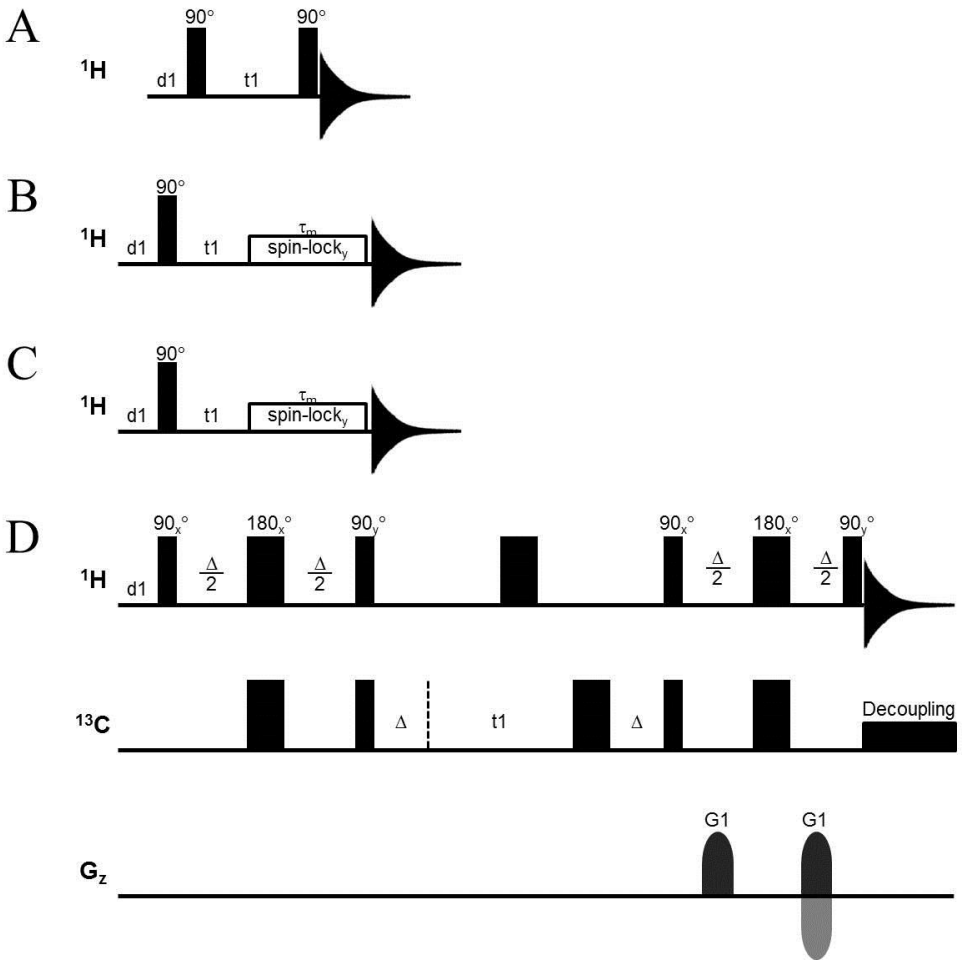

Figure 1.6. The pulse sequences used for structure elucidation of heparin and heparan sulfate oligosaccharides. (A) The COSY pulse sequence is made up of two 90° pulses separated by an evolution time, t_1. COSY cross peaks will reveal ^1H couplings usually through three bonds. (B) In the TOCSY pulse sequence, a 90° degree pulse is followed by an evolution time, t_1, and a spin-lock, τ_m. The spin-lock is made up of a series (or train) of 180° pulses separated by very small delays that cause the magnetization to evolve under the effects of the spinlock field (B_1) which is much smaller than the applied field (B_0). TOCSY cross peaks relate all the coupled protons within a spin system. (C)

The ROESY pulse sequence is similar the TOCSY, except that the spin-lock is applied in the rotating frame to allow the observation of dipolar (through-space) couplings. (D) The [^{1}H, ^{13}C] multiplicity-edited HSQC pulse sequence utilizes 90° and 180°pulses and delays that depend on the coupling constant ($1/4J_{HC}$) to transfer coherence between ^{1}H and ^{13}C. Gradients are used to remove any unwanted coherence pathways.

incremented delay, t_1, the magnetization evolves as a function of chemical shift while the second $90°_x$ pulse transfers magnetization between coupled spins. The 2D COSY spectrum of the most common heparin tetrasaccharide (ΔUA2S-GlcNS6S-IdoA2S-GlcNS6S, denoted as ISIS in Figure 1.7A) is shown in Figure 1.7B. The COSY spectrum contains a diagonal running from the bottom left to the top right corner of the contour plot which is equivalent to the ^{1}H spectrum. The off-diagonal features are cross peaks that correspond to the chemical shifts of coupled shifts protons. Starting with the well-resolved H1 resonances, the correlations are followed to the coupled H2 diagonal peak, which can then be traced to the H3 cross peak, and so on.

Like COSY, the TOCSY pulse sequence (Figure 1.6B) starts with a $90°_x$ pulse followed by an incremented t_1 delay allow for chemical shift evolution. Following t_1 is the mixing period (τ_m) constituted by a spin-lock composed of a series of composite 180° pulses separated by very short delays. During the spin-lock all spins feel the same field (B_1) which is very much less than the applied field (B_0) so that there is no evolution of chemical shift. However spin-spin coupling evolves during τ_m such that coherence is transferred between coupled spins that are part of the same spin system. The TOCSY spectrum for the ISIS tetrasaccharide is shown in Figure 1.7C. Like the COSY, the TOCSY spectrum also contains a diagonal that corresponds to the ^{1}H spectrum. The cross peaks in the TOCSY spectrum correspond to all coupled protons within the same spin system, for saccharide this means the same sugar ring. The longer-range TOCSY correlations are assigned by comparison with the COSY cross peaks which typically correspond to protons coupled through 3-bonds.

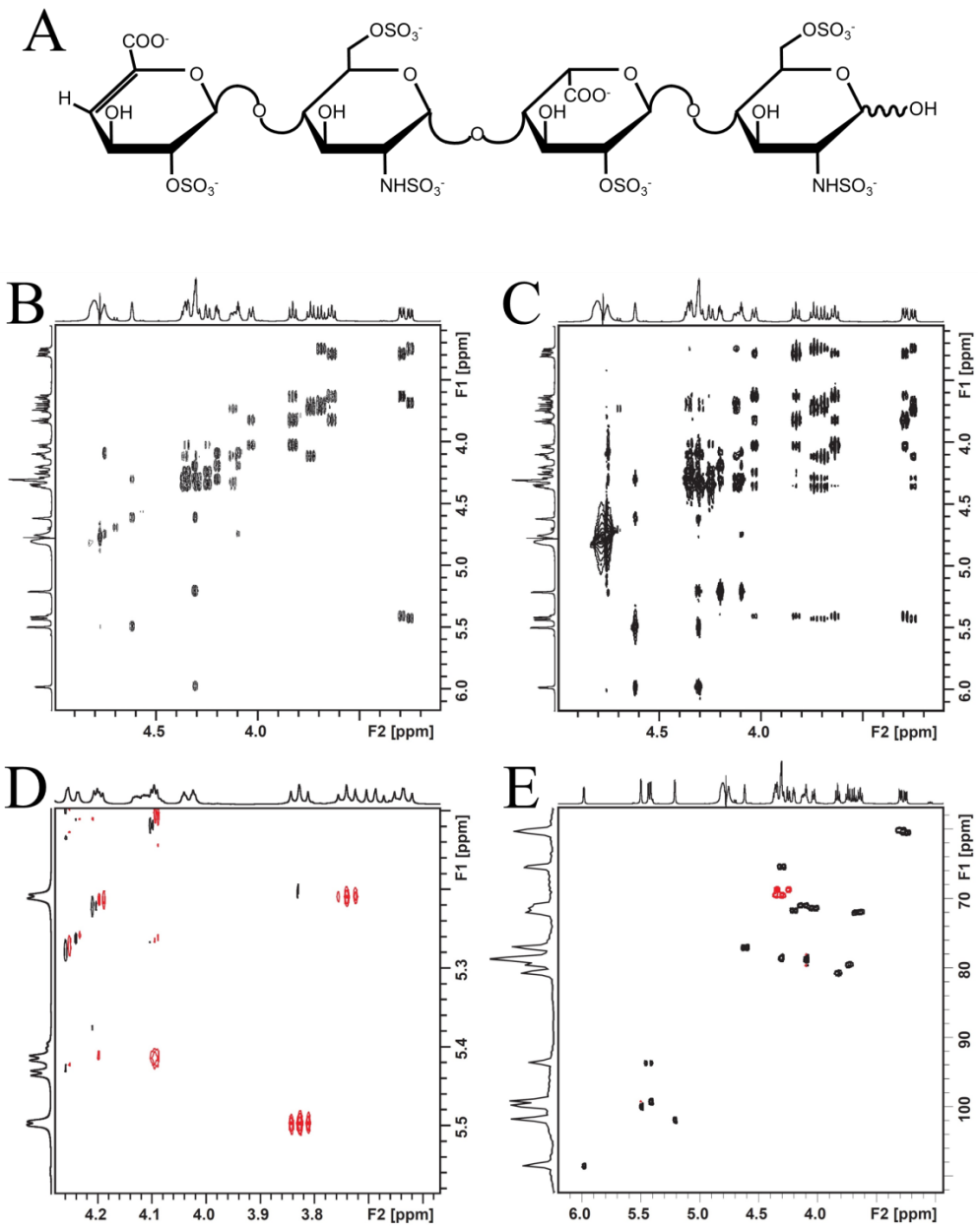

Figure 1.7. The ISIS (A) tetrasaccharide structure (ΔUA2S-GlcNS6S-IdoA2S-GlcNS6S) was elucidated using (B) COSY, (C) TOCSY, (D) ROESY, and (E) [^{1}H, ^{13}C] HSQC spectra. ISIS is the most common tetrasaccharide in heparin.

The ROESY pulse sequence (Figure 1.6D) is similar to the TOCSY in that a spin lock follows the incremented t_1 delay. ROESY is the rotating-frame version of the 2D nuclear Overhauser effect spectroscopy (NOESY) experiment. Both experiments utilize the nuclear Overhauser effect, a phenomenon in which intensity of a resonance is altered by dipolar relaxation through spins in close proximity, i.e. within 5Å. The intensity of the NOE depends on molecular tumbling, and goes through zero for medium-sized molecules, such as pentasaccharides, when measured at 14T (600 MHz). Because the ROE evolves in the rotating frame of reference, it is always positive, which is why it is preferred in this work. The ROESY spectrum of the ISIS tetrasaccharide is shown in Figure 1.7D. Like the COSY and TOCSY, the ROESY also has a diagonal corresponding to the ^{1}H spectrum. The cross peaks in a ROESY spectrum correspond to protons coupled through space, but because spin-coupled protons on adjacent carbons are within 5Å, they are also detected in both the TOCSY and ROESY spectra. In the ROESY spectrum (Figure 1.7D), the H1 proton of one sugar ring will show a cross peak to a H4 proton of an adjacent sugar ring if they are connected through a $\beta(1\rightarrow4)$ glycosidic linkage, such as those found in heparin. This provides information on ring connectivity so that in conjunction with the coupling information from the COSY and TOCSY spectra, the primary structure of GAGs is determined.

1.5.4 Heteronuclear two-dimensional NMR spectroscopy. For larger oligosaccharides, even homonuclear 2D NMR experiments may not provide sufficient resolution for unambiguous resonance assignments. Heteronuclear 2D NMR experiments provide greater resolution because of the larger chemical shift dispersion of the

heteronucleus (typically ^{13}C). The [^{1}H, ^{13}C] heteronuclear single quantum coherence (HSQC) experiment has proven useful for the analysis of heparin oligosaccharides, and has even been used for the characterization of complex LMWH heparins.[67,34,68] Multiplicity-edited [^{1}H, ^{13}C] HSQC spectra are especially useful because the CH and CH_3 proton correlations are of opposite sign from the CH_2 correlations, making them easy to distinguish. The pulse sequence (Figure 1.6D) begins by applying a ^{1}H 90° pulse followed by a delay time equal to $\Delta/2$ (where $\Delta=1/2J_{HC}$) that allows chemical shift and heteronuclear coupling evolution. A 180° pulse is applied to both ^{1}H and ^{13}C so that heteronuclear coupling continues to evolve while chemical shift is refocused after another $\Delta/2$ delay. The ^{13}C magnetization is allowed to evolve during time t1 with a ^{1}H 180° pulse in the middle to decouple any ^{1}H-^{13}C interactions. 90° pulses to both ^{1}H and ^{13}C transfer coherence back to ^{1}H. A second series of $\Delta/2$-180°-$\Delta/2$ series allows for ^{13}C magnetization to refocus. Multiplicity editing occurs by adding a Δ-180°-Δ sequence during t_1 evolution in the heteronuclear channel. Gradients remove unwanted coherence, and decoupling is applied in the heteronuclear channel during acquisition to make the spectrum less crowded in the ^{13}C dimension.

The result of the HSQC experiment is a 2D spectrum with correlations between ^{1}H (in the F2 dimension) and the ^{13}C nuclei to which they are bonded (in the F1 dimension). The ^{1}H and ^{13}C chemical shifts are unique to their chemical environment and values have been reported for a wide variety of heparin oligosaccharides, including the components of LMWHs.[69,70] For example, characteristic correlations are observed in the [^{1}H, ^{13}C] HSQC spectrum of the ISIS tetrasaccharide (Figure 1.7E). The -CH_2 (H6)

correlations of the GlcNS residues are of opposite sign relative to the -CH protons, making them easy to distinguish in an otherwise overlapped region in the NMR spectrum.

1.6 NMR relaxation mechanisms

When nuclei are placed in an external magnetic field (B_0), they align parallel to, either with or against, the magnetic field. Those nuclei aligned with the magnetic field (α) will be at a lower energy than those that are aligned against the magnetic field (β) (Figure 1.8A). Because the individual nuclear spins have angular momentum, they precess about the applied field at their Lamor frequency ($\omega = \gamma B_0$). Due to the energy difference between the α and β spin states, there will be a greater population of α spins giving rise to a net macroscopic magnetization (M). The behavior of the macroscopic magnetizaton is typically illustrated using a xyz-coordinate system, with M displayed as a vector along the +z axis, aligned with the applied magnetic field (B_0) (Figure 1.8B). The NMR experiment is most simply illustrated using a convention known as the rotating frame of reference in which the x and y axes of the coordinate system rotate (or precess) at the Larmor frequency.

At equilibrium, the spins of the individual nuclei lack coherence and precess randomly about B_0. As a result, M (the vector sum of the individual spins) does not precess about B_0 at equilibrium. Perturbation by an external radiofrequency (rf) pulse equalizes the populations of the α and β spin states and creates coherence as the individual nuclear vectors precess about B_0 as well as the B_1 field generated by the rf pulse. The effect of the pulse is visualized in Figure 1.8C as causing M to tip towards the

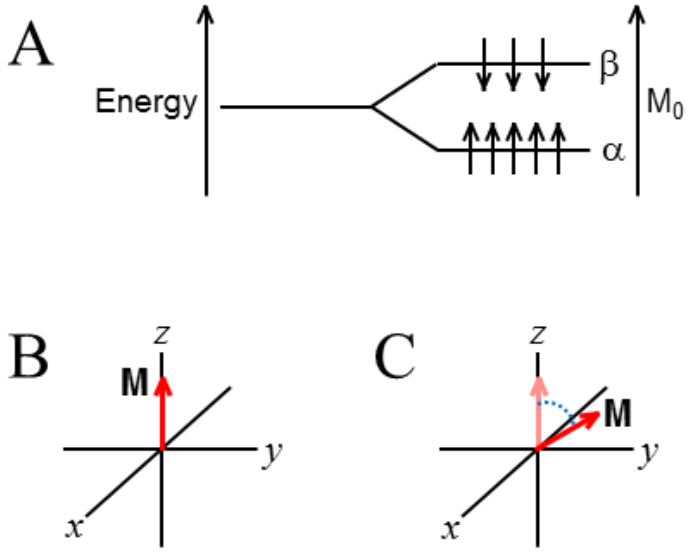

Figure 1.8. (A) When a group of spins is in the presence of an external magnetic field (M_0), some spins will align with the field (α) and some will align against the field (β). There will be a larger population of α spins, creating a bulk magnetization aligned with the magnetic field (B). This magnetization is represented by the vector, M, in the xyz coordinate system, aligned with the applied magnetic field (B_0) along the +z axis. (C) When a radiofrequency (rf) pulse is applied, the magnetization is tipped towards the xy-plane.

xy plane. After the pulse, the coherence induced in the spins causes M to precess about the z-axis (B_0). Over time, this coherence is lost and the population difference between the spin states returns to its equilibrium value. These processes are described by two different relaxation mechanisms, T_1 and T_2, as explained below.

1.6.1 T_1 relaxation. T_1 relaxation, also known as spin-lattice or longitudinal relaxation, occurs when an ensemble of spins returns to their equilibrium population. Using the vector formalism described above, T_1 relaxation can be described by the recovery of the macroscopic magnetization (M) along the z or longitudinal axis following a 90° pulse as described by Eq. 1.1:

$$M_t = M_0(1 - e^{-t/T_1}) \qquad \text{(Eq. 1.1)}$$

where M_t is the magnetization at time t following the rf pulse, M_0 is the equilibrium magnetization and T_1 is the relaxation time constant. T_1 relaxation occurs at a rate of $1/T_1$ (R_2) and after a time equivalent to one T_1, the magnetization recovers to 63% of its value at equilibrium. The value of T_1 is determined experimentally using the inversion-recovery pulse sequence shown in Figure 1.9A. In this experiment, a 180° pulse inverts the population of the spins placing the macroscopic magnetization vector along the –z axis. The magnetization recovers along the +z axis during the variable delay as the spins return to their equilibrium populations according to Eq. 1.2.

$$M_t = M_0(1 - 2e^{-t/T_1}) \qquad \text{(Eq. 1.2)}$$

Application of a 90° pulse creates transverse magnetization detected along the y axis of the rotating frame of reference (Figure 1.9B). The equation by which the magnetization returns to equilibrium is dependent on the initial rf pulse. After a 90° pulse, M_t is equal to

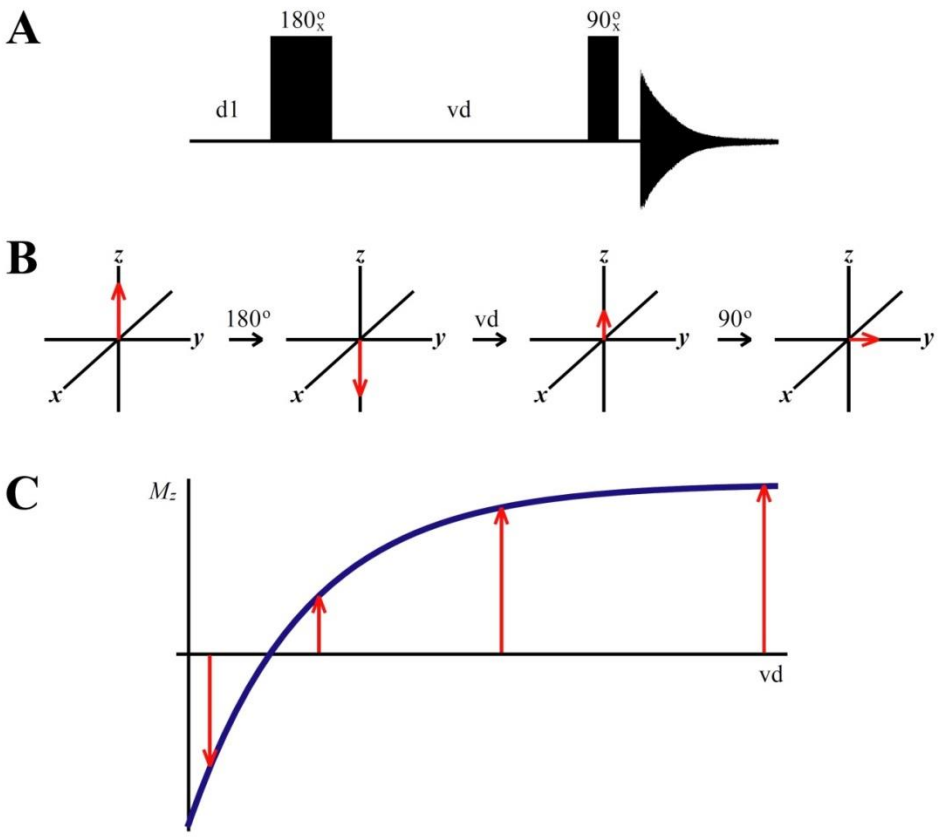

Figure 1.9. (A) The inversion recovery pulse sequence used to measure T_1 relaxation, also known as spin-lattice or longitudinal relaxation. (B) The vector diagram illustrating the effect of the inversion recovery pulse sequence on the macroscopic magnetization. Relaxation occurs during the variable delay (vd) following the 180º inversion pulse. The terminal 90º pulse enables detection of the magnetization vector along the positive y-axis. (C) The magnetization is initially inverted, passes through zero intensity and recovers to its equilibrium intensity at long values of vd.

0, so the magnetization recovers according to Eq. 1.1. After a 180° pulse, M_t is equal to $-M_0$, so the magnetization recovers according to Eq. 1.2. By varying the delay time over a series of 1D experiments, the recovery of the magnetization can be observed and the value of T_1 determined by fitting a function corresponding to Eq. 1.2 to the measured resonance intensity (M_t; Figure 1.9C). It is important to wait 5-10 times T_1 between acquisitions to allow sufficient time for magnetization to fully relax along the +z axis before another 180° pulse is applied

1.6.2 T_2 relaxation. T_2 relaxation, also known as spin-spin or transverse relaxation, represents the loss of coherence of an ensemble of spins generated by an rf pulse. This loss of coherence is observed as a dephasing of the spins reducing the intensity of M in the xy plane of the rotating frame of reference (Figure 1.10A). This relaxation process is described by an exponential decay:

$$M_t = M_0 e^{-t/T_2} \qquad \text{(Eq. 1.3)}$$

where M_t is the macroscopic magnetization at time t after the rf pulse, M_0 is the initial magnetization and T_2 is the transverse relaxation time constant in a perfectly homogeneous magnetic field. Though T_2 relaxation can occur through a variety of mechanisms, for spin ½ nuclei in a solution of low viscosity, dipolar relaxation due to molecular tumbling is the dominant mechanism. As with T_1, T_2 relaxation occurs at a rate of $1/T_2$ (R_2). The exponential decay of the FID (Figure 1.10B), denoted by T_2^* reflects both the value of T_2 and contributions from magnetic field inhomogeneity, which are minimized by a process referred to as shimming the magnet. Upon Fourier transformation

of the FID, the value of T_2* is related to the observed resonance linewidths by the following equation:

$$\omega_{1/2} = \frac{1}{\pi T_2^*} \quad \text{(Eq. 1.4)}$$

where $\omega_{1/2}$ is the resonance linewidth at half height. Longer T_2^* values produce sharper resonances.

Although T_2^* can be determined from the resonance linewidth, we are most often interested in the true T_2 relaxation time. The Hahn spin-echo experiment is useful for measuring T_2 relaxation rates. In the pulse sequence in Figure 1.11A, an initial 90° pulse is followed by delay t_D, a 180° pulse, and finally another t_D period before acquisition of the FID. The result of this experiment is an initial decay of the FID followed by appearance of another signal that is less intense than the original, called an echo (Figure 1.11B). The mechanism by which the echo forms can be explained by the vector diagram in Figure 1.11C. After the initial 90_x° pulse, the macroscopic magnetization will be along the +y axis. During the delay t_D, the macroscopic magnetization vector precesses in due to chemical shift and loses intensity due to the loss of coherence. In addition, as a result of magnetic field inhomogeneity some spins will be in a region of higher magnetic field and will appear to precess at a frequency greater than M (denoted by *f* for faster) while other spins will be in a region of lower magnetic field and will appear to precess at a frequency less than M (denoted by *s* for slower). The 180° pulse of the spin echo experiment refocuses the effects of magnetic field inhomogeneity by rotating the vectors about the x axis. The spins will continue to precess in the same direction following the 180° pulse so that after the same delay, t_D, the spins refocus along the –y axis, creating

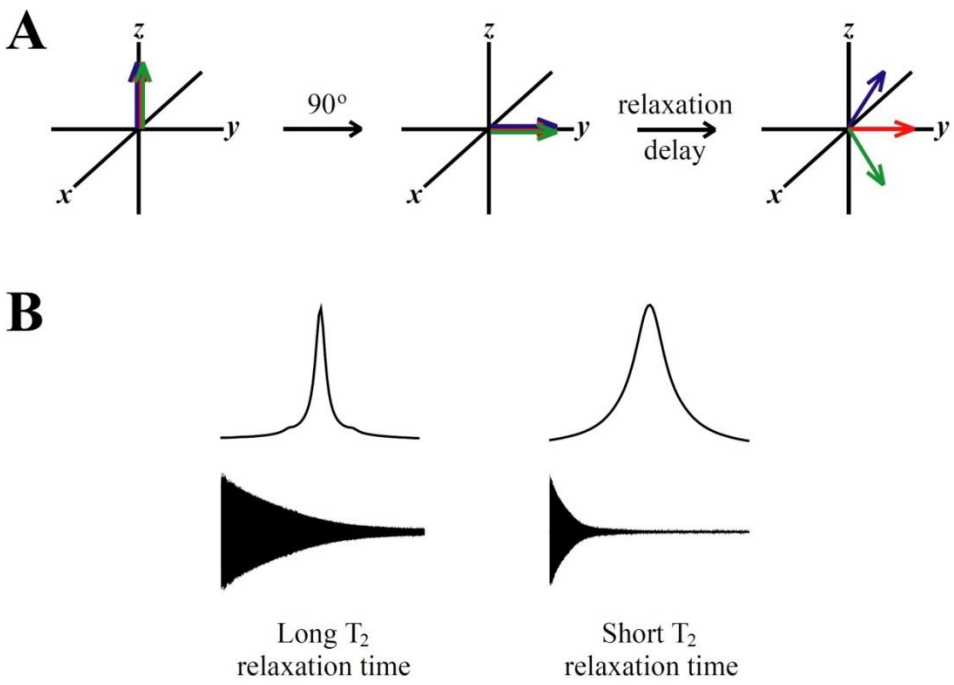

Figure 1.10. (A) A vector diagram representing T_2 relaxation, also known as spin-spin or transverse relaxation. The different color vectors represent resonances with different frequencies caused by magnetic field inhomogeneity across the sample. T_2 relaxation occurs when a group of spins loses coherence in the xy-plane. (B) The loss of intensity in free induction decay originates in part from T_2 relaxation and in part from inhomogeneities in the applied magnetic field. Longer T_2 relaxation times give rise to sharper resonances in the Fourier transformed spectrum.

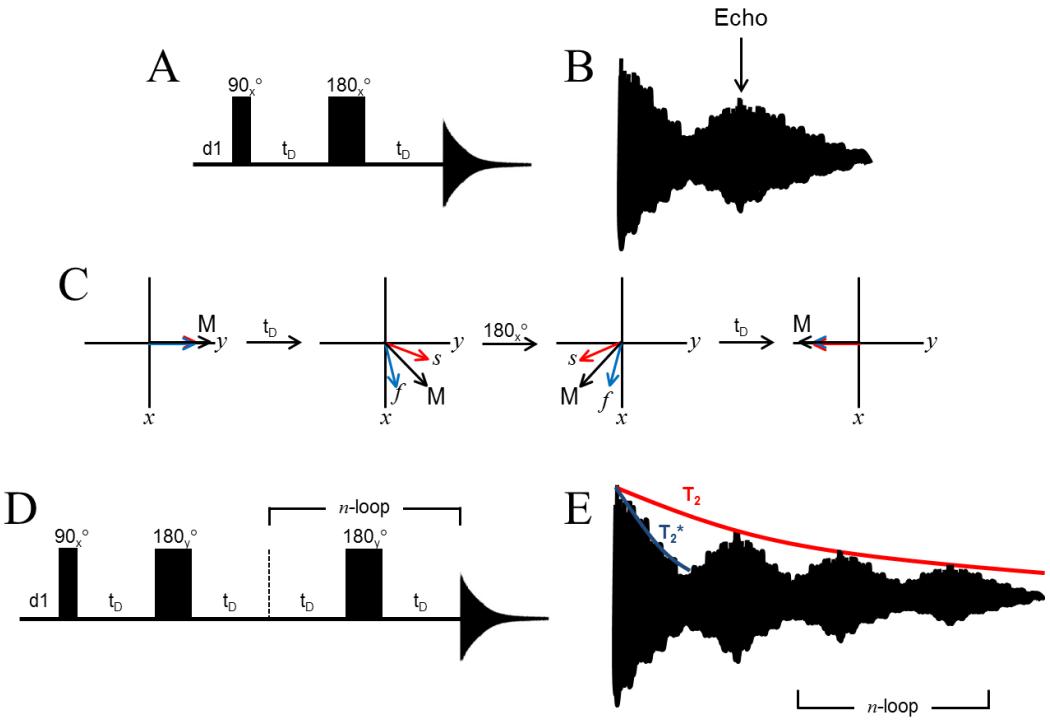

Figure 1.11. (A) The Hahn spin-echo pulse sequence. A 90°-t_D-180-t_D sequence, where t_D is a specific delay time. (B) The resulting FID shows initial decay followed by a weaker signal, called an echo, which appears and decays. (C) The mechanism by which the echo is created is illustrated with an aerial view of the xy-plane. The initial 90° pulse, tips the magnetization so that it is aligned with the +y axis. Following the pulse, the magnetization precesses according to its frequency, which is proportional to the applied magnetic field, B_0. The presence of magnetic field inhomogeneities affects the frequency of spins located in different regions of the sample, causing spins in a region of higher field to precess faster, denoted by *f* (fast), and those in a region of lower field to precess more slowly indicated as *s* (slow). The 180° pulse rotates the spins around the x axis where they will continue to travel in the same direction so that after another t_D, the vectors labeled *f* and *s* are refocused along the –y axis, creating the echo. (D) The Carr-

Purcell-Meiboom-Gill (CPMG) pulse sequence refocuses the effects of magnetic field inhomogeneity using a train of 180^{o} pulses keeping the delay between pulses short to prevent modulation of the spectra due to spin-spin coupling. (E) During the CPMG experiment the initial FID decays by the observed T_2* (depicted by the blue line), which includes the effects of magnetic field inhomogeneity. The series of echo FIDs decrease in intensity according to the actual T_2 (depicted by the red line). If a series of CPMG spectra are collected, each with an incrementally increased number of *n* loops, the signals will decay according to Eq. 1.3.

the echo. The echo is less intense than the original signal because of losses due to T_2 relaxation, but not T_2* because the effects of magnetic field inhomogeneity have been removed.

The Carr-Purcell-Meiboom-Gill (CPMG) experiment applies a 180^o pulse train composed of a series of spin echoes In the CPMG experiment, instead of applying the 180° pulses around the x axis, the pulses are applied along the ±y axis so that the magnetization always remains on the +x axis. In addition, the delay between pulses is kept short (typically 0.3 ms) to prevent phase modulation of the resonances due to J-coupling evolution, overcoming a significant limitation of the Hahn spin echo. During the train of 180^o pulses the echoes produced decay according to the true T_2. As illustrated in Figure 1.11E, each 180^o pulse in the train produces a spin echo that is less intense than the previous. The initial FID and each individual echo decays according to T_2* (blue), influenced by magnetic field inhomogeneity. In contrast the series of spin echoes produced by the CPMG pulse train decay according to the true T_2 (red). In practice, rather than recording the echoes as the pulse train is applied, the number, *n*, of loops through the CPMG pulse train is increased incrementally over a series of experiments to record a set of spectra in which the resonances decrease intensity a *n* is increased. Though the linewidth of a resonance in each CPMG spectrum reflects T_2^*, its true T_2 relaxation time can be extracted by fitting the integrated resonances measured in each experiment as a function of the CPMG pulse train time (*t*) using Eq. 1.3. T_2 relaxation times are shorter than T_1 relaxation times for larger molecules which tumble more slowly in solution.

Smaller molecules, which tumble more rapidly in solution, have equal T_1 and T_2 relaxation times; this is referred to as the extreme narrowing limit.

1.7 Chemical Exchange

The exchangeable protons of heparin and HS, introduced in section 1.5.2, include the sulfamate ($NHSO_3^-$), hydroxyl (OH), amide ($NHCOCH_3$), and amine (NH_2) protons. These protons participate in chemical exchange with the solvent water by the following reversible chemical equation:

$$ROH^* + H_2O \rightleftharpoons ROH + H_2^*O \qquad \text{(Eq. 1.5)}$$

where the proton involved in exchange is denoted by an asterisk. The rate of the exchange reaction is dependent on the proton's microenvironment and the solution conditions. The slower exchanging amide protons have been studied extensively, mainly in proteins and other GAGs such as HA.[71-75] Amide protons are detectable by NMR over a variety of temperatures and solution conditions. Sulfamate protons exchange more rapidly and are detectable over a narrow pH range.[76] Hydroxyl proton exchange in carbohydrates has been studied previously and only recently explored for heparin oligosaccharides.[26,77-81] This dissertation explores, for the first time, conditions that allow detection of carbohydrate primary amines in aqueous solution (Chapter 5). Prior to this work, the amine protons of sugars were assumed to exchange too rapidly to be detected by solution state NMR experiments.

1.7.1 NMR exchange regimes. There are three possible exchange regimes that can be considered in an NMR measurement: slow, fast, and intermediate, defined by the

exchange rate (reactions per second) and the difference in frequency (in Hz) between the two chemical environments (or sites) experienced by the exchanging protons.[82] Because of the dependence on the difference in chemical shift of the exchanging species, the appearance of the NMR spectrum can be dramatically affected when measured at different magnetic field strengths. In the slow exchange regime, the rate of exchange is much less than the frequency difference between the two sites and the protons will be detected in the NMR spectrum as two distinct resonances. In the fast exchange regime, the exchange rate is much greater than the frequency difference between the exchanging spins and a single exchange-averaged resonance is detected at a chemical shift weighted by the populations of the two species. In a typical solution of a GAG polymer or oligosaccharide, the water protons are present at such a high concentration (110 M) that the exchange-averaged chemical shift is essentially that of the water protons. Lying between these two extremes is the intermediate exchange regime, in which the exchange rate is on the same order of magnitude as the chemical shift difference between the exchanging species. In intermediate exchange, the chemical shifts of the exchanging species begin to shift towards their average value and an increase in the resonance line widths (or line broadening) is observed in the NMR spectrum.

1.7.2 Lineshape analysis. In the intermediate exchange regime, the resonance line widths of exchangeable protons are affected by their exchange with the solvent water. Because the rate of the exchange reaction increases with temperature, the resonances become broader as the temperature is raised. The relationship between resonance linewidth and temperature is described by the Eyring-Polanyi equation:

$$k = \frac{k_B T e^{-\Delta G^{\ddagger}/RT}}{\pi h} \qquad \text{(Eq. 1.6)}$$

where k is the line width at half height, k_B is the Boltzmann constant, T is temperature in K, and $\Delta G^{\ddagger}$ is the Gibbs activation energy for the exchange reaction (Eq. 1.6).[82-84] A higher value of $\Delta G^{\ddagger}$ can reflect the participation of the proton in a hydrogen bond as reported by Langeslay et al. for the internal GlcNS3S6S sulfamate proton of Arixtra.[84]

1.7.3 Saturation transfer experiments. Saturation transfer NMR experiments involve the saturation of a specific exchangeable proton signal. Chemical exchange transfers the saturation to the exchange partner, reducing its intensity. As introduced in section 1.5.2, when using presaturation and WET solvent suppression methods to suppress the water resonance, saturation is transferred to the exchangeable protons, reducing their intensity. WATERGATE and excitation sculpting, on the other hand, suppress water by using selective pulses at the frequency of water, leaving the exchangeable protons unaffected. Exchange rates and relaxation times can be extracted using the proton T_1 relaxation times (section 1.7.4).[85] Saturation transfer experiments have been utilized in studies of amide proton exchange in small molecules such as acetamide, ethyl acetimidate, acrylamide, cyanoacetamide, ethyl oxamate, and synthetic diamines.[86-88] These experiments, however, are not suitable for studying the exchange of oligosaccharide hydroxyl, sulfamate or amine protons due to their faster exchange rates.

1.7.4 Exchange spectroscopy (EXSY). Exchange spectroscopy utilizes the NOESY pulse sequence (Figure 1.12) to detect the transfer of magnetization between exchangeable spins. In aqueous solutions of heparin oligosaccharides, exchange cross

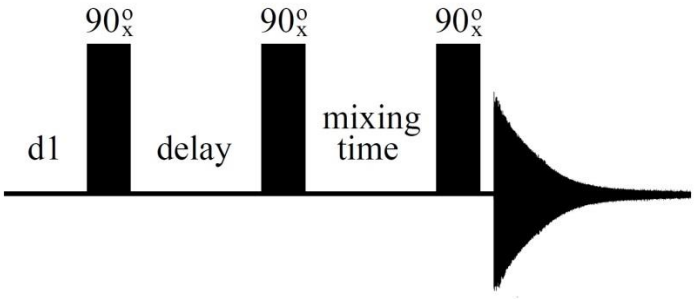

Figure 1.12. The NOESY pulse sequence used for EXSY experiments. As the mixing time is increased, the exchange cross peaks increase in intensity at a rate that corresponds to the exchange rates of the protons observed.

peaks appear between the resonances of water and the exchangeable hydroxyl and sulfamate protons.[79,89] Cross peak intensity depends on the rate of the exchange reaction, the length of the EXSY mixing time and the T_1 relaxation time. Exchange cross peaks become more intense as the mixing time is increased and eventually plateau due to T_1 relaxation. The measurement of cross peak intensity as a function of mixing time can be used to determine exchange rates. Differences in exchange rates for chemically similar protons can indicate that the more slowly exchanging protons are involved in a hydrogen bond, which is discussed in more detail in Chapter 3.

1.8 Summary

The purpose of the research presented in this dissertation is to develop methods that can be used to improve our understanding of the primary and secondary structure of heparin and HS oligosaccharides. Chapter 2 focuses on measuring ^{1}H and ^{15}N chemical shifts of individual enoxaparin tetrasaccharide SEC fractions to identify those fractions containing 3-*O*-sulfo-GlcNS residues, facilitating the isolation of component tetrasaccharides by SAX-HPLC and their structure determination by MS and NMR. Chapter 3 discusses NMR detection of oligosaccharide hydroxyl proton resonances and their use to probe for intramolecular hydrogen bonds providing insights into heparin and HS secondary structure. The rates of hydroxyl proton exchange with water are directly measured using EXSY taking into account effects from radiation damping. Analysis of the intensity of EXSY cross peaks as a function of mixing time allows the identification of two hydroxyl proton hydrogen bonds in Arixtra. Chapter 4 reports the measurement of

transverse relaxation rates (R_2) using the CPMG pulse sequence modified to incorporate excitation sculpting solvent suppression. The values of R_2 are compared with the EXSY results (Chapter 4) to evaluate whether relative transverse relaxation rates are also reflective of hydroxyl proton intramolecular hydrogen bonding. Chapter 5 reports, for the first time, the NMR detection of the amine protons of monosaccharides related to HS. The properties of the amine protons are explored including their exchange with water and acidity constants (pK_a values) to determine whether they participate in intramolecular hydrogen bonds or salt bridges. Chapter 7 summarizes the conclusions of this work and discusses future directions for the primary and secondary structural characterization of heparin and HS.

1.9 References

1. Capila, I.; Linhardt, R. J., Heparin - protein interactions. *Angew. Chem. Int. Edit.* **2002,** *41*, 391-412.

2. Whitelock, J. M.; Iozzo, R. V., Heparan sulfate: A complex polymer charged with biological activity. *Chem. Rev.* **2005,** *105*, 2745-2764.

3. Gandhi, N. S.; Mancera, R. L., The structure of glycosaminoglycans and their interactions with proteins. *Chem. Biol. Drug Des.* **2008,** *72*, 455-482.

4. Gallagher, J. T.; Walker, A., Molecular distinctions between heparan sulphate and heparin. Analysis of sulphation patterns indicates that heparan sulphate and heparin are separate families of *N*-sulphated polysaccharides. *Biochem. J.* **1985,** *230*, 665-674.

5. Hricovini, M.; Guerrini, M.; Bisio, A.; Torri, G.; Petitou, M.; Casu, B., Conformation of heparin pentasaccharide bound to antithrombin III. *Biochem. J.* **2001,** *359*, 265-272.

6. Ferro, D. R.; Provasoli, A.; Ragazzi, M.; Torri, G.; Casu, B.; Gatti, G.; Jacquinet, J. C.; Sinay, P.; Petitou, M.; Choay, J., Evidence for conformational equilibrium of the sulfated L-iduronate residue in heparin and in synthetic heparin monosaccharides and oligosaccharides: NMR and force-field studies. *J. Am. Chem. Soc.* **1986,** *108*, 6773-6778.

7. Ornitz, D. M.; Yayon, A.; Flanagan, J. G.; Svahn, C. M.; Levi, E.; Leder, P., Heparin is required for cell-free binding of basic fibroblast growth factor to a soluble receptor and for mitogenesis in whole cells. *Mol. Cell. Biol.* **1992,** *12*, 240-247.

8. Faham, S.; Hileman, R. E.; Fromm, J. R.; Linhardt, R. J.; Rees, D. C., Heparin structure and interactions with basic fibroblast growth factor. *Science* **1996,** *271*, 1116-1120.

9. Goodger, S. J.; Robinson, C. J.; Murphy, K. J.; Gasiunas, N.; Harmer, N. J.; Blundell, T. L.; Pye, D. A.; Gallagher, J. T., Evidence that heparin saccharides promote FGF2 mitogenesis through two distinct mechanisms. *J. Biol. Chem.* **2008,** *283*, 13001-13008.

10. Houck, K. A.; Leung, D. W.; Rowland, A. M.; Winer, J.; Ferrara, N., Dual regulation of vascular endothelial growth factor bioavailability by genetic and proteolytic mechanisms. *J. Biol. Chem.* **1992,** *267*, 26031-26037.

11. Ruhrberg, C.; Gerhardt, H.; Golding, M.; Watson, R.; Ioannidou, S.; Fujisawa, H.; Betsholtz, C.; Shima, D. T., Spatially restricted patterning cues provided by heparin-

binding VEGF-A control blood vessel branching morphogenesis. *Gene. Dev.* **2002,** *16*, 2684-2698.

12. Zhao, W. J.; McCallum, S. A.; Xiao, Z. P.; Zhang, F. M.; Linhardt, R. J., Binding affinities of vascular endothelial growth factor (VEGF) for heparin-derived oligosaccharides. *Bioscience Rep.* **2012,** *32*, 71-81.

13. van Barlingen, H.; Kleinveld, H. A.; Erkelens, D. W.; deBruin, T. W. A., Lipoprotein lipase-enhanced binding of lipoprotein(a) [Lp(a)] to heparan sulfate is improved by apolipoprotein E (apoE) saturation: Secretion-capture process of ApoE is a possible route for the catabolism of Lp(a). *Metabolism.* **1997,** *46*, 650-655.

14. Spillmann, D.; Lookene, A.; Olivecrona, G., Isolation and characterization of low sulfated heparan sulfate sequences with affinity for lipoprotein lipase. *J. Biol. Chem.* **2006,** *281*, 23405-23413.

15. Jee, J. P.; Nam, S. H.; Park, Y.; Lee, H. J.; Maeng, H. J.; Kim, C. K., Simplified analysis of lipoprotein lipase activity: Evaluation of lipasemic activity of low molecular weight heparin in rats. *Arch. Pharm. Res.* **2012,** *35*, 1107-1114.

16. Mummery, R. S.; Rider, C. C., Characterization of the heparin-binding properties of IL-6. *J. Immunol.* **2000,** *165*, 5671-5679.

17. Zhang, S. Y.; Condac, E.; Qiu, H.; Jiang, J. L.; Gutierrez-Sanchez, G.; Bergmann, C.; Handel, T.; Wang, L. C., Heparin-induced leukocytosis requires 6-*O*-Sulfation and is caused by blockade of selectin- and CXCL12 protein-mediated leukocyte trafficking in mice. *J. Biol. Chem.* **2012,** *287*, 5542-5553.

18. Ziarek, J. J.; Veldkamp, C. T.; Zhang, F. M.; Murray, N. J.; Kartz, G. A.; Liang, X. L.; Su, J. D.; Baker, J. E.; Linhardt, R. J.; Volkman, B. F., Heparin oligosaccharides inhibit chemokine (CXC Motif) ligand 12 (CXCL12) cardioprotection by binding orthogonal to the dimerization interface, promoting oligomerization, and competing with the chemokine (CXC Motif) receptor 4 (CXCR4) N terminus. *J. Biol. Chem.* **2013,** *288*, 737-746.

19. Rosenberg, R. D., Chemistry of hemostatic mechanism and its relationship to action of heparin. *Fed. Proc.* **1977,** *36*, 10-18.

20. Olson, S. T., Transient kinetics of heparin-catalyzed protease inactivation by antithrombin-III. Linkage of protease-inhibitor-heparin interactions in the reaction with thrombin. *J. Biol. Chem.* **1988,** *263*, 1698-1708.

21. Thunberg, L.; Backstrom, G.; Lindahl, U., Further characterization of the antithrombin-binding sequence in heparin. *Carbohyd. Res.* **1982,** *100*, 393-410.

22. Johnson, D. J. D.; Li, W.; Adams, T. E.; Huntington, J. A., Antithrombin-S195A factor Xa-heparin structure reveals the allosteric mechanism of antithrombin activation. *Embo J.* **2006,** *25*, 2029-2037.

23. Pol-Fachin, L.; Verli, H., Depiction of the forces participating in the 2-*O*-sulfo-alpha-L-iduronic acid conformational preference in heparin sequences in aqueous solutions. *Carbohyd. Res.* **2008,** *343*, 1435-1445.

24. Atha, D. H.; Lormeau, J. C.; Petitou, M.; Rosenberg, R. D.; Choay, J., Contribution of monosaccharide residues in heparin binding to antithrombin-III. *Biochemistry* **1985,** *24*, 6723-6729.

25. Langeslay, D. J.; Young, R. P.; Beni, S.; Beecher, C. N.; Mueller, L. J.; Larive, C. K., Sulfamate proton solvent exchange in heparin oligosaccharides: Evidence for a persistent hydrogen bond in the antithrombin-binding pentasaccharide Arixtra. *Glycobiology* **2012,** *22*, 1173-1182.

26. Beecher, C. N.; Young, R. P.; Langeslay, D. J.; Mueller, L. J.; Larive, C. K., Hydroxyl-proton hydrogen bonding in the heparin oligosaccharide Arixtra in aqueous solution. *J. Phys. Chem. B* **2014,** *118*, 482-491.

27. Guerrini, M.; Elli, S.; Mourier, P.; Rudd, T. R.; Gaudesi, D.; Casu, B.; Boudier, C.; Torri, G.; Viskov, C., An unusual antithrombin-binding heparin octasaccharide with an additional 3-*O*-sulfated glucosamine in the active pentasaccharide sequence. *Biochem. J.* **2013,** *449*, 343-351.

28. Shukla, D.; Liu, J.; Blaiklock, P.; Shworak, N. W.; Bai, X. M.; Esko, J. D.; Cohen, G. H.; Eisenberg, R. J.; Rosenberg, R. D.; Spear, P. G., A novel role for 3-*O*-sulfated heparan sulfate in herpes simplex virus 1 entry. *Cell* **1999,** *99*, 13-22.

29. O'Donnell, C. D.; Tiwari, V.; Oh, M.-J.; Shukla, D., A role for heparan sulfate 3-O-sulfotransferase isoform 2 in herpes simplex virus type 1 entry and spread. *Virology* **2006,** *346*, 452-459.

30. Kaner, R. J.; Baird, A.; Mansukhani, A.; Basilico, C.; Summers, B. D.; Florkiewicz, R. Z.; Hajjar, D. P., Fibroblast growth-factor receptor is a portal of cellular entry for herpes simplex virus type 1. *Science* **1990,** *248*, 1410-1413.

31. Ampofo, S. A.; Wang, H. M.; Linhardt, R. J., Disaccharide compositional analysis of heparin and heparan sulfate using capillary zone electrophoresis. *Anal. Biochem.* **1991,** *199*, 249-255.

32. Desai, U. R.; Wang, H. M.; Linhardt, R. J., Specificity studies on the heparin lyases from *Flavobacterium heparinum*. *Biochemistry* **1993,** *32*, 8140-8145.

33. Maddineni, J.; Walenga, J. M.; Jeske, W. P.; Hoppensteadt, D. A.; Fareed, J.; Wahi, R.; Bick, R. L., Product individuality of commercially available low-molecular-weight heparins and their generic versions: Therapeutic implications. *Clin. Appl. Thromb.-Hem.* **2006,** *12*, 267-276.

34. Jones, C. J.; Beni, S.; Limtiaco, J. F. K.; Langeslay, D. J.; Larive, C. K., Heparin characterization: Challenges and solutions. *Annu. Rev. Anal. Chem.* **2011**, *4*, 439-465.

35. Ziegler, A.; Zaia, J., Size-exclusion chromatography of heparin oligosaccharides at high and low pressure. *J. Chromatogr. B* **2006,** *837*, 76-86.

36. Chuang, W. L.; McAllister, H.; Rabenstein, D. L., Chromatographic methods for product-profile analysis and isolation of oligosaccharides produced by heparinase-catalyzed depolymerization of heparin. *J. Chromatogr. A* **2001,** *932*, 65-74.

37. Limtiaco, J. F. K.; Beni, S.; Jones, C. J.; Langeslay, D. J.; Larive, C. K., The efficient structure elucidation of minor components in heparin digests using microcoil NMR. *Carbohyd. Res.* **2011,** *346*, 2244-2254.

38. Powell, A. K.; Ahmed, Y. A.; Yates, E. A.; Turnbull, J. E., Generating heparan sulfate saccharide libraries for glycomics applications. *Nat. Protoc.* **2010,** *5*, 821-833.

39. Chuang, W. L.; McAllister, H.; Rabenstein, D. L., Hexasaccharides from the histamine-modified depolymerization of porcine intestinal mucosal heparin. *Carbohyd. Res.* **2002,** *337*, 935-945.

40. Zaia, J.; Costello, C. E., Compositional analysis of glycosaminoglycans by electrospray mass spectrometry. *Anal. Chem.* **2001,** *73*, 233-239.

41. Staples, G. O.; Shi, X. F.; Zaia, J., Extended *N*-sulfated domains reside at the nonreducing end of heparan sulfate chains. *J. Biol. Chem.* **2010,** *285*, 18336-18343.

42. Schumacher, V. A.; Schlotzer-Schrehardt, U.; Karumanchi, S. A.; Shi, X. F.; Zaia, J.; Jeruschke, S.; Zhang, D. S.; Pavenstaedt, H.; Drenckhan, A.; Amann, K.; Ng, C.; Hartwig, S.; Ng, K. H.; Ho, J.; Kreidberg, J. A.; Taglienti, M.; Royer-Pokora, B.; Ai, X. B., WT1-dependent sulfatase expression maintains the normal glomerular filtration barrier. *J. Am. Soc. Nephrol.* **2011,** *22*, 1286-1296.

43. Shastri, M. D.; Johns, C.; Hutchinson, J. P.; Khandagale, M.; Patel, R. P., Ion exchange chromatographic separation and isolation of oligosaccharides of intact low-molecular-weight heparin for the determination of their anticoagulant and anti-inflammatory properties. *Anal. Bioanal. Chem.* **2013,** *405*, 6043-6052.

44. Eldridge, S. L.; Korir, A. K.; Gutierrez, S. M.; Campos, F.; Limtiaco, J. F. K.; Larive, C. K., Heterogeneity of depolymerized heparin SEC fractions: to pool or not to pool? *Carbohyd. Res.* **2008,** *343*, 2963-2970.

45. Jones, C. J.; Membreno, N.; Larive, C. K., Insights into the mechanism of separation of heparin and heparan sulfate disaccharides by reverse-phase ion-pair chromatography. *J. Chromatogr. A* **2010,** *1217*, 479-488.

46. Korir, A. K.; Limtiaco, J. F. K.; Gutierrez, S. M.; Larive, C. K., Ultraperformance ion-pair liquid chromatography coupled to electrospray time-of-flight mass spectrometry for compositional profiling and quantification of heparin and heparan sulfate. *Anal. Chem.* **2008,** *80*, 1297-1306.

47. Zhang, Z.; Xie, J.; Liu, H.; Liu, J.; Linhardt, R. J., Quantification of heparan sulfate disaccharides using ion-pairing reversed-phase microflow high-performance liquid chromatography with electrospray ionization trap mass spectrometry. *Anal. Chem.* **2009,** *81*, 4349-4355.

48. Henriksen, J.; Roepstorff, P.; Ringborg, L. H., Ion-pairing reversed-phased chromatography/mass spectrometry of heparin. *Carbohyd. Res.* **2006,** *341*, 382-387.

49. Kuberan, B.; Lech, M.; Zhang, L.; Wu, Z. L.; Beeler, D. L.; Rosenberg, R. D., Analysis of heparan sulfate oligosaccharides with ion pair-reverse phase capillary high performance liquid chromatography-microelectrospray ionization time-of-flight mass spectrometry. *J. Am. Chem. Soc.* **2002,** *124*, 8707-8718.

50. Langeslay, D. J.; Urso, E.; Gardini, C.; Naggi, A.; Torri, G.; Larive, C. K., Reversed-phase ion-pair ultra-high-performance-liquid chromatography-mass spectrometry for fingerprinting low-molecular-weight heparins. *J. Chromatogr. A* **2013,** *1292*, 201-210.

51. Thanawiroon, C.; Linhardt, R. J., Separation of a complex mixture of heparin-derived oligosaccharides using reversed-phase high-performance liquid chromatography. *J. Chromatogr. A* **2003,** *1014*, 215-223.

52. Thanawiroon, C.; Rice, K. G.; Toida, T.; Linhardt, R. J., Liquid chromatography/mass spectrometry sequencing approach for highly sulfated heparin-derived oligosaccharides. *J. Biol. Chem.* **2004,** *279*, 2608-2615.

53. Patel, R. P.; Narkowicz, C.; Jacobson, G. A., Effective reversed-phase ion pair high-performance liquid chromatography method for the separation and characterization of intact low-molecular-weight heparins. *Anal. Biochem.* **2009,** *387*, 113-121.

54. Leach Iii, F. E.; Xiao, Z.; Laremore, T. N.; Linhardt, R. J.; Amster, I. J., Electron detachment dissociation and infrared multiphoton dissociation of heparin tetrasaccharides. *Int. J. Mass Spectrom.* **2011,** *308*, 253-259.

55. Leach III, F. E.; Ly, M.; Laremore, T. N.; Wolff, J. J.; Perlow, J.; Linhardt, R. J.; Amster, I. J., Hexuronic acid stereochemistry determination in chondroitin sulfate glycosaminoglycan oligosaccharides by electron detachment dissociation. *J. Am. Soc. Mass Spectr.* **2012,** *23*, 1488-1497.

56. Ganisl, B.; Valovka, T.; Hartl, M.; Taucher, M.; Bister, K.; Breuker, K., Electron detachment dissociation for top-down mass spectrometry of acidic proteins. *Chem.-Eur. J.* **2011,** *17*, 4460-4469.

57. Oh, H. B.; Leach III, F. E.; Arungundram, S.; Al-Mafraji, K.; Venot, A.; Boons, G.-J.; Amster, I. J., Multivariate analysis of electron detachment dissociation and infrared multiphoton dissociation mass spectra of heparan sulfate tetrasaccharides differing only in hexuronic acid stereochemistry. *J. Am. Soc. Mass Spectr.* **2011,** *22*, 582-590.

58. Rabenstein, D. L.; Robert, J. M.; Peng, J., Multinuclear magnetic resonance studies of the interaction of inorganic cations with heparin. *Carbohyd. Res.* **1995,** *278*, 239-256.

59. Chevalier, F.; Angulo, J.; Lucas, R.; Nieto, P. M.; Martin-Lomas, M., The heparin-Ca^{2+} interaction: Structure of the Ca^{2+} binding site. *Eur. J. Org. Chem.* **2002,** 2002, 2367-2376.

60. McEwen, I., Broadening of ^{1}H NMR signals in the spectra of heparin and OSCS by paramagnetic transition metal ions. The use of EDTA to sharpen the signals. *J. Pharmaceut. Biomed.* **2010,** *51*, 733-735.

61. Mazak, K.; Beecher, C. N.; Kraszni, M.; Larive, C. K., The interaction of enoxaparin and fondaparinux with calcium. *Carbohyd. Res.* **2014,** *384*, 13-19.

62. Hoult, D. I., Solvent peak saturation with single phase and quadrature fourier transformation. *J. Magn. Reson.* **1976,** *21*, 337-347.

63. Ogg, R. J.; Kingsley, P. B.; Taylor, J. S., WET, a T1- and B1-insensitive water-suppression method for in vivo localized ^{1}H NMR spectroscopy. *J. Magn. Reson. Ser. B* **1994,** *104*, 1-10.

64. Smallcombe, S. H.; Patt, S. L.; Keifer, P. A., WET solvent suppression and its applications to LC NMR and high-resolution NMR spectroscopy. *J. Magn. Reson. Ser. A* **1995,** *117*, 295-303.

65. Piotto, M.; Saudek, V.; Sklenar, V., Gradient-tailored excitation for single-quantum NMR spectroscopy of aqueous solutions. *J. Biomol. NMR* **1992,** *2*, 661-665.

66. Hwang, T. L.; Shaka, A. J., Water suppression that works. Excitation sculpting using arbitrary waveforms and pulsed field gradients. *J. Magn. Reson. Ser. A* **1995,** *112*, 275-279.

67. Guerrini, M.; Naggi, A.; Guglieri, S.; Santarsiero, R.; Torri, G., Complex glycosaminoglycans: Profiling substitution patterns by two-dimensional nuclear magnetic resonance spectroscopy. *Anal. Biochem.* **2005,** *337*, 35-47.

68. Langeslay, D. J.; Beecher, C. N.; Dinges, M. M.; Larive, C. K., Glycosaminoglycan structural characterization. *eMagRes*, **2013,** *2*, 205-214.

69. Mascellani, G.; Guerrini, M.; Torri, G.; Liverani, L.; Spelta, F.; Bianchini, P., Characterization of di- and monosulfated, unsaturated heparin disaccharides with terminal *N*-sulfated 1,6-anhydro-β-D-glucosamine or *N*-sulfated 1,6-anhydro-β-D-mannosamine residues. *Carbohyd. Res.* **2007,** *342*, 835-842.

70. Guerrini, M.; Guglieri, S.; Naggi, A.; Sasisekharan, R.; Torri, G., Low molecular weight heparins: Structural differentiation by bidimensional nuclear magnetic resonance spectroscopy. *Semin. Thromb. Hemost.* **2007,** *33*, 478-487.

71. Ohnishi, M.; Urry, D. W., Temperature dependence of amide proton chemical shifts: The secondary structures of gramicidin S and valinomycin. *Biochem. Bioph. Res. Co.* **1969,** *36*, 194-202.

72. Englander, S. W.; Kallenbach, N. R., Hydrogen exchange and structural dynamics of proteins and nucleic acids. *Q. Rev. Biophys.* **1983,** *16*, 521-655.

73. Andersen, N. H.; Neidigh, J. W.; Harris, S. M.; Lee, G. M.; Liu, Z. H.; Tong, H., Extracting information from the temperature gradients of polypeptide NH chemical shifts. 1. The importance of conformational averaging. *J. Am. Chem. Soc.* **1997,** *119*, 8547-8561.

74. Blundell, C. D.; Deangelis, P. L.; Almond, A., Hyaluronan: the absence of amide-carboxylate hydrogen bonds and the chain conformation in aqueous solution are incompatible with stable secondary and tertiary structure models. *Biochem. J.* **2006,** *396*, 487-98.

75. Blundell, C. D.; Almond, A., Temperature dependencies of amide ^{1}H- and ^{15}N-chemical shifts in hyaluronan oligosaccharides. *Magn. Reson. Chem.* **2007,** *45*, 430-433.

76. Langeslay, D. J.; Beni, S.; Larive, C. K., Detection of the ^{1}H and ^{15}N NMR resonances of sulfamate groups in aqueous solution: A new tool for heparin and heparan sulfate characterization. *Anal. Chem.* **2011,** *83*, 8006-8010.

77. Adams, B.; Lerner, L., Observation of hydroxyl protons of sucrose in aqueous solution: No evidence for persistent intramolecular hydrogen bonds. *J. Am. Chem. Soc.* **1992,** *114*, 4827-4829.

78. Poppe, L.; Vanhalbeek, H., The rigidity of sucrose: Just an illusion? *J. Am. Chem. Soc.* **1992,** *114*, 1092-1094.

79. Sandstrom, C.; Baumann, H.; Kenne, L., NMR spectroscopy of hydroxy protons of 3,4-disubstituted methyl α-D-galactopyranosides in aqueous solution. *J. Chem. Soc. Perk. T. 2* **1998,** 809-815.

80. Sandstrom, C.; Kenne, L., Hydroxy protons in structural studies of carbohydrates by NMR spectroscopy. *ACS Sym. Ser.* **2006,** *930,* 114-132.

81. Vilen, E. M.; Lundqvist, L. C. E.; Jouanneau, D.; Helbert, W.; Sandstrom, C., NMR sudy on hydroxy protons of κ- and κ/μ-hybrid carrageenan oligosaccharides: Experimental evidence of hydrogen bonding and chemical exchange interactions in κ/μ oligosaccharides. *Biomacromolecules* **2010,** *11*, 3487-3494.

82. Bain, A. D., Chemical exchange in NMR. *Prog. Nucl. Mag. Res. Sp.* **2003,** *43*, 63-103.

83. Eyring, H., The activated complex in chemical reactions. *J. Chem. Phys.* **1935,** *3,* 107-115.

84. Pechukas, P., Transition state theory. *Annu. Rev. of Phys. Chem.* **1981,** *32*, 159-177.

85. Forsen, S.; Hoffman, R. A., Study of moderately rapid chemical exchange reactions by means of nuclear magnetic double resonance. *J. Chem. Phys.* **1963,** *39*, 2892-2901.

86. Perrin, C. L.; Johnston, E. R., Saturation-transfer study of the mechanism of proton exchange in amides. *J. Am. Chem. Soc.* **1979,** *101*, 4753-4754.

87. Perrin, C. L.; Johnston, E. R., Saturation-transfer studies of three-site exchange kinetics. *J. Magn. Reson.* **1979,** *33*, 619-626.

88. Perrin, C. L.; Dwyer, T. J.; Rebek, J.; Duff, R. J., Exchange of amide protons. Effect of intramolecular hydrogen bonding. *J. Am. Chem. Soc.* **1990,** *112,* 3122-3125.

89. Dobson, C. M.; Lian, L. Y.; Redfield, C.; Topping, K. D., Measurement of hydrogen exchange rates using 2D NMR spectroscopy. *J. Magn. Reson.* **1986,** *69*, 201-209.

CHAPTER TWO

Screening Enoxaparin Tetra- and Hexasaccharide SEC Fractions for 3-*O*-Sulfo-*N*-Sulfoglucosamine Residues using [^{1}H, ^{15}N] HSQC NMR

Acknowledgements: I would like to thank the following people for their contributions to this research: my undergraduate mentees, Sophia Nael, Jenny Mao, Matthew S. Manighalam and Adanma F. Nwachuku, who worked with me and performed the majority of the SAX-HPLC tetra- and hexasaccharide oligosaccharide isolations. I would also like to thank Szabolcs Beni, a visiting professor from Hungary, who helped me isolate and identify many of the hexasaccharides.

Abstract: Heparin and heparan sulfate (HS) are important in mediating a variety of biological processes through binding to a myriad of different proteins. Specific structural elements along the polysaccharide chains are essential for high affinity protein-binding, such as the 3-*O*-sulfated *N*-sulfoglucosamine (GlcNS3S) residue, a relatively rare modification essential for heparin's anticoagulant activity. The isolation of 3-*O*-sulfated oligosaccharides from complex mixtures of oligosaccharides is challenging because of their low abundance. Although methods such as affinity chromatography are useful in isolating oligosaccharides that bind specific proteins with high affinity, other important 3-*O*-sulfated oligosaccharides may easily be overlooked. Screening preparative scale size-exclusion chromatography (SEC) fractions of heparin or HS digests using [^{1}H,^{15}N] HSQC NMR allows the identification of fractions containing 3-*O*-sulfated

oligosaccharides through the unique ^{1}H and ^{15}N chemical shifts of the GlcNS3S residue. Those SEC fractions containing 3-*O*-sulfated oligosaccharides can then be isolated using strong anion exchange (SAX)-HPLC. Performing SAX-HPLC analysis of individual SEC fractions, rather than a pooled sample composed of all the SEC fractions of similarly sized oligosaccharides (e.g. tetra-, hexa-, or octasaccharides) produces a less complicated chromatogram in which the 3-*O*-sulfated oligosaccharides are enriched relative to more abundant components. The utility of this approach is demonstrated for tetrasaccharide SEC fractions of the low molecular weight heparin drug enoxaparin facilitating the isolation and characterization of an unsaturated 3-*O*-sulfated tetrasaccharide containing a portion of the antithrombin-III binding sequence.

2.1. Introduction

Heparin is best known for its anticoagulant activity resulting from the binding of a specific pentasaccharide sequence to the protease inhibitor antithrombin-III (AT-III). The entire pentasaccharide sequence comprises the minimum structure required for high-affinity binding, with each residue contributing to the binding energy.[1,2] Specific structural elements of this pentasaccharide, found in only one of every three heparin chains, are critical for high affinity binding to AT-III including the flexible IdoA2S residue, which exists in equilibrium between the chair and skew-boat conformations,[3] and the internal 3,6-*O*-sulfated *N*-sulfoglucosamine (GlcNS3S6S) residue. Loss of the 3-*O*-sulfate group decreases the affinity for AT-III by 1000-fold.[1] A synthetic pentasaccharide

mimetic is currently marketed as Arixtra (fondaparinux sodium), which is examined in greater detail in Chapter 3.

3-*O*-sulfation is also important in several other biological processes involving HS though it constitutes only 0.5% of the total sulfate content of an HS chain.[4,5] For example, expression of the 3-*O*-sulfotransferase (3-*O*ST) enzyme family, including isoforms 3-*O*ST-2[6,7], -3[7,8], -4[9,10], -5[11], and -6[12], facilitate the entry of HSV-1 into cells, a process which is mediated by the binding of HS to glycoprotein-D (gD).[4,7,13] Studies have also shown that fibroblast growth factor 2 (FGF-2) prevents the HSV-1 entry into cells, most likely through competitive binding with HS.[14] Liu et al. isolated and characterized the following gD-binding octasaccharide containing a 3-*O*-sulfated glucosamine residue at the reducing end: ΔUA-GlcNS-IdoA2S-GlcNAc-UA2S-GlcNS-IdoA2S-GlcNH$_2$3S6S.[15] Although structure is important for interaction with gD; not all 3-*O*-sulfated oligosaccharides will facilitate HSV-1 entry.[16,17] Copeland et al. demonstrated that the following octasaccharide, which contains an internal 3-*O*-sulfated GlcNS residue, actually inhibits HSV-1 infection: ΔUA2S-GlcNS6S-IdoA2S-GlcNS6S-IdoA2S-GlcNS3S6S-IdoA2S-GlcNS6S.[16] Though these oligosaccharides each contain a 3-*O*-sulfated glucosamine residue, neither contains the other structural elements important for high affinity binding to AT-III.

Characterization of intact heparin and HS chains remains a challenge because of their high degree of structural heterogeneity. Rapid progress is being made in mass spectrometry approaches for GAG sequencing, however de novo sequencing of unknowns from complex low molecular weight heparins (LMWH) or HS is still on the

horizon.[18-21] Although heteronuclear NMR experiments, such as [^{1}H, ^{13}C] and [^{1}H, ^{15}N] HSQC experiments can reveal important structural components in heparin, LMWH, HS and other GAGs,[22-27] depolymerization followed by chromatographic isolation is required for absolute structural characterization of specific oligosaccharides. Heparin and HS are first depolymerized either enzymatically or chemically to form a mixture of variously sized oligosaccharides. Enzymatic digestions can be accomplished using one or more heparinase enzymes,[28,29] which introduce an unsaturated double bond between C4 and C5 in the uronic acid residue at the non-reducing end of the newly formed oligosaccharide. This chromophore allows detection of the digestion components by UV absorbance measured at 232 nm.[30] Processes for chemical digestions include β-elimination,[31] reductive deamination,[32] and oxidative depolymerization,[33] with each producing a unique structure at the reducing end. For example, the LMWH enoxaparin, which is produced by a β-elimination reaction, is known to contain reducing end modifications containing mannosamine (ManN) and (1,6-anhydro)-mannosamine (ManN(1,6-anhydro)) and -glucosamine (GlcN(1,6-anydro)) residues.[24,31] The β-elimination reaction mimics the enzymatic digestion in the introduction of a C4-C5 double bond at the non-reducing end of each cleaved oligosaccharide.

For isolation of component oligosaccharides, a partial digestion is performed and the resulting mixture separated into similarly-sized fractions using size-exclusion chromatography (SEC). High-pressure liquid chromatography (HPLC)-SEC separations coupled to MS are commonly used to screen the composition of digested GAGs.[34-39] More recently, profiling of enoxaparin was accomplished by Shastri et al. using HPLC-

SEC, with the oligosaccharides collected and subsequently analyzed by ion chromatography (IC).[40] The advantage of using HPLC-SEC is the small amount of sample required and short analysis time, μg-mg quantities separated over a period of a few hours compared to low-pressure SEC separations in which mg-g quantities are separated over a period of several days. However, in this work preparative-scale low-pressure SEC was required for the isolation of individual heparin oligosaccharides in sufficient quantities for structural characterization by NMR.

In preparative-scale low pressure SEC, the common practice is to collect each size-uniform SEC peak over multiple fractions, which are typically pooled or combined for subsequent charge-based separation using strong anion-exchange high performance liquid chromatography (SAX-HPLC).[41-43] For structural studies, each SAX peak is collected and the structure of the component oligosaccharide(s) determined by MS and NMR.[43,44] Coelution, which is particularly problematic for isomeric oligosaccharides, can complicate the structure elucidation process.

Affinity chromatography provides alternative strategy for the isolation of a specific subset of oligosaccharides that bind tightly to a protein.[45] Affinity chromatography separations are highly specific and have the advantage of providing a direct link between the isolated compounds and their biological action. However, this approach requires significant quantities of protein and is ineffective for ligands with low to medium binding affinities.[46] Obviously, it is not possible to use affinity chromatograph to target a specific oligosaccharide structural motif unless a protein with high affinity for that structure is already known.

The goal of this chapter is to develop a streamlined method for the isolation of oligosaccharides containing 3-*O*-sulfated glucosamine residues by enhancing the specificity of SEC fractionation rather than relying on an affinity-based separation. It has been demonstrated that in the preparative-scale SEC separation of a heparin digest, the composition of the SEC fractions varies along the seemingly size-uniform peaks (e.g. tetrasaccharides, hexasaccharides, etc.).[47] The sulfate groups add bulkiness, causing highly sulfated oligosaccharides to elute earlier in the separation whereas *N*-acetyl groups, reducing-end modifications, and potentially even elements of secondary structure[48,49] can affect the elution time of the various components. Given the wide array of sulfation isomers present in a heparin digest or LMWH sample, the question then arises: is there a point along the SEC separation at which the relatively rare 3-*O*-sulfated oligosaccharides elute?

Our group has previously demonstrated the potential of [^{1}H,^{15}N] HSQC NMR spectra to report on the composition of heparin and HS samples through the characteristic chemical shifts of the sulfamate groups ($NHSO_3^-$).[48] In particular, the GlcNS NH resonances of a sulfamate group adjacent to a 3-*O*-sulfate group appear at a unique chemical shift of 91.0-92.0 ppm and around 5.6 ppm in the ^{15}N and ^{1}H dimensions, respectively. The GlcNS3S6S sulfamate proton participates in a hydrogen bond with the adjacent 3-*O*-sulfate group causing the NH resonance to be sharp and easily detected over a wide range of pH values, temperatures, and at low mass concentrations.[25,48] In this Chapter we explore the use of [^{1}H,^{15}N] HSQC NMR spectra to screen individual preparative SEC tetrasaccharide fractions for the presence of enoxaparin oligosaccharides

containing GlcNS3S residues, facilitating the SAX-HPLC resolution of low-abundance 3-*O*-sulfated oligosaccharides and allowing isolation of components that would be overlooked by AT-III affinity chromatography. We also explore the possibility of utilizing this approach for longer-chain oligosaccharides, which produce more complex mixtures due to the greater structural variability that accompanies increased size.

2.2 Materials and Methods

2.2.1 Materials and Reagents. Enoxaparin sodium was purchased from the U.S. Pharmacopeia (USP, Rockville, MD). The chemical shift reagent 2,2-dimethyl-2-silapentane-5-sulfonate-d_6 sodium salt (DSS), dibutylamine (DBA) (purity > 99%) and ammonium bicarbonate (NH_4HCO_3) were purchased from Sigma Aldrich (St. Louis, MO). HPLC grade water was obtained from Burdick and Jackson (Muskegon, MI). Deuterium oxide, (D, 99.9%), deuterated hydrochloric acid, and sodium deuteroxide were purchased from Cambridge Isotope Laboratories (Andover, MA). Acetonitrile (HPLC grade), methanol (HPLC grade), and glacial acetic acid (USP grade) were purchased from Fisher-Scientific (Pittsburgh, PA). The pH meter was calibrated with pH 4.00, 7.00 and 10.00 buffers also from Fisher Scientific Co.

2.2.2 Size-exclusion chromatography (SEC). The enoxaparin oligosaccharides (1.2 g in 6.5 mL HPLC-grade water) were separated by size using a 0.5 M NH_4HCO_3 buffer, pH 7.8, at a flow rate of 0.076 mL/min on a 3.0 x 200 cm column packed with Bio-Rad Bio-Gel P-10 fine resin (Bio-Rad Laboratories Hercules, CA). Eluting oligosaccharides were collected in separate 4.5 mL fractions. The separation was

monitored offline by UV at 232 nm using a Thermo Scientific NanoDrop 2000 spectrophotometer (Wilmington, DE). SEC fractions were lyophilized separately 5 times to remove the NH_4HCO_3 and stored at -20 ºC for future use.

2.2.3 Strong anion-exchange high-performance liquid chromatography (SAX-HPLC). Each SEC fraction was further separated by SAX-HPLC using a Dionex (Sunnyvale, CA) CarboPac PA1 semi-preparative scale column (9 x 250 mm) on a Dionex 500 ion chromatography system equipped with a GP40 gradient pump and AD20 UV-visible detector. The tetra- and hexasaccharide SEC fractions were individually dissolved (without pooling) in HPLC grade water and introduced onto the column in 500 μL injections. The tetra- and hexasaccharide fractions were separated using a 50 mM phosphate buffer, pH 7.0, as mobile phase A, and 2.0 M NaCl in 50 mM phosphate buffer, pH 7.0, as mobile phase B. The following gradient profile was utilized to separate tetrasaccharides: 0 min: 100% A, 0% B; 10 min: 65% A, 35% B; 85 min: 32% A, 68% B. The following gradient profile was utilized to separate hexasaccharides: 0 min: 100%, 0% B; 10 min: 55% A, 45% B; 75 min: 25% A, 75% B. Each run was followed by a washing step of 100% B for 10 min and re-equilibration with 100% A for 20 min. SAX tetrasaccharide peaks were collected separately over multiple consecutive injections.

To reduce the salt content of the SAX isolates, each of the collected tetra- and hexasaccharide peaks was diluted 3-fold with water and reinjected onto the column as mobile phase A. This allowed the individual oligosaccharides to be retained on the column while the NaCl collected over a series of sample injections was eluted as waste. Finally, the tetrasaccharide was eluted using the gradient described above and collected

as a more concentrated sample. Each sample was lyophilized and reconstituted in the minimum amount of HPLC-grade water for desalting on a column of 1.6 x 70 cm Sephadex G-10 (superfine) obtained from GE Healthcare (Pittsburgh, PA). HPLC grade water was used as the mobile phase at a flow rate of 0.15 mL/min with the eluent collected in 1.5 mL fractions.[43] The desalting procedure was monitored offline using a NanoDrop UV spectrophotometer. Those fractions containing the desalted tetrasaccharide were combined, lyophilized, and stored at -20 ºC for future use.

2.2.4 Mass spectrometry (MS) measurements. Reverse-phase ion-pairing ultra-performance liquid chromatography-mass spectrometry (RPIP-UPLC-MS) was used as a confirmation of oligosaccharide structure.[43,50-52] Analyses were performed using a Waters Acquity UPLC with Q-TOF MS detection in negative mode. Separations were performed at 40 ºC using a 2.1 x 100 mm Waters Acquity UPLC BEH C18 column and 2.1 x 5 mm guard column both containing 1.7 μm particles and 130 Å pore size. Oligosaccharides were eluted by gradient elution with mobile phase A composed of 90% H_2O/10% MeOH, and mobile phase B 100% MeOH; both mobile phases contained 10 mM dibutylamine (DBA) as the ion-pairing reagent and 10 mM acetic acid. A gradient starting at 30% B was increased to 55% B over 15 min with a 7 min re-equilibration period between injections.[25]

2.2.5 Nuclear magnetic resonance (NMR) measurements. NMR spectra were recorded using a Bruker Avance spectrometer operating at 599.69 MHz for ^{1}H. The oligosaccharides were dissolved in 10 mM pH 8.2 aqueous phosphate buffer containing 2 mM EDTA-d_{16}, and 1 mM DSS for sulfamate proton analyses. Measurements were

performed using a 1.7 mm capillary insert with a sample volume of 35 μL centered in a 3 mm NMR tube with a Teflon holder (New Era Enterprises, Sevierville, TN) using 100% D_2O in the 3 mm tube's annular volume to provide the spectrometer lock. [^{1}H, ^{15}N] HSQC spectra were acquired using States-TPPI at 20 ºC using the Bruker pulse sequence (hsqcetf3gpsi2).[53] The spectra were acquired into 4096 complex points in t2 with 272, 288, or 304 scans coadded at each of the 112 t_1 increments, depending on the available mass. A 2.0 s relaxation delay was used with a $^{1}J_{N-H}$ of 80 Hz and GARP ^{15}N decoupling applied during acquisition. The spectral window was 6887 Hz in F1 and 1216 Hz in F2. The data were zero-filled to 8192 x 512 data points and apodized using a $\cos^2$ function and linear prediction in F1. Spectra were referenced to DSS set at a ^{1}H chemical shift of 0.00 ppm.

Additional NMR experiments were performed for the structure elucidation of isolated tetrasaccharides. Chemical shift assignments were performed using TOCSY, COSY, and ROESY spectra for structure elucidation.[44,54-56] Spectra were measured for samples dissolved in 100% D_2O containing 10 mM phosphate buffer at pD 7.0, 2 mM EDTA-d_{16}, and 1 mM DSS using a 1.7 mm capillary insert as described above. Spectra were acquired with presaturation in States-TPPI using a spectral window of 2520 Hz in the F2 and 2520 Hz in the F1 dimensions. TOCSY spectra were recorded with 40, 64, or 80 scans coadded into 2048 complex points in t2 and 176, 192, or 208 t1 increments, depending on sample concentration. A relaxation delay of 2.0 s was used with a TOCSY mixing time of 120 ms. DQF COSY spectra were recorded with 64, 80, or 96 scans coadded into 2048 complex points in t2 and 188, 224, 274, or 288 t1 increments and a

relaxation delay of 2.0 s was used. ROESY spectra were recorded with 124 or 144 scans coadded into 2048 complex pints in t2 and 284 or 300 t1 increments. A relaxation delay of 1.5 s was used with a 350 ms ROESY spinlock. All spectra were zero filled to 4096 x 512 data points with DQF-COSY were apodized using a sine function in both dimensions. TOCSY and ROESY spectra were both apodized using a cosine squared function in both dimensions.

In the cases where ManNS, ManN(1,6-anhydro), and GlcN(1,6-anhydro) residues needed to be distinguished, [^{1}H, ^{13}C] HSQC spectra were obtained.[24] Spectra were acquired at 20 ºC using the Bruker pulse sequence hsqcedetgpsisp.2 with Echo-Antiecho phase cycling. Spectra were acquired into 2048 complex points in t2 with 256, 288, 304, or 320 scans and coadded at each of the 72, 112, or 128 t_1 increments, depending on available mass. A 2 s relaxation delay was used with a $^{1}J_{C\text{-}H}$ of 145 Hz and GARP ^{13}C decoupling applied during acquisition. The spectral window was 22621 Hz in F1 and 7184 Hz in F2. The data were zero-filled to 4096 x 512 data points and linear prediction in F1 prior to apodization with a cos^2 function. Spectra were referenced to DSS set at a ^{1}H chemical shift of 0.00 ppm.

2.3 Results and Discussion

2.3.1 SEC separation. The preparative-scale SEC separation resolved enoxaparin oligosaccharides ranging from the tetrasaccharide (dp4) to the sixteen-mer (dp16) (Figure 2.1). The last eluting peak was confirmed by MS analyses to be comprised of tetrasaccharides. A limitation of the SEC method used in this work is the time required

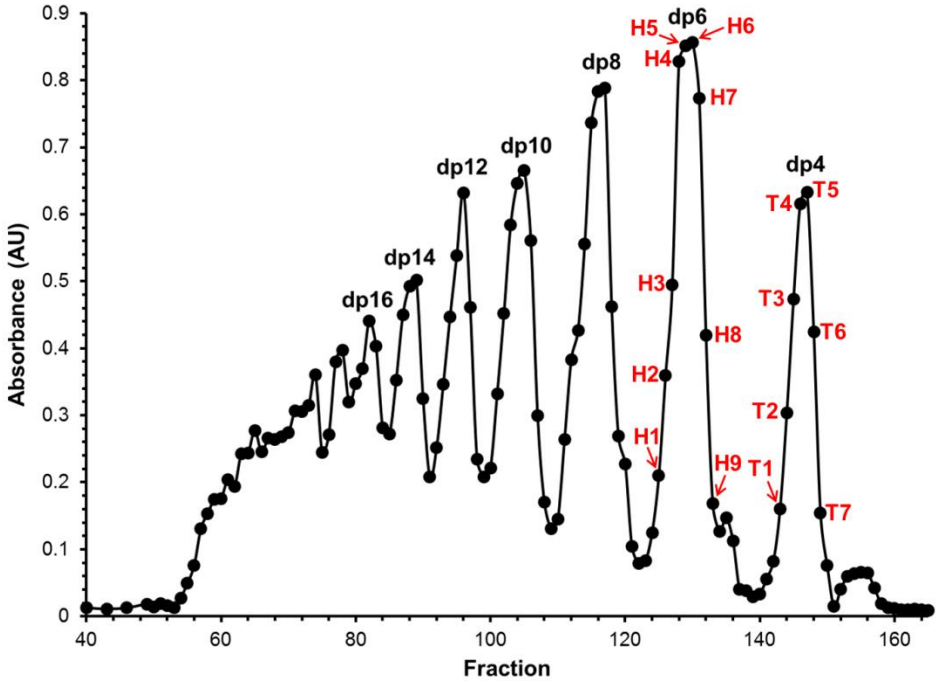

Figure 2.1. SEC chromatogram of Enoxaparin showing the depolymerization products (dp4: tetrasaccharides; dp6: hexasaccharides; etc.). Each point represents a different 4.5 mL SEC fraction. Tetrasaccharide SEC fractions are numbered T1 through T7. Hexasaccharide SEC fractions are numbered H1 through H7.

for separation. There are methods that utilize high-performance size-exclusion chromatography (HP-SEC) that are much faster, with a separation time, for example, of 85 min reported by Shastri et al. compared to 8 days using the method used in this work.[40] Despite the long separation time, we found the methods described in this work to be efficient for the purposes of isolation of individual heparin oligosaccharides in the quantities desired for structure elucidation and potential future experiments to explore their interactions with proteins. In Figure 2.1, each point in the tetrasaccharide SEC fraction is labeled T1 through T7 and each point in the hexasaccharide SEC fraction is labeled H1 through H9. The bottom-up approach employed for the fractionation and characterization of heparin oligosaccharides typically involves pooling the SEC fractions of similar size (i.e. combining all the tetrasaccharide peaks T1-T7) followed by a charge-based separation by SAX-HPLC.[42,43,55,57]

2.3.2 SAX-HPLC separation of the pooled tetrasaccharide SEC fraction. The individual fractions of the SEC tetrasaccharide peak were pooled and subsequently separated by SAX-HPLC (Figure 2.2). Individual peaks were collected separately over multiple injections and their composition analyzed by MS and NMR. The main peaks are numbered Tp1 through Tp11 (Tp stands for tetrasaccharide peak). Tp5 was discovered to have co-eluting peaks (Tp5A and Tp5), as described in more detail below. The remaining unlabeled peaks were either too dilute or insufficiently pure for structural elucidation.

The mass-to-charge ratios (m/z) of the isolated tetrasaccharides were obtained by UPLC-MS and are summarized as the doubly charged ions in Table 2.1. Tp1-Tp4 and Tp7 were each found to have an m/z of 536 Da for the doubly charged molecular ion,

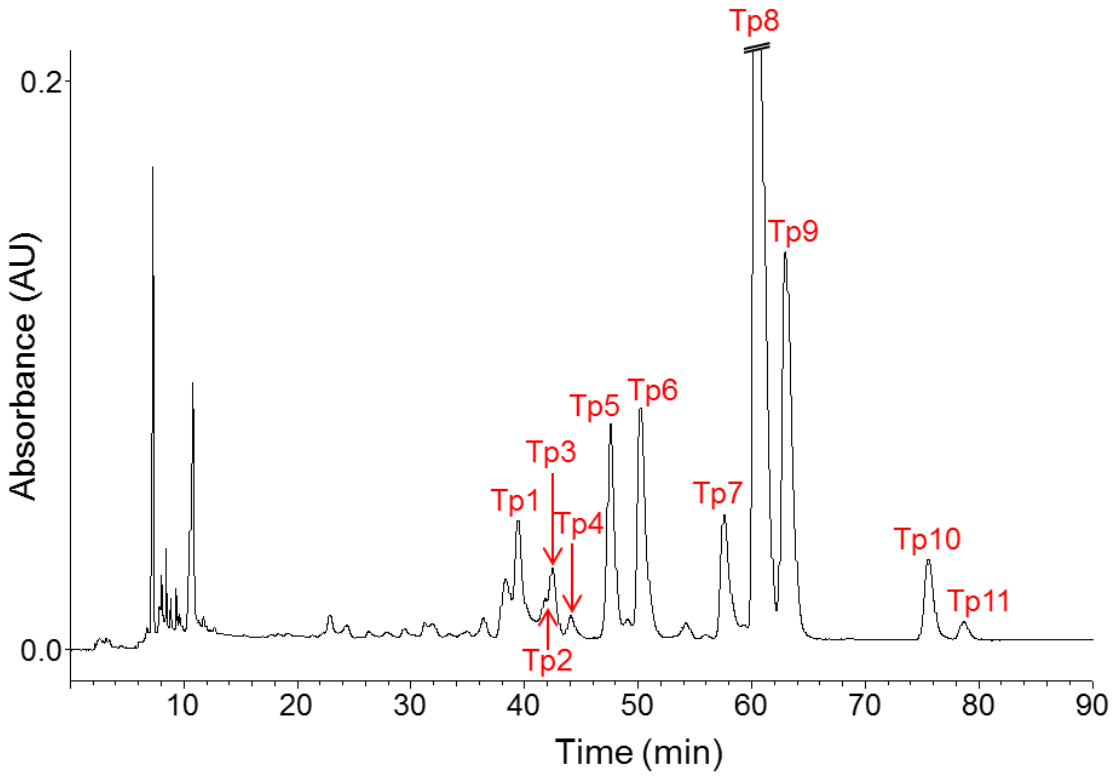

Figure 2.2. SAX-HPLC separation of the pooled tetrasaccharide (dp4) SEC fractions. The main peaks which were characterized are numbered Tp1 through Tp11 (Tp stands for tetrasaccharide peak).

Table 2.1. The identification of selected peaks in the dp4 SAX-HPLC chromatogram with the corresponding m/z for the doubly charged molecular ion.

SAX Peak	Tetrasaccharide ID	Molecular Ion (m/z)
Tp1	ΔUA2S-GlcNS6S-IdoA2S-GlcNS	535.75
Tp2	ΔUA2S-GlcNS6S-IdoA2S-ManNS	535.62
Tp3	ΔUA2S-GlcNS-IdoA2S-GlcNS6S	535.75
Tp4	ΔUA2S-GlcNS-IdoA2S-ManNS6S	535.67
Tp5	ΔUA2S-GlcNS6S-IdoA2S-GlcNS(1,6-anhydro)	526.63
Tp6	ΔUA2S-GlcNS6S-IdoA2S-ManNS(1,6-anhydro)	527.52
Tp7	ΔUA2S-GlcNS6S-GlcA-GlcNS6S	535.60
Tp8	ΔUA2S-GlcNS6S-IdoA2S-GlcNS6S	575.52
Tp9	ΔUA2S-GlcNS6S-IdoA2S-ManNS6S	575.47
Tp10	ΔUA2S-GlcNS6S-GlcA2S-GlcNS6S	575.53
Tp11	ΔUA2S-GlcNS6S-GlcA2S-ManNS6S	575.55

indicating that these tetrasaccharides each contain five sulfate groups. Two components were separated in Tp5, labeled peaks Tp5A and the original Tp5. The more abundant Tp5 had an m/z of 527 Da, indicating five sulfate groups and a loss of water. The less abundant Tp5 had an m/z of 585 Da, corresponding to six sulfate groups and addition of one molecule of water, suggesting that this oligosaccharide lacks a C4-C5 double bond at the non-reducing end. Tp6, like Tp5, had an m/z of 527 Da, also indicating five sulfate groups with a loss of water. The water loss in both Tp5 and Tp6 suggests the modification of the reducing end of the oligosaccharide chain to a GlcN(1,6-anhydro) and/or ManN(1,6-anhydro) residue, known products in the digestion process of enoxaparin.[24] Tp8- Tp11 had an m/z of 576 Da, indicating that these structures contain six sulfate groups.

Utilizing the information provided by MS, homo- and heteronuclear NMR experiments were used to determine the absolute structure of each tetrasaccharide Tp1-Tp11 isolated from the SAX-HPLC separation. The tetrasaccharide structures listed in Table 2.1 were elucidated with certainty using TOCSY, COSY and ROESY spectra. Proton chemical shifts of all tetrasaccharides are summarized in Table 2.2. For those oligosaccharides isolated in sufficient quantities, both [^{1}H, ^{13}C] and [^{1}H, ^{15}N] HSQC experiments were utilized to distinguish between the glucosamine and mannosamine residues.[25,26] Otherwise, only the more sensitive [^{1}H, ^{13}C] HSQC was used. Carbon-13 chemical shifts of selected tetrasaccharides are provided in Table 2.3, and nitrogen-15 chemical shifts of selected tetrasaccharides are provided in Table 2.4. In the SAX-HPLC separation, the more highly sulfated tetrasaccharides are more highly retained, with the

Table 2.2. ^{1}H chemical shift assignments for the main peaks in the SAX-HPLC chromatogram of the pooled Enoxaparin tetrasaccharide SEC fraction.

SAX Peak	Proton	NMR Chemical Shifts (ppm)			
Tp1		**ΔUA2S-**	**-GlcNS6S-**	**-IdoA2S-**	**-GlcNS**
	1	5.497	5.338	5.218	5.435
	2	4.62	3.29	4.30	3.23
	3	4.31	3.65	4.23	3.69
	4	5.982	3.83	4.06	3.70
	5		4.01	4.80	3.86
	6		4.24		3.92
	6’		4.34		
Tp2		**ΔUA2S-**	**-GlcNS6S-**	**-IdoA2S-**	**-ManNS**
	1	5.497	5.341	5.170	5.396
	2	4.62	3.29	4.29	3.59
	3	4.31	3.65	4.22	4.06
	4	5.982	3.82	4.06	3.67
	5		4.01	4.82	3.89
	6		4.24		3.86
	6’		4.35		
Tp3		**ΔUA2S-**	**-GlcNS-**	**-IdoA2S-**	**-GlcNS6S**
	1	5.520	5.409	5.213	5.435
	2	4.597	3.27	4.31	3.25
	3	4.23	3.61	4.20	3.69
	4	6.005	3.77	4.08	3.74
	5		3.78	4.76	4.12
	6		3.81		4.29
	6’		3.86		4.36
Tp4		**ΔUA2S-**	**-GlcNS-**	**-IdoA2S-**	**-ManNS6S**
	1	5.520	5.397	5.173	5.382
	2	4.60	3.27	4.31	3.59
	3	4.24	3.63	4.20	4.07
	4	6.007	3.78	4.09	3.69
	5		3.75	4.76	4.08
	6		3.81		4.25
	6’		3.86		4.34

Tp5		**ΔUA2S-**	**-GlcNS6S-**	**-IdoA2S-**	**-GlcNS(1,6-an)**
	1	5.50	5.35	5.34	5.602
	2	4.62	3.29	4.35	3.206
	3	4.31	3.66	4.25	3.90
	4	5.985	3.83	4.10	3.81
	5		4.01	4.630	4.08
	6		4.34		3.79
	6’		4.24		4.20
Tp6		**ΔUA2S-**	**-GlcNS6S-**	**-IdoA2S-**	**-ManNS(1,6-an)**
	1	5.499	5.36	5.35	5.558
	2	4.63	3.295	4.33	3.463
	3	4.31	3.657	4.24	4.04
	4	5.985	3.83	4.08	3.97
	5		4.01	4.550	4.81
	6		4.25		3.77
	6’		4.35		4.22
Tp7		**ΔUA2S-**	**-GlcNS6S-**	**-GlcA-**	**-GlcNS6S**
	1	5.497	5.559	4.593	5.451
	2	4.62	3.30	3.38	3.27
	3	4.32	3.64	3.85	3.72
	4	5.987	3.83	3.78	3.71
	5		3.98	3.82	4.14
	6		4.20		4.32
	6’		4.34		4.35
Tp8		**ΔUA2S-**	**-GlcNS6S-**	**-IdoA2S-**	**-GlcNS6S**
	1	5.497	5.414	5.209	5.43
	2	4.617	3.292	4.31	3.251
	3	4.31	3.64	4.20	3.69
	4	5.981	3.83	4.10	3.74
	5		4.03	4.75	4.12
	6		4.25		4.30
	6’		4.35		4.36
Tp9		**ΔUA2S-**	**-GlcNS6S-**	**-IdoA2S-**	**-ManNS6S**
	1	5.496	5.392	5.178	5.381
	2	4.62	3.30	4.31	3.60
	3	4.31	3.64	4.20	4.07
	4	5.991	3.83	4.09	3.70
	5		4.03	4.78	4.08
	6		4.25		4.30
	6’		4.35		4.36

Tp10		**ΔUA2S-**	**-GlcNS6S-**	**-GlcA2S-**	**-GlcNS6S**
	1	5.494	5.572	4.75	5.442
	2	4.614	3.28	4.14	3.26
	3	4.318	3.64	3.96	3.75
	4	5.988	3.83	3.83	3.74
	5		3.98	3.84	4.11
	6		4.21		4.19
	6’		4.35		4.58
Tp11		**ΔUA2S-**	**-GlcNS6S-**	**-GlcA2S-**	**-ManNS6S**
	1	5.494	5.571	4.73	5.451
	2	4.61	3.28	4.14	3.65
	3	4.31	3.64	3.96	4.11
	4	5.984	3.83	3.83	3.74
	5		3.99	3.84	4.06
	6		4.21		4.20
	6’		4.34		4.58

Table 2.3. ^{13}C chemical shift assignments for select enoxaparin tetrasaccharides which contain a ManNS or (1,6-anhydro) residue at the non-reducing end.

SAX Peak	Carbon	NMR Chemical Shifts (ppm)			
Tp5B		**ΔUA2S-**	**-GlcNS6S-**	**-IdoA2S-**	**-GlcNS(1,6-an)**
	1	100.1	100.2	100.2	104.0
	2	77.3	60.5	77.9	58.3
	3	65.7	72.2	70.7	72.8
	4	108.8	81.0	78.8	78.8
	5		71.6	71.0	--
	6		69.0		68.1
Tp6		**ΔUA2S-**	**-GlcNS6S-**	**-IdoA2S-**	**-ManNS(1,6-an)**
	1	100.0	99.9	101.3	103.7
	2	77.2	60.5	78.2	54.9
	3	65.7	72.2	70.9	70.9
	4	108.8	80.8	78.8	80.4
	5		71.6	71.0	76.3
	6		68.9		67.5
Tp9		**ΔUA2S-**	**-GlcNS6S-**	**-IdoA2S-**	**-ManNS6S**
	1	100.2	99.5	102.2	95.7
	2	77.3	60.3	78.4	60.2
	3	65.7	72.2	71.5	70.0
	4	108.9	80.9	78.9	77.4
	5		71.6	71.9	71.9
	6		70.0		69.8

Table 2.4. ^{15}N chemical shifts for sulfamate protons of selected enoxaparin tetrasaccharides containing a GlcN(1,6-anhydro) and/or ManN(1,6-anydro) at the reducing end.

SAX Peak	**^{15}N NMR Chemical Shifts of sulfamate protons (ppm)**			
Tp5	**ΔUA2S-** --	**-GlcNS6S-** 92.8	**-IdoA2S-** --	**-GlcNS(1,6-an)** 96.1
Tp6	**ΔUA2S-** --	**-GlcNS6S-** 92.8	**-IdoA2S-** --	**-ManNS(1,6-an)** 95.8

isomeric GlcA-containing tetrasaccharides eluting later than their IdoA-containing analogs. For example, the retention of times of Tp10 and Tp11 are longer than their IdoA-isomers, tetrasaccharides Tp8 and Tp9, respectively. A similar trend was observed in the GlcN and ManN tetrasaccharide isomers, with the ManN-containing tetrasaccharides eluting after their GlcN-containing analogs. For example, peaks Tp2, Tp4, Tp6, Tp9, and Tp11 all had longer retention times than their GlcNS isomers, peaks Tp1, Tp3, Tp5, Tp8, and Tp10, respectively.

Although the composition of the enoxaparin tetrasaccharides has been previously reported,[58] the methods utilized in this work provide a different profile of isolated tetrasaccharides. Ozug et al. used a variety of analytical methods, such as CE, HPLC, NMR, and mass spectrometry, to successfully characterize 15 different tetrasaccharides. The SAX separation of this group differs from ours in that they report elution of the ManNS(1,6-anhydro) tetrasaccharide before the GlcNS(1,6-anhydro) tetrasaccharide. This group also reports SAX separation of α- and β-anomers, which we do not observe. Although Ozug et al. mentions that a 3-*O*-sulfated tetrasaccharide was detected, it was not further explored because saturation at the non-reducing end made it difficult to detect by UV. Consequently, the SAX retention time was not reported and its structure was not fully characterized due to its low abundance.[58] None of the tetrasaccharides isolated and characterized in the present section contain a 3-*O*-sulfated glucosamine residue, prompting experiments described below to isolate and characterize the 3-*O*-sulfated tetrasaccharide.

2.3.3 NMR [^{1}H, ^{15}N] HSQC spectra of the tetrasaccharide SAX fraction Tp5.

Two cross peaks were observed in the [^{1}H, ^{15}N] HSQC spectra of the majority of isolated tetrasaccharides, one belonging to the internal and the other to the reducing end GlcNS sulfamate protons. The only spectrum which showed more than two cross peaks was that of SAX peak Tp5, which contained three cross peaks (Figure 2.3). Two of these cross peaks were identified as belonging to the more abundant component ΔUA2S-GlcNS6S-IdoA2S-GlcNS(1,6-anhydro). Based on previous assignments, [24,25] the cross peak at 5.21 ppm in ^{1}H and 92.8 ppm in ^{15}N was assigned to the internal GlcNS6S residue and that at 5.39 ppm in ^{1}H and 96.1 ppm in ^{15}N was assigned to the reducing end GlcNS(1,6-anhydro). We were excited to discover that the third cross peak at 5.54 ppm in ^{1}H and 92.1 ppm in ^{15}N is characteristic of a GlcNS sulfamate proton adjacent to a 3-*O*-sulfate group.[25] The sulfamate proton on the reducing end GlcNS residue is not observable in this spectrum most likely due to the low abundance of the tetrasaccharide and broadening due to fast exchange with the solvent water. The internal sulfamate proton in this tetrasaccharide is most likely in a hydrogen bond with its adjacent 3-*O*-sulfate group, causing it to be sharper and more easily observed by NMR. Langeslay et al. showed that in the synthetic AT-III-binding pentasaccharide, fondaparinux sodium (trade name Arixtra), the sulfamate proton is in a hydrogen bond to the adjacent 3-*O*-sulfate group which reduces the rate of exchange with water and allows it to be detected over a wide range of temperatures and pHs.[51] This discovery suggested we had found the 3-*O*-sulfated tetrasaccharide that was previously reported in the enoxaparin tetrasaccharide SEC fraction.[58] Its absolute structure could not be determined, however, without further

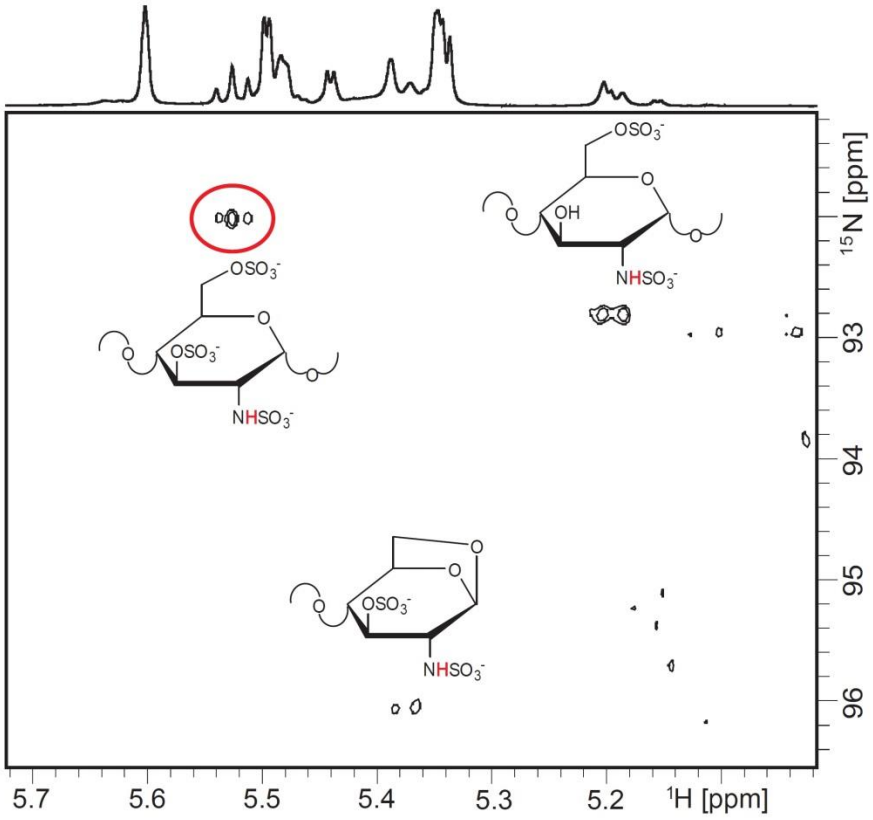

Figure 2.3. [^{1}H, ^{15}N] HSQC NMR spectrum of Tp5. The two cross peaks located at 5.21 and 5.39 ppm in ^{1}H and 92.8 and 96.1 ppm in ^{15}N, respectively, can be identified as belonging to the 1,6-anhydro tetrasaccharide. The third cross peak (circled in red) located at 5.52 ppm in ^{1}H and 92.1 ppm in ^{15}N is characteristic of a GlcNS sulfamate proton that is adjacent to a 3-*O*-sulfate group.

separation from the more abundant (1,6-anhydro) tetrasaccharide because of overlap in the NMR spectra and the low abundance of the 3-*O*-sulfated tetrasaccharide.

2.3.4 Screening of individual tetrasaccharide SEC fractions by [^{1}H, ^{15}N] HSQC NMR. We were encouraged that we could detect the [^{1}H,^{15}N] signature of a 3-*O*-sulfated tetrasaccharide as a minor component of SAX peak Tp5 and sought a strategy that would allow us to isolate and characterize the tetrasaccharide containing a 3-*O*-sulfated glucosamine residue. Because we were not able to improve the SAX separation to resolve these co-eluting components, we decided to reconsider our treatment of the SEC tetrasaccharide fractions prior to SAX-HPLC. Although the individual SEC peaks contain oligosaccharides with the same number of monosaccharide building blocks, their composition is not necessarily uniform across the peak. For example, the higher sulfated tetra- and hexasaccharides are more likely to elute earlier along the SEC separation because their bulky sulfate groups make their effective radius larger.[47] If a 3-*O*-sulfated tetrasaccharide elutes predominantly over one or two SEC fractions, then the practice of pooling all the SEC fractions effectively dilutes it with respect to the more abundant but less interesting compounds. The question remains: where along the SEC fraction do the 3-O-sulfated oligosaccharides elute?

The individual SEC fractions (Figure 2.1) were screened by [^{1}H, ^{15}N] HSQC NMR to identify the fractions containing 3-*O*-sulfated glucosamine residues. Highlighting the differences in composition across the SEC tetrasaccharide peak, the ^{1}H NMR spectra of each SEC fraction T2–T7 (Figure 2.4) show subtle differences reflecting differences in their composition. We hypothesized that recording [^{1}H, ^{15}N] HSQC spectra

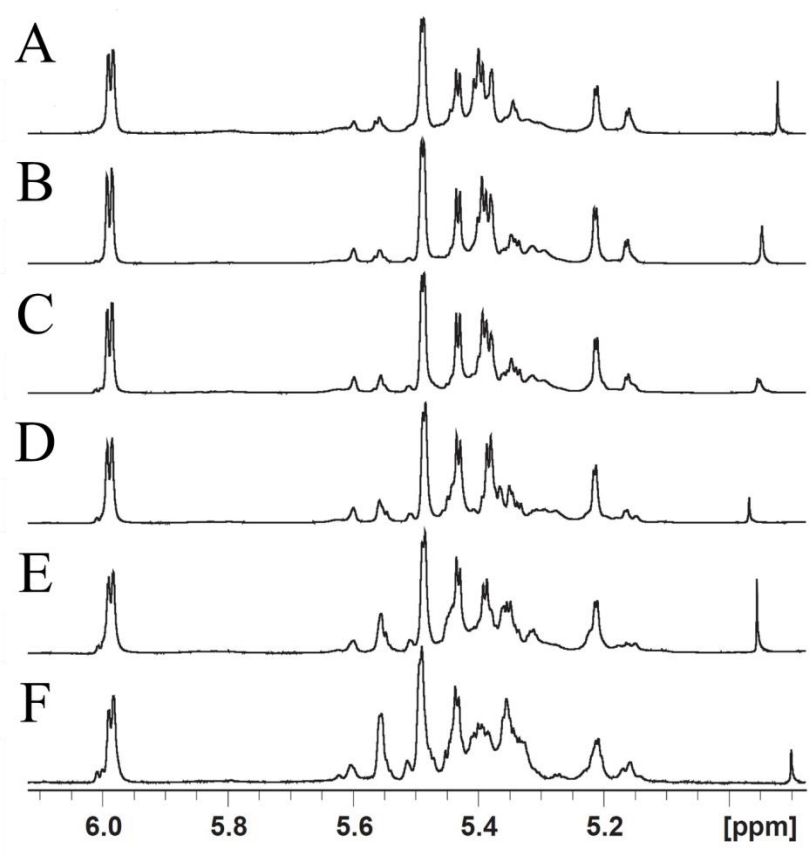

Figure 2.4. ^{1}H NMR spectra of tetrasaccharide SEC fractions: (A) T2; (B) T3; (C) T4; (D) T5; (E) T6; and (F) T7. Slight differences can be observed between the NMR spectra of different SEC fractions, suggesting compositional differences along the SEC peak.

for each SEC fraction would allow us to identify those SEC fractions containing 3-*O*-sulfated oligosaccharides. Armed with this information, we could focus our efforts on SAX-HPLC separations of the individual SEC fractions that we knew contained 3-*O*-sulfated structures of interest. We also hypothesized that the resulting SAX chromatograms would be less complex than that obtained for the pooled SEC fractions (Figure 2.2) and more easily allow identification and isolation of less abundant, yet more important, oligosaccharides.

The [^{1}H,^{15}N] HSQC spectra obtained for each SEC tetrasaccharide fraction are presented in Figure 2.5. The mass of SEC fraction T1 was too low to observe any [^{1}H, ^{15}N] HSQC correlations, which is not surprising given its lower UV absorbance (Figure 2.1). Sulfamate NH correlations are detected for SEC fraction T2 (Figure 2.5A) at 5.33 ppm (^{1}H) and 92.9 ppm ^{15}N, consistent with an internal GlcNS6S residue, the predominant glucosamine structure in enoxaparin. Correlations characteristic of oligosaccharides containing a 1,6-anhydro modification begin to appear in SEC fraction T3 (Figure 2.5B) at 5.43 and 94.0 ppm and are visible through fraction T7 (Figure 2.5E). A peak characteristic of a 3-*O*-sulfate group at 5.52 and 92.3 ppm (Figure 2.5C) is first detected in fraction T4 at the apex of the SEC peak. The intensity of this correlation increases over SEC fractions T5 and T6 (Figures 2.5D and 2.5E, respectively) and it becomes the only observable NH correlation in fraction T7 (Figure 2.5F). Our initial hypothesis was that the 3-*O*-sulfate groups would add bulkiness to the tetrasaccharides, causing them to elute at the leading edge of the SEC peak. Interestingly, the results of the spectra in Figure 2.5 reflect the opposite trend, with the 3-*O*-sulfated tetrasaccharides

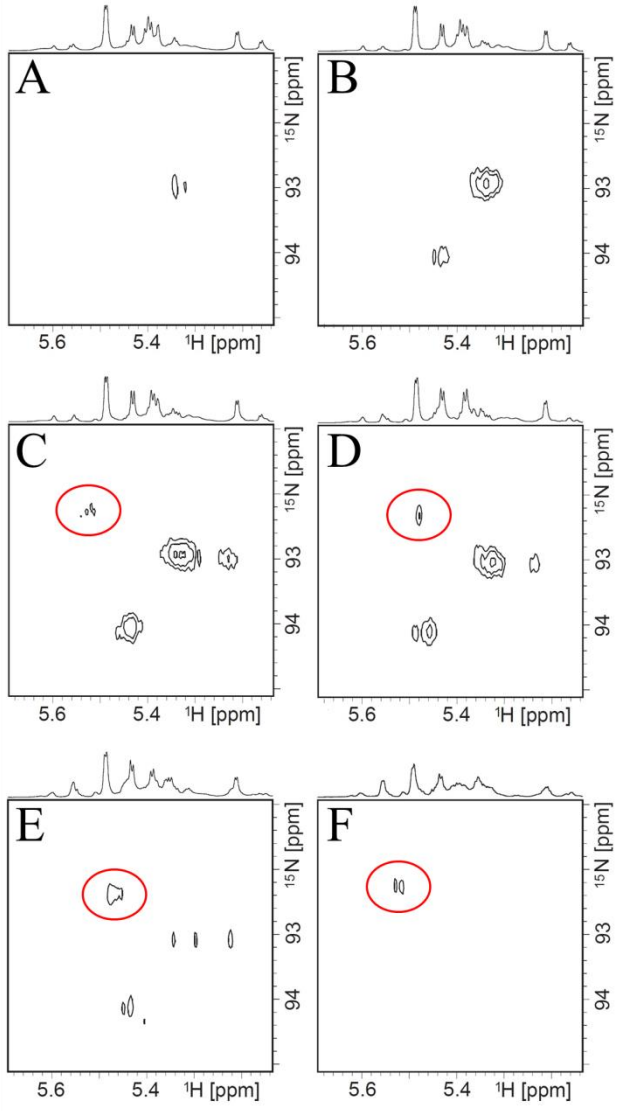

Figure 2.5. [^{1}H, ^{15}N] HSQCs of Enoxaparin sulfamate protons in SEC fractions (A) T2; (B) T3; (C) T4; (D) T5; (E) T6; and (F) T7. The sulfamate protons were not observable in the less abundant T1 fraction. The cross peak characteristic of the presence of a 3-*O*-sulfate group (circled in red) at 5.52 ppm in ^{1}H and 92.3ppm in ^{15}N starts to grow in SEC fraction T4 (C) and continues to increase in intensity. It becomes the only observable peak in SEC fraction T7 (F).

most prevalent along the trailing edge of the SEC peak. One reason for the later elution of 3-*O*-sulfated tetrasaccharides is that the 3-*O*-sulfo modification often follows a GlcA residue (as in Arixtra) and as noted in Table 2.1, GlcA containing tetrasaccharides tend to elute later than their IdoA analogs. In addition, the involvement of the GlcNS3S6S sulfamate proton in a hydrogen bond to the adjacent 3-*O*-sulfate group may make the oligosaccharide more compact contributing to its greater retention on the SEC column.[48]

2.3.5 Separation of individual SEC tetrasaccharide fractions by SAX-HPLC. SEC fractions Tp4-7 were each subjected to SAX-HPLC with the goal of isolating a 3-*O*-sulfated tetrasaccharide. Fractions Tp5-7 gave rise to an [^{1}H,^{15}N] HSQC correlation at the chemical shifts expected for a GlcNS3S residue and Tp4 was included for comparison. Only those peaks eluting between 38–85 min are shown in Figure 2.6. The less retained peaks eluting before 38 min are too dilute for structural analyses and are not shown. As expected, in the earlier eluting SEC fractions (Figures 2.6A and B) the peaks of the more highly sulfated oligosaccharides are more intense than the less sulfated oligosaccharides, which are more abundant in the later eluting SEC fractions (Figures 2.6C and D). Tp5 from in the pooled SAX-HPLC separation (Figure 2.2), suggested by our [^{1}H,^{15}N] HSQC results to contain co-eluting tetrasaccharides, decreases in intensity over SEC fractions T4-T7. In the SAX-HPLC chromatogram of SEC fraction T7 (Figure 2.6A), the two overlapping peaks are present in comparable amounts, improving their resolution as peaks Tp5A and Tp5 and allowing for their isolation as two individual samples for subsequent characterization by NMR spectroscopy.

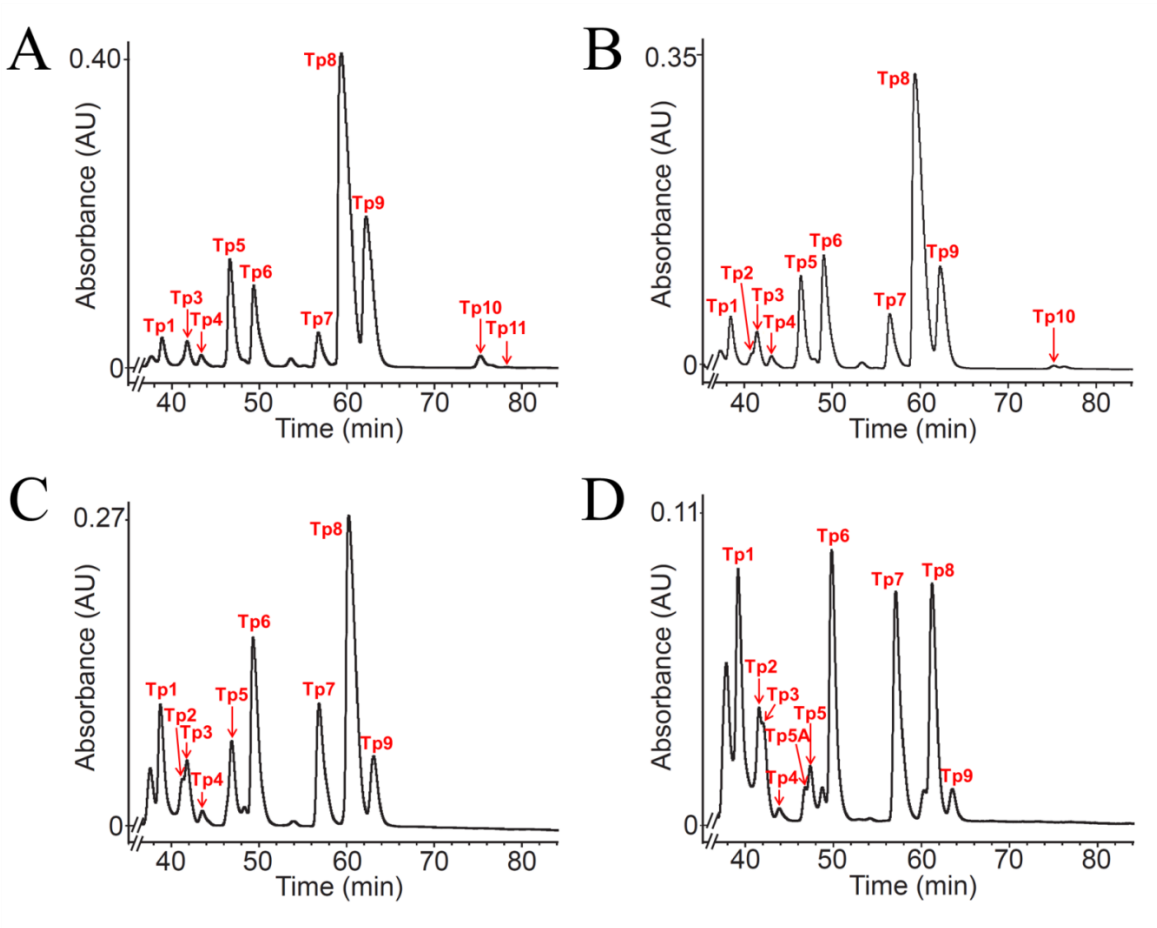

Figure 2.6. The SAX-HPLC separations of those SEC fractions which showed evidence of a 3-*O*-sulfate group in their [^{1}H, ^{15}N] HSQCs: (A) T4; (B) T5; (C) T6; (D) T7. The major peaks of the pooled. Tp5, which contained the 3-*O*-sulfated tetrasaccharide in the pooled SAX separation, decreases in intensity and eventually splits into two peaks in T7 (Tp5A and Tp5 in D).

The complexity of the spectrum of the isolated SAX peak Tp5 for the pooled tetrasaccahride fraction (Figure 2.7A) clearly indicates the presence of more than one component. Although the spectrum of the SAX peak Tp5 isolated from SEC fraction T6 (Figure 2.7B) looks similar to that of the pooled SAX peak Tp5 (Figure 2.7A), the resonances of the minor component appear enriched compared with the major component of Tp5 (ΔUA2S-GlcNS6S-IdoA2S-GlcNS(1,6-an)). For SEC fraction T7, the improved resolution of the SAX chromatogram allowed isolation of two peaks, Tp5A and Tp5, which had the structure listed in Table 2.1. Although only a small quantity of material was isolated from Tp5A, its ^{1}H spectrum (Figure 2.7C) indicated that it was fairly pure compared to the SAX peak isolated from SEC fraction T6 (Figure 2.7C). The m/z of the doubly charged tetrasaccharide (584) of peak Tp5A indicated that the isolated tetrasaccharide contains six sulfate groups and is saturated at the non-reducing end. The structure of the tetrasaccharide (Figure 2.8A) was elucidated using DQF-COSY (Figure 2.8B), TOCSY (Figure 2.8C) and ROESY (Figure 2.8D) NMR spectra. Table 2.5 shows the structure of the compound isolated as peak Tp5A: GlcA-GlcNS3S6S-IdoA2S-GlcNS6S, its mass spectral and NMR chemical shift data. The tetrasaccharide contains a GlcA at the non-reducing end without a C4-C5 double bond, and an internal 3-*O*-sulfated GlcNS residue consistent the MS data. This tetrasaccharide likely originates from the non-reducing end of an intact heparin chain. It is also interesting to note that this tetrasaccharide is part of the AT-III-binding pentasaccharide. The 6-*O*-sulfated *N*-acetylglucosamine (GlcNAc6S) residue at the non-reducing end of the AT-III-binding pentasaccharide is not present in this tetrasaccharide. Because this GlcNAc6S residue is

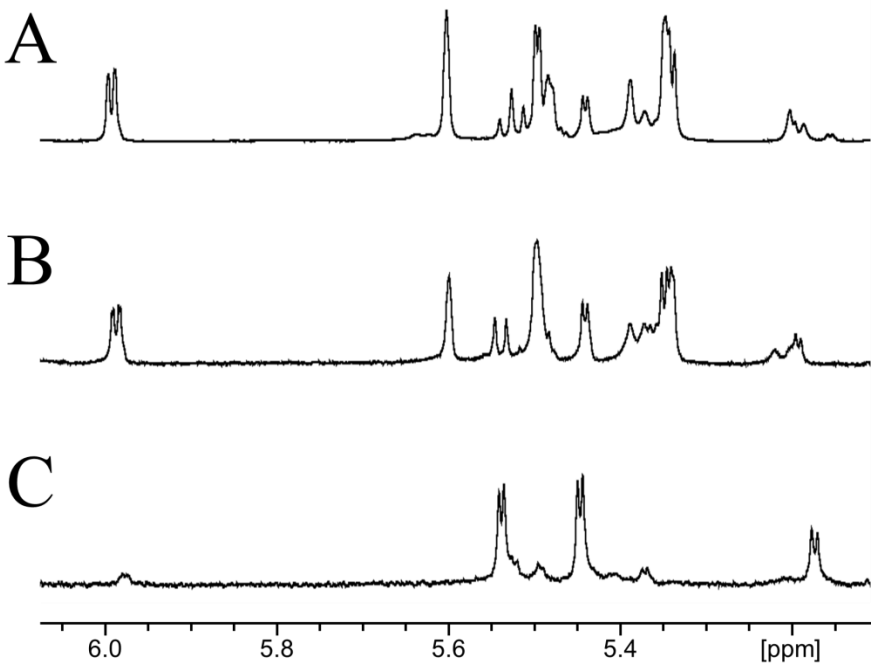

Figure 2.7. (A) The anomeric region of Tp5 from the pooled enoxaparin tetrasaccharide fraction. (B) The anomeric region of Tp5 in SEC fraction T6. The spectrum looks similar to that of the pooled Tp5 tetrasaccharide fraction, indicating there is still a mixture of different tetrasaccharides. (C) The anomeric region of the 3-*O*-sulfated tetrasaccharide, isolated in a small but fairly pure quantity.

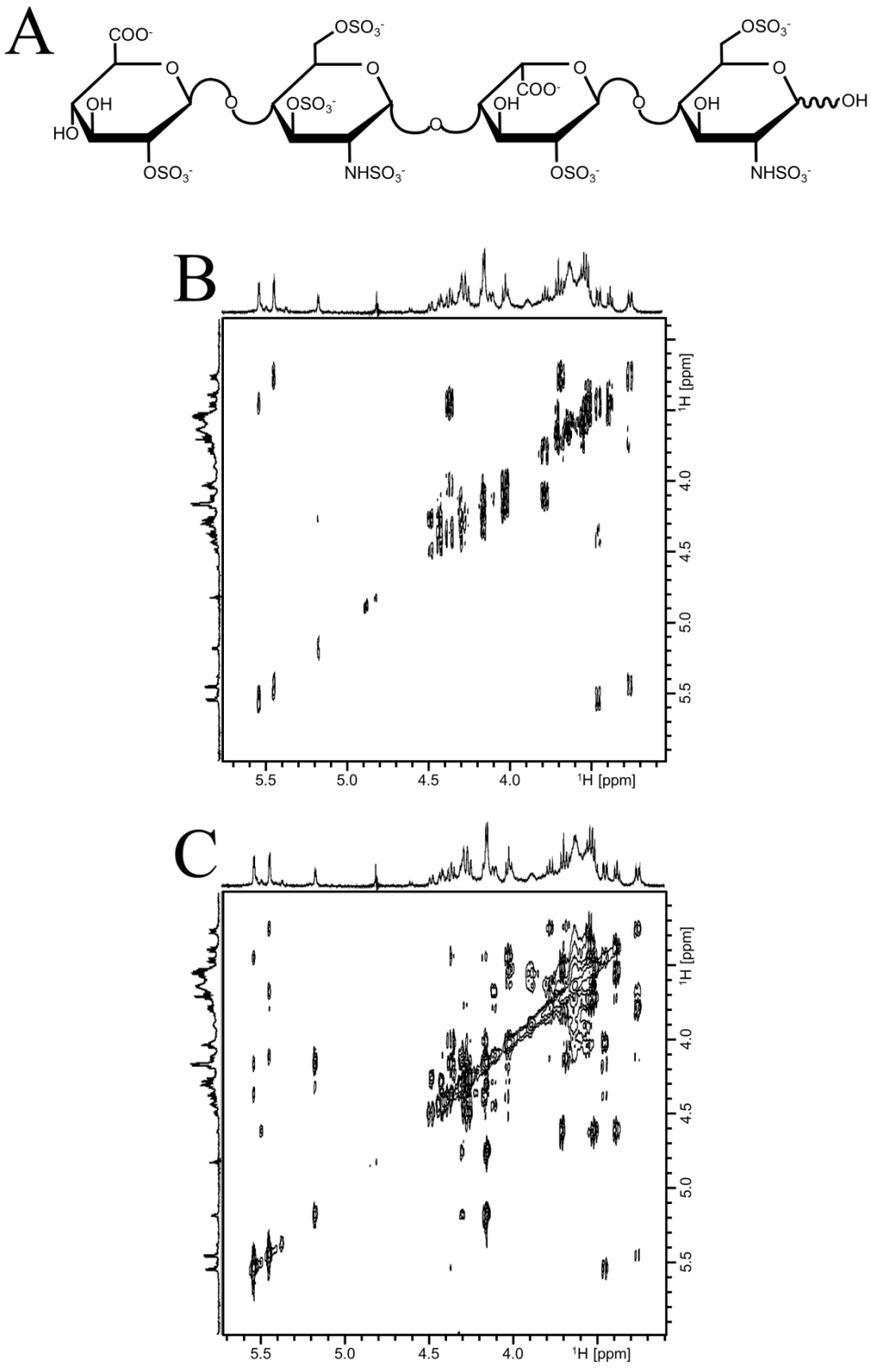
A
COO-
OSO3-
OH
HO
OSO3-
NHSO3-
OSO3-
COO-
OH
OSO3-
OSO3-
OH
OH
NHSO3-
B
C
1H [ppm]
5.5
5.0
4.5
4.0

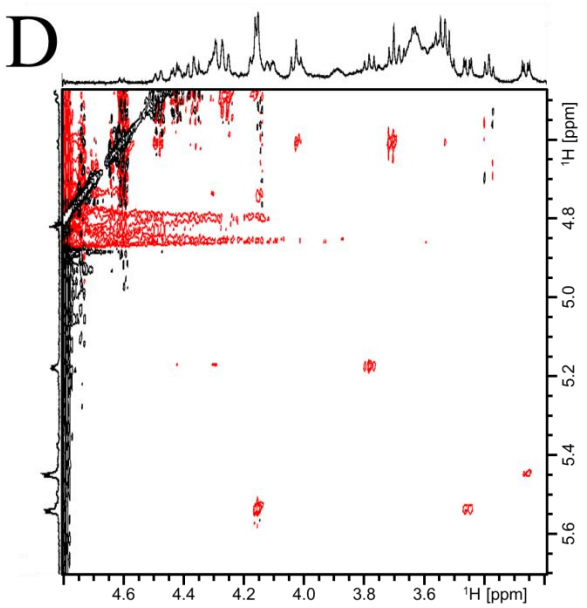

Figure 2.8. (A) The structure of the 3-*O*-sulfated tetrasaccharide isolated as Tp5A from SEC fraction T7: GlcA-GlcNS3S6S-IdoA2S-GlcNS6S. Two-dimensional (B) COSY, (C) TOCSY, and (D) ROESY spectra were used to characterize the tetrasaccharide structure.

Table 2.5. The ^{1}H NMR resonance assignments for the 3-*O*-sulfated tetrasaccharide, Tp5A. The molecular ion m/z of the doubly charged tetrasaccharide is 584.48, which corresponds to 6 sulfates and saturation at the non-reducing end.

Tp5A	**Proton**	**GlcA-**	**-GlcNS3S6S-**	**-IdoA2S-**	**-GlcNS6S**
	1	4.61	5.54	5.17	5.45
	2	3.39	3.45	4.30	3.26
	3	3.52	4.37	4.15	3.68
	4	3.52	4.02	4.15	3.78
	5	3.70	4.16	4.74	4.11
	6		4.42		4.28
	6’				4.43

known to contribute to the AT-III-binding affinity of the pentasaccharide,[4] the tetrasaccharide would likely not have been isolated by AT-III affinity chromatography.

2.3.6. SAX-HPLC separation of the hexasaccharide SEC fractions. Similar to the tetrasaccharide SEC fractions, individual fractions of the SEC hexasaccharide peak were pooled and separated by SAX-HPLC (Figure 2.9). The main peaks are labeled Hp1 through Hp7 (Hp stands for hexasaccharide peak). Each peak was collected separately over a series of multiple injections and its composition analyzed by NMR. Hexasaccharide proton chemical shift assignments are found in Table 2.6. There was no evidence of co-eluting 3-*O*-sulfated hexasaccharides in the [^{1}H, ^{15}N] HSQC spectra of the main SAX peaks. The less abundant oligosaccharides were collected together (labeled Groups 1, 2, 3, and 4) and also screened using [^{1}H, ^{15}N] HSQC experiments for sulfamate NM correlations characteristic of 3-*O*-sulfation. Although evidence of a 3-*O*-sulfated GlcNS residue was found in Groups 2 and 3, isolation of 3-*O*-sulfated oligosaccharides was not successful. The oligosaccharides collected were not very pure, making them difficult to characterize by NMR. This prompted examination of each hexasaccharide SEC fraction individually in hopes of obtaining less complex SAX-HPLC separations with better resolution of low abundance components.

2.3.7 Screening of individual hexasaccharide SEC fractions by [^{1}H, ^{15}N] HSQC NMR. Though differences are observed in the ^{1}H NMR spectra of the individual hexasaccharide SEC fractions H1 - H9 (Figure 2.10), the complexity of the mixtures and their resulting NMR spectra makes it difficult to draw conclusions about changes in composition across the SEC hexasaccharide peak. In contrast, the [^{1}H, ^{15}N] HSQC

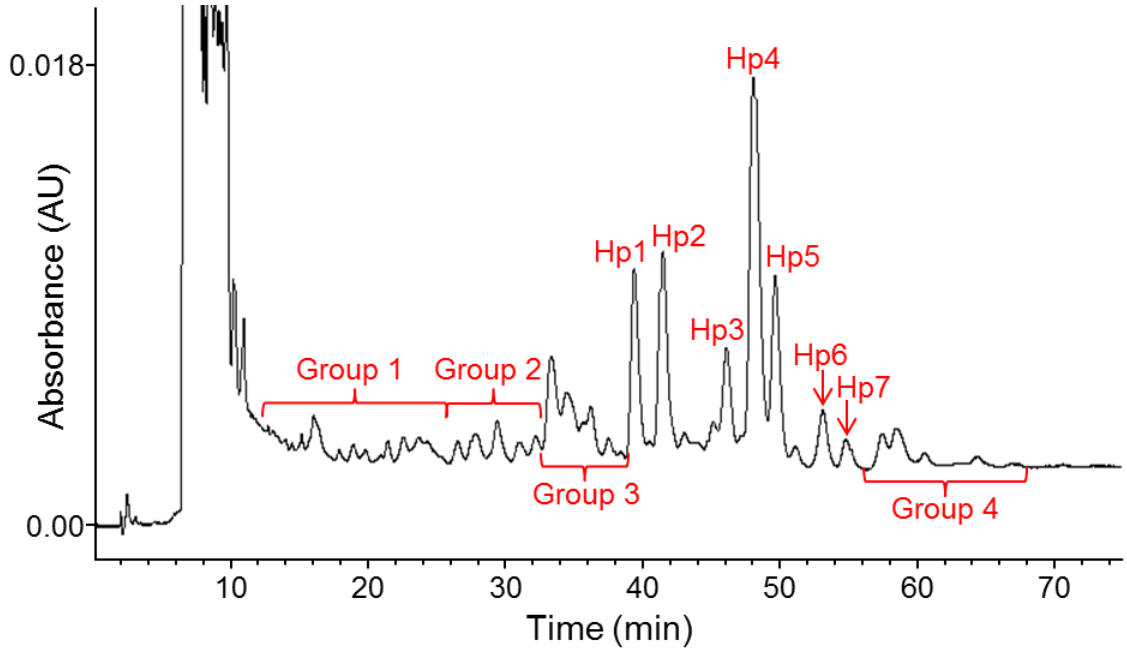

Figure 2.9. The SAX-HPLC separation of the pooled enoxaparin hexasaccharide SEC fraction. Main peaks are labeled Hp1 through Hp7 (Hp stands for hexasaccharide peak). The peaks which are labeled were discovered to be pure and in high abundance and were structurally characterized with great certainty. Groups 1, 2, 3 and 4 were measured by [^{1}H, ^{15}N] HSQC to search for evidence of a 3-*O*-sulfate group.

Table 2.6. ^{1}H chemical shift assignments for the main peaks in the SAX-HPLC separation of the pooled enoxaparin hexasaccharide SEC fraction.

SAX Peak	Proton	NMR Chemical Shifts (ppm)					
Hp1		**ΔUA2S-**	**-GlcNS6S-**	**-IdoA2S-**	**-GlcNS6S-**	**-IdoA2S-**	**-GlcNS(1,6-an)**
	1	5.51	5.413	5.216	5.381	5.335	5.614
	2	4.31	3.30	4.34	3.29	4.36	3.20
	3	4.63	3.66	4.22	3.68	4.25	3.90
	4	5.988	3.84	4.10	3.77	4.13	3.84
	5		4.05	4.82	4.02	4.64	4.83
	6		4.27		4.28		3.80
	6’		4.36		4.41		4.21
Hp2		**ΔUA2S-**	**-GlcNS6S-**	**-IdoA2S-**	**-GlcNS6S-**	**-IdoA2S-**	**-ManNS(1,6-an)**
	1	5.508	5.413	5.213	5.388	5.347	5.567
	2	4.628	3.3	4.34	3.28	4.35	3.478
	3	4.314	3.65	4.22	3.67	4.23	4.05
	4	5.987	3.84	4.10	3.77	4.11	3.98
	5		4.05	4.82	4.01	4.57	4.83
	6		4.36		4.41		4.23
	6’		4.26		4.37		3.77
Hp3		**ΔUA2S-**	**-GlcNS6S-**	**-IdoA2S-**	**-GlcNS6S-**	**-GlcA-**	**-GlcNS6S**
	1	5.495	5.38	5.221	5.573	4.60	5.448
	2	4.62	3.29	4.33	3.27	3.38	3.27
	3	4.31	3.64	4.22	3.65	3.84	3.73
	4	5.981	3.83	4.08	3.76	3.80	3.71
	5		4.03	4.81	3.96	3.79	4.15
	6		4.24		4.23		4.31
	6’		4.34		4.38		4.35

Hp4		**ΔUA2S-**	**-GlcNS6S-**	**-IdoA2S-**	**-GlcNS6S-**	**-IdoA2S-**	**-GlcNS6S**
	1	5.509	5.41	5.209	5.445	5.209	5.452
	2	4.268	3.30	4.34	3.28	4.32	3.26
	3	4.32	3.65	4.22	3.65	4.18	3.70
	4	5.989	3.84	4.10	3.77	4.13	3.76
	5		4.04	4.82	4.03	4.76	4.13
	6		4.36		4.28		4.31
	6’		4.26		4.40		4.38
Hp5		**ΔUA2S-**	**-GlcNS6S-**	**-IdoA2S-**	**-GlcNS6S-**	**-IdoA2S-**	**-ManNS6S**
	1	5.506	5.405	5.206	5.445	5.16	5.39
	2	4.625	3.29	4.33	3.28	4.31	3.60
	3	4.31	3.65	4.22	3.65	4.17	4.06
	4	5.985	3.83	4.09	3.76	4.13	3.72
	5		4.04	4.82	4.02	4.75	4.08
	6		4.26		4.27		4.31
	6’		4.35		4.39		4.40
Hp6		**ΔUA2S-**	**-GlcNS6S-**	**-GlcA-**	**-GlcNS6S-**	**-IdoA2S-**	**-GlcNS6S**
	1	5.50	5.55	4.59	5.43	5.22	5.44
	2	4.62	3.30	3.39	3.28	4.13	3.26
	3	4.31	3.64	3.84	3.68	4.18	3.69
	4	5.98	3.82	3.78	3.74	4.10	3.75
	5		4.00	3.82	4.09	4.75	4.13
	6		4.20		4.23		4.30
	6’		4.34		4.44		4.36

Hp7		ΔUA2S-	-GlcNS6S-	-GlcA-	-GlcNS6S-	-IdoA2S-	-ManNS6S
	1	5.500	5.55	4.59	5.436	5.166	5.386
	2	4.61	3.29	3.39	3.28	4.30	3.59
	3	4.31	3.63	3.84	3.68	4.17	4.05
	4	5.977	3.82	3.78	3.74	4.10	3.71
	5		3.99	3.81	4.10	4.75	4.08
	6		4.19		4.23		4.30
	6’		4.34		4.45		4.38

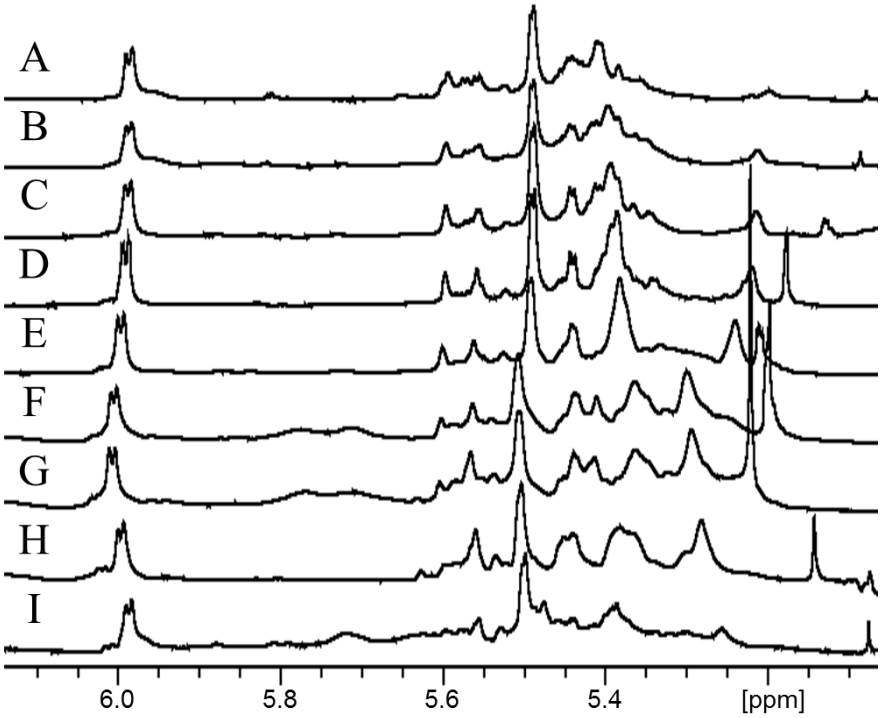

Figure 2.10. ^{1}H NMR spectra of individual hexasaccharide SEC fractions: (A) H1, (B) H2, (C) H3, (D) H4, (E) H5, (F) H6, (G) H7, (H) H8, and (I) H9. Slight differences in their NMR spectra demonstrate the compositional difference of the fractions along the SEC hexasaccharide peak.

spectra clearly indicate the SEC fractions that contain 3-*O*-sulfated oligosaccharides. No [^{1}H,^{15}N] correlations are observed in hexasaccharide SEC fractions H1, H8, and H9 due to their limited available mass. Correlations characteristic of a GlcNS sulfamate proton adjacent to a 2-*O*-sulfated uronic acid residue are detected in the [^{1}H, ^{15}N] HSQC spectrum of SEC fractions H2 (Figure 2.11A) and H3 (Figure 2.11B). A correlation at 91.9 ppm in the ^{15}N dimension (circled in red in Figure 2.11C) of the [^{1}H, ^{15}N] HSQC spectrum of SEC fraction H4 is characteristic of a GlcNS sulfamate proton adjacent to a 3-*O*-sulfate group. The intensity of this correlation increases in SEC fraction H5 (circled in red in Figure 2.11D) and two additional correlations also appear at ^{15}N chemical shifts of 90.2 and 90.5 ppm. It is suspected that these correlations belong to sulfamate protons of 3-*O*-sulfated GlcNS residues in a different microenvironment than were previously characterized. [25,53,59] Correlations are also observed in the HSQC spectrum of fraction H5 characteristic of the sulfamate protons of reducing-end GlcNS residues (93.8 ppm) and of GlcNS residues adjacent to unsubstituted uronic acid residues (93.1 ppm). All the correlations detected in fraction H5 are also observed in the spectra measured for fractions H6 and H7 (Figure 2.11E and F, respectively).

Each of the SEC fractions (H4-7) producing HSQC correlations consistent with 3-*O*-sulfatation was separated using SAX-HPLC. The SAX-HPLC chromatographs of each hexasaccharide SEC fraction had a slightly different composition (Figure 2.12). Oligosaccharides eluting earlier than 30 min are too low in abundance to characterize by NMR and are not shown in Figure 2.12. Similar to the tetrasaccharide fractions, the earlier eluting hexasaccharide SEC fractions (Figure 2.12A and B) contain a greater

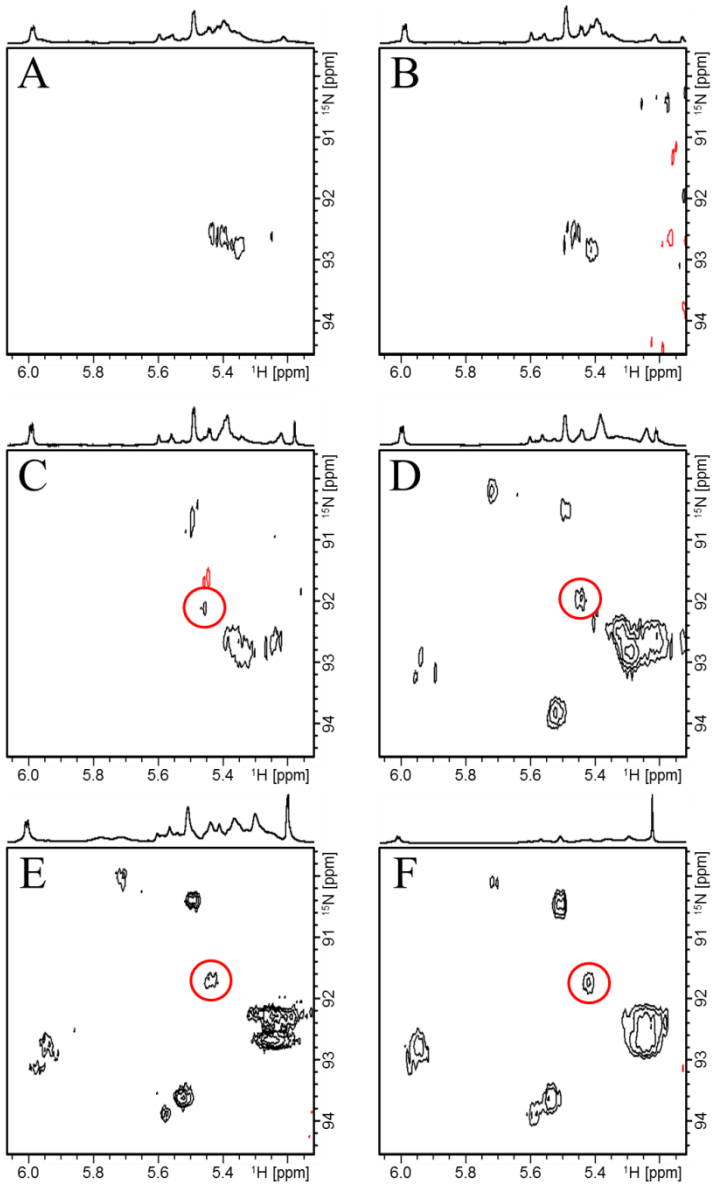

Figure 2.11. [^{1}H, ^{15}N] HSQC spectra of individual enoxaparin SEC hexasaccharide fractions: (A) H2, (B) H3, (C) H4, (D) H5, (E) H6, (F) H7. The sulfamate cross peak which is characteristic of a 3-*O*-sulfate group is circled in red and begins to appear in fraction H4 (C) and continues to increase in intensity through fraction H7 (F). All other SEC fractions were too dilute to observe any cross peaks.

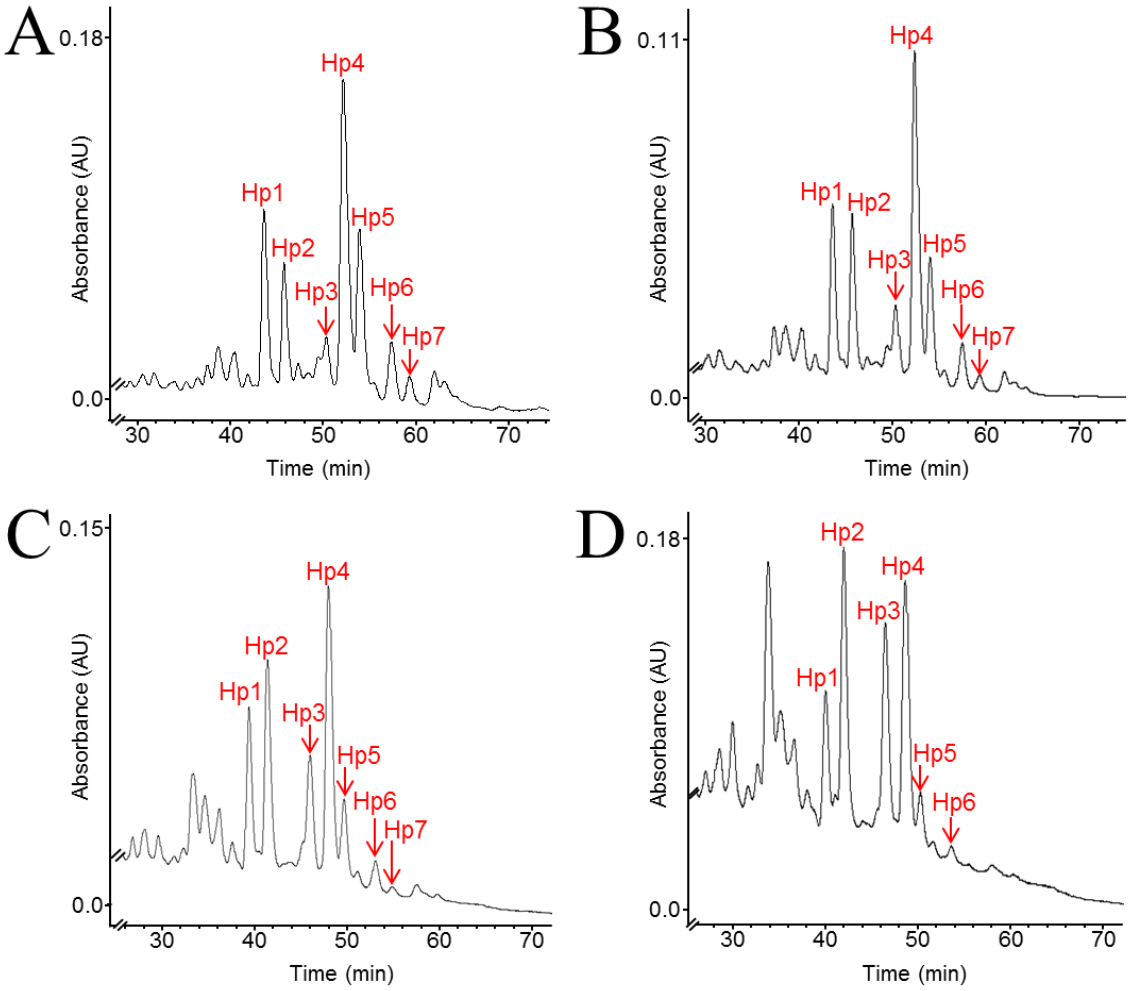

Figure 2.12. SAX-HPLC separations of individual hexasaccharide SEC fractions: (A) H4, (B) H5, (C) H6, (D) H7.

proportion of more highly sulfated oligosaccharides, while the later eluting SEC fractions contain a greater proportion of oligosaccharides with lower sulfation levels (Figure 2.12C and D).

We decided to focus our efforts on the regions of the SAX-HPLC fractions corresponding to Groups 2 and 3 of the SAX separation of the pooled SEC hexasaccharides (Figure 2.9) that originally showed evidence of 3-*O*-sulfation. In the SAX separations of the individual SEC fractions H4-H7, discrete peaks were isolated instead of collecting the peaks as a group. The NMR results indicated that the peaks were either insufficiently pure or were of too low of abundance to characterize by our 600 MHz NMR instrument. Access to a cryoprobe equipped instrument, preferably at a higher magnetic field, would have aided these measurements. Mixtures of hexasaccharides are inherently more challenging to separate than tetrasaccharides because their longer chains results in a more complex mixture of oligosaccharides containing a larger number positional isomers. As discussed in Chapter 7, an improved separation, perhaps involving an orthogonal separation method would be required to isolate the 3-*O*-sulfated hexasaccharides in high purity.

2.4 Conclusions

Using the methods described in this chapter, we successfully identified 12 tetrasaccharides, which includes a unique tetrasaccharide. Although many of these tetrasaccharides have previously been reported,[58] the methods described in this chapter provided unique SAX-HPLC separation profiles. We also reported complete ^{1}H NMR

chemical shifts of the isolated oligosaccharides. This work demonstrated a screening method using [^{1}H, ^{15}N] HSQC NMR, to identify SEC fractions containing NH correlations characteristic of 3-*O*-sulfated oligosaccharides. SAX-HPLC separations of individual SEC tetrasaccharide fractions produced less complex chromatograms and better resolution of less abundant components. The tetrasaccharide GlcA-GlcNS3S6S-IdoA2S-GlcNS6S was isolated in fairly high purity and structurally characterized by MS and NMR. Although no 3-*O*-sulfated hexasaccharides were isolated using this method, it demonstrated that their location could be narrowed down to specific regions in the SAX-HPLC chromatogram. The method presented in this chapter shows the potential to locate heparin oligosaccharides contain a 3-*O*-sulfated GlcNS residue. In the future, it might also be possible to use this strategy to locate heparan sulfate oligosaccharides containing a 3-*O*-sulfated GlcN residue. GlcN3S-containing oligosaccharides are of interest as they have been shown to be part of the binding sequence of various proteins.[15,16,17] Chapter 5 demonstrates, for the first time detection of GlcN amine protons by [^{1}H, ^{15}N] HSQC NMR, and the potential for characterizing the oligosaccharides containing GlcN residues. Isolation of additional 3-*O*-sulfated oligosaccharides would increase our library of standards and advance the understanding of protein interactions with heparin and heparan sulfate.

2.5 References

1. Atha, D. H.; Lormeau, J. C.; Petitou, M.; Rosenberg, R. D.; Choay, J., Contribution of monosaccharide residues in heparin binding to antithrombin-III. *Biochemistry* **1985,** *24*, 6723-6729.

2. Johnson, D. J. D.; Li, W.; Adams, T. E.; Huntington, J. A., Antithrombin-S195A factor Xa-heparin structure reveals the allosteric mechanism of antithrombin activation. *Embo J.* **2006,** *25*, 2029-2037.

3. Ferro, D. R.; Provasoli, A.; Ragazzi, M.; Torri, G.; Casu, B.; Gatti, G.; Jacquinet, J. C.; Sinay, P.; Petitou, M.; Choay, J., Evidence for conformational equilibrium of the sulfated L-iduronate residue in heparin and in synthetic heparin mono- and oligosaccharides: NMR and force-field studies. *J. Am. Chem. Soc.* **1986,** *108*, 6773-6778.

4. Baldwin, J.; Shukla, D.; Tiwari, V., Members of 3-*O*-sulfotransferases (3-OST) family: A valuable tool from zebrafish to humans for understanding herpes simplex virus entry. *Open Virol. J.* **2013,** *7*, 5-11.

5. Thacker, B. E.; Xu, D.; Lawrence, R.; Esko, J. D., Heparan sulfate 3-*O*-sulfation: A rare modification in search of a function. *Matrix Biol.* **2014,** *35*, 60-72.

6. O'Donnell, C. D.; Tiwari, V.; Oh, M.-J.; Shukla, D., A role for heparan sulfate 3-*O*-sulfotransferase isoform 2 in herpes simplex virus type 1 entry and spread. *Virology* **2006,** *346*, 452-459.

7. Baldwin, J.; Antoine, T. E.; Shukla, D.; Tiwari, V., Zebrafish encoded 3-*O*-sulfotransferase-2 generated heparan sulfate serves as a receptor during HSV-1 entry and spread. *Biochem. Bioph. Res. Co.* **2013,** *432*, 672-676.

8. Hubbard, S.; Darmani, N. A.; Thrush, G. R.; Dey, D.; Burnham, L.; Thompson, J. M.; Jones, K.; Tiwari, V., Zebrafish-encoded 3-*O*-sulfotransferase-3 isoform mediates herpes simplex virus type 1 entry and spread. *Zebrafish* **2010,** *7*, 181-187.

9. Tiwari, V.; O'Donnell, C. D.; Oh, M. J.; Valyi-Nagy, T.; Shukla, D., A role for 3-O-sulfotransferase isoform-4 in assisting HSV-1 entry and spread. *Biochem. Bioph. Res. Co.* **2005,** *338*, 930-937.

10. Antoine, T. E.; Yakoub, A.; Maus, E.; Shukla, D.; Tiwari, V., Zebrafish 3-*O*-sulfotransferase-4 generated heparan sulfate mediates HSV-1 entry and spread. *PLOS One* **2014,** *9*, e87302 pp. 1-9.

11. Xia, G. Q.; Chen, J. H.; Tiwari, V.; Ju, W. J.; Li, J. P.; Malmstrom, A.; Shukla, D.; Liu, J., Heparan sulfate 3-*O*-sulfotransferase isoform 5 generates both an antithrombin-binding site and an entry receptor for herpes simplex virus, type 1. *J. Biol. Chem.* **2002,** *277*, 37912-37919.

12. Xu, D.; Tiwari, V.; Xia, G. Q.; Clement, C.; Shukla, D.; Liu, J., Characterization of heparan sulphate 3-*O*-sulphotransferase isoform 6 and its role in assisting the entry of herpes simplex virus type 1. *Biochem. J.* **2005,** *385*, 451-459.

13. Shukla, D.; Liu, J.; Blaiklock, P.; Shworak, N. W.; Bai, X. M.; Esko, J. D.; Cohen, G. H.; Eisenberg, R. J.; Rosenberg, R. D.; Spear, P. G., A novel role for 3-*O*-sulfated heparan sulfate in herpes simplex virus 1 entry. *Cell* **1999,** *99*, 13-22.

14. Kaner, R. J.; Baird, A.; Mansukhani, A.; Basilico, C.; Summers, B. D.; Florkiewicz, R. Z.; Hajjar, D. P., Fibroblast growth-factor receptor is a portal of cellular entry for herpes-simplex virus type-1. *Science* **1990,** *248*, 1410-1413.

15. Liu, J.; Shriver, Z.; Pope, R. M.; Thorp, S. C.; Duncan, M. B.; Copeland, R. J.; Raska, C. S.; Yoshida, K.; Eisenberg, R. J.; Cohen, G.; Linhardt, R. J.; Sasisekharan, R., Characterization of a heparan sulfate octasaccharide that binds to herpes simplex virus type 1 glycoprotein D. *J. Biol. Chem.* **2002,** *277*, 33456-33467.

16. Copeland, R.; Balasubramaniam, A.; Tiwari, V.; Zhang, F.; Bridges, A.; Linhardt, R. J.; Shukla, D.; Liu, J., Using a 3-*O*-sulfated heparin octasaccharide to inhibit the entry of herpes simplex virus type 1. *Biochemistry* **2008,** *47*, 5774-5783.

17. Hu, Y. P.; Lin, S. Y.; Huang, C. Y.; Zulueta, M. M. L.; Liu, J. Y.; Chang, W.; Hung, S. C., Synthesis of 3-*O*-sulfonated heparan sulfate octasaccharides that inhibit the herpes simplex virus type 1 host-cell interaction. *Nat. Chem.* **2011,** *3*, 557-563.

18. Ly, M.; Leach, F. E.; Laremore, T. N.; Toida, T.; Amster, I. J.; Linhardt, R. J., The proteoglycan bikunin has a defined sequence. *Nat. Chem. Biol.* **2011,** *7*, 827-833.

19. Leach III, F. E.; Xiao, Z.; Laremore, T. N.; Linhardt, R. J.; Amster, I. J., Electron detachment dissociation and infrared multiphoton dissociation of heparin tetrasaccharides. *Int. J. Mass Spectrom.* **2011,** *308*, 253-259.

20. Leach III, F. E.; Arungundram, S.; Al-Mafraji, K.; Venot, A.; Boons, G.-J.; Amster, I. J., Electron detachment dissociation of synthetic heparan sulfate glycosaminoglycan tetrasaccharides varying in degree of sulfation and hexuronic acid stereochemistry. *Int. J. Mass Spectrom.* **2012,** *330–332*, 152-159.

21. Kailemia, M. J.; Park, M.; Kaplan, D. A.; Venot, A.; Boons, G. J.; Li, L. Y.; Linhardt, R. J.; Amster, I. J., High-field asymmetric-waveform ion mobility spectrometry

and electron detachment dissociation of isobaric mixtures of glycosaminoglycans. *J. Am. Soc. Mass Spectr.* **2014,** *25*, 258-268.

22. Guerrini, M.; Zhang, Z. Q.; Shriver, Z.; Naggi, A.; Masuko, S.; Langer, R.; Casu, B.; Linhardt, R. J.; Torri, G.; Sasisekharan, R., Orthogonal analytical approaches to detect potential contaminants in heparin. *P. Natl. Acad. Sci. USA.* **2009,** *106*, 16956-16961.

23. Guerrini, M.; Beccati, D.; Shriver, Z.; Naggi, A.; Viswanathan, K.; Bisio, A.; Capila, I.; Lansing, J. C.; Guglieri, S.; Fraser, B.; Al-Hakim, A.; Gunay, N. S.; Zhang, Z. Q.; Robinson, L.; Buhse, L.; Nasr, M.; Woodcock, J.; Langer, R.; Venkataraman, G.; Linhardt, R. J.; Casu, B.; Torri, G.; Sasisekharan, R., Oversulfated chondroitin sulfate is a contaminant in heparin associated with adverse clinical events. *Nat. Biotechnol.* **2008,** *26*, 669-675.

24. Mascellani, G.; Guerrini, M.; Torri, G.; Liverani, L.; Spelta, F.; Bianchini, P., Characterization of di- and monosulfated, unsaturated heparin disaccharides with terminal *N*-sulfated 1,6-anhydro-β-D-glucosamine or *N*-sulfated 1,6-anhydro-β-D-mannosamine residues. *Carbohyd. Res.* **2007,** *342*, 835-842.

25. Langeslay, D. J.; Beecher, C. N.; Naggi, A.; Guerrini, M.; Torri, G.; Larive, C. K., Characterizing the microstructure of heparin and heparan sulfate using *N*-sulfoglucosamine ^{1}H and ^{15}N NMR chemical shift analysis. *Anal. Chem.* **2013,** *85*, 1247-1255.

26. Pomin, V. H.; Sharp, J. S.; Li, X. Y.; Wang, L. C.; Prestegard, J. H., Characterization of glycosaminoglycans by ^{15}N NMR spectroscopy and in vivo isotopic labeling. *Anal. Chem.* **2010,** *82*, 4078-4088.

27. Keire, D. A.; Buhse, L. F.; Al-Hakim, A., Characterization of currently marketed heparin products: composition analysis by 2D-NMR. *Anal. Method.* **2013,** *5*, 2984-2994.

28. Linhardt, R. J.; Turnbull, J. E.; Wang, H. M.; Loganathan, D.; Gallagher, J. T., Examination of the substrate-specificity of heparin and heparan sulfate lyases. *Biochemistry* **1990,** *29*, 2611-2617.

29. Desai, U. R.; Wang, H. M.; Linhardt, R. J., Specificity studies on the heparin lyases from flavobacterium-heparinum. *Biochemistry* **1993,** *32*, 8140-8145.

30. Jandik, K. A.; Gu, K. A.; Linhardt, R. J., Action pattern of polysaccharide lyases on glycosaminoglycans. *Glycobiology* **1994,** *4*, 289-296.

31. Mardiguian, J. S., Heparin esters and processes for their preparation. U.S. Patent 3835112 A. September 10, 1974.

32. Shively, J. E.; Conrad, H. E., Formation of anhydrosugars in chemical depolymerization of heparin. *Biochemistry* **1976,** *15*, 3932-3942.

33. Rota, C.; Liverani, L.; Spelta, F.; Mascellani, G.; Tomasi, A.; Iannone, A.; Vismara, E., Free radical generation during chemical depolymerization of heparin. *Anal. Biochem.* **2005,** *344*, 193-203.

34. Zaia, J.; Costello, C. E., Compositional analysis of glycosaminoglycans by electrospray mass spectrometry. *Anal. Chem.* **2001,** *73*, 233-239.

35. Ziegler, A.; Zaia, J., Size-exclusion chromatography of heparin oligosaccharides at high and low pressure. *J. Chromatogr. B* **2006,** *837*, 76-86.

36. Staples, G. O.; Shi, X. F.; Zaia, J., Extended *N*-sulfated domains reside at the nonreducing end of heparan sulfate chains. *J. Biol. Chem.* **2010,** *285*, 18336-18343.

37. Schumacher, V. A.; Schlotzer-Schrehardt, U.; Karumanchi, S. A.; Shi, X. F.; Zaia, J.; Jeruschke, S.; Zhang, D. S.; Pavenstaedt, H.; Drenckhan, A.; Amann, K.; Ng, C.; Hartwig, S.; Ng, K. H.; Ho, J.; Kreidberg, J. A.; Taglienti, M.; Royer-Pokora, B.; Ai, X. B., WT1-dependent sulfatase expression maintains the normal glomerular filtration barrier. *J. Am. Soc. Nephrol.* **2011,** *22*, 1286-1296.

38. Shao, C.; Shi, X. F.; Phillips, J. J.; Zaia, J., Mass spectral profiling of glycosaminoglycans from histological tissue surfaces. *Anal. Chem.* **2013,** *85*, 10984-10991.

39. Shi, X. F.; Shao, C.; Mao, Y.; Huang, Y.; Wu, Z. L. L.; Zaia, J., LC-MS and LC-MS/MS studies of incorporation of (SO3)-S-34 into glycosaminoglycan chains by sulfotransferases. *Glycobiology* **2013,** *23*, 969-979.

40. Shastri, M.; Johns, C.; Hutchinson, J.; Khandagale, M.; Patel, R., Ion exchange chromatographic separation and isolation of oligosaccharides of intact low-molecular-weight heparin for the determination of their anticoagulant and anti-inflammatory properties. *Anal. Bioanal. Chem.* **2013,** *405*, 6043-6052.

41. Powell, A. K.; Ahmed, Y. A.; Yates, E. A.; Turnbull, J. E., Generating heparan sulfate saccharide libraries for glycomics applications. *Nat. Protoc.* **2010,** *5*, 821-833.

42. Chuang, W. L.; McAllister, H.; Rabenstein, D. L., Chromatographic methods for product-profile analysis and isolation of oligosaccharides produced by heparinase-catalyzed depolymerization of heparin. *J. Chromatogr. A* **2001,** *932*, 65-74.

43. Limtiaco, J. F. K.; Beni, S.; Jones, C. J.; Langeslay, D. J.; Larive, C. K., The efficient structure elucidation of minor components in heparin digests using microcoil NMR. *Carbohyd. Res.* **2011,** *346*, 2244-2254.

44. Jones, C. J.; Beni, S.; Limtiaco, J. F. K.; Langeslay, D. J.; Larive, C. K., Heparin characterization: Challenges and solutions. *Annu. Rev. Anal. Chem.* **2011**, *4*, 439-465.

45. Onoue, S.; Harada, S.; Nemoto, Y.; Yajima, T.; Kashimoto, K., Novel approach for preparation of heparins specific to factor Xa using affinity chromatography coupled with synthetic antithrombin III-related peptides. *Peptides* **2003,** *24*, 821-826.

46. Bisio, A.; Vecchietti, D.; Citterio, L.; Guerrini, M.; Raman, R.; Bertini, S.; Eisele, G.; Naggi, A.; Sasisekharan, R.; Torri, G., Structural features of low-molecular-weight heparins affecting their affinity to antithrombin. *Thromb. Haemostasis* **2009,** *102*, 865-873.

47. Eldridge, S. L.; Korir, A. K.; Gutierrez, S. M.; Campos, F.; Limtiaco, J. F. K.; Larive, C. K., Heterogeneity of depolymerized heparin SEC fractions: To pool or not to pool? *Carbohyd. Res.* **2008,** *343*, 2963-2970.

48. Langeslay, D. J.; Young, R. P.; Beni, S.; Beecher, C. N.; Mueller, L. J.; Larive, C. K., Sulfamate proton solvent exchange in heparin oligosaccharides: Evidence for a persistent hydrogen bond in the antithrombin-binding pentasaccharide Arixtra. *Glycobiology* **2012,** *22*, 1173-1182.

49. Beecher, C. N.; Young, R. P.; Langeslay, D. J.; Mueller, L. J.; Larive, C. K., Hydroxyl-proton hydrogen bonding in the heparin oligosaccharide Arixtra in aqueous solution. *J. Phys. Chem. B* **2014,** *118*, 482-491.

50. Brustkern, A. M.; Buhse, L. F.; Nasr, M.; Al-Hakim, A.; Keire, D. A., Characterization of currently marketed heparin products: Reversed-phase ion-pairing liquid chromatography mass spectrometry of heparin digests. *Anal. Chem.* **2010,** *82*, 9865-9870.

51. Jones, C. J.; Membreno, N.; Larive, C. K., Insights into the mechanism of separation of heparin and heparan sulfate disaccharides by reverse-phase ion-pair chromatography. *J. Chromatogr. A* **2010,** *1217*, 479-488.

52. Wang, B.; Buhse, L. F.; Al-Hakim, A.; Ii, M. T. B.; Keire, D. A., Characterization of currently marketed heparin products: Analysis of heparin digests by RPIP-UHPLC-QTOF-MS. *J. Pharmaceut. Biomed.* **2012,** *67-68*, 42-50.

53. Langeslay, D. J.; Beni, S.; Larive, C. K., Detection of the ^{1}H and ^{15}N NMR resonances of sulfamate groups in aqueous solution: A new tool for heparin and heparan sulfate characterization. *Anal. Chem.* **2011,** *83*, 8006-8010.

54. Pervin, A.; Gallo, C.; Jandik, K. A.; Han, X. J.; Linhardt, R. J., Preparation and structural characterization of large heparin-derived oligosaccharides. *Glycobiology* **1995,** *5*, 83-95.

55. Chuang, W.-L.; Christ, M. D.; Rabenstein, D. L., Determination of the primary structures of heparin- and heparan sulfate-derived oligosaccharides using band-selective homonuclear-decoupled two-dimensional ^{1}H NMR experiments. *Anal. Chem.* **2001,** *73*, 2310-2316.

56. Langeslay, D. J.; Beecher, C. N.; Dinges, M. M.; Larive, C. K., Glycosaminoglycan structural characterization. *eMagRes*, **2013,** *2*, 205-214.

57. Chuang, W. L.; McAllister, H.; Rabenstein, D. L., Hexasaccharides from the histamine-modified depolymerization of porcine intestinal mucosal heparin. *Carbohyd. Res.* **2002,** *337*, 935-945.

58. Ozug, J.; Wudyka, S.; Gunay, N. S.; Beccati, D.; Lansing, J.; Wang, J.; Capila, I.; Shriver, Z.; Kaundinya, G. V., Structural elucidation of the tetrasaccharide pool in enoxaparin sodium. *Anal. Bioanal. Chem.* **2012,** *403*, 2733-2744.

59. Langeslay, D. J.; Beni, S.; Larive, C. K., A closer look at the nitrogen next door: ^{1}H-^{15}N NMR methods for glycosaminoglycan structural characterization. *J. Magn. Reson.* **2012,** *216*, 169-174.

CHAPTER THREE

Detection and Identification of Hydroxyl Proton Hydrogen Bonds in Arixtra and other Heparin Oligosaccharides

Based on a paper published in the Journal of Physical Chemistry B

J. Phys. Chem. B. 2014, 118:482-491

Acknowledgements: I would like to thank the following people for their contributions to this research: Robert Young for his contribution of the molecular dynamics simulations, Dr. Leonard Mueller for his help in the derivation of radiation damping effects on T_1 and in using the Mathematica software, and Dr. Derek Langeslay for his help with the NMR and Mathematica software.

Abstract: Heparin is best known for its anticoagulant activity, which is mediated by the binding of a specific pentasaccharide sequence to the protease inhibitor antithrombin-III (AT-III). Although heparin oligosaccharides are thought to be flexible in aqueous solution, the recent discovery of a hydrogen bond between the sulfamate ($NHSO_3^-$) proton and the adjacent 3-*O*-sulfo group of the 3,6-*O*-sulfated *N*-sulfoglucosamine residue of the Arixtra^{TM} (fondaparinux sodium) pentasaccharide demonstrates that definable elements of local structure exist in solution. Molecular dynamics simulations of Arixtra suggest the presence of additional hydrogen bonds involving the C3-OH groups of the glucuronic acid and 2-*O*-sulfo-iduronic acid residues. NMR measurements of temperature coefficients, chemical shift differences, and solvent exchange rate constants

provide experimental confirmation of these hydrogen bonds. The extraction of rate constants from cross peak build-up curves in 2D exchange spectroscopy is complicated by the presence of radiation damping in aqueous solution. A straight-forward model is presented that explicitly takes into account the effect of radiation damping on the water proton relaxation and is sufficiently robust to provide an accurate measure of the proton exchange rate between the analyte hydroxyl protons and water. The effects of catalysis of hydroxyl proton – solvent exchange by dissolved CO_2 are also discussed.

3.1 Introduction

Heparin exhibits a variety of biological effects including inhibition of angiogenesis and tumor growth through well-characterized interactions with fibroblast growth factors (FGF),[1-3] vascular endothelial growth factor (VEGF),[4-6] lipases[7-9] and cytokines,[10-12] but is best known for its role as an anticoagulant and antithrombotic, acting by binding to the protease inhibitor antithrombin-III (AT-III).[13,14] The anticoagulant activity of heparin has been studied extensively, and the structure of the native pentasaccharide sequence responsible for high affinity AT-III binding is known.[15] A synthetic pentasaccharide that mimics this binding sequence is currently used clinically and marketed as Arixtra™ (fondaparinux sodium). A critical structural element of the AT-III binding pentasaccharide is the internal 3,6-*O*-sulfated *N*-sulfoglucosamine (GlcNS3S6S) residue. Removal of the 3-*O*-sulfo moiety decreases the affinity of the pentasaccharide for AT-III by 1000-fold.[16] The conformational flexibility of the 2-*O*-sulfated iduronic acid (IdoA2S) residue of the pentasaccharide is also important for AT-

III binding. The IdoA2S residue can exist in two different conformations: chair ($^1C_4$) and skew boat (^2S_O), that interconvert on a rate that is fast on the NMR timescale. In oligosaccharides in which the IdoA2S residue is connected to a 6-*O*-sulfated GlcNS residue at its non-reducing end, the equilibrium slightly favors the $^1C_4$ conformer ($^1C_4$:^2S_O = 60:40). If this GlcNS residue is 3,6-*O*-sulfated, however, equilibrium of the adjacent IdoA2S shifts to favor the ^2S_O conformer (>60%).[17] In the AT-III complex, however, the IdoA2S residue of the pentasaccharide is exclusively in the ^2S_O conformation causing the "kink" observed in the otherwise linear oligosaccharide chain.[18] The 6-*O*-sulfo group at the non-reducing end GlcNS6S residue of the pentasaccharide also contributes to its AT-III binding affinity and in the crystal structure is involved in a hydrogen bond to the side chain of Arg129.[19] Although the glucuronic acid (GlcA) residue of the pentasaccharide has been reported to be neutral with respect to the binding energy,[16] the crystal structure reveals a hydrogen bond between the GlcA carboxylate moiety and the side chain of Lys125 as well as a salt bridge with Asn45.[19]

Understanding how elements of local structure impact the solution conformation of heparin oligosaccharides can potentially provide insights into the nature of heparin-protein interactions. Although oligosaccharides are thought to be flexible in solution, specific structural motifs may favor formation of intramolecular hydrogen bonds that restrict the conformation and pre-organize a local structure for high-affinity protein binding. For example, a persistent hydrogen bond involving the Arixtra GlcNS3S6S sulfamate NH was identified through ^{1}H NMR spectra examining the pH and temperature dependence of the $NHSO_3^-$ resonances in a series of heparin oligosaccharides.[20]

Molecular dynamics experiments suggested the presence of this hydrogen bond in both IdoA2S conformations of Arixtra and identified the hydrogen bond acceptor as the adjacent 3-*O*-sulfo group.[20] These molecular dynamics simulations also predicted that additional intramolecular hydrogen bonds involving the Arixtra hydroxyl protons may further stabilize its secondary structure, a possibility explored experimentally in this Chapter.

Several experimental strategies have been used to quantitatively assess hydroxyl proton hydrogen bonding in aqueous solutions of oligosaccharides. A small hydroxyl proton temperature coefficient (the slope of the line obtained by plotting chemical shift vs temperature) suggests protection from exchange with water, most likely by participation in a hydrogen bond, although chemical shift changes may also arise from conformational changes. Differences in hydroxyl proton chemical shift compared to their corresponding monosaccharide values ($\Delta\delta = \delta_{oligo} - \delta_{mono}$) can also be diagnostic of hydrogen bonding.[21] A positive $\Delta\delta$ value suggests additional hydration from other exchangeable protons while a negative $\Delta\delta$ indicates close spatial proximity of the hydroxyl proton to an electronegative atom, as would be expected in a hydrogen bond.[22] For example, through analysis of temperature coefficients, $\Delta\delta$ values and ROESY cross peaks, Vilen et al. identified hydroxyl proton hydrogen bonds in κ/μ-hybrid carrageenan that are absent in the structurally related κ-carrageenan oligosaccharides.[21] Chemical shift differences can also result from isotope participation in hydrogen bonding, which the O'Leary group used to determine the presence of hydrogen bonds in partially deuterated diols.[22]

Results of similar studies for sucrose have been more controversial. For example, Adams and Lerner evaluated sucrose in water/acetone solution using hydroxyl proton temperature coefficients, coupling constants and solvent exchange rates and concluded that intramolecular hydrogen bonds were not sufficiently persistent to be detected by NMR.[23] Poppe and van Halbeek also studied sucrose in water/acetone solution detecting interresidue NOE contacts and OH-OH ROESY chemical exchange peaks consistent with a hydrogen bond between the glucose OH2 and the fructose OH1. Although their results supported the persistence of the interresidue hydrogen bond detected in the sucrose crystal structure, Poppe and van Halbeek concluded that in solution sucrose does not behave as a rigid body but has a high degree of internal flexibility.[24] Recently, Battistel et al. reported the results of NMR measurements for a super-cooled aqueous solutions of sucrose at high concentrations (e.g. 300 mM). The ^{13}C HSQC-TOCSY experiment was used to directly detect interresidue cross peaks indicative of intramolecular hydroxyl hydrogen bonds, which were confirmed by $^{2}J_{OH\text{-}OH}$ coupling detected in the COSY spectrum.[25] MD simulations and DOSY experiments were used to discriminate intramolecular hydrogen bonding from possible aggregation-induced intermolecular hydrogen bonds. The Freedberg group used a similar experimental strategy to directly detect patterns of hydrogen bonding in a ^{15}N,^{13}C labeled α2-8 sialic acid tetramer providing direct evidence of hydrogen bonding through the CBCANH NMR experiment.[26]

Inspired by recent reports of hydrogen bonding in oligosaccharides,[21,25,27,28] and motivated by our prior molecular dynamics study,[20] we embarked on an investigation of

hydroxyl group hydrogen bonding in aqueous solutions of Arixtra. The limited quantity of Arixtra available and the necessity of performing the measurements without the benefit of ^{13}C and ^{15}N isotopic enrichment precluded the direct detection of hydrogen bonds as described by Battistel et al.[25,26] In addition, in heparin oligosaccharides we anticipate OH hydrogen bonding through *N*- or *O*-sulfate groups which would be challenging to detect through long-range couplings, especially at natural abundance levels of ^{15}N and ^{13}C.

In this study, ^{1}H NMR experiments were performed to evaluate temperature coefficients, differences in hydroxyl proton chemical shifts relative to their monosaccharide values, and solvent exchange rates for the Arixtra hydroxyl protons in aqueous solution. To accomplish our experimental objectives, the contribution of water radiation damping to the exchange rate calculations was also addressed. To our knowledge, this study provides the first experimental evidence of solution state hydrogen bonds involving the hydroxyl protons of a heparin oligosaccharide.

The quantification of hydroxyl proton-solvent exchange rates through measurement of cross peak intensity in two-dimensional chemical exchange spectroscopy (EXSY) spectra acquired as a function of mixing time can also provide evidence for hydrogen bonding.[28,29] A slower rate of increase (or build-up) of EXSY cross peak intensity indicates that a hydroxyl proton is protected from exchange with water due to hydrogen bonding. In aqueous solution, radiation damping induced by the water magnetization makes a significant contribution to the observed longitudinal relaxation of the hydroxyl protons. The observed magnetization dynamics of water and exchanging protons are governed by a radiation damped relaxation mechanism, T_{RD}, described by

Chen and Mao for the exchange of the NH protons of guanidine chloride with water.[30] Therefore, a challenge in interpreting the results of EXSY measurements for dilute aqueous solutions of heparin oligosaccharides is that analysis of the hydroxyl proton build-up curves must consider both the T_{RD} contribution as well as the hydroxyl proton T_1 relaxation rates. Here we adapt the radiation-damped exchange model of Chen and Mao to the case of 2D EXSY correlation spectroscopy. While radiation damping complicates the analysis, quantitative determination of the exchange rates are accomplished in a robust manner.

3.2 Materials and methods

3.2.1 Materials and reagents. Arixtra (fondaparinux sodium), formulated as prefilled syringes for clinical use, was obtained from the University Pharmacy and Department of Pharmacy Administration of Semmelweis University. 2,2-dimethyl-2-silapentane-5-sulfonate-d_6 sodium salt (DSS), and the GlcNS6S and D-GlcA monosaccharides were purchased from Sigma Aldrich (Saint Louis, MO). HPLC grade water was obtained from Burdick and Jackson (Muskegon, MI). Acetone-d_6 (D, 99.9%) and deuterium oxide, (D, 99.9%), deuterated hydrochloric acid, and sodium deuteroxide were purchased from Cambridge Isotope Laboratories (Andover, MA). Sodium chloride (NaCl) and sodium bicarbonate ($NaHCO_3$) were purchased from Fisher Scientific (Hampton, NH).The pH meter was calibrated with buffers 4.00, 7.00 and 10.00 purchased from Fisher Scientific.

3.2.2 Solution preparation for NMR measurements. To reduce the solvent exchange rate of the hydroxyl protons, Arixtra and monosaccharide NMR samples were prepared at concentrations of 1 – 2 mM under an N_2 atmosphere and studied at reduced temperatures in 85% H_2O/15% acetone-d_6 containing 0.15 M NaCl.[21,23] Acetone-d_6 was added to avoid freezing the sample and 0.15 M NaCl was added to allow stable measurements of pH and to control the ionic strength. Samples were prepared using deionized HPLC grade water that had been boiled to remove CO_2 that could catalyze proton exchange. Spectra were recorded as a function of pH using dilute solutions of CO_2 free HCl and NaOH and the pH was set to 8.1 for subsequent measurements. Solution pH measurements were made prior to the addition of acetone-d_6 using a Fisher Scientific AB15 pH meter with a double junction Ag/AgCl micro-pH electrode (Thermo Scientific, Beverly, MA). NMR measurements were performed in 5 mm NMR tubes using a 600 μL sample.

A separate set of Arixtra solutions were prepared to test the effects of dissolved CO_2 on hydroxyl proton exchange. Two sets of 1 mM Arixtra solutions with 0.15 M NaCl were prepared open to the atmosphere at pH 8.1 and 8.3. One set was prepared in HPLC-grade water and the other in Millipore water to compare the impact of water source. EXSY exchange rates were measured for the Millipore sample at pH 8.28. Two stock solutions of $NaHCO_3$ were prepared at concentrations of 0.030 and 0.30 M at a pH of 8.26 and slowly titrated into the Arixtra sample in 0.5 – 2 μL increments to achieve the concentrations of bicarbonate between 0.010 and 6.9 mM. The EXSY exchange rates were also measured for the same Arixtra sample after the addition of 0.59 mM $NaHCO_3$.

3.2.3 NMR measurements of Arixtra hydroxyl proton resonances. Solvent suppression was accomplished using excitation sculpting to avoid the signal attenuation often observed with WATERGATE.[31] One-dimensional NMR spectra were recorded at -14.5 °C using two Bruker 600 MHz Avance spectrometers each equipped with a TXI probe, one operating at 600.13 MHz and the second operating at 599.58 MHz.[32] Temperature coefficients were measured by recording ^{1}H NMR spectra over the temperature range -14.5 ºC to 11.5 ºC in approximately 4-5 ºC increments. The temperature was calibrated using an external methanol standard.[32] Chemical shifts were referenced using the residual ^{1}H resonance of acetone-d_6 at 2.204 ppm. The $\Delta\delta$ values for each monosaccharide were determined at -10.0 °C.

Chemical shift assignments of the Arixtra hydroxyl protons were determined using COSY and TOCSY NMR spectra recorded at -14.5 °C in 85% H_2O/15% acetone-d_6 at pH 8.1 building on the previous assignments of the carbon-bound protons.[33,34] Both spectra were recorded using excitation sculpting and States-TPPI. Spectra with 96 scans coadded into 2048 complex points in t_2 and 160 (COSY) or 144 (TOCSY) t_1 increments. The optimal TOCSY mixing time for the hydroxyl protons was found to be 60 ms. A spectral window of 7000 Hz in the F2 and 6200 Hz in the F1 dimension and a relaxation delay of 1.5 s were used for both spectra. Spectra were zero filled to 4096 x 512 data points.

EXSY spectra were acquired using the Bruker NOESY pulse program "noesyesgpph" at -14.5 ºC using excitation sculpting solvent suppression and mixing times ranging from 0 to 24 ms in 3 ms increments. 2048 complex-valued time-domain

points in t_2 and 128 complex time-domain points in t_1 were acquired using a relaxation delay of 1.5 s and the coaddition of 32 scans per t_1 increment. A spectral window of 4440 Hz was used in both F1 and F2 frequency domains. The spectra were zero-filled to 16384 x 4096 points to obtain more accurate volume integrals of the hydroxyl cross peaks and apodized using a cosine function. Build-up curves were plotted as the volume integral of the hydroxyl exchange cross peaks as a function of mixing time. The cross peak volume integrals were measured using the TopSpin 3.1 integration program and are normalized to the diagonal peak for each resonance. In cases where peaks were slightly overlapped, the volume was determined only for the portion of the cross peak that was well resolved. To provide consistency, the same chemical shift regions were used for cross peak volume integration in each experiment. Initial rate constants were calculated from the EXSY data using Bloch equations modified to include chemical exchange and to accommodate the fact that the relaxation of the water protons is governed by radiation damping, T_{RD}, as discussed below.[29,30]

3.2.4 Molecular dynamics simulations. The combined results of hydrogen-bonding analyses of five molecular dynamics (MD) simulations of Arixtra in explicit solvent are reported. One 5 ns MD simulation was previously described in Langeslay et al.[20] and the results were combined with the four additional simulations described herein. The initial heavy atom coordinates for two of the four additional simulations, 6 ns and 75 ns in duration, were extracted from the X-ray crystal structure of the bound pentasaccharide with Antithrombin-S195A factor Xa, PDB ID 2GD4.[19] The final two simulations were initiated from starting coordinates better approximating the solution

conformation of Arixtra by extracting structures from individual frames of the first MD run. These included one of each observed conformation of the IdoA2S residue, $^{1}C_{4}$ and $^{2}S_{O}$, and were additionally modified by adjusting the interglycosidic dihedral angles φ_H (H1-C1-O1-C4') and ψ_H (C1-O1-C4'-H4') to the same values listed as the free-state averages by Hricovíni et al. using the VEGA ZZ program.[18,35] The last two simulations were 9.3 ns in duration. Table 3.1 lists the average φ_H and ψ_H dihedral angles measured during each trajectory. The AmberTools 11 *xleap* module was used to parameterize Arixtra with the GLYCAM06g force field, to neutralize the system charge by adding sodium ions (ff99SB force field), and to construct a rectangular water box of TIP3P parameterized water molecules with faces extending at least 12 Å from the solute.[36-39] NAMD 2.8 was used to calculate all minimization, heating, equilibration, and production trajectories.[40] Conjugate gradient minimization was applied to the solvent, solutes, and finally the entire system to remove bad contacts. The system was heated slowly in the constant NVE ensemble from 0 to 298K in 398 ps, including a 100 ps hold at the target temperature. Equilibration and production runs were conducted in the constant NPT ensemble with a pressure of 1 atm and temperature of 298K. The temperature was maintained using the Langevin thermostat with a damping coefficient of 5 ps^{-1} and the pressure controlled by NAMD's Nosé-Hoover Langevin piston method.[40] The non-bonded interactions were cutoff at 12Å with a smooth switching function applied at 10Å. The VDW and electrostatic 1-4 scaling factors were set to unity for consistency with the GLYCAM06g parameterization.[37] Periodic boundary conditions were applied throughout and the Particle Mesh Ewald summation was employed to handle long-range

Table 3.1. Average dihedral angles in degrees (+/- std. dev.) for φ_H (H1-C1-O1-C4') and ψ_H (C1-O1-C4'-H4') observed for the indicated simulation and IdoA2S conformation (Conf.).

Simulation	Conf.[a]	Frames[b]	ϕ_H1	ψ_H1	ϕ_H2	ψ_H2	ϕ_H3	ψ_H3	ϕ_H4	ψ_H4
1	$^1C_4$	8,000	-51 (8)	-34 (9)	41 (10)	3 (11)	-36 (12)	-15 (15)	42 (10)	-4 (19)
1	^2S_O	8,901	-50 (8)	-33 (10)	44 (10)	9 (11)	-46 (14)	-39 (15)	46 (10)	7 (15)
1	$^1C_4$	31,000	-49 (8)	-31 (9)	50 (11)	14 (11)	-39 (11)	-22 (12)	38 (11)	-19 (22)
2	^2S_O	60,000	-49 (9)	-31 (9)	49 (11)	16 (11)	-49 (11)	-40 (14)	45 (11)	0 (21)
3	^2S_O	1,815	-46 (12)	-32 (10)	48 (11)	16 (10)	-48 (12)	-39 (14)	48 (10)	9 (16)
3	$^1C_4$	29,364	-48 (9)	-31 (9)	49 (11)	16 (11)	-34 (24)	-21 (17)	25 (27)	-24 (62)
3	^2S_O	2,749	-42 (13)	-29 (12)	47 (11)	16 (11)	-49 (10)	-37 (14)	48 (10)	8 (18)
3	$^1C_4$	16,632	-48 (9)	-31 (9)	40 (28)	10 (17)	-29 (29)	-18 (16)	35 (14)	-25 (21)
3	$^1C_4$	21,301	-48 (9)	-31 (10)	31 (37)	7 (21)	-23 (33)	-17 (15)	35 (18)	-21 (23)
4	^2S_O	93,000	-43 (17)	-27 (14)	48 (11)	15 (11)	-48 (11)	-38 (15)	47 (10)	8 (18)
5	$^1C_4$	32,600	-49 (9)	-32 (9)	48 (11)	15 (11)	-38 (18)	-24 (17)	39 (10)	-21 (22)
5	^2S_O	14,548	-49 (8)	-31 (9)	49 (11)	18 (10)	-47 (11)	-36 (14)	46 (10)	2 (22)
5	$^1C_4$	44,996	-49 (8)	-31 (9)	48 (12)	15 (11)	-39 (14)	-18 (16)	41 (11)	-13 (25)

[a]Conf. indicates the conformation of the IdoA2S residue.

[b]Frames indicates the number of frames included in the analysis. In simulations where conformational changes of the IdoA2S residue occurred the trajectories were divided per conformation and the transition periods ommitted from the hydrogen bonding analysis.

electrostatics with a grid spacing of 1 Å.[41] Only the hydrogen-oxygen bonds within water molecules were held rigid using the SETTLE algorithm.[42] All simulations were integrated in 1 fs time steps. The trajectory output was saved every 1000 fs for the 75 ns duration simulation and every 100 fs for all other simulations. VMD 1.9 was used for the visualization of trajectories as well as to monitor temperature, pressure, and energy data.[43] AmberTools 11 *ptraj* module was used to compute dihedral angles, interatomic distances, and to analyze hydrogen bonding.[36] The hydrogen bonding analysis included a 3.5 Å heavy atom cutoff distance and a 120° angle cutoff. M. Forster's *mdxvu* program was used to compute and monitor the Cremer-Pople ring puckering parameters of all five rings over the course of the simulation production runs.[44] In three of the five simulations, the IdoA2S residue was observed to transition between the $^{2}S_{O}$ and $^{1}C_{4}$ conformations. The trajectories where this occurred were divided according to IdoA2S conformation and the periods corresponding to the transitions, which took place in less than 14 ps each, were excluded from the hydrogen bonding analyses. Plots of the Cremer-Pople θ parameter versus time for each monomer and histograms of the φ_2 parameter for the IdoA2S residue when in the $^{2}S_{O}$ conformation are found in Figure 3.1. The results of the hydrogen bonding analyses per IdoA2S conformation were then weighted by frames and averaged. In terms of frames from the resulting MD trajectories, the population ratio of $^{2}S_{O}$ to $^{1}C_{4}$ conformers observed for the IdoA2S residue was approximately 50:50. Experimental studies of Arixtra in solution indicate that the ratio of IdoA2S conformations best satisfying observed $^{3}J_{HH}$ coupling constants is approximately 60:40 ($^{2}S_{O}$:$^{1}C_{4}$).[45,46] The results of the hydrogen bonding analysis indicated that some hydrogen

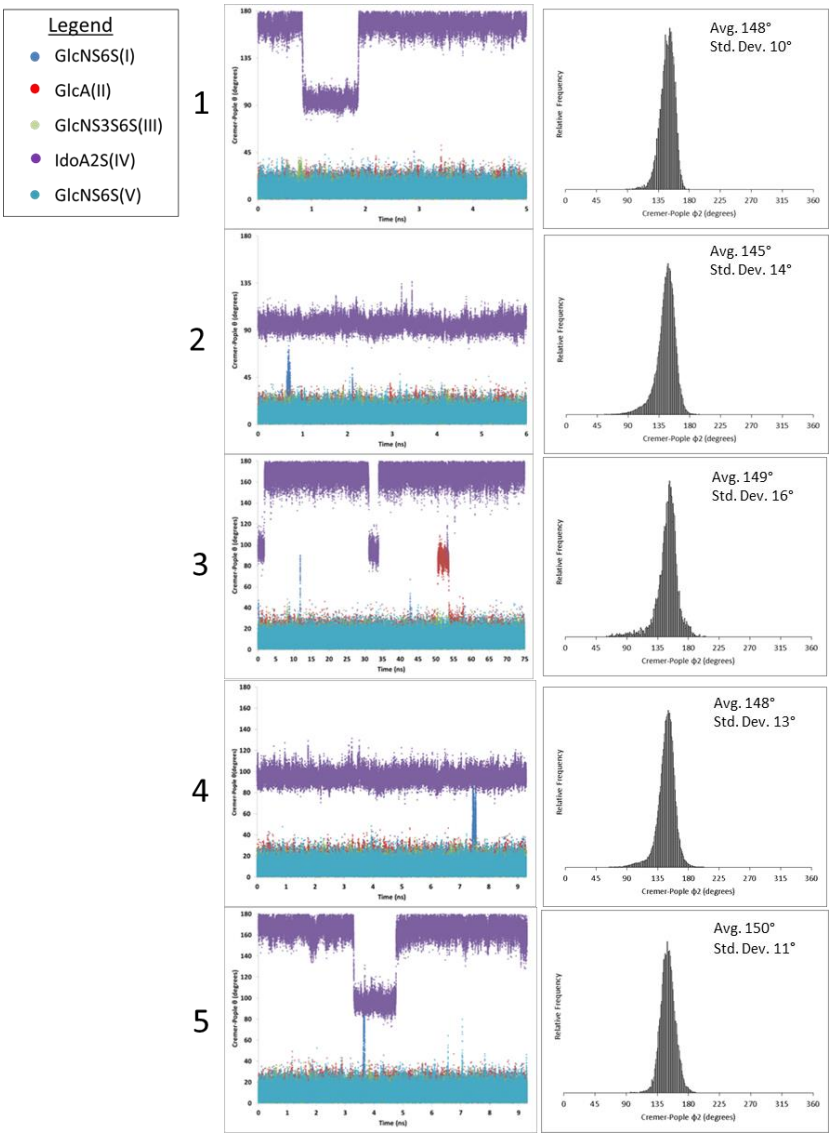

Figure 3.1. Plots of the Cremer-Pople θ parameter versus time (left) and histograms (right) of the IdoA2S residue φ2 parameter for the $^{2}S_{O}$ conformational state for the five MD simulations analyzed in this study.

bonds are affected by the conformation of the IdoA2S residue and, therefore, to compute overall average hydrogen bond occupancy percentages, the weights of 60:40 $^{2}S_{O}$:$^{1}C_{4}$ were applied.

3.3 Results and discussion

3.3.1 Challenges in solution preparation. The fast exchange rates of the hydroxyl protons make optimizing solution conditions a challenge. Previous studies of hydroxyl protons were conducted in unbuffered solutions composed of 85% H_2O (CO_2 free)/15% acetone-d_6 to be able to reduce the temperature to below the freezing point of water.[21,23,24,27] Adams and Lerner demonstrated that a low concentration of acetone does not significantly affect the relative temperature coefficients and exchange rates of sugar hydroxyl protons.[23,24] Unlike the amide and sulfamate protons which can be detected in the presence of a phosphate buffer, buffers catalyze the exchange of the hydroxyl protons.[25] Maintaining, and even measuring, a stable pH in unbuffered aqueous solutions is very difficult. Addition of 0.15 M NaCl was found to enhance the stability of the pH measurements and the reproducibility of the spectral measurements. It should also be noted, however, that chemical exchange is strongly influenced by solution composition, pH, and temperature so that care must be taken when directly comparing the hydroxyl proton exchange between two solutions.[27]

Solution preparation was initially conducted under an N_2 atmosphere in a glovebox in an attempt to reduce contamination by CO_2. Dissolved CO_2 forms carbonic

acid (H_2CO_3) or bicarbonate (HCO_3^-) in solution that can catalyze hydroxyl proton exchange.[23,27] Dissolved CO_2 was removed by boiling the HPLC-grade water followed by bubbling with N_2. The solution was allowed to cool in a capped vial prior to the addition of any solute. An antistatic mat was used to alleviate the static build-up caused by the dry N_2 environment of the glove box that could potentially interfere with pH readings.

3.3.2 Detection and identification of hydroxyl protons by NMR. An NMR pH titration of the Arixtra hydroxyl protons was performed to determine the optimum pH for their detection by ^{1}H NMR. Arixtra hydroxyl resonances were observed to be most intense over the pH range 7.8 - 8.8 (Figure 3.2), which is consistent with the optimum conditions for measurement of the Arixtra exchangeable NH resonances of the GlcNS sulfamate ($NHSO_3^-$) groups.[20,47,48] The optimum pH chosen for the hydroxyl proton hydrogen bonding experiments was pH 8.1. The use of excitation sculpting for solvent suppression works well for the detection of exchangeable protons by NMR.[31]

The structure of Arixtra with its residues labeled is shown in Figure 3.3A. The position of the individual monosaccharide residues within the oligosaccharide is indicated by a Roman numeral, starting from the non-reducing end. Visual examination of Figure 3.3B reveals differences in the line widths of the six Arixtra hydroxyl protons, which are each in a different chemical environment. For some protons, the resonances are sufficiently sharp so that even small couplings are resolved, while other peaks are broader, suggesting differences in the solvent exchange rate within a given oligosaccharide. Chemical shift assignments of the Arixtra hydroxyl protons were

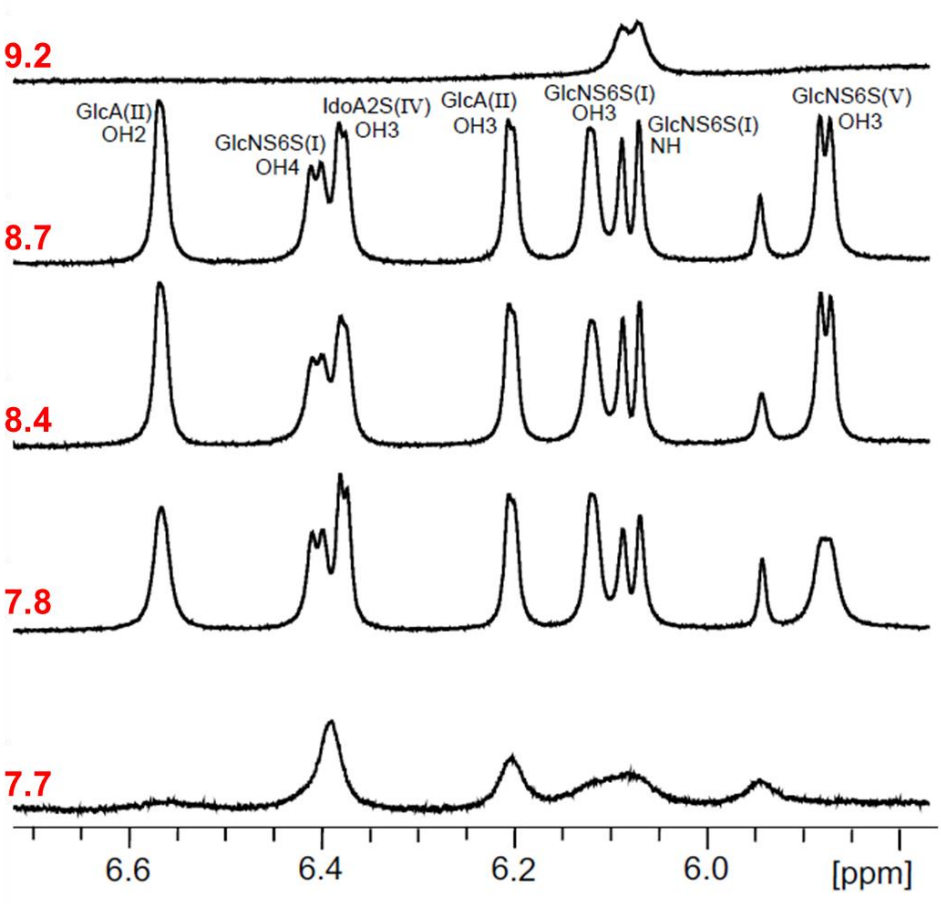

Figure 3.2. The pH dependence of the Arixtra hydroxyl proton NMR resonances.

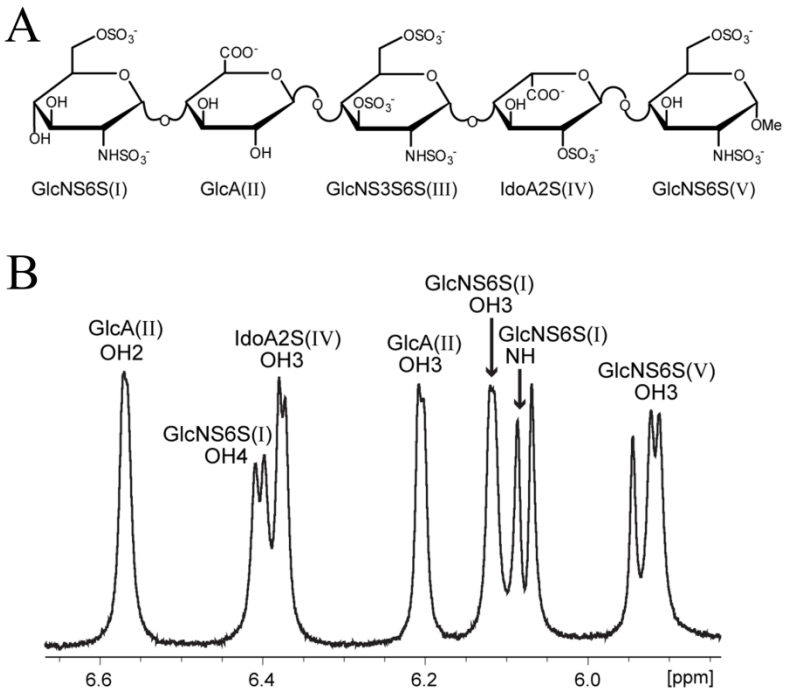

Figure 3.3. (A) Structure of Arixtra with residues labeled. (B) ^{1}H NMR spectrum of Arixtra measured in 85% H_2O/15% acetone-d_6 at pH 8.1 and -14.5 C with hydroxyl and sulfamate proton resonances indicated.

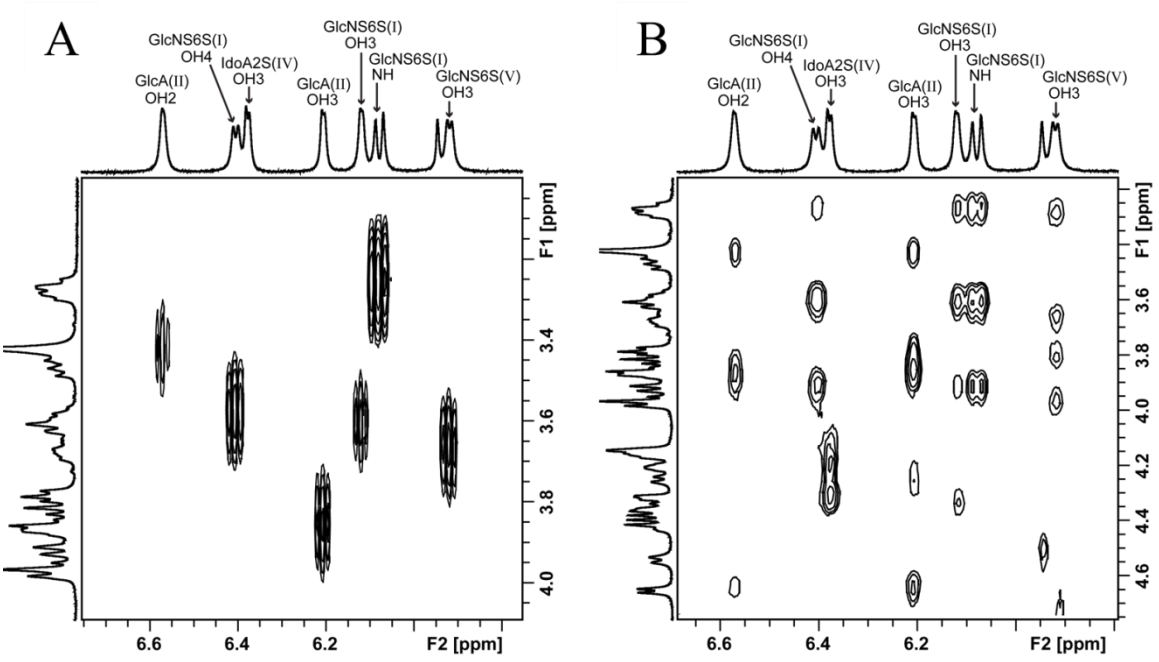

Figure 3.4. (A) COSY and (B) TOCSY spectra of Arixtra used to assign hydroxyl proton resonances at -14.5 °C in 85% H_2O/15% acetone-d_6 and pH 8.1.

determined using the COSY (Figure 3.4A) and TOCSY (Figure 3.4B) NMR spectra with excitation sculpting solvent suppression at pH 8.1.[33,34] Assignments were made based on previously reported carbon-bound proton chemical shifts.[49,50] The Arixtra hydroxyl proton chemical shifts are summarized in Table 3.2.

3.3.3 Proton exchange with solvent in the presence of radiation damping. In 2D exchange correlation spectroscopy (Figure 3.5A),[51] the cross peak intensity shows a time response that depends on the exchange rate and the spin relaxation properties. In this case the suppression of the solvent resonance is applied directly after the mixing period. For analyte protons undergoing exchange with water in aqueous solution, this process is complicated by radiation damping – the significantly enhanced drive to equilibrium for intense resonances in highly concentrated solutions.[30,52,53] In radiation damping, the large transverse sample magnetization induces a substantial signal voltage across the detection coil, which in turn generates a magnetic "reaction" field 90^{o} out of phase with the transverse component, rotating it back toward alignment with the field in a nearly selective manner. Because of this, proton spins in water do not relax exponentially, but with a rate proportional to their transverse magnetization, complicating the analysis of EXSY cross-peaks.

Chen and Mao demonstrated that quantitative analysis of exchange is still possible (and is some ways enhanced) under radiation damping.[30,54] Here we adapt their analysis to the problem of cross-peak intensity in the EXSY experiment. The cross-peak of interest is that from water to the analyte and in our experiments the water is placed on resonance – a requirement in the analysis that follows, which assumes that the bulk water

Table 3.2. Arixtra hydroxyl proton chemical shift assignments in 85% H_2O/15% acetone-d_6 at pH 8.1 and -14.5 °C.

Hydroxyl Proton	Chemical shift (ppm)
GlcNS6S(I) OH3	6.117
GlcNS6S(I) OH4	6.403
GlcA(II) OH2	6.568
GlcA(II) OH3	6.204
IdoA2S(IV) OH3	6.375
GlcNS6S(V) OH3	5.916

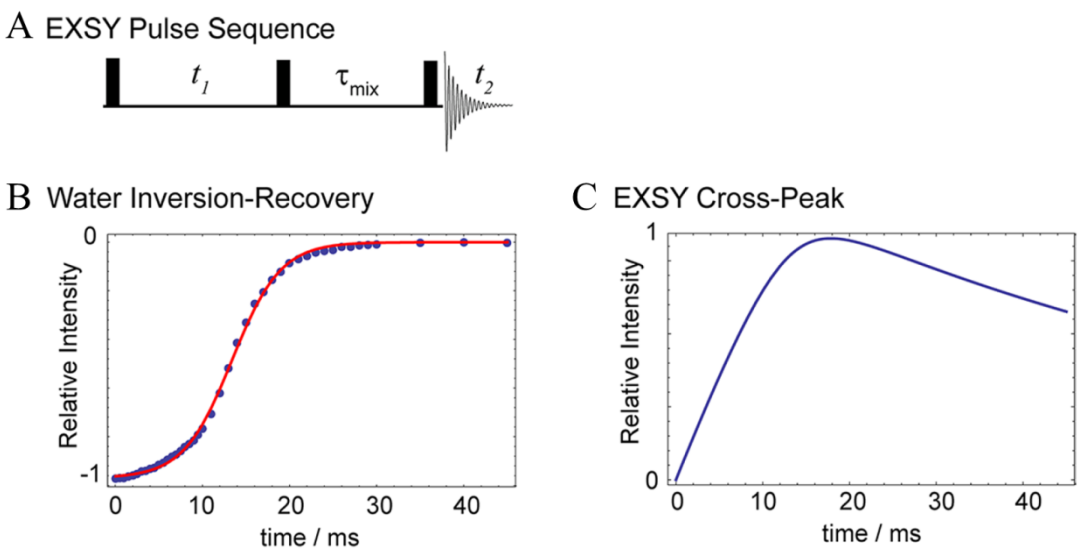

Figure 3.5. (A) Pulse sequence for 2D exchange correlation spectroscopy (EXSY). (B) Inversion recovery of water magnetization performed and phase cycled using the EXSY pulse sequence with $t_1 = 0$ and τ_{mix} varied. The blue data points were fit by Eq. 3.2 to give T_{RD} = 5.5 ms and t_0 = 13.4 ms. (C) Intensity predicted from Eq. 3.5 for a cross-peak between water (subject to radiation damping with T_{RD} = 5.5 ms and t_0 = 13.4 ms) and an analyte with k = 15 s^{-1}.

magnetization is aligned either parallel or antiparallel to the magnetic field at the start of τ_{mix}. Indeed, to suppress zero-frequency artifacts in the indirect dimension (due to relaxation during t_1 and τ_{mix}), standard phase cycling in EXSY experiments alternately places the water magnetization along and against the field, with a corresponding 180° phase shift of the receiver.[55] For full inversion of the water resonance, the z-magnetization recovers under radiation damping according to

$$M_{H_2O,z}(t) = M^o_{H_2O,z} \tanh[(t - t_0)/T_{RD}], \quad (3.1)$$

where $M^o_{H_2O,z}$ is the net equilibrium magnetization, $1/T_{RD}$ is the radiation damping rate constant, t_0 is the latency interval that is related to the initial angular deviation of the inversion from 180°, and T_1 relaxation of water is ignored.[53] When the magnetization is placed in alignment with the field, the radiation damping mechanism is not operative and the bulk magnetization persists. Thus, the net water decay in the EXSY experiment has the form

$$M_{H_2O,z}(t) = M^o_{H_2O,z}\{\tanh[(t - t_0)/T_{RD}] - 1\}/2. \quad (3.2)$$

Figure 2B shows a simple inversion recovery experiment, phase cycled as described above and using the pulse sequence shown with t_1=0. This signal is fit well by Eq. 3.2 with T_{RD} = 5.5 ms and t_0 = 13.4 ms.

During the mixing time of the EXSY experiment, protons exchange between water and the analyte. Because of the vastly different concentrations of the analyte (<2 mM) and water (55 M x 2 protons per water molecule), exchange with the analyte does not significantly perturb the water magnetization, and Eq. 3.2 continues to be an excellent

model for the water nuclear spin magnetization. The build-up of cross-peak intensity from water to the analyte can then be written:

$$\begin{aligned}\frac{dM_{\text{analyte},z}(t)}{dt} &= -k\,M_{\text{analyte},z}(t) - \frac{M_{\text{analyte},z}(t)}{T_1} + k\,X_{analyte}\,\frac{M_{\text{H}_2\text{O},z}(t)}{2} \\ &= -k\,M_{\text{analyte},z}(t) - \frac{M_{\text{analyte},z}(t)}{T_1} + \frac{k\,X_{analyte}\,M^{o}_{\text{H}_2\text{O},z}}{4}\left\{\tanh\left[(t-t_0)/T_{\text{RD}}\right]-1\right\}, \\ &= -k\,M_{\text{analyte},z}(t) - \frac{M_{\text{analyte},z}(t)}{T_1} + \frac{k\,M^{o}_{analyte,z}}{2}\left\{\tanh\left[(t-t_0)/T_{\text{RD}}\right]-1\right\}\end{aligned} \quad (3.3)$$

where k is the proton exchange rate from the analyte to water, X_{analyte} is the mole fraction of analyte (note that $k\,M^{\text{o}}_{\text{analyte},z} = k\,X_{analyte}\,M^{\text{o}}_{\text{H}_2O,z}/2$ follows from detailed balance), and $1/T_1$ is the analyte longitudinal relaxation rate. This equation can be integrated (performed here within Mathematica[56]) subject to the cross-peak initial condition, $M_{\text{analyte},z}(0)=0$, to give a closed from solution in terms of the generalized hypergeometric function ${}_2F_1$(a,b; c; x)[57]

$$\begin{aligned}\frac{M_{\text{analyte},z}(t)}{M^{o}_{\text{analyte},z}} &= \frac{\left\{1-e^{-(k+1/T_1)t}\right\}kT_1}{1+kT_1} + \frac{e^{2(t-t_0)/T_{RD}}kT_1}{1+kT_1+2T_1/T_{RD}}\;{}_2F_1\left(1,\frac{1+kT_1+2T_1/T_{RD}}{2T_1/T_{RD}};\frac{1+kT_1+4T_1/T_{RD}}{2T_1/T_{RD}};-e^{2(t-t_0)/T_{RD}}\right) \\ &\quad + \frac{e^{-(k+1/T_1)t-2t_0/T_{RD}}kT_1}{1+kT_1+2T_1/T_{RD}}\;{}_2F_1\left(1,\frac{1+kT_1+2T_1/T_{RD}}{2T_1/T_{RD}};\frac{1+kT_1+4T_1/T_{RD}}{2T_1/T_{RD}};-e^{-2t_0/T_{RD}}\right)\end{aligned} \quad (3.4)$$

One additional approximation that is typically valid for small molecules is that the longitudinal relaxation time of the analyte is much longer than T_{RD} and $1/k$, allowing Eq. 3.4 to be written

$$\begin{aligned}\frac{M_{\text{analyte},z}(t)}{M^{o}_{\text{analyte},z}} &= 1-e^{-kt} + \frac{e^{2(t-t_0)/T_{RD}}k}{k+2/T_{RD}}\;{}_2F_1\left(1,\frac{2+kT_{RD}}{2};\frac{4+kT_{RD}}{2};-e^{2(t-t_0)/T_{RD}}\right) \\ &\quad + \frac{e^{-kt-2t_0/T_{RD}}k}{k+2/T_{RD}}\;{}_2F_1\left(1,\frac{2+kT_{RD}}{2};\frac{4+kT_{RD}}{2};-e^{-2t_0/T_{RD}}\right)\end{aligned}. \quad (3.5)$$

In the fits described below, we find negligible differences in the extracted rate constants k and radiation damping parameters T_{RD} and t_0 using either Eq. 3.4 or Eq. 3.5, with nearly identical qualities of fit.

As an example, Figure 3.5C shows the predicted time response of the cross-peak intensity using the radiation damping parameters from Figure 3.5B and an exchange rate of 15 s^{-1}. Initially, radiation damping is slow and the cross-peak intensity increases with a rate

$$\frac{d}{dt}\left(\frac{M_{\text{analyte},z}(t)}{M^{o}_{\text{analyte},z}}\right)_{t=0} = \frac{k}{2}\left\{1+\tanh\left[t_0 / T_{\text{RD}}\right]\right\} \approx k\,. \tag{3.6}$$

But a characteristic of radiation damping is that the solvent magnetization quickly transitions from full polarization to zero between times t_0-T_{RD} and t_0+T_{RD}. This rapid depletion of source magnetization coincides with the cross-peak reaching its maximum intensity and then decaying exponentially under the influence of exchange and T_1. At first sight, radiation damping might seem to complicate the analysis of exchange; but upon further examination, the switching off of the solvent magnetization and subsequent free decay of the analyte magnetization provides a robust mechanism for segregating the effect of exchange and the relaxation properties of water and the analyte. The process of extracting the exchange rate is made even more straightforward if an independent measurement of T_{RD} and t_0 is made, as we do below for the sample mixtures of Arixtra in water.

3.3.4 Molecular dynamics simulations. The results of the hydrogen bonding analyses of the five MD simulations are summarized in Table 3.3 and in Figure 3.6 as the

Table 3.3. Combined results of MD hydrogen bonding analyses as percent (%) of frames occupied per IdoA2S residue conformation and overall (*weighted 60% $^{2}S_{O}$ and 40% $^{1}C_{4}$). Only hydrogen bonds with a percent occupancy of greater than 20% for either conformation are listed.

Donor	Acceptor	$^{2}S_{O}$	$^{1}C_{4}$	Overall*
GlcA(II)3OH	GlcNS6S(I) 2-*N*-sulfo	85	92	88
GlcNS3S6S(III) 2NH	GlcNS3S6S(III) 3-*O*-sulfo	89	63	79
IdoA(IV) 3OH	GlcNS3S6S(III) *N*-sulfo	35	2	22
IdoA(IV) 3OH	IdoA2S(IV) 2-*O*-sulfo	49	0	29
GlcNS6S(V) 3OH	IdoA(IV) O5 (ring oxygen)	32	61	43

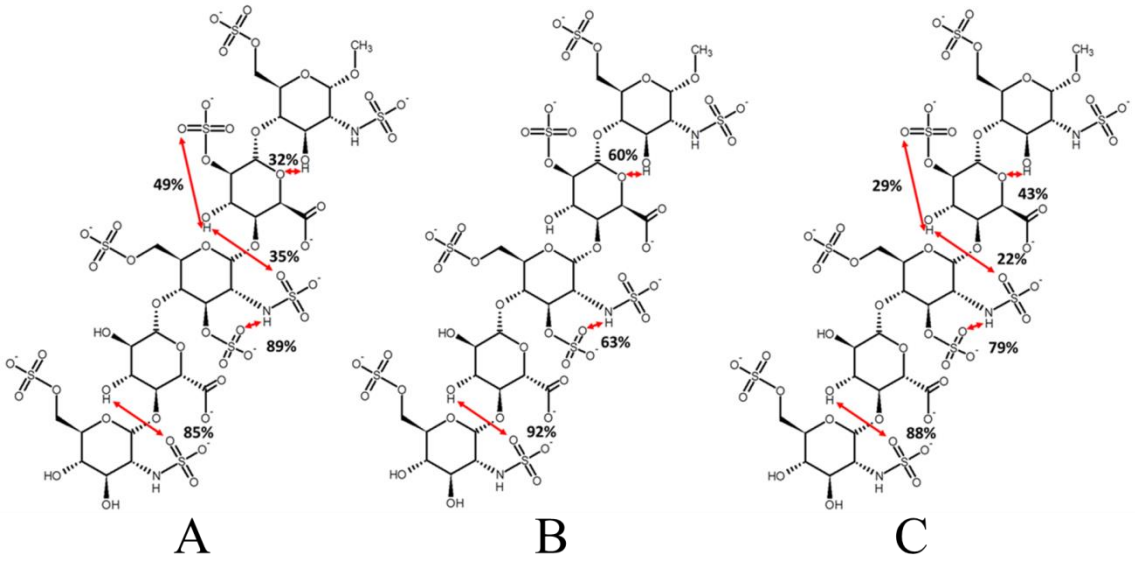

Figure 3.6. Graphical depiction of intramolecular hydrogen bonding predicted from MD simulations of Arixtra as a percentage lifetime of frames occupied by the IdoA2S residue conformations (A) $^{2}S_{O}$, (B) $^{1}C_{4}$, and (C) overall (weighted 60% $^{2}S_{O}$ and 40% $^{1}C_{4}$). Only the hydrogen bonds with percentage occupancies greater than 20% are depicted.

percent of frames in which the given hydrogen bonds were detected. Only hydrogen bonds detected at greater than 20% occupancy for either conformation are listed in the table. Although numerous intramolecular hydrogen bonds were detected, only four hydrogen bond donors, GlcA(II)OH3, GlcNS3S6S(III)NH2, IdoA2S(IV)OH3, and the GlcNS6S(V)OH3, were consistently involved in hydrogen bonds with an overall combined percent occupancy of greater than 40%. The next highest occupancy was 12%. The IdoA2S(IV)3OH was observed to alternate its hydrogen bond donation between the GlcNS3S6S(III) 2-sulfamate oxygen atoms and the IdoA2S(IV) 2-sulfo oxygen atoms when in the $^{2}S_{O}$ conformation that, when weighted 60% $^{2}S_{O}$ and 40% $^{1}C_{4}$, still resulted in an overall occupancy of 51%.

3.3.5 Hydroxyl proton temperature coefficients and chemical shift differences. To investigate experimentally the occurrence of the hydroxyl hydrogen bonds predicted by our MD simulations, Arixtra hydroxyl proton resonance temperature coefficients, chemical shift differences, and relative rates of chemical exchange with water were compared. The temperature dependence of the ^{1}H NMR resonances of exchangeable protons can provide a qualitative indication of hydrogen bonding.[20,23,58-60] As illustrated in Figure 3.7, the Arixtra hydroxyl resonances broaden and shift linearly upfield as the temperature is increased. Visual inspection of the spectra in Figure 3.7 shows differences in the extent of line broadening as the temperature is raised. The line widths of the IdoA2S(IV)OH3 and GlcA(II)OH3 resonances increase more gradually than the other OH resonances as the temperature increases. The temperature coefficients, calculated as the change in chemical shift as a function of temperature, are summarized in Table 3.4.

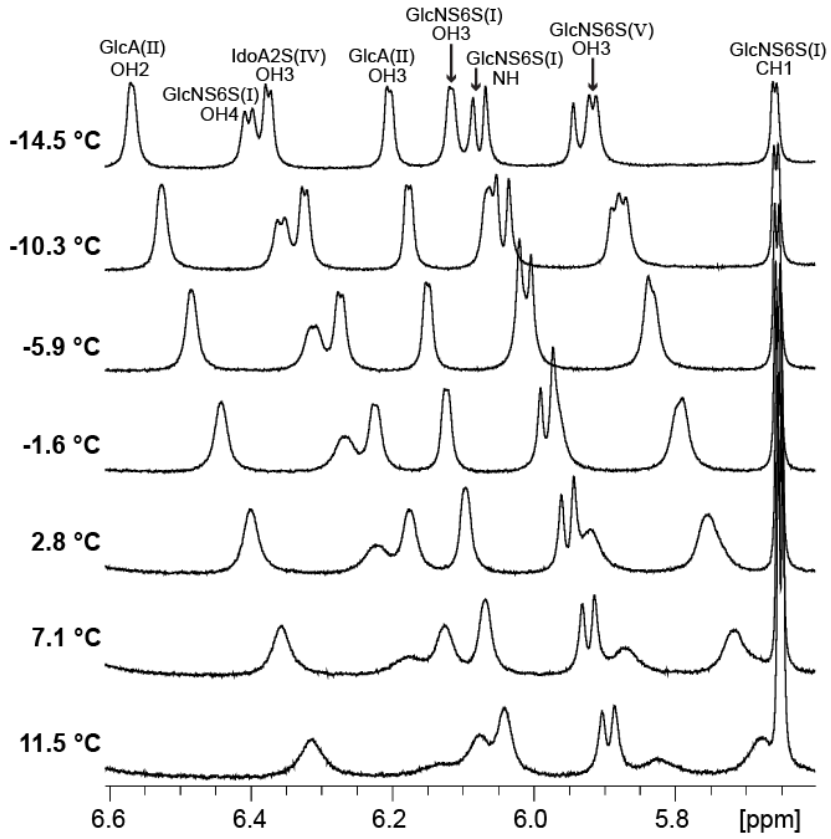

Figure 3.7. Exchangeable hydroxyl and sulfamate proton resonances of Arixtra experience a linear shift toward the water resonance as the temperature increases, whereas the resonances of the carbon-bound protons are unaffected. Exchange broadening of the hydroxyl proton resonances is also observed as the temperature is increased.

Table 3.4. Chemical shift differences, temperature coefficients, and exchange rate constants of the Arixtra hydroxyl protons. N/A indicates that the result was not available.

Hydroxyl Proton	Temperature Coefficient (ppb/K)	Δδ (ppm)	Initial Build-Up Rate (k_{ex}, s^{-1})
GlcNS6S(I) OH3	11.2	-0.008	13.8
GlcNS6S(I) OH4	10.5	-0.160	14.2
GlcA(II) OH2	9.9	-0.006	22.6
GlcA(II) OH3	6.4	-0.278	4.72
IdoA2S(IV) OH3	11.4	N/A	5.73
GlcNS6S(V) OH3	9.1	-0.199	25.9

The GlcA(II) OH3 resonance has the smallest temperature coefficient, 6.4 ppb/K, with the other hydroxyl resonances producing temperature coefficients greater than 9 ppb/K. This result suggests a qualitatively different environment for the GlcA(II)OH3, consistent with the results of the molecular dynamics simulation (Figure 3.6) which showed this OH group to be involved in a persistent hydrogen bond with the GlcNS6S(I) sulfamate group. Although the MD simulations also predict a hydrogen bond involving the IdoA2S(IV)OH3 hydroxyl proton, this is not reflected in the temperature coefficient measured for this resonance. The MD simulation suggests that the IdoA2S(IV)OH3 hydrogen bond alternates between two different sulfate groups which could be responsible for the larger temperature coefficient (11.4 ppb/K) of this resonance.

A large negative deviation in the chemical shift of an oligosaccharide hydroxyl proton resonance relative to is value in the corresponding monosaccharide can be indicative of close spatial proximity to an electronegative atom, as expected in a hydrogen bond.[21,27] The $\Delta\delta$ ($\Delta\delta = \delta_{oligo} - \delta_{mono}$) values of the hydroxyl protons in each Arixtra residue are summarized in Table 3.4. Unfortunately, the IdoA2S monosaccharide was not available, so the chemical shift comparison for this residue is omitted from Table 3.4. In Arixtra, the GlcA(II)OH3 has the largest $\Delta\delta$ value, -0.278 ppm, which is consistent with its reduced temperature coefficient and the hydrogen bond predicted by the MD simulations. We also observed a large $\Delta\delta$ value (-0.199 ppm) for GlcNS6S(V)OH3 though the chemical shift of the non-reducing end GlcNS6S(I)OH3 is very close to that of the monosaccharide. As highlighted in Figure 3.6, the MD simulations predict the GlcNS6S(V)OH3 proton to be involved in a hydrogen bond with

the IdoA2S 5O ring oxygen 43% of the time (Table 3.2). To provide more conclusive evidence of hydrogen bonding we turned to differences in the rates of chemical exchange of the hydroxyl protons with water.

3.3.6 Solvent exchange rates. Chemical exchange of the sugar hydroxyl and water protons produces prominent exchange cross peaks in the EXSY spectra of oligosaccharides in aqueous solution. Examination of the relative intensities of the exchange cross peaks of the Arixtra hydroxyl proton resonances, shown in Figure 3.8, suggests differences in their solvent exchange rates, especially for GlcA(II)OH3 which gives rise to a much weaker cross peak than the other hydroxyl groups. Exchange rates were calculated from the buildup curves (Figure 3.9) for each of the Arixtra hydroxyl protons and are summarized in Table 3.4.[29,51] The largest exchange rates were measured for GlcA(II)OH2 (22.6 s^{-1}) and GlcNS6S(V)OH3 (25.9 s^{-1}) while intermediate rate were observed for the non-reducing end GlcNS6S(I)OH3 (13.8 s^{-1}) and OH4 (14.2 s^{-1}). Although the large $\Delta\delta$ value (-0.199 ppm) for GlcNS6S(V)OH3 and the MD simulation suggested partial involvement of this hydroxyl proton in a hydrogen bond, this is not supported by its exchange rate. In an MD study of factors influencing the conformational preference of the IdoA2S residue, Pol-Fachin and Verli also indicated the presence of a hydrogen bond in IdoA2S(1→4)GlcNS6S disaccharides between the OH3 of the GlcNS6S residue and the IdoA2S residue's ring oxygen in both IdoA2S conformations, as predicted in this work.[61] The GlcA(II)OH3 and IdoA2S(IV)OH3 hydroxyl protons have the lowest exchange rate constants of 4.72 and 5.73 s^{-1}, respectively. The small exchange rate constant, along with the reduced temperature coefficient and $\Delta\delta$ value

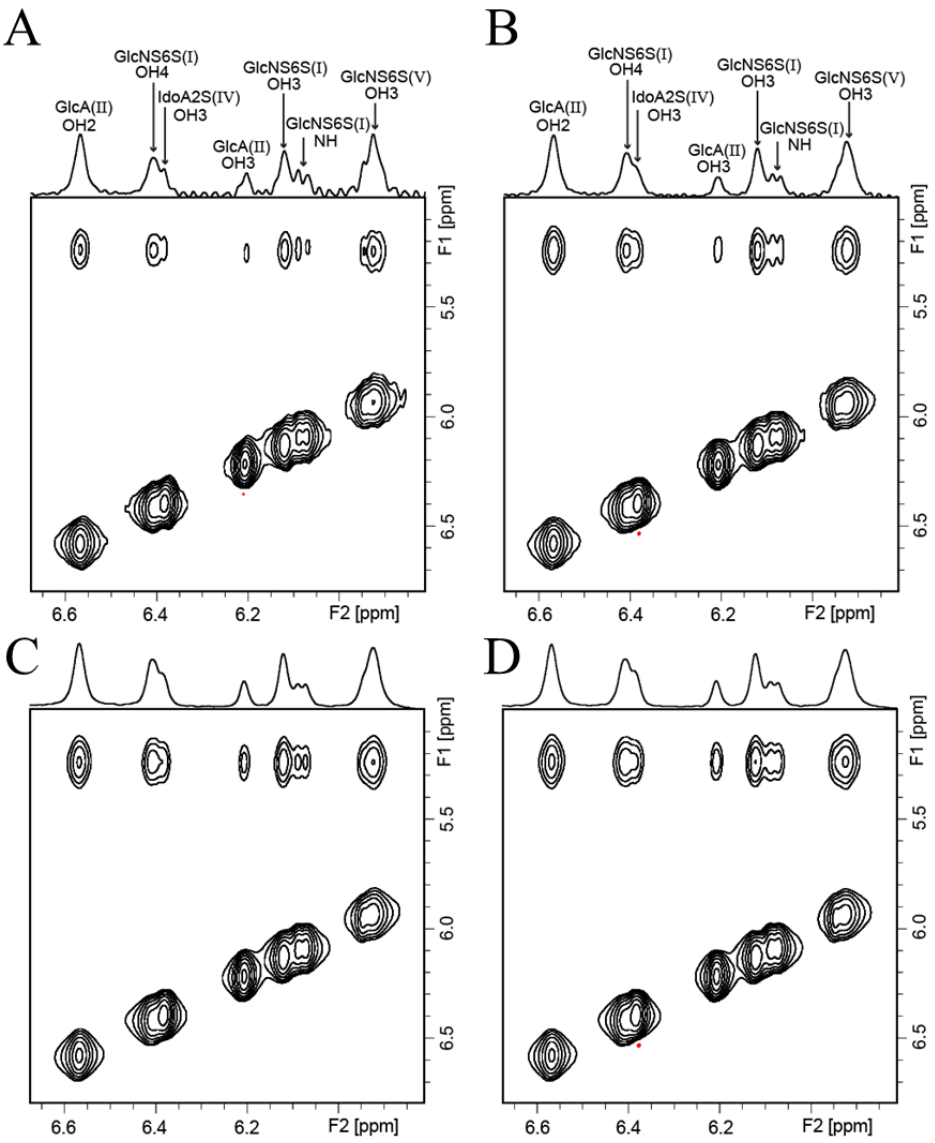

Figure 3.8. EXSY spectra of Arixtra at mixing times of (A) 6 ms, (B) 12 ms, (C) 18 ms, (D) 24 ms showing differences in the exchange cross-peak intensity of each hydroxyl proton. Traces through the exchange cross-peaks at the water chemical shift (5.2 ppm) are plotted at the top of each contour map. Note the lower intensity of the GlcA(II) OH3 exchange cross-peak relative to the other hydroxyl protons.

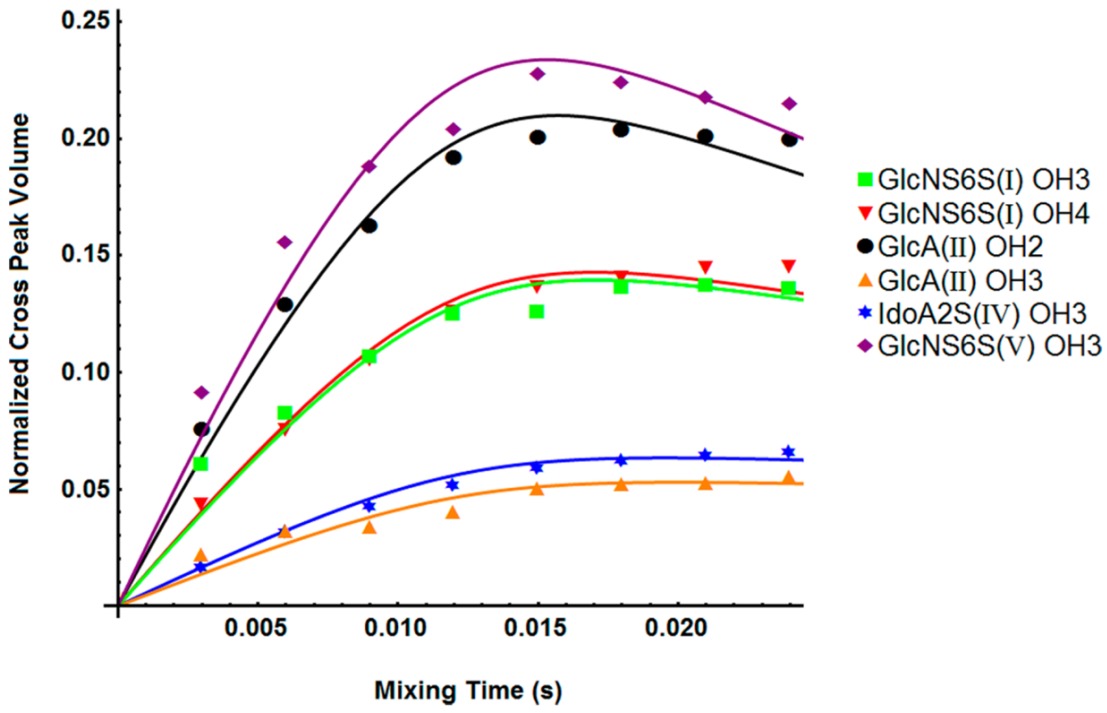

Figure 3.9. Exchange cross-peak intensity of the Arixtra hydroxyl protons as a function of mixing time. The lower build-up rate observed for the GlcA(II) OH3 and IdoA2S(IV) OH3 protons suggests their involvement in a hydrogen bond, consistent with the predictions of the MS simulations in Figure 3.6.

together provide strong evidence for a GlcA(II)OH3 hydrogen bond, which was predicted in 88% of the structures calculated in the MD simulations. The low exchange rate measured for the IdoA(IV)OH3 hydroxyl proton also suggests that it may be involved in hydrogen bond despite its larger temperature coefficient. The MD simulations indicate that the IdoA2S(IV)OH3 is involved in a hydrogen bond roughly 51% of the time, switching between the GlcNS3S6S and IdoA2S sulfate groups, which may explain its higher temperature coefficient. The two strongest hydroxyl hydrogen bonds found in Arixtra are that of the GlcA(II)OH3 and IdoA2S(IV)OH3 protons. In addition to the interaction the GlcA carboxyl group with AT-III,[19,62] its participation in a hydroxyl proton hydrogen bond may also help stabilize the secondary structure of Arixtra for binding to AT-III. Similarly, the participation of the IdoA2S(IV) residue in a hydroxyl proton hydrogen bond may stabilize its conformational shift towards the $^{2}S_{O}$ conformation to prepare it for binding to AT-III.[20,63]

3.3.7 Effects of dissolved CO_2 and bicarbonate on hydroxyl proton exchange rate measurements. The reproducibility of the EXSY exchange rate constant measurements was tested by preparing five different Arixtra solutions over a range of pH values between 7.67 and 8.50. Hydroxyl proton resonances were sharp in the spectra measured for some samples, but broad in others and did not follow a clear trend with pH (Figure 3.10). The fact that these solutions were prepared in exactly the same manner led us to suspect that the poor reproducibility of our data might arise from contamination by dissolved CO_2.

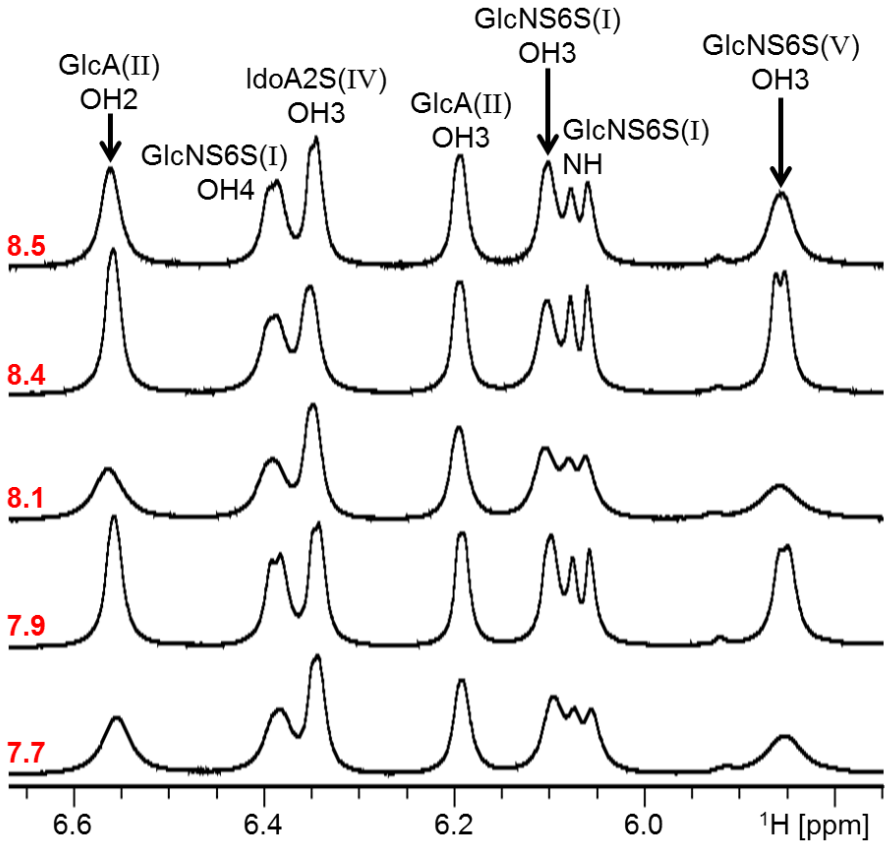

Figure 3.10. A pH titration of Arixtra hydroxyl protons from 7.67 to 8.50 with resonances labeled. Samples were prepared on separate days and are composed of 85% H_2O/15% acetone-d_6 and 0.15 M NaCl at a temperature of -14.6 °C.

In an attempt to reduce the extent of contamination from dissolved CO_2, our samples were prepared with ultra-high purity (UHP) N_2 instead of the industrial-grade N_2 that was originally utilized.[64] To our surprise, we found that UHP N_2 actually appeared increased the rate of hydroxyl protons exchange, as evidenced by broader resonances compared to the spectra obtained with industrial grade N_2 (Figure 3.11A). We were even more surprised to find that the NMR spectra of solutions prepared open to the atmosphere were much sharper and more reproducible than those previously prepared in an N_2 atmosphere and by bubbling the solution with N_2 (Figure 3.11B). We found that the most common contaminants regulated in N_2 tanks are O_2, moisture, and hydrocarbons, but that CO_2 is not monitored by the supplier. This led us to hypothesize that bubbling our solutions with N_2 introduced CO_2 which was responsible for our sample to sample variability. Note that dissolved CO_2 can introduce variability in our experiments through two mechanisms. First, since our samples do not contain a buffer, dissolved CO_2 (H_2CO_3) can alter the solution pH, and as shown in Figure 3.2, pH has a marked effect on the quality of the spectra observed. In addition, H_2CO_3, or more likely HCO_3^-, the dominant species in neutral to slightly basic pH solution, can catalyze hydroxyl proton exchange. The relatively consistent (and apparently lower) CO_2 content in samples prepared open to the atmosphere produced spectra with less variability than those prepared in a N_2 atmosphere.

To test the hypothesis that dissolved CO_2 introduced by the N_2 used in the preparation of our samples was responsible for variability in our results, an Arixtra sample was prepared at pH 8.3 open to the atmosphere and a series of EXSY experiments

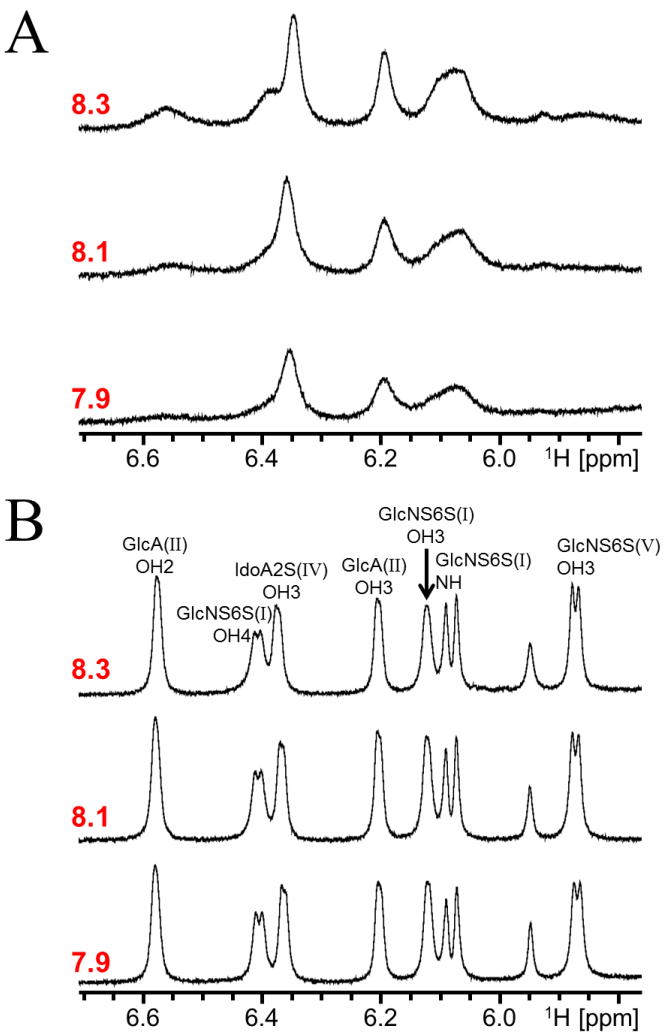

Figure 3.11. A pH titration of Arixtra hydroxyl protons (A) after the solution had been bubbled with ultra-high purity (UHP) N_2 and prepared in a glove box and (B) without bubbling with N_2 and preparing solutions open to the atmosphere. Solutions were measured in 85% Millipore H_2O/15% acetone-d_6 at -14.6 °C.

was performed to measure initial hydroxyl proton exchange rates. We then added a $NaHCO_3^-$ solution at pH 8.26 to the sample in 0.5 - 2 μL increments achieving concentrations between 0.010 and 6.9 mM HCO_3^- and recorded the ^1H NMR spectra of these solutions (Figure 3.12). As $NaHCO_3^-$ is a buffer in this pH range, its addition allowed us to evaluate the extent to which it catalyzes the exchange of the hydroxyl protons without having to worry about changes resulting from changes in pH. It was observed that, in general, the hydroxyl proton resonances become broader with the addition of HCO_3^-. However, it is interesting that as the HCO_3^- is added, the both the GlcA(II)OH2 and GlcN6S(V)OH3 resonances initially sharpen before beginning to broaden at a rate comparable to the GlcA(II)OH3 resonance, a proton for which we have consistent experimental evidence is in a hydrogen bond.[64] The resonance of the IdoA2S(IV)OH3 proton broadens and decreases in intensity relatively quickly upon addition of bicarbonate, behaving similarly to the GlcNS6S(I)OH3 and OH4 hydroxyl protons.

Additional evidence that samples prepared in an N_2 atmosphere contained dissolved CO_2 that catalyzed hydroxyl proton exchange was provided by EXSY measurements. Arixtra solutions prepared in the open atmosphere required longer EXSY mixing times to achieve plateaus in the build-up curves. The normalized cross peak volume integrals were plotted as a function of mixing time in Figure 3.13A and EXSY exchange rate constants are summarized in Table 3.5. The two hydroxyl protons with the lowest exchange rates, GlcA(II)OH3 (3.50 s^{-1}) and IdoA2S(IV)OH3 (5.32 s^{-1}) protons, are in good agreement with rates reported in section 3.3.6 and are consistent with their

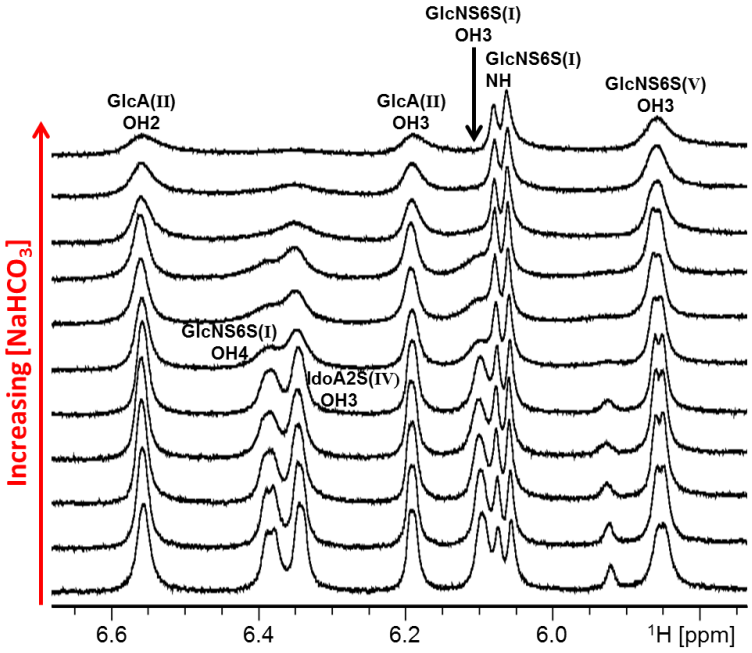

Figure 3.12. Arixtra bicarbonate titration with hydroxyl proton resonances labeled. Initial solution was prepared open to the atmosphere in 85% Millipore H_2O/15% acetone-d_6 at pH 8.28. Sodium bicarbonate at pH 8.26 was titrated in 0.5 – 2 μL increments and the NMR spectra measured at -14.6 °C.

Table 3.5. EXSY initial build-up rates of Arixtra hydroxyl protons. **A** is an Arixtra solution set to pH 8.28 and prepared open to the atmosphere. **B** is the same solution (**A**) after the addition of 0.59 mM HCO_3^-. The rates for the hydroxyl protons in **C** were calculated from the average normalized cross-peak volumes of three separate measurements using a stock Arixtra solution. Each solution was set to pH 8.3 and also prepared open to the atmosphere. It is hypothesized that **C** may have absorbed some CO_2 from the atmosphere, thus resulting in relative rates that are more comparable to **B** than to **A**.

Hydroxyl Proton	**Initial Build-Up Rate (k_{ex}, s^{-1})**		
	A	**B**	**C**
GlcNS6S(I) OH3	13.0	12.9	10.3
GlcNS6S(I) OH4	14.0	16.0	12.4
GlcA(II) OH2	17.7	6.01	6.11
GlcA(II) OH3	3.50	1.20	1.49
IdoA2S(IV) OH3	5.32	9.23	6.64
GlcNS6S(V) OH3	25.5	5.13	5.87

involvement in a hydrogen bond.[64] The exchange rates of the GlcNS6S(V)OH3 proton (25.5 s^{-1}) and the GlcNS6S(I)OH3 and OH4 protons (13.0 and 14.0 s^{-1}, respectively) are also in agreement with the values reported in section 3.3.6. The only proton with an exchange rate that deviates noticeably from that previously reported[64] is the GlcA(II)OH2 proton (17.7 s^{-1}) which exchanges more slowly in this sample. This difference could be caused by slight differences in solution composition between samples (for example pH, which is very difficult to determine in unbuffered solution), prompting the reproducibility experiments discussed in section 3.3.8.

The EXSY NMR measurements were repeated for the Arixtra solution following the addition of 0.59 mM sodium bicarbonate (Figure 3.12B) and the resulting buildup curves had very different profiles than those in Figure 3.12A. Interestingly the hydroxyl proton exchange rates, summarized in Table 3.4, were not uniformly affected by HCO_3^- catalysis. The exchange rate constants determined for GlcA(II) OH2 (6.01 s^{-1}) and IdoA2S(IV)OH3 (9.23 s^{-1}) nearly doubled following HCO_3^- addition, while the rates for GlcNS6S(I)OH3 and OH4 (13.0 and 16.0 s^{-1}, respectively) were similar to those determined from the results in Figure 3.13A The exchange rate constant measured for GlcNS6S(V) OH3 (5.13 s^{-1}) is actually slower than the value measured for this solution before addition of HCO_3- and is also lower than the value reported in section 3.3.6.

We originally hypothesized that HCO_3^- would have a greater effect on the exchange of hydroxyl protons not involved in hydrogen bonds, reasoning that the hydrogen bonds might protect the hydroxyl group from the effects of HCO_3^- catalysis. The results of our titration suggest that the microstructural environment also has a large

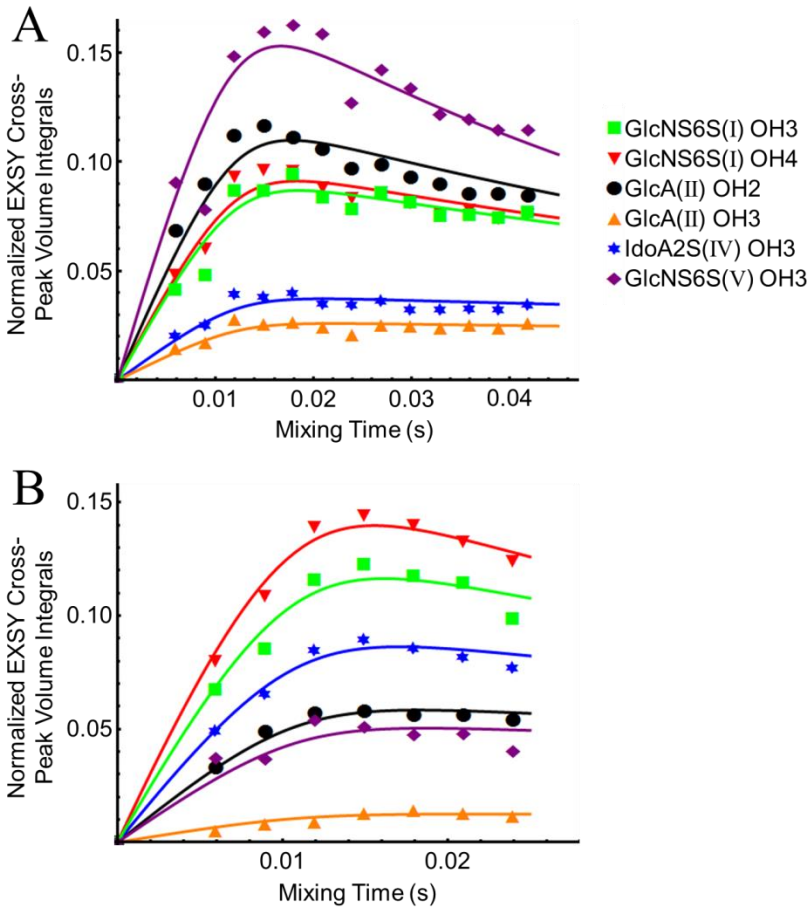

Figure 3.13. (A) EXSY cross peak build-up curves of Arixtra hydroxyl protons measured at -14.6 °C prior to the addition of sodium bicarbonate. The solution was prepared open to the atmosphere and composed of 85% Millipore H_2O/15% acetone-d_6 at pH 8.28 with 0.15 M NaCl. (B) EXSY cross peak build-up curves of Arixtra hydroxyl protons constants after the addition of sodium bicarbonate to a concentration of 0.59 mM.

impact. The negatively charged Arixtra sulfate and carboxylate groups may repel HCO_3^- reducing its impact on hydroxyl protons in close proximity to carboxylate and sulfate moieties. Supporting this idea, the GlcNS6S(I) OH3 and OH4 protons that appear to exchange faster in the presence of HCO_3^- are also the most solvent exposed.

It seems reasonable that HCO_3^- could also disrupt the intramolecular hydrogen bonding network, especially for the IdoA(IV) residue. IdoA(IV) is involved in a conformational equilibrium that results in two different hydrogen bonds for the IdoA(IV) OH3 proton depending on whether it is in the $^1C_4$ or ^2S_O conformation. The results in Figure 3.13 suggest that interactions with HCO_3^- may disrupt the IdoA(IV) OH3 intramolecular hydrogen bonds and catalyze its exchange. To avoid discrepancies caused by the differences in CO_2 content, future studies of hydroxyl proton exchange should be conducted with samples prepared in a glove box and by incorporating scrubbing of the N_2 to remove trace amounts of CO_2.

3.3.8 Error in EXSY exchange rate constant measurements. To test the reproducibility of our EXSY NMR determination of hydroxyl proton exchange rates, replicate measurements were performed for three similarly prepared Arixtra samples. The same Arixtra stock solution was utilized for all three trials to avoid variance that could be introduced by small differences in sample composition. Solutions were set to a pH of 8.3 prior to the addition of acetone-d_6 and NMR spectra immediately recorded. The Arixtra stock solution was stored in the refrigerator between measurements. Normalized cross-peak volumes of all three EXSY data sets were determined and the average values with

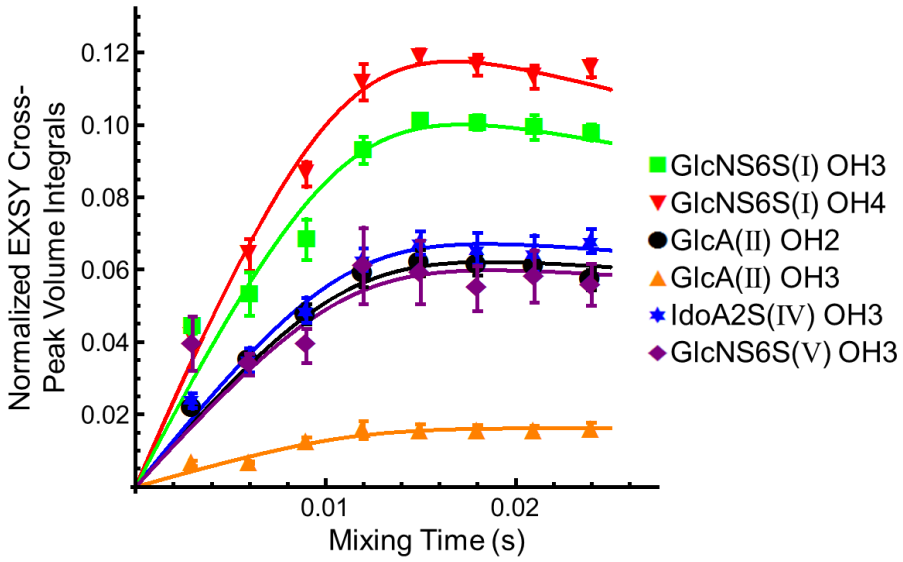

Figure 3.14. EXSY build-up curves of Arixtra hydroxyl protons. The error bars were calculated at each mixing time using the standard error of three trials. The three measurements were performed on the same Arixtra stock solution to keep solution composition consistent. A fresh NMR sample was made for each measurement using the same Arixtra stock solution. Each solution was composed of 85% H_2O/15% acetone-d_6 with 0.15 M NaCl at pH 8.3 and -14.6 °C.

standard errors are plotted as a function of mixing time in Figure 3.14. The exchange rate constants are summarized in Table 3.4.

The error associated with the EXSY measurements suggests that exchange rate constant measurements are reproducible within the same sample. CO_2 is absorbed easily from the atmosphere by a sample at a basic pH, making it concentration difficult to control. Hydroxyl proton exchange rates should be compared within the same sample and only to other samples which are of the same or similar composition. The exchange rate constants obtained from the data shown in Figure 3.14 correspond well with those reported for the Arixtra sample containing 0.59 mM HCO_3^- in section 3.3.7. The GlcA(II) OH3 proton exchanges the slowest at a rate of 1.49 s^{-1}. It is the only proton found to be in a persistent hydrogen bond. The IdoA(IV) OH3 proton exchanges at a rate (6.64 s^{-1}) comparable to those of the GlcNS6S(I) OH3 and OH4 protons (10.3 and 12.4 s^{-1}, respectively). The GlcA(II) OH2 and GlcNS6S(V) OH3 protons exchange relatively slowly (6.11 and 5.87 s^{-1}, respectively).

3.4 Conclusions

This work provides the first experimental evidence for intramolecular hydrogen bonds involving the hydroxyl protons in a heparin oligosaccharide. Hydroxyl hydrogen bonds were identified by the use of exchange rates taken together with temperature coefficient and $\Delta\delta$ measurements. These results highlight the power of MD simulations which predicted the existence of the GlcA OH3 and IdoA2S OH3 hydrogen bonds and indicated the hydrogen bond acceptors. To our knowledge, this is also the first work to

address the issue of radiation damping in aqueous solutions when extracting solvent exchange rates of hydroxyl protons. The error associated with the exchange rate measurements was also evaluated. It was determined that CO_2 content could dramatically affect the relative exchange rates of hydroxyl protons within a sample and that care must be taken when comparing exchange rates between samples. Because EXSY exchange rate constants were determined to be fairly reproducible within the same sample, exchange rate measurements reported in subsequent chapters will not contain error bars.

3.5 References

1. Ornitz, D. M.; Yayon, A.; Flanagan, J. G.; Svahn, C. M.; Levi, E.; Leder, P., Heparin is required for cell-free binding of basic fibroblast growth-factor to a soluble receptor and for mitogenesis in whole cells. *Mol. Cell. Biol.* **1992,** *12*, 240-247.

2. Faham, S.; Hileman, R. E.; Fromm, J. R.; Linhardt, R. J.; Rees, D. C., Heparin structure and interactions with basic fibroblast growth factor. *Science* **1996,** *271*, 1116-1120.

3. Goodger, S. J.; Robinson, C. J.; Murphy, K. J.; Gasiunas, N.; Harmer, N. J.; Blundell, T. L.; Pye, D. A.; Gallagher, J. T., Evidence that heparin saccharides promote FGF2 mitogenesis through two distinct mechanisms. *J. Biol. Chem.* **2008,** *283*, 13001-13008.

4. Zhao, W. J.; McCallum, S. A.; Xiao, Z. P.; Zhang, F. M.; Linhardt, R. J., Binding affinities of vascular endothelial growth factor (VEGF) for heparin-derived oligosaccharides. *Bioscience Rep.* **2012,** *32*, 71-81.

5. Houck, K. A.; Leung, D. W.; Rowland, A. M.; Winer, J.; Ferrara, N., Dual regulation of vascular endothellial growth-factor bioavailability by genetic and proteolytic mechanisms. *J. Biol. Chem.* **1992,** *267*, 26031-26037.

6. Ruhrberg, C.; Gerhardt, H.; Golding, M.; Watson, R.; Ioannidou, S.; Fujisawa, H.; Betsholtz, C.; Shima, D. T., Spatially restricted patterning cues provided by heparin-binding VEGF-A control blood vessel branching morphogenesis. *Gene. Dev.* **2002,** *16*, 2684-2698.

7. Jee, J. P.; Nam, S. H.; Park, Y.; Lee, H. J.; Maeng, H. J.; Kim, C. K., Simplified analysis of lipoprotein lipase activity: Evaluation of lipasemic activity of low molecular weight heparin in rats. *Arch. Pharm. Res.* **2012,** *35*, 1107-1114.

8. Spillmann, D.; Lookene, A.; Olivecrona, G., Isolation and characterization of low sulfated heparan sulfate sequences with affinity for lipoprotein lipase. *J. Biol. Chem.* **2006,** *281*, 23405-23413.

9. van Barlingen, H. H.; Kleinveld, H. A.; Erkelens, D. W.; deBruin, T. W. A., Lipoprotein lipase-enhanced binding of lipoprotein(a) [Lp(a)] to heparan sulfate is improved by apolipoprotein E (apoE) saturation: Secretion-capture process of apoE is a possible route for the catabolism of Lp(a). *Metabolism.* **1997,** *46*, 650-655.

10. Mummery, R. S.; Rider, C. C., Characterization of the heparin-binding properties of IL-6. *J. Immunol.* **2000,** *165*, 5671-5679.

11. Zhang, S. Y.; Condac, E.; Qiu, H.; Jiang, J. L.; Gutierrez-Sanchez, G.; Bergmann, C.; Handel, T.; Wang, L. C., Heparin-induced leukocytosis requires 6-*O*-sulfation and is caused by blockade of selectin- and CXCL12 protein-mediated leukocyte trafficking in mice. *J. Biol. Chem.* **2012,** *287*, 5542-5553.

12. Ziarek, J. J.; Veldkamp, C. T.; Zhang, F. M.; Murray, N. J.; Kartz, G. A.; Liang, X. L.; Su, J. D.; Baker, J. E.; Linhardt, R. J.; Volkman, B. F., Heparin oligosaccharides inhibit chemokine (CXC Motif) ligand 12 (CXCL12) cardioprotection by binding orthogonal to the dimerization interface, promoting oligomerization, and competing with the chemokine (CXC Motif) receptor 4 (CXCR4) N terminus. *J. Biol. Chem.* **2013,** *288*, 737-746.

13. Rosenberg, R. D., Chemistry of hemostatic mechanism and its relationship to action of heparin. *Fed. Proc.* **1977,** *36*, 10-18.

14. Olson, S. T., Transient kinetics of heparin-catalyzed protease inactivation by antithrombin-III. Linkage of protease-inhibitor-heparin interactions in the reaction with thrombin. *J. Biol. Chem.* **1988,** *263*, 1698-1708.

15. Thunberg, L.; Backstrom, G.; Lindahl, U., Further characterization of the antithrombin-binding sequence in heparin. *Carbohyd. Res.* **1982,** *100*, 393-410.

16. Atha, D. H.; Lormeau, J. C.; Petitou, M.; Rosenberg, R. D.; Choay, J., Contrubution of monosaccharide residues in heparin binding to antithrombin-III. *Biochemistry* **1985,** *24*, 6723-6729.

17. Ferro, D. R.; Provasoli, A.; Ragazzi, M.; Torri, G.; Casu, B.; Gatti, G.; Jacquinet, J. C.; Sinay, P.; Petitou, M.; Choay, J., Evidence for conformational equilibrium of the sulfated L-iduronate residue in heparin and in synthetic heparin mono- and oligosaccharides: NMR and force-field studies. *J. Am. Chem. Soc.* **1986,** *108*, 6773-6778.

18. Hricovini, M.; Guerrini, M.; Bisio, A.; Torri, G.; Petitou, M.; Casu, B., Conformation of heparin pentasaccharide bound to antithrombin-III. *Biochem. J.* **2001,** *359*, 265-272.

19. Johnson, D. J. D.; Li, W.; Adams, T. E.; Huntington, J. A., Antithrombin-S195A factor Xa-heparin structure reveals the allosteric mechanism of antithrombin activation. *Embo J.* **2006,** *25*, 2029-2037.

20. Langeslay, D. J.; Young, R. P.; Beni, S.; Beecher, C. N.; Mueller, L. J.; Larive, C. K., Sulfamate proton solvent exchange in heparin oligosaccharides: Evidence for a persistent hydrogen bond in the antithrombin-binding pentasaccharide Arixtra. *Glycobiology* **2012,** *22*, 1173-1182.

21. Vilen, E. M.; Lundqvist, L. C. E.; Jouanneau, D.; Helbert, W.; Sandstrom, C., NMR study on hydroxy protons of κ- and κ/μ-hybrid carrageenan oligosaccharides: Experimental evidence of hydrogen bonding and chemical exchange interactions in κ/μ oligosaccharides. *Biomacromolecules* **2010,** *11*, 3487-3494.

22. Vasquez, T. E.; Bergset, J. M.; Fierman, M. B.; Nelson, A.; Roth, J.; Khan, S. I.; O'Leary, D. J., Using equilibrium isotope effects to detect intramolecular OH/OH hydrogen bonds: Structural and solvent effects. *J. Am. Chem. Soc.* **2002,** *124*, 2931-2938.

23. Adams, B.; Lerner, L., Observation of hydroxyl protons of sucrose in aqueous solution: No evidence for persistent intramolecular hydrogen bonds. *J. Am. Chem. Soc.* **1992,** *114*, 4827-4829.

24. Poppe, L.; Vanhalbeek, H., The rigidity of sucrose: just an illusion? *J. Am. Chem. Soc.* **1992,** *114*, 1092-1094.

25. Battistel, M. D.; Pendrill, R.; Widmalm, G.; Freedberg, D. I., Direct evidence for hydrogen bonding in glycans: A combined NMR and molecular dynamics study. *J. Phys. Chem. B* **2013,** *117*, 4860-4869.

26. Battistel, M. D.; Shangold, M.; Trinh, L.; Shiloach, J.; Freedberg, D. I., Evidence for helical structure in a tetramer of α2-8 sialic acid: Unveiling a structural antigen. *J. Am. Chem. Soc.* **2012,** *134*, 10717-10720.

27. Sandstrom, C.; Kenne, L., Hydroxy protons in structural studies of carbohydrates by NMR spectroscopy. *ACS. Sym. Ser.* **2006,** *930*, 114-132.

28. Sandstrom, C.; Baumann, H.; Kenne, L., NMR spectroscopy of hydroxy protons of 3,4-disubstituted methyl α-D-galactopyranosides in aqueous solution. *J. Chem. Soc. Perk. T. 2* **1998,** 809-815.

29. Dobson, C. M.; Lian, L. Y.; Redfield, C.; Topping, K. D., Measurement of hydrogen exchange rates using 2D NMR spectroscopy. *J. Magn. Reson.* **1986,** *69*, 201-209.

30. Chen, J. H.; Mao, X. A., Measurement of chemical exchange rate constants with solvent protons using radiation damping. *J. Magn. Reson.* **1998,** *131*, 358-361.

31. Hwang, T. L.; Shaka, A. J., Water suppression that works. Excitation sculpting using arbitrary wave-forms and pulsed-field gradients. *J. Magn. Reson. Ser. A* **1995,** *112*, 275-279.

32. Van Geet, A. L., Calibration of methanol and glycol nuclear magnetic resonance thermometers with a static thermistor probe. *Anal. Chem.* **1968,** *40*, 2227-2229.

33. Langeslay, D. J.; Beni, S.; Larive, C. K., A closer look at the nitrogen next door: ^{1}H-^{15}N NMR methods for glycosaminoglycan structural characterization. *J. Magn. Reson.* **2012,** *216*, 169-174.

34. Mazak, K.; Beecher, C. N.; Kraszni, M.; Larive, C. K., The interaction of enoxaparin and fondaparinux with calcium. *Carbohyd. Res.* **2014,** *384*, 13-19.

35. Pedretti, A.; Villa, L.; Vistoli, G., VEGA: a versatile program to convert, handle and visualize molecular structure on Windows-based PCs. *J. Mol. Graph. Model.* **2002,** *21*, 47-49.

36. Case, D. A.; Darden, T. A.; Cheatham III, T. E.; Simmerling, C. L.; Wang, J.; Duke, R. E.; Luo, R.; Walker, R. C.; Zhang, W.; Merz, K. M., **2011**, *Amber 11*.

37. Kirschner, K. N.; Yongye, A. B.; Tschampel, S. M.; Gonzalez-Outeirino, J.; Daniels, C. R.; Foley, B. L.; Woods, R. J., GLYCAM06: A generalizable biomolecular force field. Carbohydrates. *J. Comput. Chem.* **2008,** *29*, 622-655.

38. Hornak, V.; Abel, R.; Okur, A.; Strockbine, B.; Roitberg, A.; Simmerling, C., Comparison of multiple amber force fields and development of improved protein backbone parameters. *Proteins.* **2006,** *65*, 712-725.

39. Jorgensen, W. L.; Chandrasekhar, J.; Madura, J. D.; Impey, R. W.; Klein, M. L., Comparison of simple potential functions for simulating liquid water. *J. Chem. Phys.* **1983,** *79*, 926-935.

40. Phillips, J. C.; Braun, R.; Wang, W.; Gumbart, J.; Tajkhorshid, E.; Villa, E.; Chipot, C.; Skeel, R. D.; Kale, L.; Schulten, K., Scalable molecular dynamics with NAMD. *J. Comput. Chem.* **2005,** *26*, 1781-1802.

41. Darden, T.; York, D.; Pedersen, L., Particle mesh Ewald: An N•log(N) method for Ewald sums in large systems. *J. Chem. Phys.* **1993,** *98*, 10089-10092.

42. Miyamoto, S.; Kollman, P. A., SETTLE: An analytical version of SHAKE and RATTLE algorithm for rigid water models. *J. Comput. Chem.* **1992,** *13*, 952-962.

43. Humphrey, W.; Dalke, A.; Schulten, K., VMD: Visual molecular dynamics. *J. Mol. Graph. Model.* **1996,** *14*, 33-38.

44. Forster, M. J. *mdxvu – molecular dynamics X11 viewer*; **2008**; available at http://sourceforge.net/projects/mdxvu/ (accessed 01/04/2014).

45. Ragazzi, M.; Ferro, D. R.; Perly, B.; Sinay, P.; Petitou, M.; Choay, J., Conformation of the pentasaccharide corresponding to the binding site of heparin to antithrombin III. *Carbohyd. Res.* **1990,** *195*, 169-185.

46. Ragazzi, M.; Ferro, D. R.; Perly, B.; Torri, G.; Casu, B.; Sinaÿ, P.; Petitou, M.; Choay, J., Conformation of the pentasaccharide corresponding to the binding site of heparin to antithrombin-III. *Carbohyd. Res.* **1987,** *165*, C1-C5.

47. Langeslay, D. J.; Beni, S.; Larive, C. K., Detection of the ^{1}H and ^{15}N NMR resonances of sulfamate groups in aqueous solution: A new tool for heparin and heparan sulfate characterization. *Anal. Chem.* **2011,** *83*, 8006-8010.

48. Langeslay, D. J.; Beecher, C. N.; Naggi, A.; Guerrini, M.; Torri, G.; Larive, C. K., Characterizing the microstructure of heparin and heparan sulfate using *N*-sulfoglucosamine ^{1}H and ^{15}N NMR chemical shift analysis. *Anal. Chem.* **2013,** *85*, 1247-1255.

49. Langeslay, D. J.; Beecher, C. N.; Dinges, M. M.; Larive, C. K., Glycosaminoglycan structural characterization. *eMagRes*, **2013,** *2*, 205-214.

50. Limtiaco, J. F. K.; Beni, S.; Jones, C. J.; Langeslay, D. J.; Larive, C. K., The efficient structure elucidation of minor components in heparin digests using microcoil NMR. *Carbohyd. Res.* **2011,** *346*, 2244-2254.

51. Jeener, J.; Meier, B. H.; Bachmann, P.; Ernst, R. R., Investigation of exchange processes by two-dimensional NMR spectroscopy. *J. Chem. Phys.* **1979,** *71*, 4546-4553.

52. Bloembergen, N.; Pound, R. V., Radiation damping in magnetic resonance experiments. *Phys. Rev.* **1954,** *95*, 8-12.

53. Chen, J. H.; Cutting, B.; Bodenhausen, G., Measurement of radiation damping rate constants in nuclear magnetic resonance by inversion recovery and automated compensation of selective pulses. *J. Chem. Phys.* **2000,** *112*, 6511-6514.

54. Chen, J. H.; Mao, X. A., Radiation damping transfer in nuclear magnetic resonance experiments via chemical exchange. *J. Chem. Phys.* **1997,** *107*, 7120-7126.

55. Berger, S.; Braun, S., *200 and More NMR Experiments: A Practical Course*, 3rd ed.; Wiley-VCH: Weinheim, Germany, **2004**.

56. Wolfram, S., *Mathematica: A System for Doing Mathematiccs by Computer*, 2nd ed.; Addison-Wesley Publishing Company: Reading, MA, **1991**.

57. Abramowitz, M.; Stegun, I. A., *Handbook of Mathematical Functions with Formulas, Graphs, and Mathematical Tables*; U.S. Government Printing Office: Washington, D.C., **1964**.

58. Baxter, N. J.; Williamson, M. P., Temperature dependence of ^{1}H chemical shifts in proteins. *J. Biomol. NMR.* **1997,** *9*, 359-369.

59. Kindahl, L.; Sandstrom, C.; Norberg, T.; Kenne, L., ^{1}H NMR studies of hydroxy protons of Asn- and Ser-linked disaccharides in aqueous solution. *J. Carbohyd. Chem.* **2000,** *19*, 1291-1303.

60. Kindahl, L.; Sandstrom, C.; Norberg, T.; Kenne, L., ^{1}H NMR studies of hydroxy protons of the V[β-Gal(1→3)-α-GalNAc(1→O)]THPGY glycopeptide. *Carbohyd. Res.* **2001,** *336*, 319-323.

61. Pol-Fachin, L.; Verli, H., Depiction of the forces participating in the 2-*O*-sulfo-α-L-iduronic acid conformational preference in heparin sequences in aqueous solutions. *Carbohyd. Res.* **2008,** *343*, 1435-1445.

62. van Boeckel, C. A. A.; Petitou, M., The unique antithrombin-III- binding domain of heparin: A lead to new synthetic antithrombotics. *Angew. Chem. Int. Edit.* **1993,** *32*, 1671-1690.

63. Guerrini, M.; Elli, S.; Gaudesi, D.; Torri, G.; Casu, B.; Mourier, P.; Herman, F.; Boudier, C.; Lorenz, M.; Viskov, C., Effects on molecular conformation and anticoagulant activities of 1,6-anhydrosugars at the reducing terminal of antithrombin-binding octasaccharides isolated from low-molecular-weight heparin enoxaparin. *J. Med. Chem.* **2010,** *53*, 8030-8040.

64. Beecher, C. N.; Young, R. P.; Langeslay, D. J.; Mueller, L. J.; Larive, C. K., Hydroxyl-proton hydrogen bonding in the heparin oligosaccharide Arixtra in aqueous solution. *J. Phys. Chem. B* **2014,** *118*, 482-491.

CHAPTER FOUR

Hydroxyl Proton Hydrogen Bonding in Heparin Oligosaccharides in Aqueous Solution

Acknowledgements: I would like to thank the following people for their contributions to this research: Dr. Leonard Mueller for his help with the EXSY initial build-up rate calculations and Robert Young for his efforts to perform molecular dynamic simulations of the oligosaccharides studied in this Chapter, which are currently underway.

Abstract

Heparin is best known for its anticoagulant activity, which is mediated by the binding of a specific pentasaccharide sequence to the protease inhibitor antithrombin-III (AT-III). Although heparin oligosaccharides are known to flexible in aqueous solution, the recent discovery of a hydrogen bond between the sulfamate ($NHSO_3^-$) proton and the adjacent 3-*O*-sulfate group of the GlcNS3S6S residue in the Arixtra pentasaccharide demonstrates the potential of ^{1}H NMR to elucidate elements of secondary structure. Chapter 3 discussed the hydroxyl proton hydrogen bonds present in Arixtra. The present chapter examines intramolecular hydrogen bonds involving the hydroxyl protons of heparin oligosaccharides which are structurally related to Arixtra through measurements of temperature coefficients, chemical shift differences, and rate constants for solvent proton exchange calculated from EXSY initial build-up rate data. In the series of oligosaccharides examined, several structural motifs were observed to give rise to

hydrogen bonds involving specific hydroxyl groups of glucuronic acid (GlcA) and glucosamine (GlcNS) residues and are dependent on local structure.

4.1 Introduction

Heparin oligosaccharides are known to be flexible in solution, but can also adopt local secondary structure through participation of the exchangeable protons in an intramolecular hydrogen bonds, as described in Arixtra in Chapter 3. Structurally specific hydrogen bonds may play a role in orienting the heparin chain to facilitate protein-binding. As described in Chapter 3, various methods can be utilized to measure the exchange rates of the heparin exchangeable protons to probe for hydrogen bonds. These include temperature coefficients,[1-5] differences in chemical shift between in the oligo- and monosaccharide ($\Delta\delta = \delta_{oligo} - \delta_{mono}$),[6] and more direct measurements of exchange rates including evaluation of the energy of activation for chemical exchange ($\Delta G^{\ddagger}$)[2,7-9] and determination of exchange rate constants using EXSY.[1,10-12] Molecular dynamic (MD) simulations of Arixtra predicted a hydrogen bond between a sulfamate NH proton and adjacent 3-*O*-sulfate group within the same glucosamine residue of Arixtra.[2] These MD simulations also predicted structurally specific hydrogen bonds involving the Arixtra hydroxyl protons. In Chapter 3 we experimentally confirmed the results of the MD simulations, discovering hydroxyl proton hydrogen bonds involving the GlcA(II)OH3 and IdoA2S(IV)OH3 hydroxyl protons of Arixtra using temperature coefficients, $\Delta\delta$ values, and EXSY initial build-up rate constants (k_{ex}).[1]

In this chapter, the results of ^{1}H NMR experiments are examined comparing hydroxyl proton hydrogen bonding patterns for aqueous solutions of heparin oligosaccharides structurally related to Arixtra that were isolated from the low molecular weight heparin (LMWH) enoxaparin. The isolated oligosaccharides do not contain the 3-*O*-sulfate group required for formation of the GlcNS3S sulfamate NH-3-*O*-sulfate hydrogen bond. The goal of this chapter was to experimentally evaluate the impact of structural variations on hydrogen bonding in heparin oligosaccharides. MD simulations are currently underway by our collaborator, Robert Young, to support experimental results and predict hydrogen bond acceptors.

4.2 Materials and methods

4.2.1 Materials and reagents. Enoxaparin sodium was purchased from the U.S. Pharmacopeia (USP, Rockville, MD). Oligosaccharides structurally related to the Arixtra pentasaccharide were isolated from enoxaparin as described in Chapter 2. Hydrochloric acid (HCl), sodium chloride (NaCl), and sodium hydroxide (NaOH) were purchased from Fisher Scientific Co. (Fair Lawn, NJ). The GlcNS6S and D-GlcA monosaccharides were purchased from Sigma Aldrich (Saint Louis, MO). HPLC-grade water was obtained from Burdick and Jackson (Muskegon, MI). Acetone-d_6 (D, 99.9%) and deuterium oxide, (D_2O; D, 99.9%) were purchased from Cambridge Isotope Laboratories (Andover, MA). The pH meter was calibrated with buffers at 4.00, 7.00 and 10.00 purchased from Fisher Scientific Co.

4.2.2 Solution preparation. To reduce the solvent exchange rate of the hydroxyl protons, oligosaccharide NMR samples were prepared under an N_2 atmosphere to reduce catalysis of exchange by dissolved CO_2. To reduce contamination by CO_2, solutions were not bubbled with N_2 (section 3.3.7). Solutions were prepared in 85% H_2O/15% acetone-d_6 with 0.15 M NaCl at concentrations of oligosaccharide ranging from 1 to 2 mM.[1,3-6] The pH was set to 8.1 using dilute solutions of CO_2-free HCl and NaOH. Solution pH measurements were made using a Fisher Scientific AB15 pH meter with a double junction Ag/AgCl micro-pH electrode (Thermo Scientific, Beverly, MA) and measured prior to the addition of acetone-d_6. NMR measurements were performed in 5 mm NMR tubes using a 600 µL sample.

4.2.3 NMR measurements. One-dimensional NMR spectra were acquired at -14.5 °C using a Bruker 600 MHz Advance spectrometer equipped with a TXI probe operating at 600.13 MHz. Solvent suppression was accomplished using excitation sculpting.[13] The temperature coefficients were measured by recording ^{1}H NMR spectra over the temperature range -15 ºC and 12 ºC in approximately 4-5 ºC increments. Temperatures were calibrated using an external methanol standard.[14] Chemical shifts were referenced using the residual ^{1}H resonance of acetone-d_6 at 2.204 ppm. The $\Delta\delta$ values for each monosaccharide were determined at -10.0 °C.

Hydroxyl proton resonances were assigned using two-dimensional COSY and TOCSY NMR spectra. Both were acquired in States-TPPI. Double-quantum filtered (DQF)- COSY spectra were acquired into 2048 complex points in t2 with 64, 80, or 128 scans coadded at each of 208, 256, or 272 t1 increments, depending on solution

concentration. Phase sensitive TOCSY spectra incorporating excitation sculpting for solvent suppression were acquired into 2048 complex points in t2 with 64, 80, or 128 scans coadded at each of 192, 256, or 272 t1 increments, depending on solution concentration. A spectral window of 7000 Hz in F2, 6200 Hz in F1 and a relaxation delay of 1.5 s were used in both the COSY and TOCSY experiments. The optimal TOCSY mixing time for the hydroxyl protons was found to be 60 ms. Spectra were zero-filled to 4096 x 512 data points and apodized using a sine squared function (for the COSY) and a cosine squared function (for the TOCSY) in both dimensions.

EXSY spectra were measured at -14.5 ºC using excitation sculpting for solvent suppression. A series of EXSY spectra were acquired using mixing times between 0 and 24 ms in 3 ms increments for the more abundant oligosaccharides. Due to experiment time restrictions, the less abundant oligosaccharide was measured using mixing times between 0 and 18 ms in 3 ms increments with one experiment using 22 ms mixing time.[1,12] Spectra were acquired in 2048 complex points in t_2 with 32 scans for the more abundant oligosaccharide and 128 scans for the less abundant oligosaccharide. EXSY experiments used 128 t_1 increments with a relaxation delay of 1.5 s. Spectral windows of 4440 Hz were used in F1 and F2. Spectra were zero-filled to 16384 x 4096 points and apodized by multiplication by a cosine squared function to obtain more accurate volume integrals of hydroxyl proton exchange cross peaks. EXSY build-up curves were plotted as the volume integral of the hydroxyl cross peaks as a function of mixing time and rate constants were calculated using modified Bloch equations as described in Chapter 3.[1,10,15]

4.3 Results and discussion

4.3.1 Heparin oligosaccharide hydroxyl proton detection and identification. Our goal is to determine the influence that local structure has on heparin hydroxyl proton hydrogen bonding, building on the hydrogen bonds characterized in the pentasaccharide, Arixtra (Chapter 3).[1] The following isolated heparin tetra- and hexasaccharides, characterized in Chapter 2, are structurally similar to Arixtra but do not contain the important glucosamine 3-*O*-sulfate group: ΔUA2S-GlcNS6S-GlcA-GlcNS6S (Figure 4.1A); ΔUA2S-GlcNS6S-IdoA2S-GlcNS6S (Figure 4.1B); ΔUA2S-GlcNS6S-IdoA2S-GlcNS6S-GlcA-GlcNS6S (Figure 4.1C). These heparin oligosaccharides will be referred to in the text as oligosaccharides [1], [2] and [3], respectively. As described in greater detail in Chapter 3, temperature coefficients, chemical shift differences ($\Delta\delta = \delta_{oligo} - \delta_{mono}$), and EXSY initial build-up rate constants (k_{ex}) were used to probe for hydroxyl proton hydrogen bonds in these oligosaccharides.

In order to slow down chemical exchange and make the hydroxyl protons observable by NMR, oligosaccharide solutions were prepared in 85% H_2O/15% acetone-d_6 and spectra were measured at -14.5 °C using excitation sculpting solvent suppression.[1,5,6, 12,13] Differences in resonance linewidth are observed between the different hydroxyl protons in the ^{1}H NMR spectrum of each oligosaccharide (Figure 4.2). The GlcNS6SOH3 hydroxyl proton resonances of each compound appear relatively sharp, suggesting these protons exchange more slowly. Hydroxyl proton resonances were assigned for each oligosaccharide using two-dimensional COSY and TOCSY spectra (Figure 4.3).

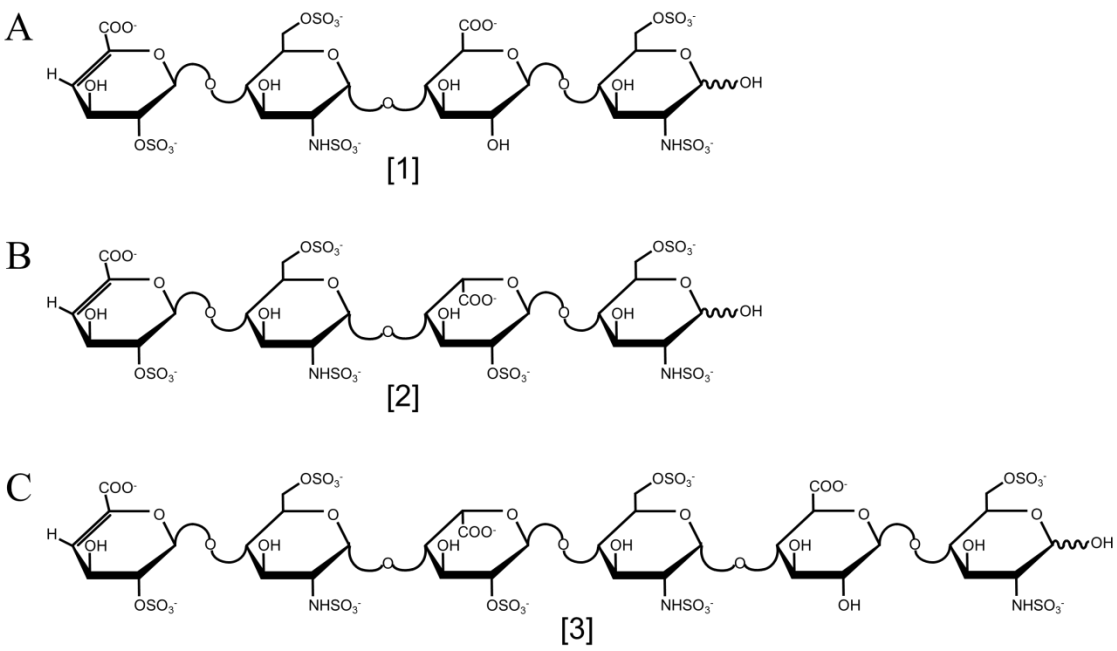

Figure 4.1. Isolated heparin oligosaccharides (A) ΔUA2S-GlcNS6S-GlcA-GlcNS6S, referred to as [1], (B) ΔUA2S-GlcNS6S-IdoA2S-GlcNS6S, referred to as [2], and (C) ΔUA2S-GlcNS2S-IdoA2S-GlcNS6S-GlcA-GlcNS6S, referred to as [3] are structurally related to Arixtra but do not contain the important 3-*O*-sulfate group. The oligosaccharides (A), (B), and (C) are referred to as [1], [2], and [3], respectively in the text.

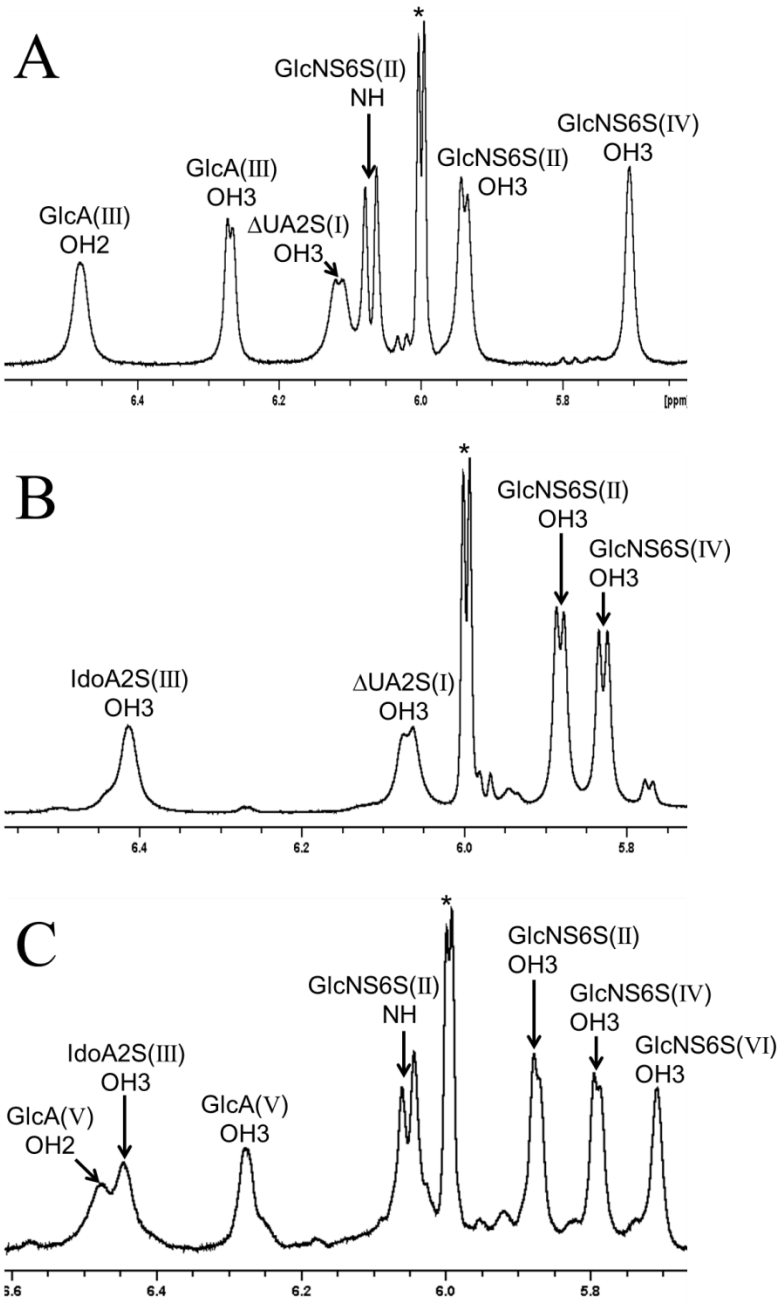

Figure 4.2. ^{1}H NMR spectra of the hydroxyl proton region of oligosaccharide (A) [1], (B) [2], and (C) [3]. Hydroxyl and sulfamate proton resonances are labeled. Carbon-bound protons are indicated with an asterisk.

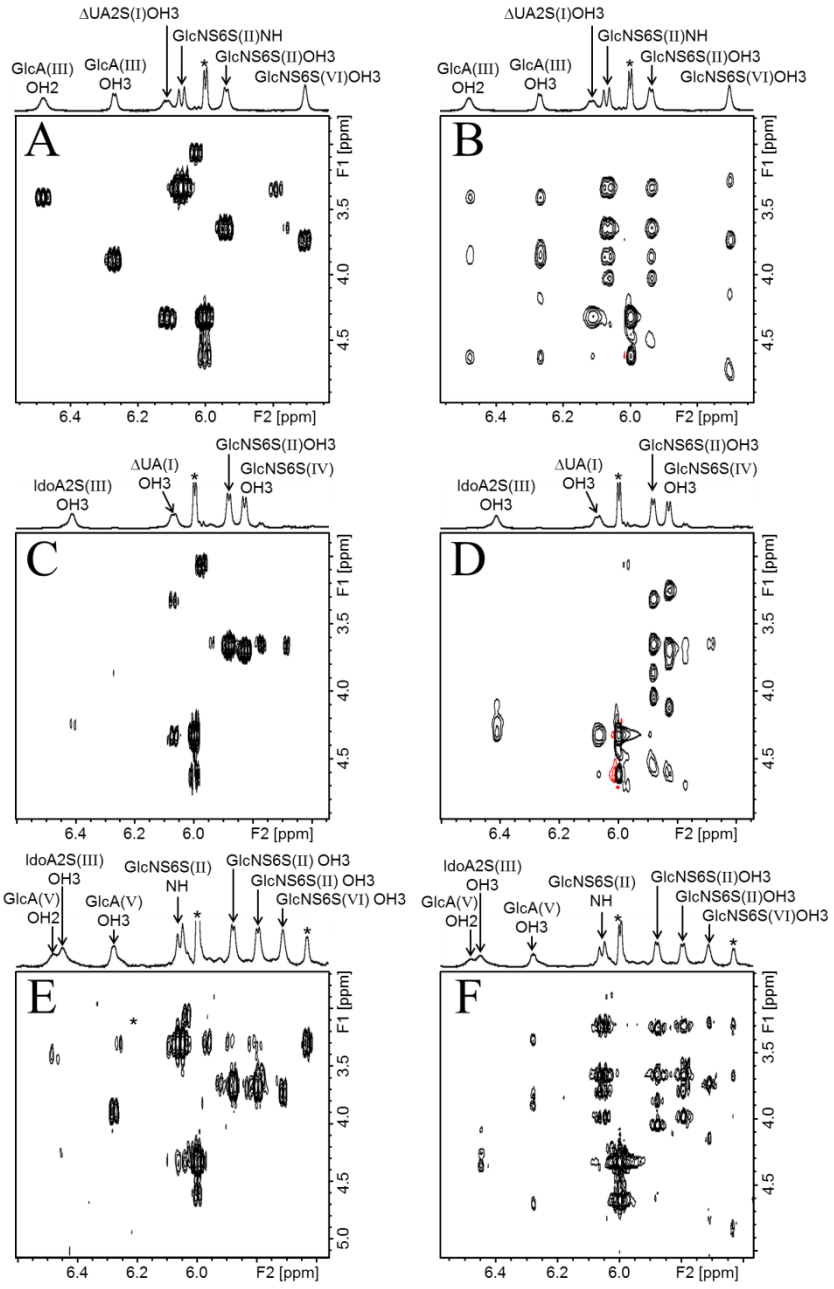

Figure 4.3. Hydroxyl proton resonances were identified using two-dimensional COSY and TOCSY spectra. COSY spectra are labeled for oligosaccharides (A) [1], (C) [2], and (E) [3]. TOCSY spectra are labeled for oligosaccharides (B) [1], (D) [2], and (F) [3]. Carbon-bound protons are marked with an asterisk.

4.3.2 Temperature coefficients. As discussed in section 3.1, a lower temperature coefficient can indicate that a proton is involved in a hydrogen bond. The ^{1}H NMR hydroxyl proton resonances shift linearly upfield with an increase in temperature (Figure 4.4). When chemical shifts are plotted as a function of temperature (Figure 4.5), the absolute values of the slopes are taken as the temperature coefficients (summarized in Table 4.1). The temperature coefficients of the anomeric hydroxyl protons were not measured because they exchange too quickly at this pH and are unlikely to participate in a hydrogen bond.

The GlcNS6S(II) and GlcA(III)OH3 hydroxyl protons in oligosaccharide [1] have the smallest relative temperature coefficients of 6.2 and 6.6 ppb/K, respectively, which are comparable to the GlcA(II)OH3 proton of Arixtra which participates in a hydrogen bond (Chapter 3).[1] The temperature coefficients of the reducing end GlcNS6S(IV)OH3 (8.6 ppb/K) and GlcA(III)OH2 (10.8 ppb/K) are similar to the values measured for the corresponding residues of Arixtra.[1] It is not too surprising that the ΔUA2S(I)OH3 proton has the largest temperature coefficient (12.7 ppb/K) as this modified residue at the tetrasaccharide's non-reducing end has a rigid partially planar conformation and is not expected to contribute to hydroxyl proton hydrogen bonding.

The GlcNS6S(II) and GlcNS6S(IV)OH3 protons in oligosaccharide [2] have temperature coefficients of 8.5 and 8.8 ppb/K, respectively, which are comparable to reducing end GlcNS6SOH3 protons in both Arixtra and in oligosaccharide [1]. The temperature coefficient of IdoA2S(III)OH3 hydroxyl proton is relatively large (11.0 ppb/K) and similar to that in Arixtra (Chapter 3).[1] Although the temperature coefficient

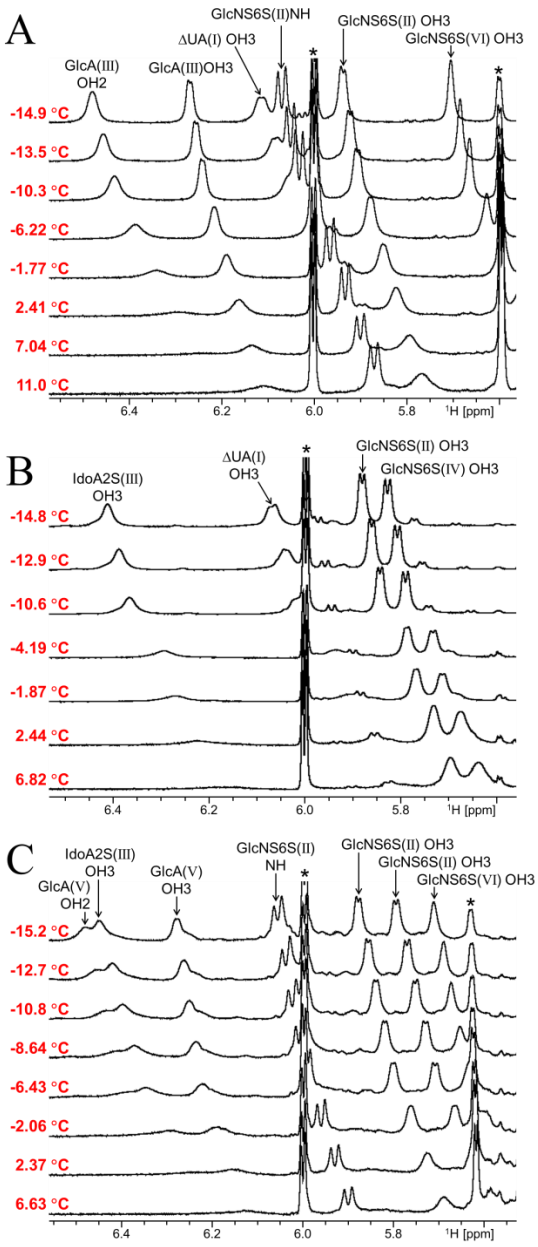

Figure 4.4. The hydroxyl proton resonances (labeled) of each oligosaccharide (A) [1], (B), [2], and (C) [3] experience a linear upfield shift as the temperature is increased. The exchangeable sulfamate protons also shift upfield with an increase in temperature while the carbon-bound protons (marked with an asterisk) remain unaffected.

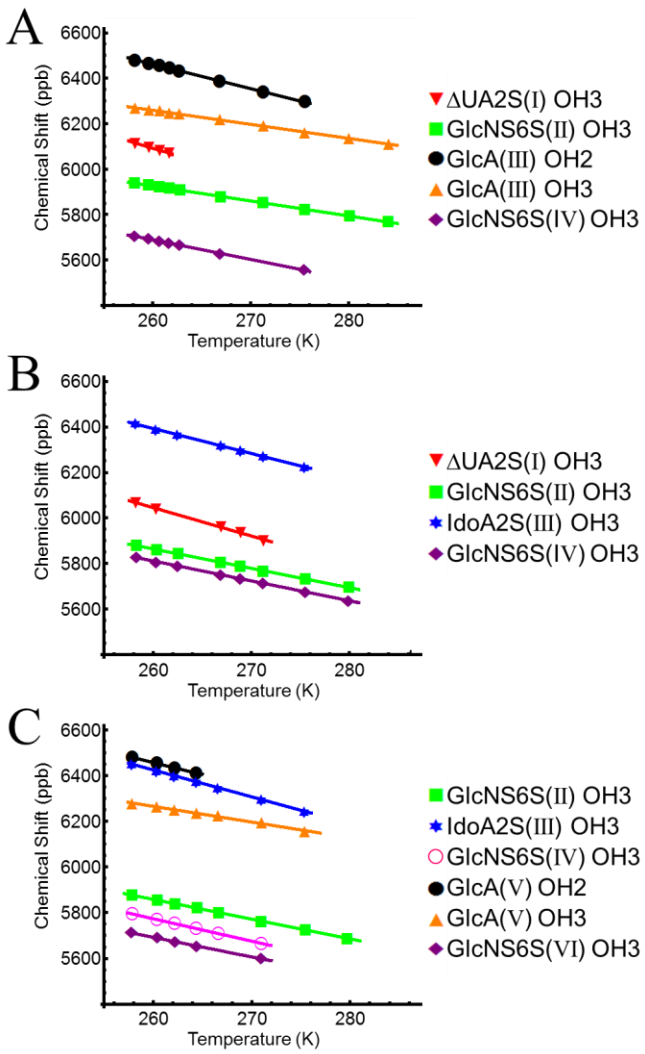

Figure 4.5. Temperature coefficient plots for the hydroxyl protons of oligosaccharides (A) [1], (B) [2], and (C) [3]. Chemical shifts are plotted as a function of temperature and the absolute values of the slopes are taken as the temperature coefficients.

Table 4.1. Chemical shift differences, temperature coefficients, and exchange rate constants of three oligosaccharides studied. These were compared to the results of the Arixtra hydroxyl proton exchange studies, found in Table 3.4.

Oligosaccharide	Hydroxyl Proton	Δδ (ppm)	Temperature Coefficient (ppb/K)	Initial Build-Up Rate (k_{ex}, s^{-1})
ΔUA2S-GlcNS6S-GlcA-GlcNS6S [1]	ΔUA2S(I) OH3	N/A	12.7	24.3
	GlcNS6S(II) OH3	-0.167	6.6	9.70
	GlcA(III) OH2	-0.103	10.8	24.5
	GlcA(III) OH3	-0.216	6.2	7.33
	GlcNS6S(IV) OH3	-0.410	8.6	9.13
ΔUA2S-GlcNS6S-IdoA2S-GlcNS6S [2]	ΔUA2S(I) OH3	N/A	9.2	20.7
	GlcNS6S(II) OH3	-0.234	8.5	6.71
	IdoA2S(III) OH3	N/A	11.0	18.9
	GlcNS6S(IV) OH3	-0.288	8.8	4.95
ΔUA2S-GlcNS6S-IdoA2S-GlcNS6S-GlcA-GlcNS6S [3]	IdoA2S(III) OH3	N/A	11.7	37.9
	GlcA(V) OH2	-0.108	10.5	30.0
	GlcA(V) OH3	-0.212	6.9	11.1
	GlcNS6S(II) OH3	-0.241	8.6	6.73
	GlcNS6S(IV) OH3	-0.330	9.8	1.75
	GlcNS6S(VI) OH3	-0.407	8.5	9.61

of the ΔUA2S(I)OH3 proton (9.2 ppb/K) is slightly lower than its counterpart in oligosaccharide [1], it is still greater than the hydrogen bonded Arixtra GlcA(II)OH3 proton.

Temperature coefficients of hydroxyl protons in oligosaccharide [3] are comparable to protons in similar microenvironments in oligosaccharides [1] and [2]. The GlcA(V)OH3 hydroxyl proton has the smallest temperature coefficient (6.9 ppb/K), comparable to the GlcA(III)OH3 proton in oligosaccharide [1]. The reducing end GlcNS6S(VI)OH3 proton has a larger temperature coefficient (8.5 ppb/K), comparable to the reducing end OH3 protons of both oligosaccharides [1] and [2]. The temperature coefficients of the OH3 protons of the reducing end GlcNS6S residues appear to be unaffected by the identity of the adjacent uronic acid residue. The internal GlcNS6S(II)OH3 proton also has a relatively large temperature coefficient (8.6 ppb/K) that is comparable to the GlcNS6S(II)OH3 proton of oligosaccharide [2]. Both protons are also in a similar microenvironment, flanked by a ΔUA2S residue at their non-reducing end and an IdoA2S residue at their reducing end. Both the GlcA(V)OH2 and IdoA2S(III)OH3 protons have the largest temperature coefficients (10.5 and 11.7 ppb/K, respectively), and are comparable to their counterparts in both oligosaccharides [1] and [2], respectively. The ΔUA2S(I)OH3 hydroxyl proton could not be evaluated in oligosaccharide [3] due to resonance overlap with carbon-bonded protons.

4.3.3 Chemical shift differences (Δδ). Chemical shift differences report on the hydroxyl proton microenvironment. A larger negative Δδ ($\Delta\delta = \Delta\delta_{oligo} - \Delta\delta_{mono}$) value (summarized in Table 4.1) indicates close proximity to an electronegative atom and a

greater possibility of participation in a hydrogen bond.[1,5,6]. The IdoA2S and ΔUA2S monosaccharides were not available, so their Δδ values are not included in Table 4.1.

In oligosaccharide [1], the GlcNS6S(IV)OH3 proton has the largest negative Δδ (-0.410 ppm), which is much larger than that of the Arixtra hydrogen bonded GlcA(II)OH3 hydroxyl proton (Chapter 3). Similar to temperature coefficients, Δδ values are also influenced by factors other than hydrogen bonding. The GlcA(III)OH3 proton has a Δδ value of -0.216 ppm, which is comparable to its counterpart in Arixtra and is consistent with its smaller temperature coefficient. The GlcNS6S(II)OH3 hydroxyl proton has a smaller negative Δδ value (-0.167 ppm). The GlcA(III)OH2 proton has the smallest negative Δδ (-0.103 ppm), corresponding to its smaller temperature coefficient.

Because monosaccharide standards are not available for ΔUA2S and IdoA2S, Δδ values could only be determined for the GlcNS6S(II) and GlcNS6S(IV)OH3 protons (-0.234 and -0.288 ppm, respectively) of oligosaccharide [2]. The Δδ values of both GlcNS6S OH3 protons are comparable to that of the GlcA(II)OH3 proton in Arixtra. The differences in temperature coefficients between the reducing end GlcNS6S(IV)OH3 proton of oligosaccharide [2] and that of oligosaccharide [1] could reflect differences in their microenvironment. The reducing end GlcNS6S residue in oligosaccharide [1] is adjacent to a GlcA residue whereas the reducing end GlcNS6S residue in oligosaccharide [2] is adjacent to an IdoA2S residue.

In oligosaccharide [3], the reducing end GlcNS6S(VI)OH3 proton has the largest negative Δδ (-0.407 ppm), comparable to its counterpart in oligosaccharide [1]. The similarity in these values is most likely attributed to similarities in their

microenvironments. Both residues are adjacent to a GlcA residue at their non-reducing end. The internal GlcNS6S(II)OH3 proton has a relatively large negative Δδ (-0.241 ppm), which is also comparable to its counterpart in oligosaccharide [2]. Both are in a similar microenvironment, flanked by a ΔUA2S residue at their non-reducing end and an IdoA2S residue at their reducing end. Although the relatively large temperature coefficient of the internal GlcNS6S(IV)OH3 proton suggests fast exchange, its relatively large Δδ (-0.330 ppm) suggests participation in a hydrogen bond. This residue has a unique microenvironment flanked by both GlcA and IdoA2S residues. The GlcA(V)OH2 and OH3 proton Δδ values (-0.108 and -0.212 ppm, respectively) are in good agreement with their temperature coefficients and are comparable to their respective counterparts in oligosaccharide [1]. Though chemical shift differences between the oligo- and monosaccharide can be a qualitative indicator of hydrogen bonding, the exchange rate constants, discussed in section 4.3.4, provide stronger evidence of hydroxyl proton hydrogen bonding.

4.3.4 Solvent exchange rates. The rate of hydroxyl proton-solvent exchange can be a direct indicator hydroxyl proton hydrogen bonding. To evaluate the exchange rates, EXSY spectra were acquired with mixing times between 0 and 24 ms for oligosaccharides [1] and [2] and between 0 and 22 ms for oligosaccharide [3]. EXSY spectra using 24 ms mixing time for oligosaccharides [1] and [2] (Figure 4.6A and 4.6B, respectively) and using 22 ms mixing time for oligosaccharide [3] (Figure 4.6C) show differences in the intensity of the water exchange cross peaks for the various hydroxyl proton resonances. To obtain exchange rate constants, the normalized exchange cross

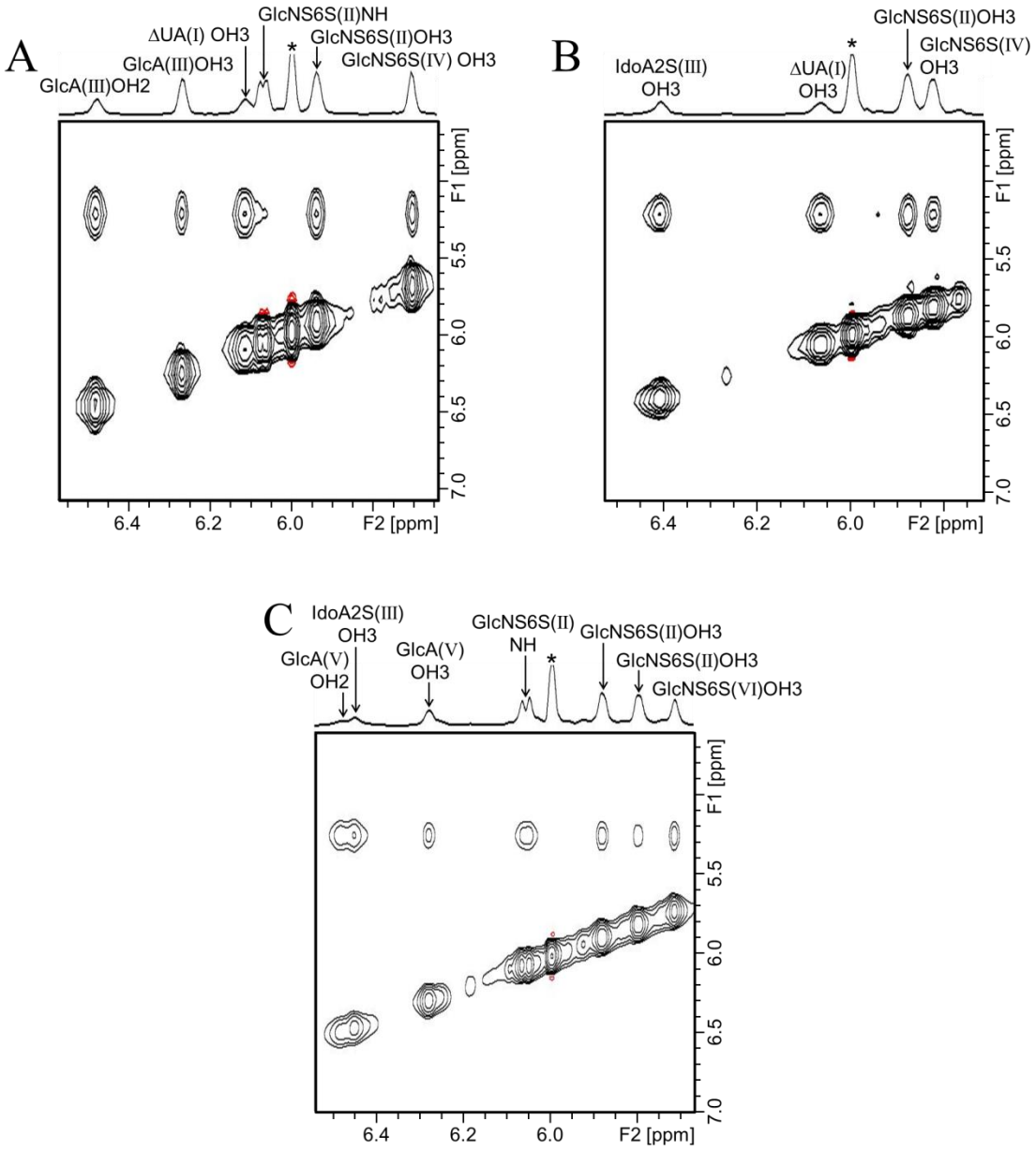

Figure 4.6. Hydroxyl proton EXSY spectra of oligosaccharides (A) [1], (B) [2] and 24 ms mixing time and oligosaccharide (C) [3] at 22 ms mixing time. Hydroxyl proton resonances are labeled. Sulfamate protons also give rise to an exchange cross peak to the solvent water. Carbon-bound protons are indicated with an asterisk.

peak volumes are plotted as a function of mixing time for each oligosaccharide (Figure 4.7). Initial build-up rate constants are calculated as described in Chapter 3 and are summarized in Table 4.1.[1]

The EXSY initial build-up rates (k_{ex}) of the oligosaccharide [1] hydroxyl protons suggest participation of the GlcA(III)OH3 proton in a hydrogen bond as this proton has the smallest initial build-up rate (7.33 s^{-1}). Although the initial build-up rates of GlcNS6S(II) and GlcNS6S(IV)OH3 protons are slightly higher (9.70 and 9.13 s^{-1}, respectively) than that of the GlcA(III)OH3 proton, they are significantly lower than those of the ΔUA2S(I)OH3 and GlcA(III)OH2 protons (24.3 and 24.5 s^{-1}, respectively). It is possible that the two GlcNS6S OH3 protons also participate in hydrogen bonds in oligosaccharide [1]. MD simulations would provide additional evidence to clarify the experimental results.

In oligosaccharide [2], the EXSY initial build-up rates show evidence of hydrogen bonding only in the GlcNS6S(II) and GlcNS6S(IV)OH3 hydroxyl protons with fairly small initial build-up exchange rates (6.71 and 4.95 s^{-1}, respectively). With an initial build-up rate of 18.9 s^{-1}, it appears that the IdoA2SOH3 does not participate in a hydrogen bond. The IdoA2S residue changes its conformation from majority $^{2}S_{O}$ to majority $^{1}C_{4}$ without the adjacent glucosamine 3-*O*-sulfate group.[16] This most likely moves the IdoA2SOH3 proton away from the sulfamate protons to which it is hydrogen bonded in Arixtra (Chapter 3). MD simulations would provide more insight into the effects of structure on hydroxyl proton hydrogen bonding patterns.

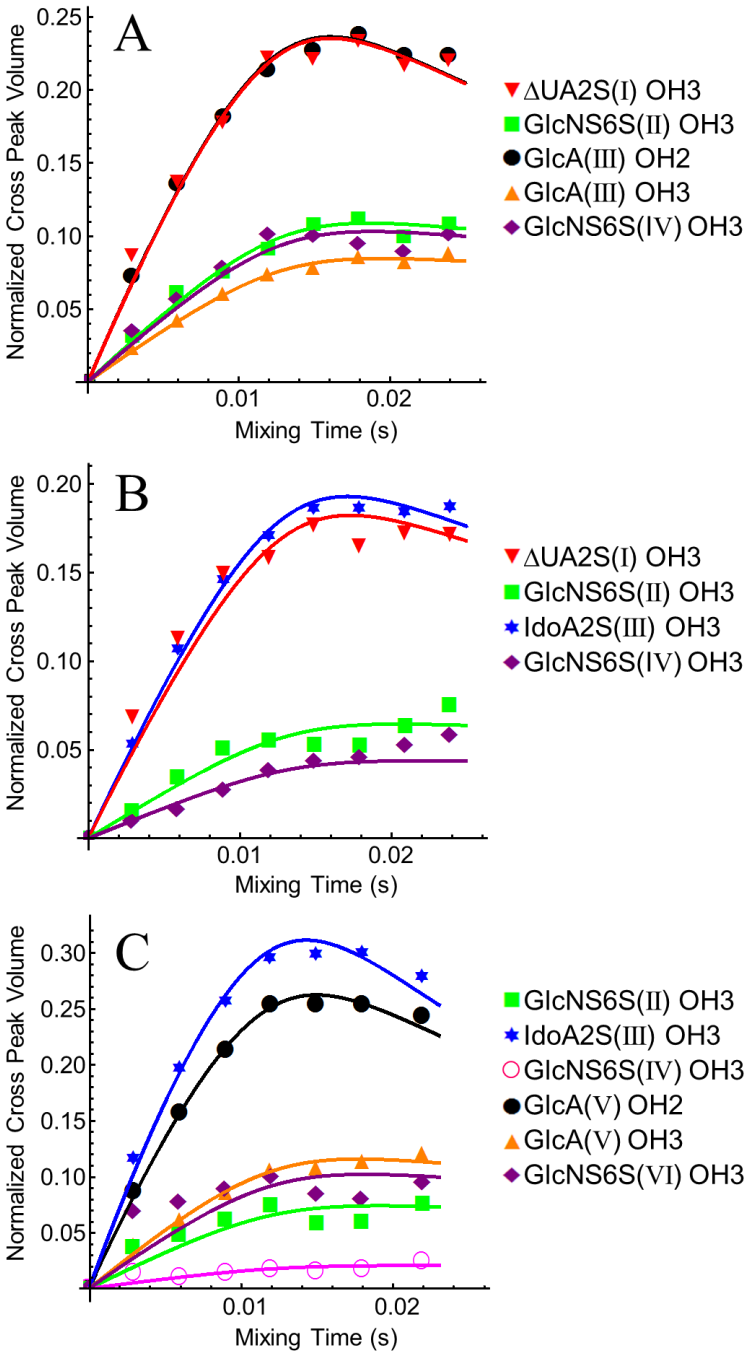

Figure 4.7. EXSY initial build-up rate curves for the hydroxyl protons of oligosaccharides (A) [1], (B) [2], and (C) [3].

The hydroxyl proton hydrogen bond patterns in oligosaccharide [3] are similar to those in oligosaccharides [1] and [2] but differ from those measured in Arixtra. No evidence of a hydrogen bond was found in the IdoA2S(III)OH3 proton in oligosaccharide [3]. Its initial build-up rate (37.9 s^{-1}) is much larger than that of the GlcA(V)OH2 proton (30.0 s^{-1}). The GlcNS6S(IV)OH3 proton has the smallest initial build-up rate (1.75 s^{-1}), suggesting its participation in a hydrogen bond. The GlcNS6S(II)OH3 proton also has a relatively small initial build-up rate (6.73 s^{-1}) which suggests that it may also be involved in a hydrogen bond. The reducing end GlcNS6S(VI)OH3 proton initial build-up rate (9.61 s^{-1}) is slightly larger, but is comparable to that of the reducing end OH3 proton of oligosaccharide [1]. Interestingly, both GlcNS6S(II) and GlcNS6S(VI)OH3 proton initial build-up rates, temperature coefficients, and $\Delta\delta$ values are comparable to their respective counterparts in oligosaccharides [2] and [1], respectively. Experimental evidence suggests that the GlcNS6SOH3 protons of oligosaccharide [3] all participate in hydrogen bonds. The GlcA(V)OH3 proton initial build-up rate (11.1 s^{-1}) is slightly higher than the GlcNS6SOH3 protons of oligosaccharide [1] or Arixtra. It is possible that this proton is no longer participating in a strong hydrogen bond in oligosaccharide [3]. MD simulations would provide further insight into the presence of hydroxyl proton hydrogen bonds and the hydrogen bond acceptor in these oligosaccharides.

4.3.5 Effects of microstructure on hydroxyl proton chemical exchange. The hydroxyl proton temperature coefficients, $\Delta\delta$ values, and initial build-up rates are influenced by their surrounding microstructure, supporting our assertion that differences in heparin microstructure affect local hydrogen bonding patterns. Experimental evidence

suggests that the IdoA2SOH3 proton no longer participates in a hydrogen bond without an adjacent GlcNS3S6S residue. The GlcAOH3 proton shows evidence of participation in a hydrogen bond without an adjacent GlcNS3S6S residue only if an IdoA2S residue is also not present. The results presented in this chapter also suggest that the GlcNS6SOH3 protons are involved in a hydrogen bond when the 3-*O*-sulfate group is not present.

4.3.6 Effects of CO_2 on hydroxyl proton exchange. In Chapter 3 we demonstrated that CO_2 contamination introduced by bubbling the sample with N_2 changed the relative hydrogen bonding patterns within the pentasaccharide Arixtra. The samples evaluated in this chapter were not bubbled with N_2, to help minimize their exposure to CO_2. The results presented in this chapter are comparable for hydroxyl protons in similar microenvironments within different oligosaccharides, suggesting that these results are not strongly affected by CO_2 contamination. Future experiments should be performed which look further into the effect that CO_2 contamination has on all oligosaccharide chains studied and to reduce CO_2 contamination by removing it from the N_2 feed (Chapter 7).

4.4. Conclusions

Hydroxyl hydrogen bonds were identified using solvent exchange rates taken together with temperature coefficient and $\Delta\delta$ measurements of isolated heparin oligosaccharides that are structurally similar to Arixtra. It was demonstrated that oligosaccharides that do not contain a 3-*O*-sulfate group have different hydroxyl proton hydrogen bond patterns than those observed for Arixtra. The most significant finding of this work is that the internal GlcNS6SOH3 protons show evidence of hydrogen bonding in oligosaccharides

that do not have a glucosamine 3-*O*-sulfate group. The IdoA2SOH3 proton, on the other hand, does not appear to participate in a hydrogen bond without an adjacent GlcNS3S6S residue. It appears that the GlcAOH3 proton participates in a hydrogen bond without the 3-*O*-sulfate group only if the IdoA2S residue is also absent. The results presented in this Chapter highlight the role that heparin's structural microheterogeneity plays in adoption of local secondary structure.

4.5. References

1. Beecher, C. N.; Young, R. P.; Langeslay, D. J.; Mueller, L. J.; Larive, C. K., Hydroxyl-proton hydrogen bonding in the heparin oligosaccharide arixtra in aqueous solution. *J. Phys. Chem. B* **2014,** *118*, 482-491.

2. Langeslay, D. J.; Young, R. P.; Beni, S.; Beecher, C. N.; Mueller, L. J.; Larive, C. K., Sulfamate proton solvent exchange in heparin oligosaccharides: Evidence for a persistent hydrogen bond in the antithrombin-binding pentasaccharide Arixtra. *Glycobiology* **2012,** *22*, 1173-1182.

3. Kindahl, L.; Sandstrom, C.; Norberg, T.; Kenne, L., ^{1}H NMR studies of hydroxy protons of Asn- and Ser-linked disaccharides in aqueous solution. *J. Carbohyd. Chem.* **2000,** *19*, 1291-1303.

4. Kindahl, L.; Sandstrom, C.; Norberg, T.; Kenne, L., ^{1}H NMR studies of hydroxy protons of the V[β-Gal(1→3)-α-GalNAc(1→O)]THPGY glycopeptide. *Carbohyd. Res.* **2001,** *336*, 319-323.

5. Vilen, E. M.; Lundqvist, L. C. E.; Jouanneau, D.; Helbert, W.; Sandstrom, C., NMR study on hydroxy protons of κ- and κ/μ-hybrid carrageenan oligosaccharides: Experimental evidence of hydrogen bonding and chemical exchange interactions in κ/μ oligosaccharides. *Biomacromolecules* **2010,** *11*, 3487-3494.

6. Sandstrom, C.; Kenne, L., Hydroxy protons in structural studies of carbohydrates by NMR spectroscopy. *ACS. Sym. Ser.* **2006,** *930*, 114-132.

7. Eyring, H., The Activated Complex in Chemical Reactions. *J. Chem. Phys.* **1935,** *3* (2), 107-115.

8. Pechukas, P., Transition state theory. *Annu. Rev. of Phys. Chem.* **1981,** *32*, 159-177.

9. Bain, A. D., Chemical exchange in NMR. *Prog. Nucl. Mag. Res. Sp.* **2003,** *43*, 63-103.

10. Dobson, C. M.; Lian, L. Y.; Redfield, C.; Topping, K. D., Measurement of hydrogen exchange rates using 2D NMR spectroscopy. *J. Magn. Reson.* **1986,** *69*, 201-209.

11. Jeener, J.; Meier, B. H.; Bachmann, P.; Ernst, R. R., Investigation of exchange processes by two-dimensional NMR spectroscopy. *J. Chem. Phys.* **1979,** *71*, 4546-4553.

12. Sandstrom, C.; Baumann, H.; Kenne, L., NMR spectroscopy of hydroxy protons of 3,4-disubstituted methyl α-D-galactopyranosides in aqueous solution. *J. Chem. Soc. Perk. T. 2* **1998,** 809-815.

13. Hwang, T. L.; Shaka, A. J., Water suppression that works. Excitation sculpting using arbitrary wave-forms and pulsed-field gradients. *J. Magn. Reson. Ser. A* **1995,** *112*, 275-279.

14. Van Geet, A. L., Calibration of methanol and glycol nuclear magnetic resonance thermometers with a static thermistor probe. *Anal. Chem.* **1968,** *40*, 2227-2229.

15. Chen, J. H.; Mao, X. A., Measurement of chemical exchange rate constants with solvent protons using radiation damping. *J. Magn. Reson.* **1998,** *131*, 358-361.

16. Ferro, D. R.; Provasoli, A.; Ragazzi, M.; Torri, G.; Casu, B.; Gatti, G.; Jacquinet, J. C.; Sinay, P.; Petitou, M.; Choay, J., Evidence for conformational equilibrium of the sulfated L-iduronate residue in heparin and in synthetic heparin mono- and oligosaccharides: NMR and force-field studies. *J. Am. Chem. Soc.* **1986,** *108*, 6773-6778.

CHAPTER FIVE

Detection of the Amine and Hydroxyl Protons of Heparan Sulfate Related Monosaccharides and Characterization of their Solvent Exchange Properties

Based on a paper published in Analytical Chemistry

Anal. Chem. 2015, ASAP, DOI: 10.1021/acs.analchem.5b01181

Abstract: Glucosamine is an important constituent of the heterogeneous glycosaminoglycans heparin and heparan sulfate occurring in *N*-acetylated and *N*-sulfated forms, and as the unmodified amine. Though the ^{1}H and ^{15}N NMR chemical shifts of *N*-acetyl- and *N*-sulfoglucosamine residues have been extensively characterized, this study provides the first direct NMR characterization of the amine groups of glucosamine and 3-*O*-sulfoglucosamine in aqueous solution. The solvent exchange properties of the amine protons are examined and the possibility of a salt bridge between the sulfate and amine groups of 3-*O*-sulfoglucosamine was explored through ^{1}H NMR pK_a measurements, but is not supported by the experimental results.

5.1 Introduction

More than 400 heparin binding proteins have been identified,[1] however, for many of these proteins the native ligand is believed to be the structurally-related cell-surface proteoglycan heparan sulfate. Glucosamine 3-*O*-sulfation, a relatively rare modification, is critical for high affinity binding of heparin and heparan sulfate to antithrombin-III resulting in its activation as a potent thrombin inhibitor.[2-4] 3-*O*-sulfation also increases the

affinity of heparan sulfate for the herpes simplex virus glycoprotein D facilitating viral fusion,[5-10] and is implicated in binding to fibroblast growth factors,[11,12] cyclophilin B,[13] and stabilin.[14,15] Evidence is also emerging about the importance of glucosamine 3-*O*-sulfation in development and cancer.[16]

NMR spectroscopy is a well-established analytical tool for the structural characterization of heparin and heparan sulfate.[17,18] Because they are linear repeating polymers composed of variously substituted uronic acid-glucosamine disaccharide subunits, NMR detection of the ^{1}H and ^{15}N chemical shifts of *N*-acetylated (GlcNAc), *N*-sulfated (GlcNS) and unmodified (GlcN) glucosamine residues can provide important insights into heparin and heparan sulfate structure. NMR measurements of the amide protons of GlcNAc residues are well-established and are easily executed due to their slow exchange in acidified aqueous solution.[19-21] In contrast, conditions that permit detection of the more rapidly exchanging GlcNS NH resonances have only been reported recently.[22] GlcNS sulfamate ($NHSO_3^-$) ^{1}H and ^{15}N chemical shifts have been used to provide important structural information for complex samples like low molecular weight heparins.[23,24] In addition, exploration of the solvent exchange properties of the sulfamate protons led to the identification of a hydrogen bond in the synthetic ultra-low molecular weight heparin drug Arixtra™ (fondaparinux).[25] To our knowledge there have been no prior reports of direct NMR measurements of the GlcN amine protons because of their rapid exchange in solution. Although the glucosamine ^{15}N chemical shift has been indirectly recorded using the [^{1}H,^{15}N] HMBC experiment, it from poor sensitivity due to small values of $^{3}J_{NH}$.[26]

Building on our recent success in using ^{1}H NMR to study the hydroxyl protons of heparin oligosaccharides,[27,28] we report herein the NMR characterization of the amine groups of the GlcN and 3-*O*-sulfoglucosamine (GlcN3S) monosaccharides through the measurement of ^{1}H and [^{1}H,^{15}N] HSQC spectra. We further explore the solvent exchange properties of these protons, and through measurement of the amine group pK_a values examine the possibility of a salt bridge between the adjacent amine and sulfate groups of GlcN3S.

5.2 Materials and methods

5.2.1 Materials and reagents. The monosaccharides D-glucosamine (GlcN) and D-glucosamine-3-sulfate (GlcN3S) were purchased from Sigma-Aldrich (Saint Louis, MO). Deuterated acetone (acetone-d_6, 99.9% D) and deuterium oxide (D_2O, 99% D) were purchased from Cambridge Isotope Laboratories (Andover, MA). DSS-d_6 (3-(trimethylsilyl)-1-propanesulfonic acid sodium salt) was purchased from Isotech (Miamisburg, OH). High-performance liquid chromatography (HPLC-) grade water was obtained from Burdick and Jackson (Muskegon, MI). The pH meter was calibrated with buffers at pH 4.00, 7.00, and 10.00 purchased from Fisher Scientific (Hampton, NH). The hydrochloric acid (HCl) and dibasic sodium phosphate were purchased from Fisher Scientific (Hampton, NH) and the sodium hydroxide (NaOH) was purchased from Macron Fine Chemicals (Center Valley, PA).

5.2.2 Solution preparation for NMR measurements Solutions for NMR resonance assignment and exchange experiments were composed of 85% H_2O/15% acetone-d_6 at

pH 3.65 and were recorded at -14.5 °C.[27-31] All pH measurements were performed at room temperature using a double-junction Ag/AgCl micro-pH electrode (Thermo Scientific, Beverly, MA) prior to the addition of acetone-d_6. The pH optima for NMR detection of the amine protons of GlcN and GlcN3S were determined through pH titrations performed under an N_2 atmosphere in our attempt to avoid catalyzed exchange from dissolved carbon dioxide (CO_2).[2,27] Solutions were prepared using HPLC-grade water that had been boiled and then bubbled with N_2 to remove dissolved CO_2. These experiments were performed prior to our studies in section 3.3.7 which noted contamination of the N_2 by CO_2. The potential impact of dissolved CO_2 on these measurements is discussed in section 5.3.3.

The pK_a values of the amine group of the GlcN and GlcN3S monosaccharides were determined by ^{1}H NMR by following the chemical shift of the carbon-bound H2 proton as a function of pH. Monosaccharide solutions (10 mM) in 90% H_2O/10% D_2O solution containing 10 mM phosphate buffer and 1 mM DSS were titrated from pH 3.07 to pH 10.50 (GlcN) or from pH 3.01 to pH 10.42 (GlcN3S) using HCl and NaOH dissolved in of 90% H_2O/10% D_2O. NMR measurements were performed at 25 °C.

5.2.3 NMR experimental parameters. One-dimensional ^{1}H NMR spectra were obtained for each of the GlcN and GlcN3S samples at a temperature of -14.5 °C on a Bruker Avance 600 MHz spectrometer operating at 599.58 MHz using excitation sculpting for solvent suppression ("zgesgp").[32] A total of 32 scans for GlcN and 128 scans for GlcN3S were coadded into 32768 complex points. A spectral window of 8389 Hz and relaxation delay of 2.0 s were used with a 90° pulse of 8.5 μs at a power level of -

5.00 dB. Spectra were zero-filled using 32768 points and line-broadening of 0.30 Hz. For solutions containing acetone-d_6, spectra were referenced to the residual ^{1}H acetone-d_6 signal at 2.204 ppm. For solutions containing DSS, spectra were referenced to the residual ^{1}H signal set to 0.00 ppm. Resonances were assigned using double quantum filtered (DQF)-COSY spectra.

DQF-COSY spectra were measured using excitation sculpting solvent suppression (Bruker pulse program "cosyfesgpph") for 10 mM GlcN and 10 mM GlcN3S in 85% H_2O/15% acetone-d_6 at pH 4.02 and -14.5 °C. Spectra were acquired using States-TPPI with 64 scans coadded into 2048 complex points in F2 with 192 increments in F1. A spectral window of 7183 Hz was used in both F2 and F1 dimensions. A relaxation delay of 2.0 s was used with a 90° pulse of 8.72 μs for GlcN and 8.93 μs for GlcN3S at a power level of -5.00 dB. Spectra were zero filled to 4096 points in F1 and 512 points in F2 and were apodized using a cosine squared function.

Two-dimensional [^{1}H, ^{15}N] HSQC experiments were measured at pH 3.65 using echo-antiecho phase cycling. Spectra were acquired into 4096 complex points. For GlcN 240 scans were coadded in F1 over 128 scans in F2 while for GlcN3S 384 coadded scans in F2 were collected over 144 scans. A spectral window of 6887 Hz was used in the ^{1}H dimension and 2430 Hz was used in the ^{15}N dimension with the ^{15}N frequency set to 35 ppm. A value of 90 Hz was used for J_{HN} with a relaxation delay of 2.0 s. Spectra were zero-filled using 8192 points in F2 and 256 points in F1 and apodized in each dimension using a cosine squared function with 0.50 Hz line broadening in F2 and 0.30 Hz line broadening in F1.

One-dimensional ^{1}H NMR spectra were measured as a function of temperature using excitation sculpting solvent suppression for GlcN and GlcN3S samples at pH 3.65. Temperature coefficients were calculated by taking the absolute value of the best fit line obtained by plotting chemical shift as a function of temperature.[25,29,31,33] The resonances were fit to a Lorentzian function in Mathematica to extract the widths at half-height ($\omega_{1/2}$) which were plotted as a function of temperature and fit to the Eyring-Polanyi equation (Eq. 1.5) to determine the energetic barrier to solvent exchange, $\Delta G^{\ddagger}$.[25,34,35]

The rates of chemical exchange of the amine protons with water were measured by exchange spectroscopy (EXSY) using the NOESY pulse sequence incorporating excitation sculpting solvent suppression. All spectra were recorded at a temperature of -14.5 °C. A total of nine EXSY spectra were recorded for each sample using mixing times that ranged from 0 to 24 ms in 3 ms intervals.[27,30] Spectra were recorded with 2048 complex points using 128 experiments, each with 32 coadded scans using States-TPPI. A spectral window of 7184 Hz was used in both F1 and F2 with a 1.5 s relaxation delay. A power level of -5.00 dB was used with 90º pulses (pulse widths 8.85 - 9.05 μs). EXSY spectra were processed using 16384 complex points in F2 and 4096 complex points in F1 and apodized using a cosine squared function in both dimensions. Amine and hydroxyl proton cross peaks were integrated using the Topspin 3.1 software. Cross peak volumes were normalized to the corresponding diagonal peak volume and plotted as a function of mixing time. EXSY build-up curves were fit using Mathematica.[27,36]

5.3 Results and discussion

The structures of the GlcN and GlcN3S monosaccharides are given in Figure 5.1. In aqueous solution, glucosamine exists as an equilibrium mixture of α- and β-anomers. Because the rate of mutarotation is slow on the NMR timescale, the spectrum contains the resonances of both anomeric species.

The glucosamine amine and hydroxyl protons are also involved an equilibrium in which they exchange with the solvent water as indicated by the chemical reaction listed below, using the amine protons as an example:

$$RNH_3^+ + HOH^* \rightleftharpoons RNH^*H_2^+ + HOH$$

where the asterisk denotes a proton that exchanges between water and the glucosamine amine group during the time in which the FID is acquired. The rate of the chemical exchange reaction is pH dependent as indicated by Eq. 5.1.

$$k_{overall} = k_{H+} \times [H^+] + k_{OH-} \times [OH^-] \qquad \text{(Eq. 5.1)}$$

The solvent exchange reaction is both acid and base catalyzed. Therefore in very acidic or basic solution the rate of the exchange reaction will be fast on the NMR timescale and the resonance of the amine protons will not be observed in the NMR spectrum. Because the rate constants for the acid (k_{H+}) and base (k_{OH-}) catalyzed terms are not equal, the minimum in the exchange rate (indicated by $k_{overall}$) typically does not occur at neutral pH. For example, the exchange rate is minimized for amide protons around pH 3 – 4,[19,20,21] and for the sulfamate protons the exchange minimum occurs in slightly basic solution, around pH 8.[22]

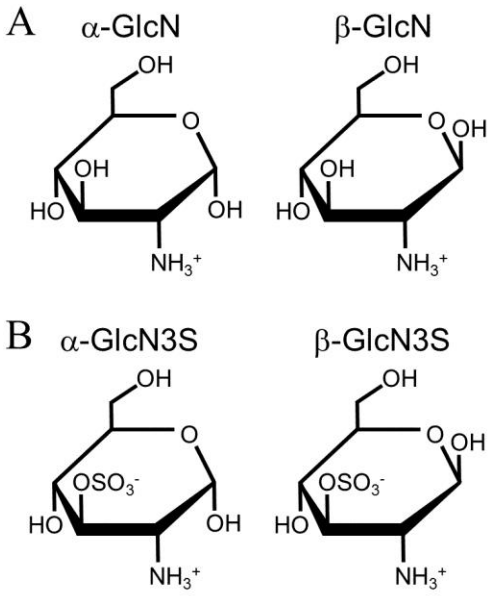

Figure 5.1. The structures of the α- and β-anomers of (A) GlcNS and (B) GlcN3S.

5.3.1. Detection and identification of the GlcN and GlcN3S amine protons. To identify the solution conditions conducive for detection of the resonances of the glucosamine amine protons, NMR spectra were recorded at -14.5 ºC in 85% H_2O/15% acetone-d_6, conditions used previously to characterize sugar hydroxyl proton resonances, which also undergo solvent exchange with water.[27,29] Upon dissolution at room temperature, glucosamine gives rise to a solution at pH 5.30. Though the α-anomeric hydroxyl (OH1) resonance is visible as a broad peak at 7.47 ppm in Figure 5.2A, at pH 5.30 the sharper resonances of the other hydroxyl resonances of the GlcN α- and β-anomers are observed between 5.8 and 7.1 ppm. In addition, the hemiacetal resonance of acetone (marked with an asterisk) appears at 6.94 ppm. As the pH is lowered, most of the OH resonances broaden until they are no longer detected. Conversely, the amine resonances of the GlcN α- and β-anomers sharpen as the solution pH (measured at room temperature) is lowered to 3.65, behavior mirrored by the OH1 resonance of the α-anomer. A similar trend is observed for the GlcN3S amine and OH protons (Figure 5.2B). The amine and α-OH1 proton resonances were identified using the DQF-COSY spectra (Figure 5.3).

The regions of the one-dimensional ^{1}H NMR spectra containing the amine resonances of GlcN and GlcN3S are compared in Figures 5.4A and 5.4B, respectively. The presence of the 3-*O*-sulfate group in GlcN3S produces a slight upfield shift of the amine resonances of both anomers. Notably, the α-OH1 resonances of GlcN and GlcN3S are also observed at pH 3.65 (Figure 5.4). In Chapters 3 and 4, more basic solution conditions were used to minimize the solvent exchange of the hydroxyl protons of *N*-

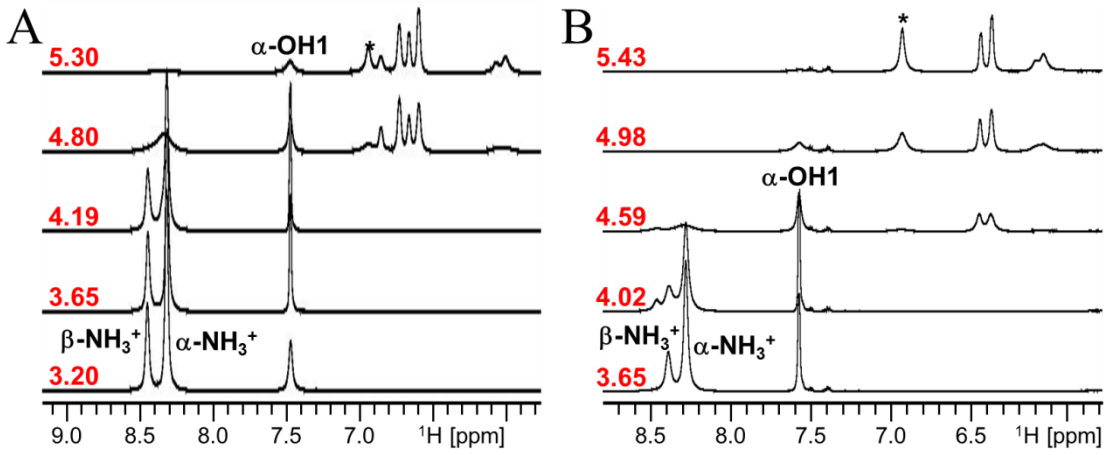

Figure 5.2. Results of the pH titration of (A) GlcN and (B) GlcN3S to determine the optimum pH for amine proton detection by NMR. Though the spectra were measured at -14.5 ºC in 85% H_2O/15% acetone-d_6, the solution pH values were recorded at room temperature prior to the addition of acetone. The resonance of the hemiacetal form of acetone at 6.94 ppm is indicated by an asterisk.

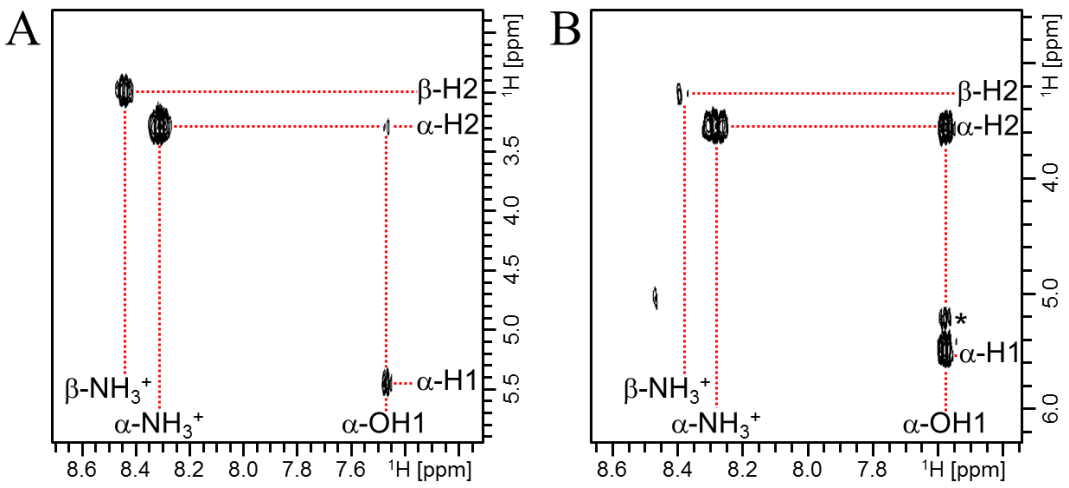

Figure 5.3. Double-quantum filtered COSY spectra of (A) GlcN and (B) GlcN3S in 85% H_2O/15% acetone-d_6 at pH 4.02 and -14.5 °C. The assignments of the amine and OH1 resonances are indicated on the contour plots. The crosspeak indicated with an asterisk is an artifact at the chemical shift of water.

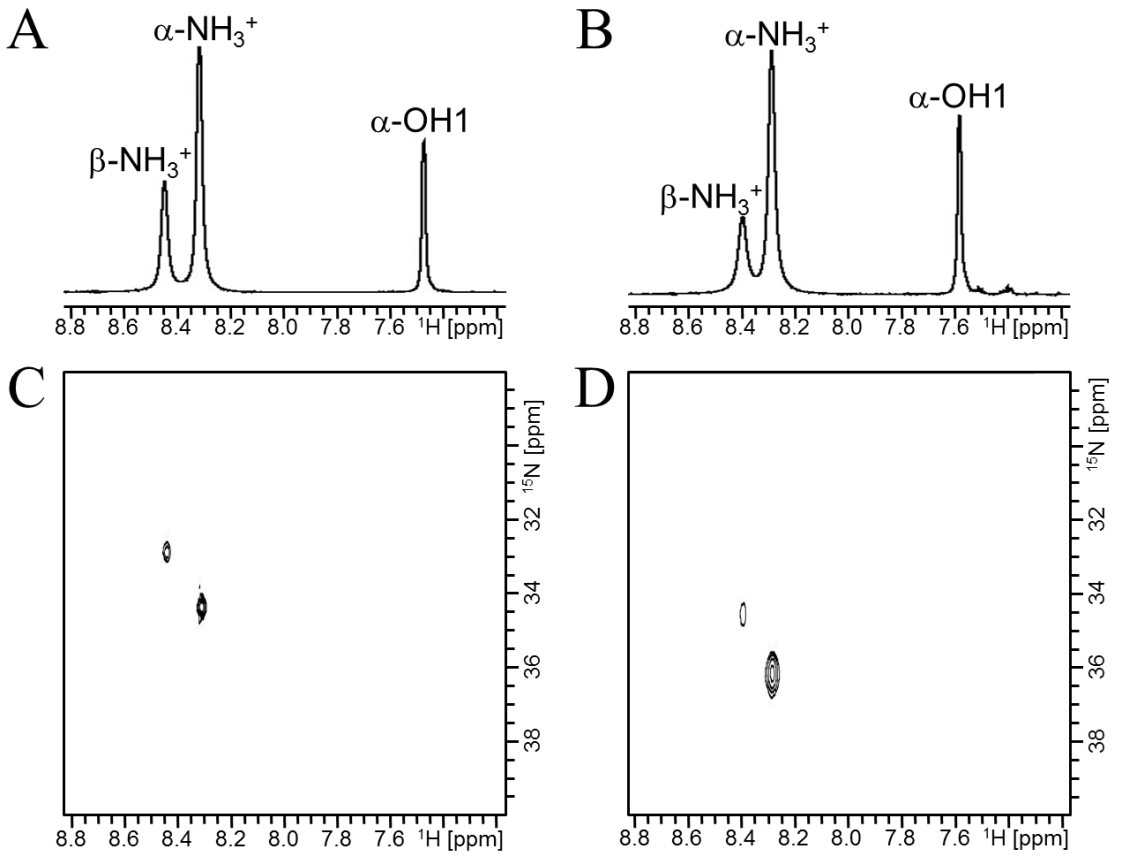

Figure 5.4. Expansions of the one-dimensional ^{1}H NMR spectra of (A) GlcN and (B) GlcN3S measured in 85% H_2O/15% acetone-d_6 at -14.5 °C. The [^{1}H,^{15}N] HSQC spectra of (C) GlcN and (D) GlcN3S show the one-bond ^{1}H-^{15}N correlations of the α- and β-anomer amine groups. Since it is not coupled to a nitrogen atom, no HSQC correlation is expected for the α-OH1 proton.

sulfated heparin oligosaccharides.[27] The stabilization of the GlcN and GlcN3S α-OH1 resonances at low pH reflects a decrease in the rate of the acid catalyzed exchange term in Eq. 5.1, which may arise due to charge repulsion of H^+ by the adjacent positively charged amine group. Supporting this hypothesis, the resonance of the β-OH1 is not observed at this pH, similar to the other GlcN and GlcN3S hydroxyl protons, likely because in the chair conformation the β-OH1 is in the equatorial position pointing away from the amine. Although the absolute pH minimum for the amine protons is not 3.65, this pH was chosen because it falls within the range of pH 3.20 and 4.19 where the amine protons appear the sharpest (Figure 5.2).

Two-dimensional [^{1}H,^{15}N] HSQC spectra were measured for GlcN (Figure 5.4C) and GlcN3S (Figure 5.4D) with the ^{1}H and ^{15}N chemical shifts summarized in Table 5.1. The [^{1}H,^{15}N] HSQC experiment detects correlations between ^{1}H and ^{15}N nuclei coupled through one bond, and therefore no peak is expected for the α-OH1 proton because it does not have a ^{1}H-^{15}N bond. The presence of the 3-*O*-sulfate group produces a 2 ppm downfield shift in the^{15}N frequency. The ^{15}N chemical shifts of the α-GlcN (34.4 ppm) and α-GlcN3S (36.2 ppm) are also consistently downfield of the corresponding β-GlcN (32.9 ppm) and β-GlcN3S (34.5 ppm) due to deshielding by nearby OH1 oxygen in the α-anomer. Overall, the ^{15}N chemical shifts determined are slightly downfield of the values previously reported using HMBC, most likely due to temperature differences between the two sets of measurements.[26] Detection by HSQC through one-bond ^{1}H-^{15}N couplings is much more sensitive than indirect detection by HMBC through long-range couplings. The sensitivity improvement resulting from HSQC detection, especially when

Table 5.1. The ^{1}H and ^{15}N chemical shifts and pK_a values of α- and β-anomers of the GlcN and GlcN3S amine moieties. The ^{15}N chemical shifts were measured -14.5 °C in 85% H_2O/15% acetone-d_6 at a room temperature pH of 3.65. The pK_a values were measured at 25 °C in a 90% H_2O/10% D_2O solution containing 10 mM phosphate buffer and 1 mM DSS.

Saccharide	Group	^{1}H Chemical Shift (ppm)	^{15}N Chemical Shift (ppm)	pK_a
GlcN	α-NH_3^+	8.31	34.4	7.84
	β-NH_3^+	8.44	32.9	7.44
GlcN3S	α-NH_3^+	8.28	36.2	7.40
	β-NH_3^+	8.39	34.5	7.16

coupled with higher field and/or cryoprobe equipped magnets, should make it feasible to use this approach to characterize the amine groups of heparin and heparan sulfate oligosaccharides, which are typically available in very limited quantities.

5.3.2. Chemical exchange properties of the GlcN and GlcN3S amine protons. The observation of an intramolecular hydrogen bond between the 3,6-*O*-sulfo-*N*-sulfoglucosamine (GlcNS3S6S) sulfamate NH and the adjacent 3-*O*-sulfate group in the Arixtra pentasaccharide[25] raises the possibility that that the amine protons of GlcN and GlcN3S may also participate in hydrogen bonds or that the GlcN3S amine group could form a salt bridge with the adjacent 3-*O*-sulfate group. With the ability to detect the amine protons by NMR, we can probe for hydrogen bonds or salt bridge interactions through measurements of temperature coefficients, energy barriers for solvent exchange ($\Delta G^{\ddagger}$), and solvent exchange rates determined using EXSY. The values determined in this study are summarized in Table 5.2.

The effects of temperature on the amine and α-OH1 resonances can be observed in the spectra shown in Figure 5.5 for GlcN3S. As the temperature is increased from -15.3 °C to 6.8 °C, the α- and β-amine and α-OH1 protons experience a linear upfield shift and broaden. Temperature coefficients were calculated from the absolute value of the slope of the lines obtained by plotting chemical shift as a function of temperature (Figure 5.6). The GlcN β-amine protons have a slightly larger temperature coefficient (4.49 ppb/K) compared with that of the α-anomer (4.14 ppb/K). A similar trend is observed for GlcN3S with the temperature coefficient of the β-amine protons (3.60 ppb/K) larger than the α-anomer (2.99 ppb/K). The temperature coefficients of the α-

Table 5.2. The temperature coefficients, $\Delta G^{\ddagger}$ values and solvent exchange rate constants determined for the amine and α-OH1 protons of GlcN and GlcN3S.

Saccharide	Group	Temperature Coefficient (ppb/K)	$\Delta G^{\ddagger}$ (kcal/mol)	Solvent Exchange Rate Constants (s^{-1})
GlcN	α-NH_3^+	4.14	14.0	4.27
	β-NH_3^+	4.49	13.7	11.3
	α-OH1	4.39	14.8	9.84
GlcN3S	α-NH_3^+	2.99	13.6	22.2
	β-NH_3^+	3.60	13.3	37.3
	α-OH1	4.07	14.6	11.5

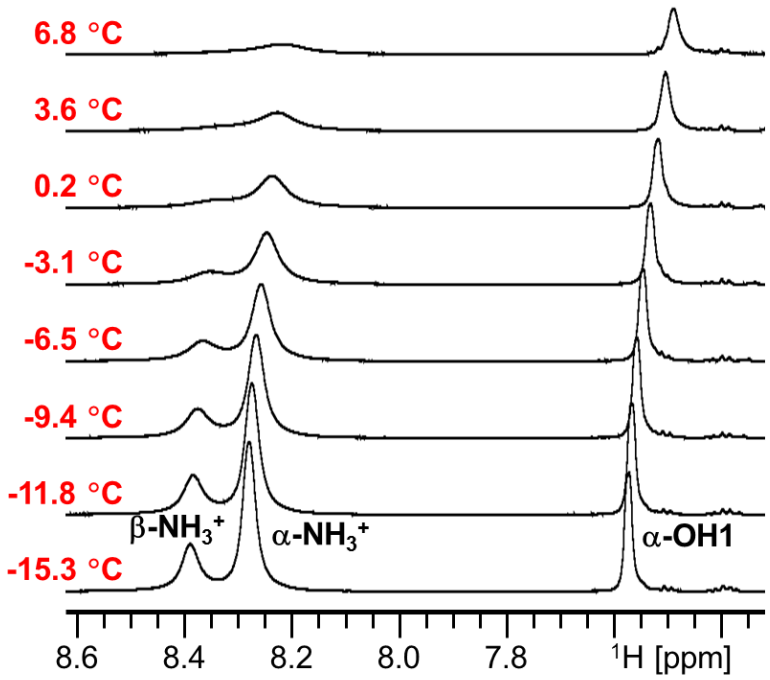

Figure 5.5. Increasing temperature causes the α- and β-NH_3^+ and α-OH1 resonances of GlcN3S to shift linearly upfield and broaden as the rate of solvent exchange increases.

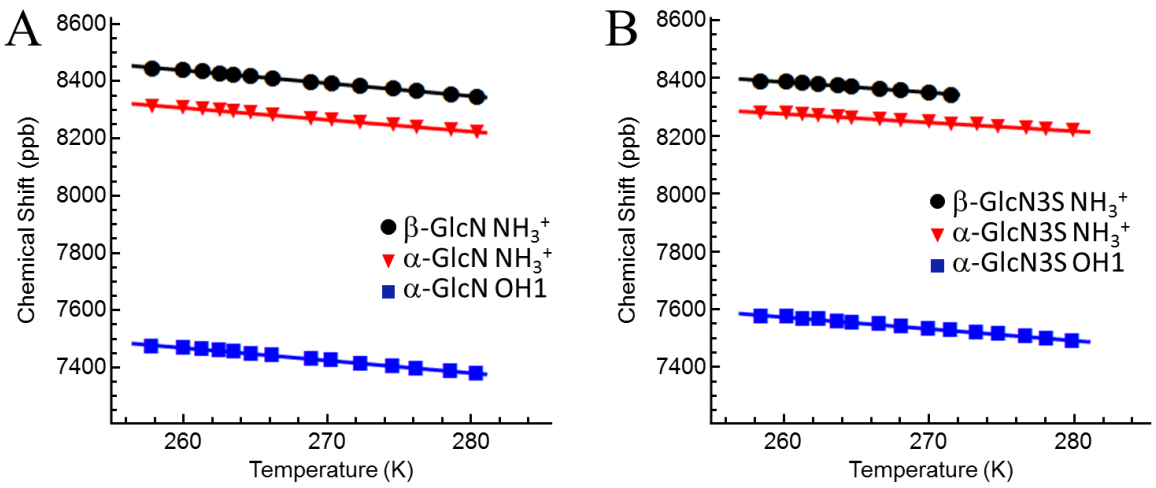

Figure 5.6. The temperature coefficient plots for the amine and α-OH1 proton of (A) GlcN and (B) GlcN3S.

OH1 resonances of GlcN (4.39 ppb/K) is slightly larger than that of GlcN3S (4.07 ppb/K), similar to the trend observed in the amine protons of GlcN and GlcN3S. Though amide proton temperature coefficients are a well-established qualitative indicator of hydrogen bonding peptides and proteins,[37-40] because this is the first NMR study of amine groups in sugars, an extensive literature is not available to provide a basis of comparison. The GlcN3S amine temperature coefficients are somewhat lower than those reported in our prior study of the sulfamate protons of GlcNS or 6-*O*-sulfo-*N*-sulfoglucosamine (GlcNS6S), which ranged from 3.8 to 7.4 ppb/K, but higher than the 1.0 ppb/K of the GlcNS3S6S sulfamate proton involved in a hydrogen bond to the adjacent 3-*O*-sulfate group.[25] The temperature coefficients of the GlcN and GlcN3S α-OH1 protons are in general lower than the values reported for the Arixtra hydroxyl protons at pH 8.1 (section 3.3.5).

Though temperature coefficients do not provide a direct indication of hydrogen bonding, they can be used to support insights provided through other means, including the results of lineshape analysis. As observed in Figure 5.4, as the temperature is raised resonances broaden due to an increase in the solvent exchange rate. Resonance linewidths were plotted as a function of temperature and the value of the energetic barrier for solvent exchange, $\Delta G^{\ddagger}$, calculated by fitting the results for GlcN (Figure 5.7) and GlcN3S (Figure 5.8) to the Eyring-Polanyi equation:

$$k = \frac{k_B T}{h} e^{-\frac{\Delta G^{\ddagger}}{RT}} \qquad \text{(Eq. 5.2)}$$

where k is the peak width at half height, k_B is the Boltzmann constant, h is Planck's constant, $\Delta G^{\ddagger}$ is Gibbs energy of activation, and T is temperature in Kelvin.[25,34-36,41] The

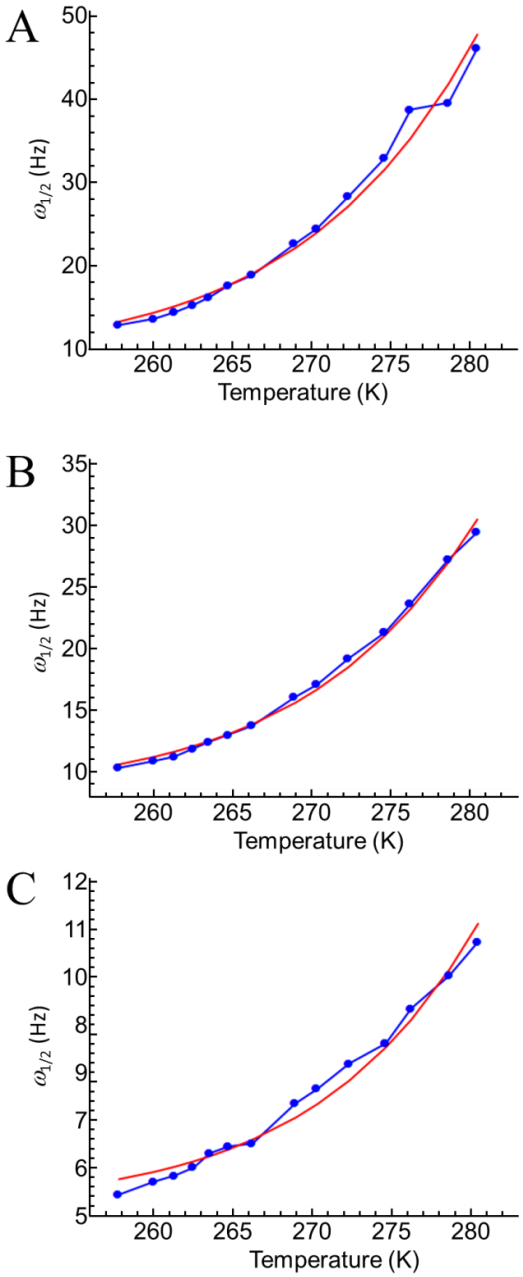

Figure 5.7. The linewidths of GlcN (A) α-NH_3^+, (B) β-NH_3^+, and α-OH1 protons plotted as a function of temperature (shown as blue points). The fits to the Eyring-Polyani equation (smooth red line) are shown overlapped with the data.

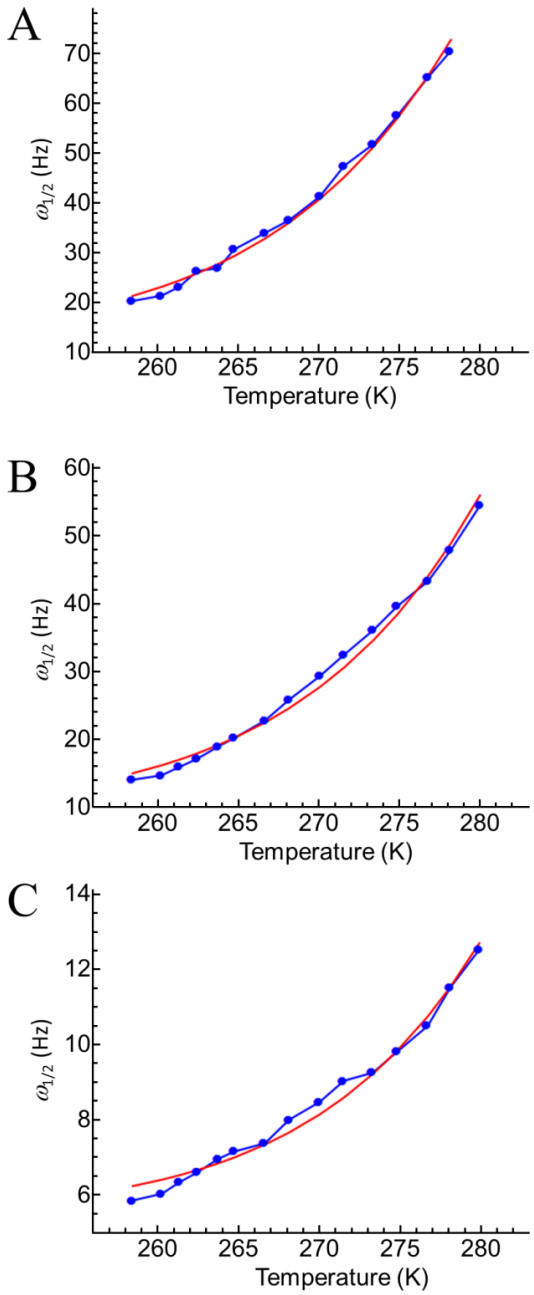

Figure 5.8. The linewidths of GlcN3S (A) α-NH_3^+, (B) β-NH_3^+, and α-OH1 protons plotted as a function of temperature (shown as blue points). The fits to the Eyring-Polyani equation (smooth red line) are shown overlapped with the data.

$\Delta G^{\ddagger}$ values summarized in Table 5.2 correlate well with the temperature coefficients. The β-amine protons have the lowest energy barriers for solvent exchange in GlcN (13.7 kcal/mol) and GlcN3S (13.3 kcal/mol) consistent with their larger temperature coefficients and their equatorial orientation. The $\Delta G^{\ddagger}$ values of the α-anomer amine protons in GlcN (14.0 kcal/mol) and GlcN3S (13.6 kcal/mol) are similar and slightly higher than the corresponding values for the β-anomer. The differences in the $\Delta G^{\ddagger}$ values between the α- and β-anomer pairs likely are attributable to the greater steric hindrance caused by the axial OH1 in the α-anomer and are far below the 2-3 kcal/mol expected for a hydrogen bond or salt bridge. They are also lower than the barriers measured for solvent exchange for the sulfamate protons of α- and β-GlcNS (15.6 and 15.1 kcal/mol, respectively), consistent with the observation of the sulfamate proton resonances at temperatures well above 0 °C.[25] The $\Delta G^{\ddagger}$ values of the α-OH1 of GlcN (14.6 kcal/mol) and GlcN3S (14.8 kcal/mol) are similar.

A direct method for measuring solvent exchange is through EXSY experiments.[42,43] As illustrated for GlcN3S in Figure 5.9, in EXSY the increase in the normalized intensity of the solvent exchange cross peaks is measured as a function of the mixing time. The EXSY build-up curves for GlcN (Figure 5.10A) and GlcN3S (Figure 5.10B) provide additional direct evidence for the slower exchange of the α-amine protons. The solvent exchange rates extracted from these build-up curves are summarized in Table 5.2. The solvent exchange rates of the α-OH1 protons in GlcN and GlcN3S are similar, consistent with their similar $\Delta G^{\ddagger}$ values. For both GlcN and GlcN3S, the

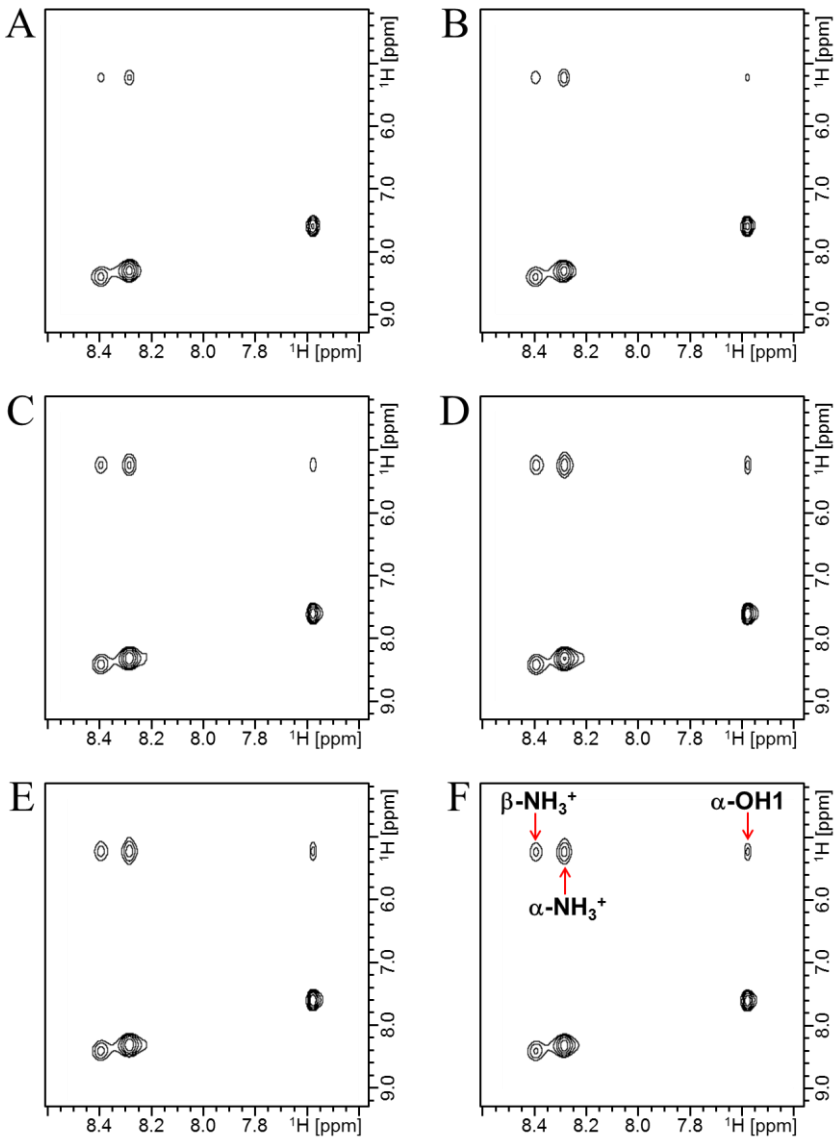

Figure 5.9. EXSY spectra for GlcN3S showing the buildup of the solvent exchange cross peak intensities of the α- and β-NH_3^+ and α-OH1 protons at mixing times of (A) 9 ms, (B) 12 ms, (C) 15 ms, (D) 18 ms, (E) 21 ms, and (F) 24 ms. The assignments are indicated for each water-exchange cross peak in (F).

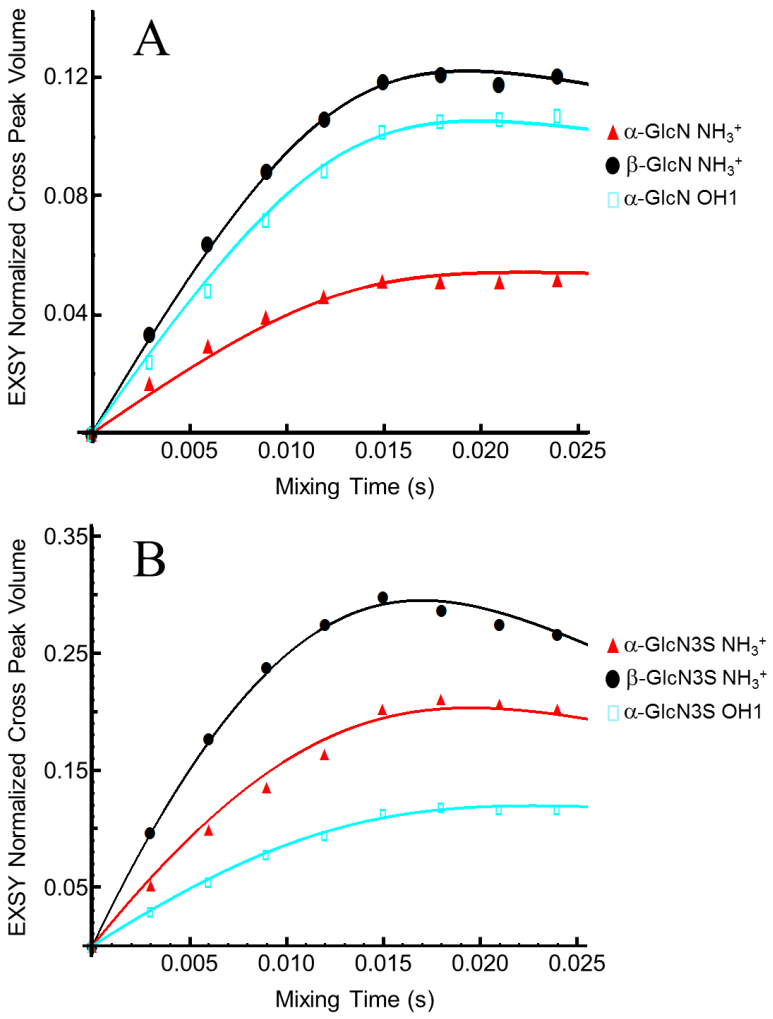

Figure 5.10. The EXSY build up curves for solvent exchange of the amine and α-OH1 protons of (A) GlcN and (B) GlcN3S. In both GlcN and GlcN3S, the α-NH_3^+ protons exchange more slowly than those of the β-anomer.

exchange rates of the α-amine protons is less than that of the corresponding β-anomer. Comparison of the complete set of results obtained for GlcN and GlcN3S suggests that introduction of the 3-*O*-sulfate moiety actually lowers the energetic barrier to solvent exchange ($\Delta G^{\ddagger}$) while increasing the exchange rate of the amine protons. If the GlcN3S amine participated in a hydrogen bond or salt bridge with the adjacent 3-*O*-sulfate group, we would expect to observe a slower exchange rate and a higher barrier to solvent exchange than observed for GlcN.

5.3.3 Effects of dissolved CO_2 on measurements of GlcN and GlcN3S amine proton exchange. Like the sulfamate protons, which were detected in the presence of phosphate buffer, the amine protons appear to be less sensitive to buffer-catalyzed exchange than the hydroxyl protons. This can be attributed to the lower pH optimum (pH 3-4) for detection of the amine resonances which gives rise to a more stable pH, and to the ability of glucosamine to self-buffer in this pH range. In addition, the solubility of CO_2 is less at low pH than in slightly basic solution. Therefore, compared with the measurements performed with Arixtra in section 3.3.6, we expect less contamination from CO_2 in solutions in the pH range 3-4. Finally, it is also possible that H_2CO_3 is less effective than HCO_3^- in catalyzing proton exchange because its proton acceptor sites are saturated. As a result of these considerations, we are not concerned that CO_2 contamination was a complicating factor in this initial study, however in future studies, this problem should be avoided by scrubbing the N_2 to remove CO_2 prior to use.

5.3.4 Comparison of pK_a values for the GlcN and GlcN3S amine groups. It is possible that salt bridge between the positively charged amine group and the adjacent

negatively charged 3-*O*-sulfate group of a GlcN3S residue helps to stabilize heparan sulfate secondary structure and prepare for protein-binding. Salt bridges in proteins are typically detected by measuring the pK_a values of the carboxylate and amine groups by NMR.[44-46] Salt bridge formation stabilizes the ionic species involved, decreasing the carboxylate pK_a and increasing the pK_a of the protonated amine.[44-46] Comparison of the pK_a values of the amine groups of GlcN and GlcN3S should reflect the formation of a salt bridge if one were present. Because of the effect of the amine group protonation state on nearby carbon-bound protons, direct observation of the amine protons is not required for the pK_a determination and the NMR titration can be performed in 90% H_2O/10% D_2O at room temperature. Figure 5.11 shows the region of the ^1H NMR spectra of GlcN and GlcN3S containing the carbon-bound H2 protons which experience the greatest chemical shift change over the course of the titration. Note that a unique advantage of NMR is the ability to simultaneously determine the pK_a values of both anomeric species. The pK_a values of GlcN and GlcN3S were determined by plotting the chemical shifts of the carbon-bound H2 protons (δ_{obs}) as a function of pH and fitting the results in Mathematica according to Eq. 5.3:[36]

$$\delta_{obs} = \delta_U + \frac{\delta_P + \delta_U}{1 + 10^{n(pK_a - pH)}} \quad \text{(Eq. 5.3)}$$

where δ_U is the chemical shift of the neutral, unprotonated amine, δ_P is the chemical shift of the positively charged, protonated amine, and *n* is Hill's coefficient (which should be 1 in this case).[47,48] The pK_a values of the GlcN α- (7.84) and β-amine (7.44) are larger than the values determined for corresponding GlcN3S α- (7.40) and β-amine (7.16) groups. These values indicate that the GlcN3S amine group does not participate in a salt bridge

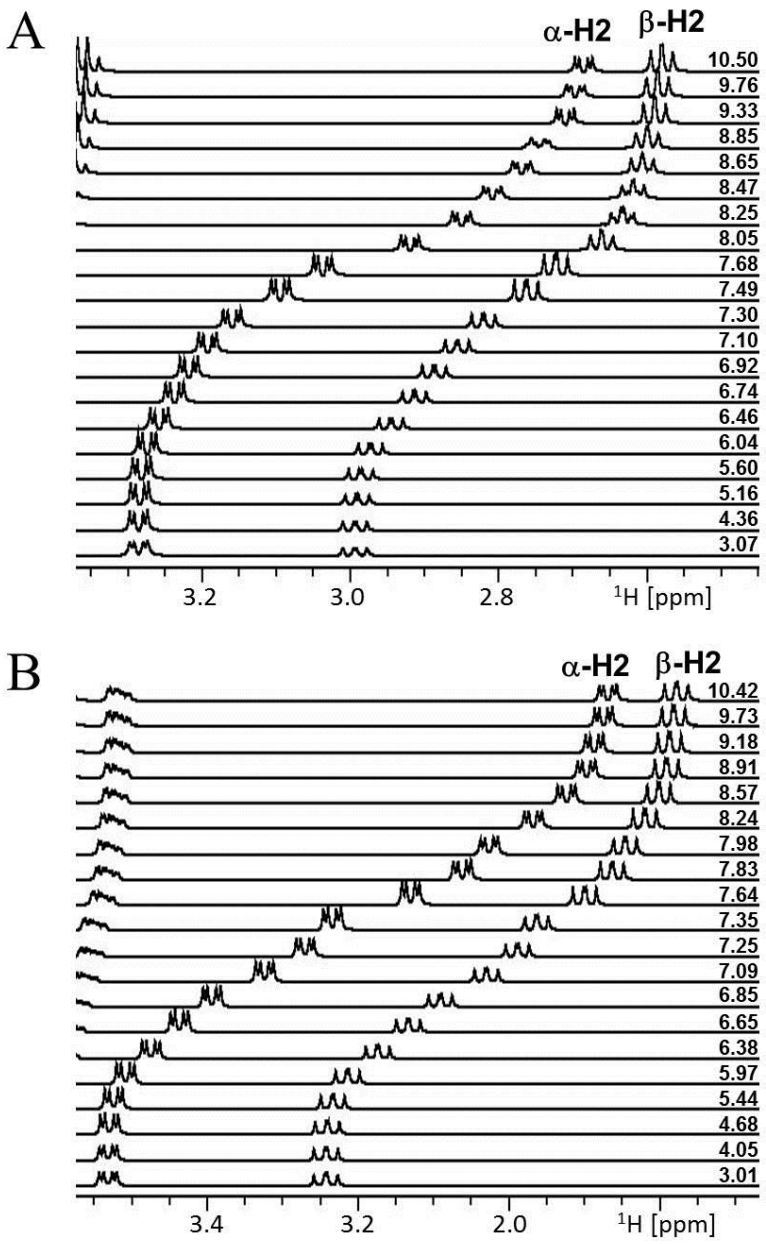

Figure 5.11. ^{1}H NMR spectra of (A) GlcN and (B) GlcN3S showing the effect of pH on the the α- and β-anomer H2 resonance. Chemical shifts extracted from these spectra were plotted as a function of pH and fit using Eq. 5.3 to calculate pK_a.

with the adjacent 3-*O*-sulfate group, as a salt bridge would be expected to increase the amine group pK_a.

5.4 Conclusions

This work presents for the first time the direct NMR detection of the amine protons of the heparan sulfate related glucosamine monosaccharides GlcN and GlcN3S. The ability to detect the sugar amine protons opens the door for measurement of ^{15}N chemical shifts by [^{1}H,^{15}N] HSQC experiments. A detailed characterization of the exchange properties of the amine protons is now possible by evaluation of temperature coefficients, measurements of the energy barrier to solvent exchange, and determination of solvent exchange rates, which taken altogether can reflect the participation of the amine protons in a hydrogen bond or salt bridge. The presence of a salt bridge can be further evaluated through NMR pH titrations to determine the amine group pK_a. Though no evidence was obtained to support the presence of a hydrogen bond or salt bridge in these simple monosaccharides, the approach demonstrated in this work paves the way for future studies of the amine groups in larger isolated or synthetic heparan sulfate oligosaccharides that might favor their formation.

5.5 References

1. Peysselon, F.; Ricard-Blum, S., Heparin–protein interactions: From affinity and kinetics to biological roles. Application to an interaction network regulating angiogenesis. *Matrix Biol.* **2014,** *35*, 73-81.

2. Lindahl, U.; Backstrom, G.; Hook, M.; Thunberg, L.; Fransson, L. A.; Linker, A., Structure of the antithrombin-binding site in heparin. *P. Natl. Acad. Sci. USA* **1979,** *76*, 3198-3202.

3. Thunberg, L.; Backstrom, G.; Lindahl, U., Further characterization of the antithrombin-binding sequence in heparin. *Carbohyd. Res.* **1982,** *100*, 393-410.

4. Atha, D. H.; Lormeau, J. C.; Petitou, M.; Rosenberg, R. D.; Choay, J., Contribution of monosaccharide residues in heparin binding to antithrombin-III. *Biochemistry* **1985,** *24*, 6723-6729.

5. Shukla, D.; Liu, J.; Blaiklock, P.; Shworak, N. W.; Bai, X. M.; Esko, J. D.; Cohen, G. H.; Eisenberg, R. J.; Rosenberg, R. D.; Spear, P. G., A novel role for 3-*O*-sulfated heparan sulfate in herpes simplex virus 1 entry. *Cell* **1999,** *99*, 13-22.

6. O'Donnell, C. D.; Tiwari, V.; Oh, M.-J.; Shukla, D., A role for heparan sulfate 3-*O*-sulfotransferase isoform 2 in herpes simplex virus type 1 entry and spread. *Virology* **2006,** *346*, 452-459.

7. Kaner, R. J.; Baird, A.; Mansukhani, A.; Basilico, C.; Summers, B. D.; Florkiewicz, R. Z.; Hajjar, D. P., Fibroblast growth-factor receptor is a portal of celluar entry for herpes-simplex virus type-1. *Science* **1990,** *248*, 1410-1413.

8. Hu, Y. P.; Lin, S. Y.; Huang, C. Y.; Zulueta, M. M. L.; Liu, J. Y.; Chang, W.; Hung, S. C., Synthesis of 3-*O*-sulfonated heparan sulfate octasaccharides that inhibit the herpes simplex virus type 1 host-cell interaction. *Nature Chem.* **2011,** *3*, 557-563.

9. Copeland, R.; Balasubramaniam, A.; Tiwari, V.; Zhang, F. M.; Bridges, A.; Linhardt, R. J.; Shukla, D.; Liu, J., Using a 3-O-sulfated heparin octasaccharide to inhibit the entry of herpes simplex virus type 1. *Biochemistry* **2008,** *47* (21), 5774-5783.

10. Liu, J.; Shriver, Z.; Pope, R. M.; Thorp, S. C.; Duncan, M. B.; Copeland, R. J.; Raska, C. S.; Yoshida, K.; Eisenberg, R. J.; Cohen, G.; Linhardt, R. J.; Sasisekharan, R., Characterization of a heparan sulfate octasaccharide that binds to herpes simplex virus type 1 glycoprotein D. *J. Biol. Chem.* **2002,** *277*, 33456-33467.

11. McKeehan, W. L.; Wu, X. C.; Kan, M., Requirement for anticoagulant heparan sulfate in the fibroblast growth factor receptor complex. *J. Biol. Chem.* **1999,** *274*, 21511-21514.

12. Ye, S.; Luo, Y. D.; Lu, W. Q.; Jones, R. B.; Linhardt, R. J.; Capila, I.; Toida, T.; Kan, M.; Pelletier, H.; McKeehan, W. L., Structural basis for interaction of FGF-1, FGF-2, and FGF-7 with different heparan sulfate motifs. *Biochemistry* **2001,** *40*, 14429-14439.

13. Vanpouille, C.; Deligny, A.; Delehedde, M.; Denys, A.; Melchior, A.; Lienard, X.; Lyon, M.; Mazurier, J.; Fernig, D. G.; Allain, F., The heparin/heparan sulfate sequence that interacts with cyclophilin B contains a 3-*O*-sulfated *N*-unsubstituted glucosamine residue. *J. Biol. Chem.* **2007,** *282*, 24416-24429.

14. Borjigin, J.; Deng, J.; Sun, X.; De Jesus, M.; Liu, T. C.; Wang, M. M., Diurnal pineal 3-*O*-sulphotransferase 2 expression controlled by beta-adrenergic repression. *J. Biol. Chem.* **2003,** *278*, 16315-16319.

15. Pempe, E. H.; Xu, Y. M.; Gopalakrishnan, S.; Liu, J.; Harris, E. N., Probing structural selectivity of synthetic heparin binding to stabilin protein receptors. *J. Biol. Chem.* **2012,** *287*, 20774-20783.

16. Thacker, B. E.; Xu, D.; Lawrence, R.; Esko, J. D., Heparan sulfate 3-*O*-sulfation: A rare modification in search of a function. *Matrix Biol.* **2014,** *35*, 60-72.

17. Guerrini, M.; Naggi, A.; Guglieri, S.; Santarsiero, R.; Torri, G., Complex glycosaminoglycans: Profiling substitution patterns by two-dimensional nuclear magnetic resonance spectroscopy. *Anal. Biochem.* **2005,** *337*, 35-47.

18. Jones, C. J.; Beni, S.; Limtiaco, J. F. K.; Langeslay, D. J.; Larive, C. K., Heparin characterization: Challenges and solutions. *Annu. Rev. Anal. Chem.* **2011**, *4*, 439-465.

19. Blundell, C. D.; DeAngelis, P. L.; Day, A. J.; Almond, A., Use of ^{15}N-NMR to resolve molecular details in isotopically-enriched carbohydrates: sequence-specific observations in hyaluronan oligomers up to decasaccharides. *Glycobiology* **2004,** *14*, 999-1009.

20. Blundell, C. D.; Deangelis, P. L.; Almond, A., Hyaluronan: The absence of amide-carboxylate hydrogen bonds and the chain conformation in aqueous solution are incompatible with stable secondary and tertiary structure models. *Biochem. J.* **2006,** *396*, 487-98.

21. Blundell, C. D.; Almond, A., Temperature dependencies of amide ^{1}H- and ^{15}N-chemical shifts in hyaluronan oligosaccharides. *Magn. Reson. Chem.* **2007,** *45*, 430-433.

22. Langeslay, D. J.; Beni, S.; Larive, C. K., Detection of the ^{1}H and ^{15}N NMR resonances of sulfamate groups in aqueous solution: A new tool for heparin and heparan sulfate characterization. *Anal. Chem.* **2011,** *83*, 8006-8010.

23. Langeslay, D. J.; Beni, S.; Larive, C. K., A closer look at the nitrogen next door: ^{1}H-^{15}N NMR methods for glycosaminoglycan structural characterization. *J. Magn. Reson.* **2012,** *216*, 169-174.

24. Langeslay, D. J.; Beecher, C. N.; Naggi, A.; Guerrini, M.; Torri, G.; Larive, C. K., Characterizing the microstructure of heparin and heparan sulfate using *N*-sulfoglucosamine ^{1}H and ^{15}N NMR chemical shift analysis. *Anal. Chem.* **2013,** *85*, 1247-1255.

25. Langeslay, D. J.; Young, R. P.; Beni, S.; Beecher, C. N.; Mueller, L. J.; Larive, C. K., Sulfamate proton solvent exchange in heparin oligosaccharides: Evidence for a persistent hydrogen bond in the antithrombin-binding pentasaccharide Arixtra. *Glycobiology* **2012,** *22*, 1173-1182.

26. Limtiaco, J. F.; Langeslay, D. J.; Beni, S.; Larive, C. K., Getting to know the nitrogen next door: HNMBC measurements of amino sugars. *J. Magn. Reson.* **2011,** *209*, 323-331.

27. Beecher, C. N.; Young, R. P.; Langeslay, D. J.; Mueller, L. J.; Larive, C. K., Hydroxyl-proton hydrogen bonding in the heparin oligosaccharide Arixtra in aqueous solution. *J. Phys. Chem. B* **2014,** *118*, 482-491.

28. Beecher, C. N.; Larive, C. K., In *Glycosaminoglycans – Chemistry and Biology*; Balagurunathan, K.; Nakoto, H.; Desai, U. R., Eds.; Springer: **2015**; pp 173-187.

29. Adams, B.; Lerner, L., Observation of hydroxyl protons of sucrose in aqueous solution – no evidence of persistent intramolecular hydrogen bonds. *J. Am. Chem. Soc.* **1992,** *114*, 4827-4829.

30. Sandstrom, C.; Baumann, H.; Kenne, L., NMR spectroscopy of hydroxy protons of 3,4-disubstituted methyl α-D-galactopyranosides in aqueous solution. *J. Chem. Soc. Perk. T. 2* **1998,** 809-815.

31. Sandstrom, C.; Kenne, L., Hydroxy protons in structural studies of carbohydrates by NMR spectroscopy. *ACS. Sym. Ser.* **2006,** *930*, 114-132.

32. Hwang, T. L.; Shaka, A. J., Water suppression that works – excitation sculpting using arbitrary wave-forms and pulsed-field gradients. *J. Magn. Reson. Ser. A* **1995,** *112*, 275-279.

33. Vilen, E. M.; Lundqvist, L. C. E.; Jouanneau, D.; Helbert, W.; Sandstrom, C., NMR study on hydroxy protons of κ- and κ/μ-hybrid carrageenan oligosaccharides: Experimental evidence of hydrogen bonding and chemical exchange interactions in κ/μ oligosaccharides. *Biomacromolecules* **2010,** *11*, 3487-3494.

34. Bain, A. D., Chemical exchange in NMR. *Prog. Nucl. Mag. Res. Sp.* **2003,** *43*, 63-103.

35. Pechukas, P., Transition state theory. *Annu. Rev. Phys. Chem.* **1981,** *32*, 159-177.

36. Wolfram, S., *Mathematica: A System for Doing Mathematics by Computer*, 2nd ed.; Addison-Wesley Publishing Company: Reading, MA, **1991**.

37. Ohnishi, M.; Urry, D. W., Temperature dependence of amide proton chemical shifts – secondary structures of gramicidin S and valinomycin. *Biochem. Bioph. Res. Co.* **1969,** *36*, 194-202.

38. Andersen, N. H.; Neidigh, J. W.; Harris, S. M.; Lee, G. M.; Liu, Z. H.; Tong, H., Extracting information from the temperature gradients of polypeptide NH chemical shifts. 1. The importance of conformational averaging. *J. Am. Chem. Soc.* **1997,** *119*, 8547-8561.

39. Baxter, N. J.; Williamson, M. P., Temperature dependence of ^{1}H chemical shifts in proteins. *J. Biomol. NMR* **1997,** *9*, 359-369.

40. Cierpicki, T.; Otlewski, J., Amide proton temperature coefficients as hydrogen bond indicators in proteins. *J. Biomol. NMR* **2001,** *21*, 249-261.

41. Eyring, H., The activated complex in chemical reactions. *J. Chem. Phys.* **1935,** *3*, 107-115.

42. Jeener, J.; Meier, B. H.; Bachmann, P.; Ernst, R. R., Investigation of exchange processes by two-dimensional NMR spectroscopy. *J. Chem. Phys.* **1979,** *71*, 4546-4553.

43. Dobson, C. M.; Lian, L. Y.; Redfield, C.; Topping, K. D., Measurement of hydrogen exchange rates using 2D NMR spectroscopy. *J. Magn. Reson.* **1986,** *69*, 201-209.

44. Bosshard, H. R.; Marti, D. N.; Jelesarov, I., Protein stabilization by salt bridges: Concepts, experimental approaches and clarification of some misunderstandings. *J. Mol. Recognit.* **2004,** *17*, 1-16.

45. Anderson, D. E.; Becktel, W. J.; Dahlquist, F. W., pH-induced denaturation of proteins: A single salt bridge contributes 3-5 kcal/mol to the free energy of folding of T4 lysozyme. *Biochemistry* **1990,** *29*, 2403-2408.

46. Williamson, M. P.; Hounslow, A. M.; Ford, J.; Fowler, K.; Hebditch, M.; Hansen, P. E., Detection of salt bridges to lysines in solution in barnase. *Chem. Comm.* **2013,** *49*, 9824-9826.

47. Gao, G. H.; Prasad, R.; Lodwig, S. N.; Unkefer, C. J.; Beard, W. A.; Wilson, S. H.; London, R. E., Determination of lysine pK values using [5-^{13}C] lysine: Application to the lyase domain of DNA pol β. *J. Am. Chem. Soc.* **2006,** *128*, 8104-8105.

48. Gao, G. H.; DeRose, E. F.; Kirby, T. W.; London, R. E., NMR determination of lysine pK_a values in the pol λ lyase domain: Mechanistic implications. *Biochemistry* **2006,** *45*, 1785-1794.

CHAPTER SIX

Evaluation of Oligosaccharide Hydroxyl Proton Transverse Relaxation Rates (R_2)

Abstract: NMR detection of intramolecular hydrogen bonding in aqueous solutions of carbohydrates is of considerable current interest as it has the potential to provide insights into polysaccharide secondary structure and dynamics. Various NMR measurements can be used to probe for intramolecular hydrogen bonds involving carbohydrate exchangeable protons. These approaches include indirect methods such as the measurement of temperature coefficients, analysis of differences in monosaccharide and oligosaccharide chemical shifts, and determination of the activation barriers for solvent exchange through lineshape analysis. Perhaps the most compelling evidence for the involvement of an exchangeable proton in an intramolecular hydrogen bond is provided by a reduced rate of solvent exchange, which can be directly assessed using exchange spectroscopy (EXSY). This Chapter evaluates the use of transverse relaxation rates (R_2) measured for the exchangeable protons of glucosamine (GlcN), 3-*O*-sulfoglucosamine (GlcN3S), and Arixtra as a complementary approach to investigate hydroxyl proton exchange rates. The CPMG pulse sequence used to measure R_2 values effectively removes the contribution of radiation damping to transverse relaxation. We were encouraged that plots of R_2 vs EXSY exchange rates gave a linear correlation for the GlcN and GlcN3S hydroxyl protons, however, plots for the Arixtra hydroxyl protons provided poorer correlations. The results obtained for Arixtra suggest that for longer oligosaccharides other factors can influence relaxation rates, such as molecular motion and conformational flexibility.

Because NMR measurements of the Arixtra hydroxyl protons are carried out in slightly basic solution, catalysis of exchange by bicarbonate may also contribute to differences in the solvent exchange and transverse relaxation rates. Therefore, EXSY exchange rates, as used in Chapters 3 and 4, are a more robust indicator of hydrogen bonding and caution should be used in attributing differences in hydroxyl proton transverse relaxation rates and resonance linewidths to hydrogen bonding.

6.1 Introduction

Heparin is known to mediate a variety of important biological processes through binding to over 400 different proteins.[1-3] Although many of the mechanisms of specific heparin-protein interactions are not yet understood at the molecular level, heparin's anticoagulant activity has been studied extensively.[4-7] A specific pentasaccharide sequence, found in only one of every three heparin chains, contains the minimum structural requirements for high affinity binding to the protease inhibitor antithrombin-III (AT-III).[8,9] In particular, the internal *N*-,3,6-*O*-sulfated glucosamine (GlcNS3S6S) residue contains a critical 3-*O*-sulfate group that increases the affinity of the pentasaccharide for AT-III 1000-fold.[10] The flexibility of the 2-*O*-sulfated IdoA (IdoA2S) residue is also important for AT-III binding.[11,12] A synthetic ultralow molecular weight heparin drug, fondaparinux sodium, based on this pentasaccharide structural motif is marketed for pharmaceutical use under the trade name Arixtra.[13]

Though methods for elucidation of the primary structure of oligosaccharides, such as those derived from heparin, are well-established[14,15] fewer studies probe secondary

structure. Intramolecular hydrogen bonds involving the exchangeable protons of heparin may help stabilize a particular conformation locally within a specific structural motif.[16,17] The methods for characterizing hydrogen bonding in oligosaccharides are similar to the well-established methods for peptides and proteins developed over several decades of study.[18-21] Temperature coefficients and chemical shift differences have been used as indicators of hydrogen bonds in various carbohydrates.[22-25] Differences in the energetic barriers for chemical exchange ($\Delta G^{\ddagger}$) were used to identify a hydrogen bond in Arixtra involving the GlcNS3S6S sulfamate ($NHSO_3^-$) proton and the adjacent 3-*O*-sulfo group.[16] Analysis of the $\Delta G^{\ddagger}$ values for Arixtra's hydroxyl protons proved less fruitful most likely because resonance overlap and the lack of observable *J*-couplings prevented accurate measurements. As described in Chapters 3 and 4, two-dimensional exchange spectroscopy (EXSY) measurements of relative rates of solvent exchange provide direct approach to investigate hydroxyl proton hydrogen bonding,[17,25-27] and we utilized these rates to discover a persistent hydrogen bond involving the GlcA(II)OH3 of Arixtra.[17] Noting that differences in hydroxyl proton resonance line widths roughly correlate with their EXSY exchange rates prompted us to question whether transverse relaxation rates (R_2) might provide a simpler and faster means to identify hydroxyl proton hydrogen bonds.

The T_2 relaxation time of water depend on chemical exchange with the exchangeable protons of carbohydrates, polymers, and solutions such as methanol and glycerol.[28-35] Fabri et al. studied T_2 relaxation times in sugar solutions as well as aqueous solutions of glycol and glycerol and determined that the T_2 relaxation of the water

changes as a function of the percent exchangeable protons.[32] Calucci et al. utilized spin-spin relaxation times to provide insight into the hydration mechanism of poly(amidoamine) hydrogels.[33] To our knowledge, direct measurements of the T_2 relaxation times of individual hydroxyl protons of heparin oligosaccharides have not been used to investigate their solvent exchange rates. Although radiation damping needed to be accounted for in the hydroxyl proton EXSY exchange rate constant calculations,[17] Mao et al. demonstrated that the Carr-Purcell-Meiboom-Gill (CPMG)[36,37] pulse sequence effectively removes radiation damping from the measurement of the T_2 relaxation times in a solution of acetone-d_6 in 80% (v/v) benzene.[38]

In this Chapter the hydroxyl proton R_2 values for the D-glucosamine (GlcN) and 3-*O*-sulfated D-glucosamine (GlcN3S) monosaccharides, and Arixtra are compared to the solvent exchange rates (k_{ex}) measured using EXSY. The effect of radiation damping on transverse relaxation rates is also explored in this using various mixtures of H_2O/D_2O.

6.2 Methods and Materials

6.2.1 Materials and reagents. Monosaccharides GlcN and GlcN3S were purchased from Sigma-Aldrich (Saint Louis, MO). Arixtra (fondaparinux sodium), formulated as prefilled syringes for clinical use, was obtained from the University of Pharmacy and Department of Pharmacy Administration of Semmelweis University (Budapest, Hungary). Arixtra was desalted, freeze-dried, and stored at -20 °C between measurements. Acetone-d_6 (99.9% D) and deuterium oxide (99.9% D) were purchased from Cambridge Isotope Laboratories. Sodium chloride (NaCl) and sodium bicarbonate

($NaHCO_3$) were purchased from Fisher Scientific (Pittsburgh, PA). High-performance-liquid-chromatography (HPLC) grade water was obtained from Burdick and Jackson (Muskegon, MI). Ultrapure Millipore water with resistivity of 18.2 MΩ•cm was obtained using a Millipore Simplicity UV Water Purification System (Billerica, MA). The pH meter was calibrated with buffers of 4.00, 7.00, and 10.00 purchased from Fisher Scientific. The pH was adjusted using hydrochloric acid (HCl) purchased from Fisher Scientific and sodium hydroxide (NaOH) purchased from Macron Fine Chemicals (Center Valley, PA).

6.2.2 Hydroxyl proton detection and identification. Solutions of 10 mM GlcN and 3 mM GlcN3S containing 0.15 M NaCl were prepared in a CO_2 free environment using HPLC-grade water which had been boiled to remove dissolved CO_2. A pH titration was performed to determine the pH optimum for GlcN and GlcN3S hydroxyl protons. Arixtra solution preparation is described in detail Chapter 3. Five separate solutions of 1 mM Arixtra at pH 7.67, 7.95, 8.10, 8.37, and 8.50 (referred to Arixtra solutions 1, 2, 3, 4, and 5, respectively) were prepared with HPLC-grade water. A solution of 1 mM Arixtra at pH 8.28 was prepared open to the atmosphere using Millipore water and then titrated with 0.59 mM $NaHCO_3$. Measurements were performed on this solution before and after the addition of bicarbonate. All solutions were composed of 85% H_2O/15% acetone-d_6 and pH adjustments made using CO_2 free 0.1 M HCl and 0.1 M NaOH prior to the addition of acetone-d_6[17] using a Fisher Scientific AB15 pH meter with a double-junction Ag/AgCl micro-pH electrode (Thermo Scientific, Beverly, MA).

One-dimensional ^{1}H NMR spectra were recorded using a Bruker 600 MHz Avance spectrometer equipped with a triple gradient inverse probe operating at 599.58 MHz using a 600 μL sample in 5 mm NMR tubes. The temperature of the NMR probe was set to -14.5 °C, measured using an external methanol standard.[39] Chemical shifts were referenced to the residual ^{1}H resonance of acetone-d_6 at 2.204 ppm.

GlcN and GlcN3S hydroxyl protons resonances were assigned using two-dimensional COSY spectra with excitation sculpting solvent suppression. Double-quantum filtered (DQF-) COSY spectra were acquired in States-TPPI with 2048 complex points in t2 with 64 scans coadded at each of 192 t1 increments for both GlcN and GlcN3S. A spectral window of 7200 Hz was used in both dimensions. A 2.0 s relaxation delay was used. The spectra were zero filled to 4096 x 512 data points.

6.2.3 NMR measurements of hydroxyl proton transverse relaxation rates. To determine the effects of radiation damping on the values of R_2 measured using the CPMG pulse sequence, water transverse relaxation rates were measured in solutions containing 5%, 15%, 25%, 35%, 45%, 55%, 65%, 75%, and 85% H_2O in D_2O. Measurements were performed at 25 °C with 1 mM DSS-d_6 the chemical shift reference using the CPMG pulse sequence (Bruker pulse program cpmg), which consists of a 90° pulse followed by a spin-echo pulse train: $90°-(t_D-180°-t_D)_n$ (Chapter 1, Figure 1.11D). Delay times (t_D) of 0.3, 0.5, and 1.0 ms were used with values of *n* ranging from 2 to 10000 m, as listed in Table 6.1. The relaxation delay was 10.0 s and 8 scans were coadded. A 7.60 μs 90° pulse was used at a power level of -5 dB. The spectral window was 7000 Hz and spectra were recorded using 32768 complex points.

Table 6.1. The number of spin echo pulse trains (*n*) looped per CPMG cycle for each delay time (t_D) for all H_2O/D_2O solutions.

Delay time (t_D)	**0.3 ms**	**0.5 ms**	**1.0 ms**
Spin echo pulse train (*n*)	2	2	20
	20	20	80
	40	40	100
	60	60	150
	80	80	200
	100	100	250
	150	150	350
	200	200	500
	250	250	700
	350	350	850
	500	500	1000
	700	700	1200
	850	850	1500
	1000	1000	1700
	1200	1200	2000
	1500	1500	2500
	1700	1700	3000
	2000	2000	4000
	2500	2500	5000
	3000	3000	6000
	4000	4000	7000
	5000	5000	8000
		6000	9000
			10000

Spectra were processed using Topspin 3.1 as a pseudo two-dimensional experiment and zero-filled with 32768 points in t2. The free induction decays (FIDs) were apodized by multiplication with an exponential function equivalent to 0.3 Hz line broadening prior to Fourier transformation. The water resonance was integrated, plotted as a function of the length of the CPMG pulse train, *t*, (where $t = 2nt_D$) and the resulting decays fit using Mathematica[40] to the following equation:

$$M_t = M_0 e^{-t/T_2} \qquad \text{(Eq. 6.1)}$$

where M_t is the net magnetization magnitude at time t and M_0 is the initial net magnetization (Chapter 1, Eq. 1.3).

The transverse relaxation rates of the GlcN, GlcN3S, and Arixtra hydroxyl protons were determined using a CPMG pulse sequence with excitation sculpting solvent suppression obtained from Hoffmann et al.[41] Spectra were recorded using 32768 complex points in t2 with a spectral window of 7000 Hz. A total of 34 experiments were obtained for each solution by coadding 16 scans for GlcN and 64 scans for both GlcN3S and Arixtra over values of *n* ranging from 2 to 500 (Table 6.2). A CPMG spin-echo t_D delay of 0.30 ms was used with a relaxation delay of 10.0 s. The 90° pulses were calibrated at a power level of -5 dB as 9.0 μs for GlcN and GlcN3S and 8.6 μs for Arixtra.

Spectra were processed as a pseudo two-dimensional experiment, with zero-filling to 32768 points. Individual spectra were extracted and the hydroxyl proton resonance integrals measured using TopSpin 3.1. Integrals for each hydroxyl proton were plotted as a function of CPMG pulse train length, *t*, and the resulting plots were fit to Eq. 6.1 using Mathematica.[40]

Table 6.2. The number of spin echo pulse trains (*n*) looped per CPMG cycle for the hydroxyl protons of each solution with a delay time (t_D) of 0.3 ms.

Spin echo pulse train (*n*)
2
4
6
8
10
12
14
16
18
20
22
24
26
28
30
36
40
46
50
56
60
70
80
90
100
130
150
180
200
250
300
350
400
500

6.2.4 NMR measurements of hydroxyl proton solvent exchange rates. EXSY spectra for GlcN and GlcN3S hydroxyl protons were acquired using the Bruker NOESY pulse program "noesyesgpph" using excitation-sculpting solvent suppression and mixing times ranging from 0 to 24 ms in 3-ms increments.[17] Spectra were recorded into 2048 complex points in t2 and coadding 32 scans at each of 128 t1 increments. A relaxation delay of 1.5 s and spectral windows of 4440 Hz were used in both and dimensions. For each solution, the EXSY experiments were performed immediately following the CPMG experiments so that the results would be directly comparable.

The EXSY spectra were zero-filled using 16384 x 4096 points to obtain more accurate volume integrals of the hydroxyl proton cross peaks and apodized using a cosine squared function. The cross peak volume integrals were measured using TopSpin 3.1, normalized to the diagonal peak of each hydroxyl proton resonance, and plotted as a function of mixing time. Initial rate constants were calculated from the EXSY build-up curves using modified Bloch equations as described in Chapter 3.[17]

6.3 Results and Discussion

A convenient and fast one-dimensional NMR method for evaluating differences in hydroxyl proton exchange properties would streamline studies of hydrogen bonding in oligosaccharides. Although resonance lineshape analysis of ^{1}H NMR spectra measured as a function of temperature have been used to identify hydrogen bonds involving amide and sulfamate protons by calculating the energy barrier ($\Delta G^{\ddagger}$) for chemical exchange,[16,41] we found that this method does not work as well for the hydroxyl protons due to peak

overlap and the lack of observable *J*-couplings. In the spectra presented in Chapters 3 and 4, we observed that the hydroxyl protons within a given oligosaccharide have different resonance linewidths, and that these differences in general are consistent with differences in the EXSY exchange rates.[17] In this Chapter we explore quantitatively whether exchange contributions to T_2 relaxation are reflective of differences in hydroxyl proton exchange rates, and therefore a potential predictor of hydrogen bonding.

6.3.1 Transverse relaxation rates of H_2O/D_2O mixtures. Radiation damping can produce significant non-uniform decreases in relaxation times.[42] Chen and Mao demonstrated that when the T_1 relaxation rate of water is governed by radiation damping it must be included when measuring proton longitudinal relaxation rates.[42] In EXSY measurements of the exchange rates of sugar hydroxyl protons with water, we also considered the effects of radiation damping (Chapter 3).[17] In contrast, for T_2 relaxation measurements, Mao et al. report that the 180° pulses of the CPMG pulse train remove the effects of radiation damping, along with the effects of magnetic field inhomogeneity.[38]

To experimentally determine the effects of radiation damping on hydroxyl proton relaxation rate measurements, R_2 ($R_2 = 1/T_2$) values for determined for the water resonance in solutions with various ratios of H_2O/D_2O. The measured R_2 values plotted as a function of the percent H_2O for three different CPMG spin-echo delays (t_D) are shown in Figure 6.1. The transverse relaxation rates measured using the shortest spin-echo delay time (t_D = 0.3 ms) range from 0.111 to 0.198 s^{-1} as the percentage of H_2O increases. Such a small difference in R_2 between solutions could be attributed to the difference in the dipole-dipole interactions between H_2O and D_2O.[43] At any given

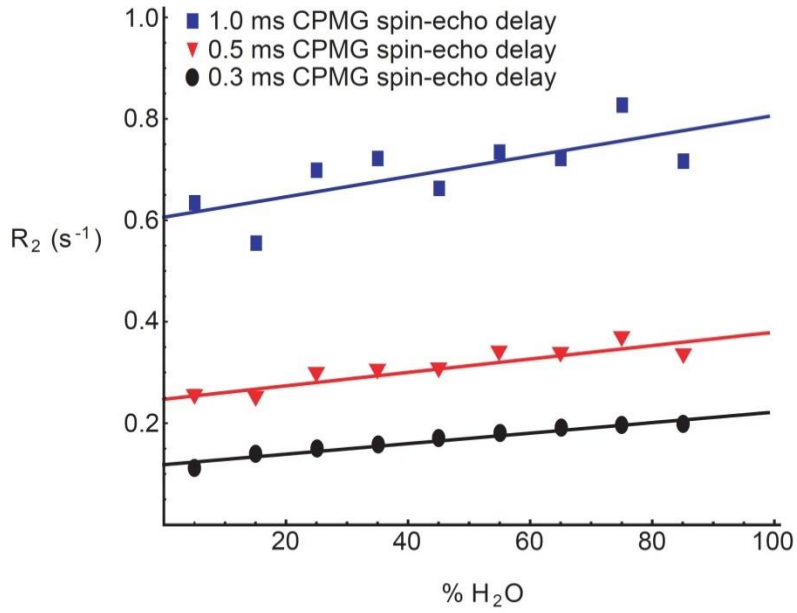

Figure 6.1. The water transverse relaxation rates (R_2) determined for various combinations of H_2O in D_2O using the CPMG pulse sequence. CPMG spin-echo delays (t_D) of 1.0 ms, 0.5 ms, and 0.3 ms were used to measure the correlation between R_2 values and the concentration of H_2O.

percentage of water the three different CPMG spin-echo delays produced different values of the water R_2 (Figure 6.1). In addition, a greater deviation of the R_2 values from a linear correlation is observed for larger values of t_D. This is most likely due to the incomplete realignment of relaxing magnetization with a slower duty cycle, along with a greater contribution from translational diffusion during the longer delay times.[44] Dramatic effects due to radiation damping on the transverse relaxation rate of water are not observed in Figure 6.1.

6.3.2 Comparison of GlcN and GlcN3S hydroxyl proton solvent exchange and transverse relaxation rates. As discussed in Chapter 3, observation of the hydroxyl proton NMR resonances requires determination of experimental conditions under which their solvent exchange is sufficiently slow to allow detection. The optimum pH for the hydroxyl protons was found to be between pH 5.3 and 5.8 for GlcN (Figure 6.2A) and between pH 5.4 and 6.0 for GlcN3S (Figure 6.2B). The hydroxyl proton resonances of both GlcN and GlcN3S were assigned using COSY spectra with excitation sculpting solvent suppression (Figures 6.3A and 6.3B, respectively). The pH optimum for the hydroxyl protons of GlcN is slightly more acidic than that of GlcN3S. This difference is likely due to the overall positive charge of GlcN compared to the net neutral charge of the zwitterionic GlcN3S.[17,45] Solutions of GlcN at 5.3 and of GlcN3S at pH 6.0 were used for the EXSY and CPMG experiments.

For both GlcN and GlcN3S, the hydroxyl proton R_2 values are in good agreement with the EXSY solvent exchange rates (Table 6.3). The GlcN EXSY build-up curves (Figure 6.4A) and CPMG decay curves (Figure 6.4B) show that there are two hydroxyl

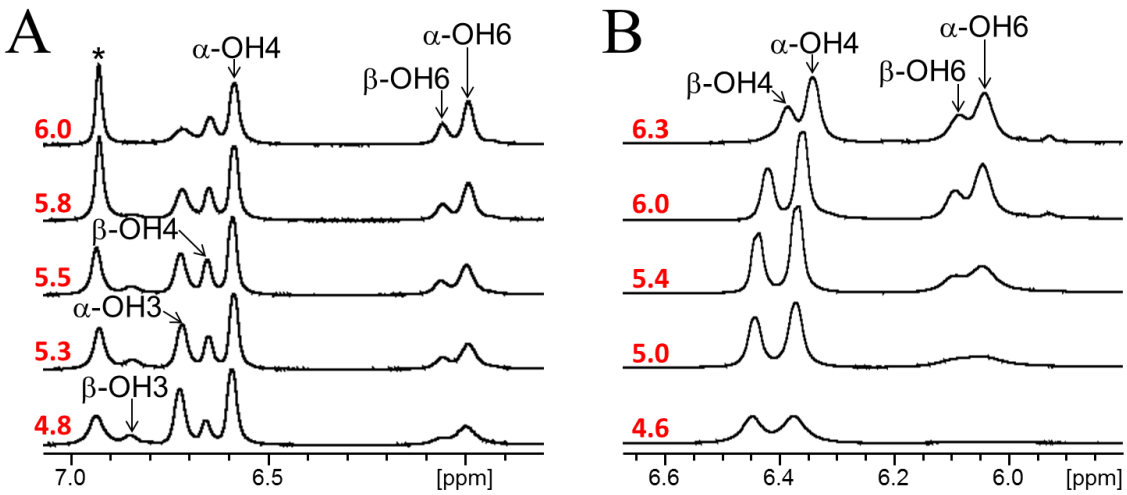

Figure 6.2. ^{1}H NMR spectra showing the hydroxyl proton resonances of (A) GlcN and (B) GlcN3S as a function of pH. Titrations were performed at -14.5 °C in 85% H_2O/15% acetone-d_6. The asterisk at 6.94 ppm indicates the acetone hemiacetal resonance.

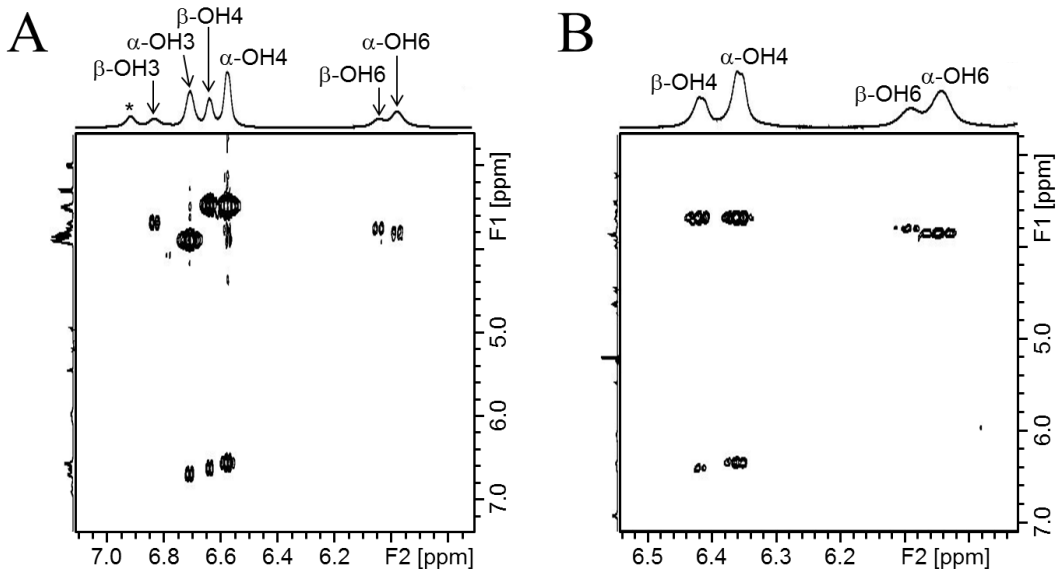

Figure 6.3. The hydroxyl proton resonances of (A) GlcN and (B) GlcN3S were assigned using COSY spectra with excitation sculpting solvent suppression. Spectra were measured at -14.5 °C in 85% H_2O/15% acetone-d_6. The asterisk at 6.94 ppm indicates the acetone hemiacetal resonance.

Table 6.3. EXSY solvent exchange rates and CPMG R_2 values for the GlcN and GlcN3S hydroxyl protons. The measurements were performed for solutions composed of 85% H_2O/15% acetone-d_6 at -14.5 °C. The GlcN and GlcN3S solutions were measured at pH 5.3 and 6.00, respectively.

Proton	GlcN		GlcN3S	
	EXSY k_{ex} (s^{-1})	**CPMG R_2 rate (s^{-1})**	**EXSY k_{ex} (s^{-1})**	**CPMG R_2 rate (s^{-1})**
α-OH3	36.9	37.8	---	---
β-OH3	59.9	64.3	---	---
α-OH4	21.2	25.0	13.4	16.0
β-OH4	22.2	26.6	14.2	16.4
α-OH6	73.1	69.7	34.9	31.2
β-OH6	60.2	57.1	34.6	32.4

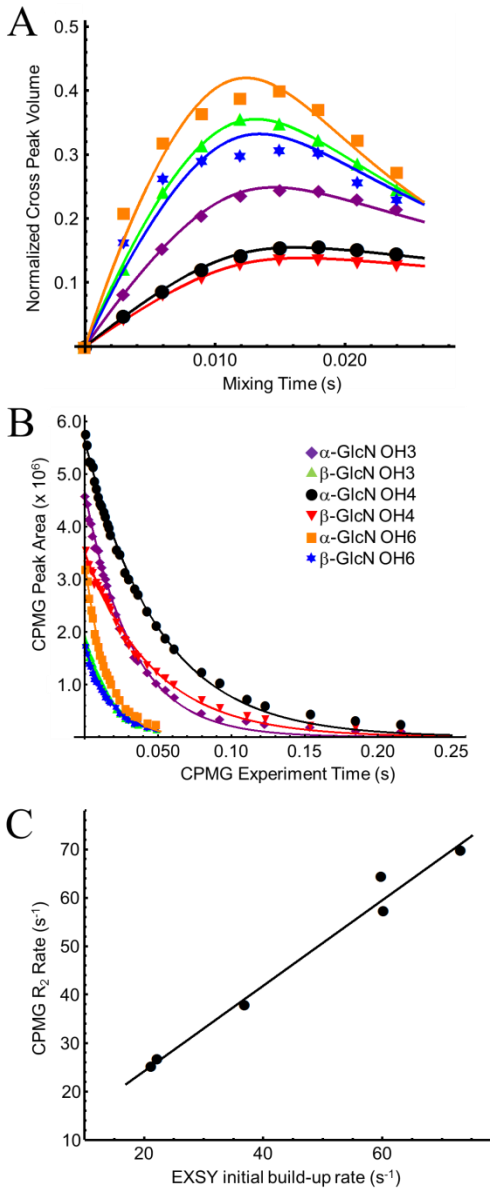

Figure 6.4. GlcN hydroxyl proton (A) EXSY build-up curves, and (B) CPMG decay curves measured in 85% H_2O/15% acetone-d_6 at pH 5.3 and -14.5 °C. (C) Correlation of R_2 values and EXSY solvent exchange rates. The slope and correlation coefficient for the linear fit of the data are 0.883 and 0.981, respectively. The OH1 proton resonance was not observed at this pH.

protons, α- and β-GlcN OH4, that exchange more slowly than the other protons. Their solvent exchange rates (21.2 and 22.2 s^{-1}, respectively) correlate well to their measured R_2 values (25.0 and 26.6 s^{-1}, respectively). The α- and β-OH6 protons, on the other hand, exchange more rapidly with rates of 73.1 and 60.2 s^{-1}, respectively, and R_2 values of 69.7 and 57.1 s^{-1}, respectively. Interestingly, there appear to be some structural differences even for this simple monosaccharide. The β-OH3 proton exchanges fairly quickly, with solvent exchange and transverse relaxation rates of 59.9 and 64.3 s^{-1}, respectively, while the α-OH3 proton exchanges more slowly, with a solvent exchange rate of 36.9 s^{-1} and an R_2 value of 37.8 s^{-1}. When the R_2 values of all the GlcN hydroxyl protons are plotted as a function of their solvent exchange rates determined by EXSY, a linear correlation is obtained (Figure 6.4C). The slope of this line is 0.883 with a good linear correlation coefficient (R^2) of 0.981. The deviation of the slope from a value of 1.0 likely arises because there are additional contributions to the resonance linewidth other than solvent exchange.

The GlcN3S hydroxyl protons cluster in two groups, as observed in EXSY build-up plots(Figure 6.5A) and CPMG decay curves (Figure 6.5B). Just as in GlcN, the α- and β-OH4 hydroxyl protons have the smallest initial build-up rates (13.4 and 14.2 s^{-1}, respectively), which correspond well to their R_2 values (16.0 and 16.4 s^{-1}, respectively). The α- and β-GlcN3S OH6 protons have larger relative initial build-up rates (34.9 and 34.6 s^{-1}, respectively), which also correlate well to their R_2 values (31.2 and 32.4 s^{-1}, respectively). The plot of R_2 as a function of initial build-up rates for the GlcN3S hydroxyl protons also follows a linear relationship (Figure 6.5C) with a slope of 0.745

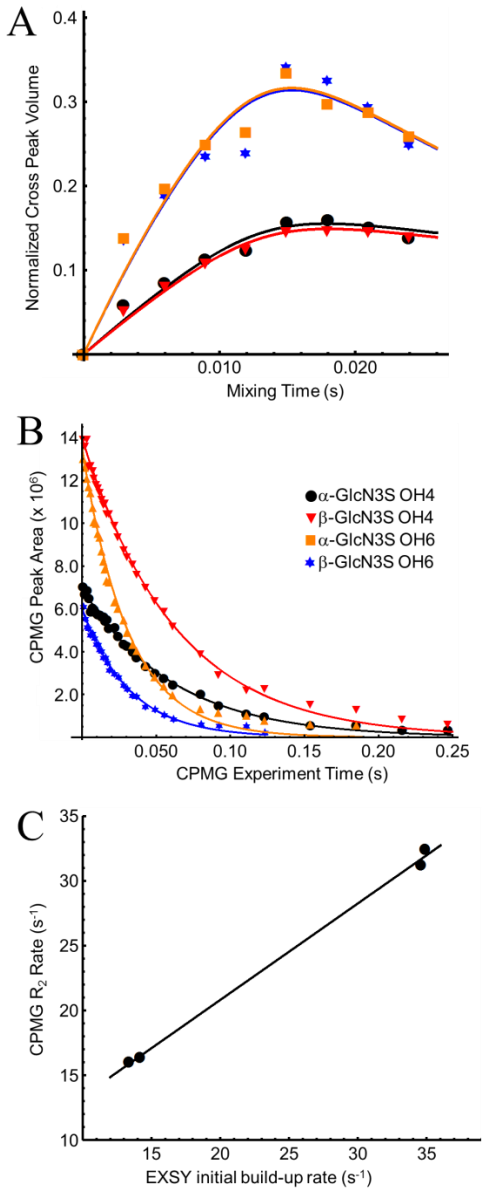

Figure 6.5. GlcN3S hydroxyl proton (A) EXSY build-up curves, and (B) CPMG decay curves measured in 85% H_2O/15% acetone-d_6 at pH 6.0 and -14.5 °C. (C) Correlation of R_2 values and EXSY solvent exchange rates. The slope and correlation coefficient for the linear fit of the data are 0.745 and 0.995, respectively. The OH1 proton was not observed at this pH.

and a linear correlation coefficient of 0.995. As observed for GlcN, a slope less than 1.0 for this plot likely reflects contributions to transverse relaxation in addition to solvent exchange.

6.3.3 Comparison of Arixtra hydroxyl proton solvent exchange and transverse relaxation rates. The relationship between hydroxyl proton solvent exchange rates measured using EXSY, and transverse relaxation times measured with CPMG, was also investigated for two Arixtra solutions. Because of the effects of dissolved CO_2 noted in Chapter 3, the Arixtra solution was prepared open to the atmosphere (conditions that minimize CO_2 contamination) and analyzed before and after addition of bicarbonate. The Arixtra solutions showed differences in the patterns of solvent exchange rates measured by EXSY (Figure 3.13), prompting investigation of their hydroxyl proton transverse relaxation rates.

In an attempt to ensure comparable results, CPMG and EXSY experiments were performed back-to-back for both Arixtra solutions. The CPMG decay curves for the Arixtra hydroxyl protons in the solution without added bicarbonate are shown in Figure 6.6A. Transverse relaxation rates were calculated for each hydroxyl proton using Eq. 6.1 and are compared with the EXSY solvent exchange rates in Table 6.4. The plot of R_2 as a function of solvent exchange rates (Figure 6.6B) has a slope of 0.906 and a correlation coefficient of 0.927. This result is comparable to our findings for GlcN (Figure 6.4C) and GlcNS (Figure 6.5C).

The CPMG decay curves for the Arixtra hydroxyl protons in the solution containing 0.59 mM added bicarbonate are shown in Figure 6.6C. The plot of R_2 as a

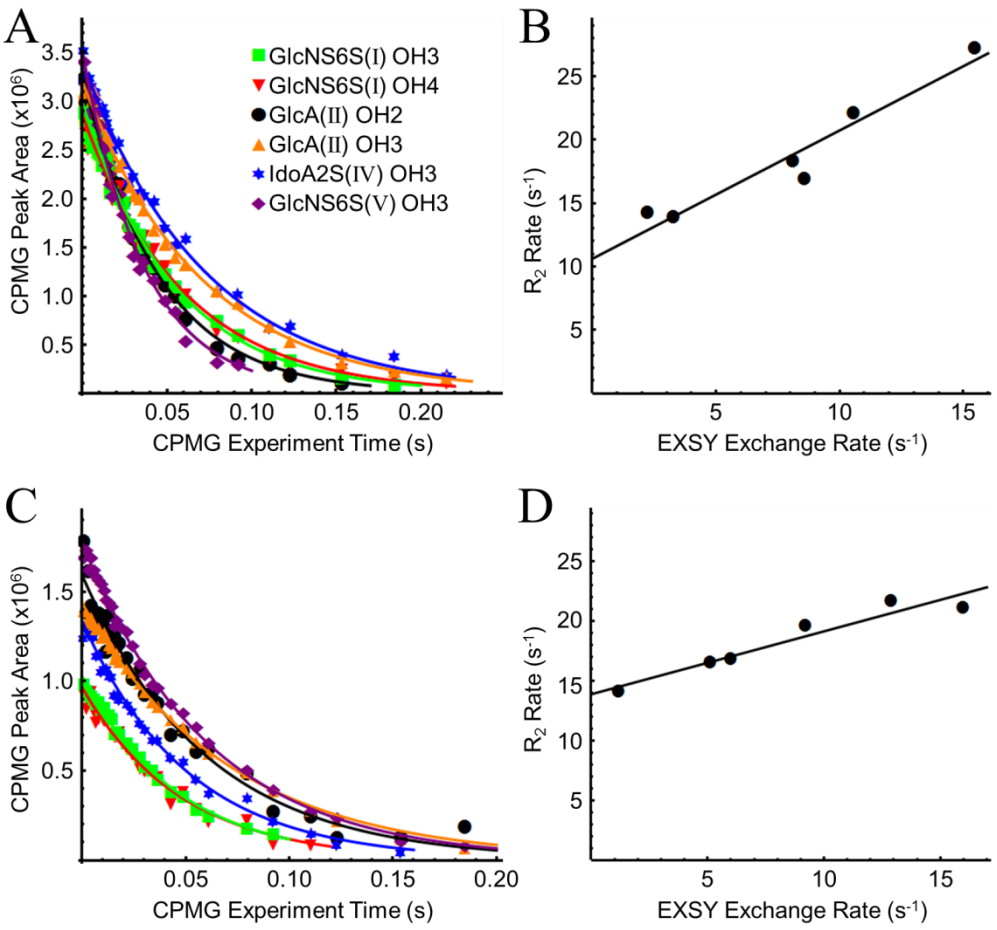

Figure 6.6. (A) CPMG decay curves for the Arixtra hydroxyl protons in 85% H_2O/15% acetone-d_6 at pH 8.3 and -14.5 °C before the addition of sodium bicarbonate (Chapter 3). (B) A plot of the R_2 values as a function of EXSY solvent exchange rates. (C) CPMG decay curves of Arixtra hydroxyl protons in 85% H_2O/15% acetone-d_6 at pH 8.3 and -14.5 °C after the addition of 0.59 mM sodium bicarbonate. (D) A plot of the R_2 values as a function of EXSY solvent exchange rates. EXSY and CPMG measurements were performed back-to-back for each sample.

Table 6.4. EXSY solvent exchange and CPMG transverse relaxation rates (R_2) of the Arixtra hydroxyl protons in the solutions studied. Measurements were performed in solutions of 85% H_2O/15% acetone-d_6 at -14.5 °C. Solutions indicated with an asterisk were prepared open to the atmosphere at pH 8.28 while the remaining were prepared under an N_2 atmosphere at the pH values indicated.

	Rate (s^{-1})	GlcNS6S (I) OH3	GlcNS6S (I) OH4	GlcA (II) OH2	GlcA (II) OH3	IdoA (IV) OH3	GlcNS6S (V) OH3	Slope	R^2
Arixtra prior to bicarbonate addition*	EXSY k_{ex}	8.15	8.60	10.6	2.25	3.29	15.3	0.906	0.927
	CPMG R_2	18.3	16.9	22.1	14.2	13.9	27.2		
Arixtra with 0.59 mM bicarbonate*	EXSY k_{ex}	12.9	16	6.01	1.2	9.23	5.13	0.527	0.921
	CPMG R_2	21.7	21.1	16.8	14.1	19.6	16.5		
Solution **1** pH 7.8	EXSY k_{ex}	36.4	24.1	6.61	7.00	20.3	43.9	0.973	0.914
	CPMG R_2	44.5	25.4	17.8	20.3	28.4	57.3		
Solution **2** pH 7.9	EXSY k_{ex}	9.26	8.70	3.07	4.61	7.66	11.1	0.733	0.682
	CPMG R_2	18.4	14.1	13.1	12.5	14.4	20.8		
Solution **3** pH 8.1	EXSY k_{ex}	37.1	27.9	8.09	8.82	21.1	50.6	1.264	0.944
	CPMG R_2	55.4	32.9	18.7	22.2	35.9	75.3		
Solution **4** pH 8.4	EXSY k_{ex}	5.50	10.8	5.33	1.8	8.95	4.93	0.427	0.87
	CPMG R_2	15.7	17.9	16.8	13.9	17.6	16.1		
Solution **5** pH 8.5	EXSY k_{ex}	18.0	12.8	3.69	3.76	10.9	21.5	1.102	0.805
	CPMG R_2	27.5	17.4	14.1	15.3	18.8	36.6		

function of solvent exchange rate (Figure 6.6D) has a slope of 0.527 and a linear correlation coefficient of 0.921. Although the plots in Figure 6.6B and 6.6D have similar correlation coefficients, they have very different slopes. The significant decrease in slope observed for the plot in Figure 6.6D for the Arixtra solution after bicarbonate addition suggests that the transverse relaxation rates are affected by bicarbonate catalysis to a much greater degree than the solvent exchange rates determined using EXSY.

Looking further into the correlation between R_2 and initial build-up rates, hydroxyl proton exchange was investigated in the five different Arixtra solutions prepared in Chapter 3 at the following pH values: 7.7, 7.9, 8.1, 8.4, and 8.5, referred to as Arixtra solutions **1**, **2**, **3**, **4**, and **5**, respectively. Because these samples were prepared before we realized that the compressed nitrogen tanks are a significant source of CO_2, these samples were prepared under a N_2 atmosphere and were bubbled with N_2. As the hydroxyl proton resonance linewidths of their do not follow a clear trend with pH (Figure 3.10 in Chapter 3), we hypothesize that each solution contains an unknown and variable amount of CO_2 contamination. The EXSY solvent exchange rates and CPMG R_2 values of the hydroxyl protons in each Arixtra solution are summarized in Table 6.4, along with the slopes and linear correlation coefficients of their respective R_2 vs. solvent exchange rate plots.

Hydroxyl proton solvent exchange and transverse relaxation rates for Arixtra solutions **1**, **3**, and **5** follow a similar trend as a group and as compared to the results in (Figure 6.6B) for the Arixtra solution prepared open to the atmosphere and prior to bicarbonate addition. The solvent exchange rates of the GlcA(II)OH3 hydroxyl protons

in solutions **1**, **3**, and **5** (6.61, 8.09, 3.69 s^{-1}, respectively) and those of the IdoA(IV)OH3 hydroxyl protons (7.00, 8.82, and 3.76 s^{-1}, respectively) are relatively slow, consistent with their involvement in a hydrogen bond as postulated in Chapter 3. The R_2 values correspond well to the solvent exchange rates for both the GlcA(II)OH3 hydroxyl proton (17.8, 18.7, 14.1 s^{-1}, respectively) and the IdoA2S(IV)OH3 hydroxyl proton (20.3, 22.2, 15.3 s^{-1}, respectively). The GlcA(II)OH2 hydroxyl protons in solutions **1**, **3**, and **5** have relatively fast initial build-up exchange rates (36.4, 37.1, and 18.0 s^{-1}, respectively) and R_2 values (44.5, 55.4, and 27.5 s^{-1}, respectively), similar to the Arixtra solution prior to the addition of bicarbonate. Although there is a fair amount of spread among the R_2 values for the three sets of experiments, within an experiment, the relative ranking of R_2 values for a given hydroxyl proton are more consistent. As a result, the slopes of the plots of hydroxyl proton R_2 as a function of solvent exchange rates for solutions **1** (0.973), **3** (1.26), and **5** (1.10), are similar and close to 1.0 with roughly similar values for the linear correlation coefficients (0.914, 0.944, and 0.805, respectively).

In contrast, the hydroxyl proton solvent exchange and transverse relaxation for Arixtra solutions **2** and **4** are more similar to the patterns observed for the Arixtra solution after the addition of 0.59 mM bicarbonate. In solutions **2** and **4**, only the GlcA(II)OH3 proton exchanges slowly with initial build-up rates of 1.67 and 1.80 s^{-1}, respectively, and R_2 values of 12.5 and 13.9 s^{-1}, respectively. In comparison, the IdoA(IV)OH3 proton exchanges relatively rapidly and in the case of solution **4** has a solvent exchange rate (5.33 s^{-1}) comparable to those of GlcA(II)OH2 (5.50 s^{-1}) and GlcNS(V)OH3 (4.93 s^{-1}) protons. For solution **4**, the slope (0.427) of the plot of the

hydroxyl proton R_2 values as a function of solvent exchange rate deviated the most from unity, although a fairly good linear correlation (0.870) was still obtained. The corresponding plot for solution **2** had a slope (0.733) that is closer to 1.0 but this data did not produce good linear correlation coefficient (0.682).

In Figure 6.7, the overall correlation of hydroxyl proton R_2 and solvent exchange rates of each Arixtra solution (**1**, **2**, **3**, **4**, and **5**) are compared with the results for the Arixtra solution prepared open to the atmosphere before and after bicarbonate addition. Figure 6.7A shows the combined results for Arixtra (no added bicarbonate) and solutions **1**, **3**, and **5**. The slope of the plot of R_2 as a function of solvent exchange rate (1.12) is close to 1.0 and has a linear correlation coefficient of 0.911. The combined results for Arixtra (0.59 mM bicarbonate) and solutions **2** and **4** (Figure 6.7B) show a lower slope (0.587) and a much poorer linear correlation coefficient of 0.728. The results in Figure 6.7B indicate that bicarbonate catalysis of solvent exchange affects transverse relaxation rates to a much greater extent than the solvent exchange rates, and plots of R_2 vs solvent exchange rate may provide a good indication of CO_2 contamination. Further investigation is needed to confirm the relationship between R_2 and solvent exchange rates under conditions that rigorously avoid CO_2 contamination (Chapter 7).

6.4 Conclusions

The results of this study demonstrate that it is possible to use transverse relaxation rates to study hydroxyl proton solvent exchange, but that these measurements must be interpreted with caution. Though the transverse relaxation rates of the GlcN and GlcN3S

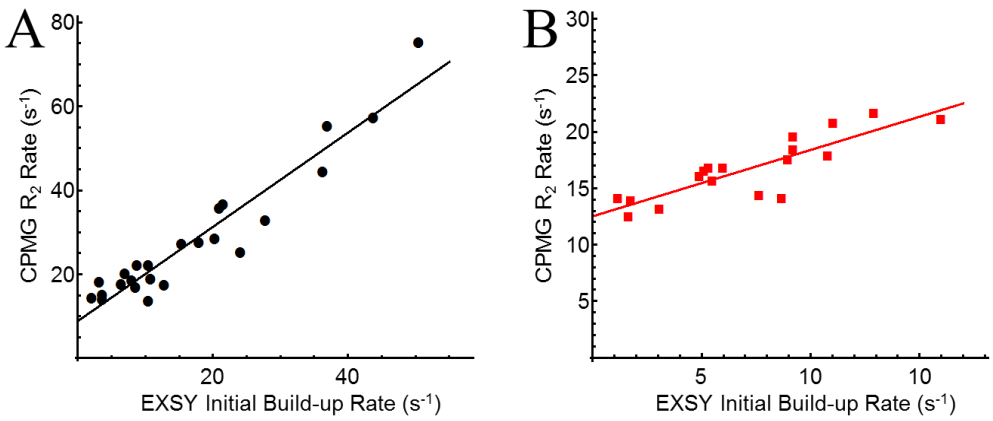

Figure 6.7. (A) Hydroxyl proton R_2 values plotted as a function of EXSY solvent exchange rates for Arixtra (no added bicarbonate) and solutions **1**, **3**, **5**. The linear plot has a slope of 1.12 and a correlation coefficient of 0.911. (B) Hydroxyl proton R_2 values plotted as a function of EXSY solvent exchange rates for Arixtra (0.59 mM bicarbonate) and solutions **2**, and **4**. The slope of this line is 0.587 and its linear correlation coefficient is 0.728.

monosaccharide hydroxyl protons correlated reasonably well with their EXSY solvent exchange rates, a much poorer correlation was obtained for the Arixtra hydroxyl protons, especially when bicarbonate contamination was significant. In addition, to the effects of bicarbonate catalysis, in longer oligosaccharides R_2 values may also be affected by dynamic processes such as conformational change and local molecular motion. Given these limitations, transverse relaxation measurements for oligosaccharide hydroxyl protons are not likely to be useful as a method to identify hydrogen bonds. Still, poor correlations between R_2 values and solvent exchange rates could be useful as a means of confirming the presence of other relaxation mechanisms, for example bicarbonate catalysis of solvent exchange.

6.5 References

1. Capila, I.; Linhardt, R. J., Heparin - Protein interactions. *Angew. Chem. Int. Edit.* **2002,** *41*, 391-412.

2. Multhaupt, H. A. B.; Couchman, J. R., Heparan sulfate biosynthesis: Methods for investigation of the heparanosome. *J Histochem Cytochem* **2012,** *60*, 908-915.

3. Peysselon, F.; Ricard-Blum, S., Heparin–protein interactions: From affinity and kinetics to biological roles. Application to an interaction network regulating angiogenesis. *Matrix Biol.* **2014,** *35*, 73-81.

4. Rosenberg, R. D.; Goldman, P.; Bing, D.; Glass, J., Actions and interactions of antithrombin and heparin. *New Engl. J. Med.* **1975,** *292*, 146-151.

5. Rosenberg, R. D.; Lam, L., Correlation between structure and function of heparin. *P. Natl. Acad. Sci. USA* **1979,** *76*, 1218-1222.

6. Petitou, M.; Casu, B.; Lindahl, U., 1976-1983, A critical period in the history of heparin: The discovery of the antithrombin binding site. *Biochimie* **2003,** *85*, 83-89.

7. Damus, P. S.; Hicks, M.; Rosenber.Rd, Anticoagulant action of heparin. *Nature* **1973,** *246*, 355-357.

8. Lindahl, U.; Backstrom, G.; Hook, M.; Thunberg, L.; Fransson, L. A.; Linker, A., Strucure of the antithrombin-binding site in heparin. *P. Natl. Acad. Sci. USA* **1979,** *76*, 3198-3202.

9. Thunberg, L.; Backstrom, G.; Lindahl, U., Further characterization of the antithrombin-binding sequence in heparin. *Carbohyd. Res.* **1982,** *100*, 393-410.

10. Atha, D. H.; Lormeau, J. C.; Petitou, M.; Rosenberg, R. D.; Choay, J., Contribution of monosaccharide residues in heparin binding to antithrombin-III. *Biochemistry* **1985,** *24*, 6723-6729.

11. Ferro, D. R.; Provasoli, A.; Ragazzi, M.; Torri, G.; Casu, B.; Gatti, G.; Jacquinet, J. C.; Sinay, P.; Petitou, M.; Choay, J., Evidence for conformational equilibrium of the sulfated L-iduronate residue in heparin and in synthetic heparin monosaccharides and oligosaccharides: NMR and force-field studies. *J. Am. Chem. Soc.* **1986,** *108*, 6773-6778.

12. Ragazzi, M.; Ferro, D. R.; Perly, B.; Sinay, P.; Petitou, M.; Choay, J., Conformation of the pentasaccharide corresponding to the binding site of heparin for antithrombin-III. *Carbohyd. Res.* **1990,** *195*, 169-185.

13. Sourena, N.; Smoot, J. T.; Vanartsdalen, J. A., Process for preparing fondaparinux sodium and intermediates useful in the synthesis thereof. Google Patents: 2012.

14. Jones, C. J.; Beni, S.; Limtiaco, J. F. K.; Langeslay, D. J.; Larive, C. K., Heparin Characterization: Challenges and Solutions. In *Annual Review of Analytical Chemistry, Vol 4*, Cooks, R. G.; Yeung, E. S., Eds. Annual Reviews: Palo Alto, 2011; Vol. 4, pp 439-465.

15. Langeslay, D. J.; Beecher, C. N.; Dinges, M. M.; Larive, C. K., Glycosaminoglycan Structural Characterization. In *eMagRes*, John Wiley & Sons, Ltd: 2007.

16. Langeslay, D. J.; Young, R. P.; Beni, S.; Beecher, C. N.; Mueller, L. J.; Larive, C. K., Sulfamate proton solvent exchange in heparin oligosaccharides: Evidence for a persistent hydrogen bond in the antithrombin-binding pentasaccharide Arixtra. *Glycobiology* **2012,** *22*, 1173-1182.

17. Beecher, C. N.; Young, R. P.; Langeslay, D. J.; Mueller, L. J.; Larive, C. K., Hydroxyl-proton hydrogen bonding in the heparin oligosaccharide Arixtra in aqueous solution. *J. Phys. Chem. B* **2014,** *118*, 482-491.

18. Ohnishi, M.; Urry, D. W., Temperature dependence of amide proton chemical shifts: Secondary structures of gramicidin S and valinomycin. *Biochem. Biophys. Res. Co.* **1969,** *36*, 194-202.

19. Englander, S. W.; Kallenbach, N. R., Hydrogen exchange and structural dynamics of proteins and nucleic acids. *Q. Rev. Biophys.* **1983,** *16*, 521-655.

20. Andersen, N. H.; Neidigh, J. W.; Harris, S. M.; Lee, G. M.; Liu, Z. H.; Tong, H., Extracting information from the temperature gradients of polypeptide NH chemical shifts. 1. The importance of conformational averaging. *J. Am. Chem. Soc.* **1997,** *119*, 8547-8561.

21. Maity, H.; Lim, W. K.; Rumbley, J. N.; Englander, S. W., Protein hydrogen exchange mechanism: Local fluctuations. *Protein Sci.* **2003,** *12*, 153-160.

22. Sandstrom, C.; Kenne, L., Hydroxy protons in structural studies of carbohydrates by NMR spectroscopy. *ACS. Sym. Ser.* **2006,** *930*, 114-132.

23. Blundell, C. D.; Almond, A., Temperature dependencies of amide ^{1}H- and ^{15}N-chemical shifts in hyaluronan oligosaccharides. *Magn. Reson. Chem.* **2007,** *45*, 430-433.

24. Blundell, C. D.; Deangelis, P. L.; Almond, A., Hyaluronan: The absence of amide-carboxylate hydrogen bonds and the chain conformation in aqueous solution are

incompatible with stable secondary and tertiary structure models. *Biochem. J.* **2006,** *396*, 487-98.

25. Nestor, G.; Kenne, L.; Sandstrom, C., Experimental evidence of chemical exchange over the β(1→3) glycosidic linkage and hydrogen bonding involving hydroxy protons in hyaluronan oligosaccharides by NMR spectroscopy. *Org. Biomol. Chem.* **2010,** *8*, 2795-2802.

26. Sandstrom, C.; Baumann, H.; Kenne, L., NMR spectroscopy of hydroxy protons of 3,4-disubstituted methyl α-D-galactopyranosides in aqueous solution. *J. Chem. Soc. Perk. T. 2* **1998,** 809-815.

27. Dobson, C. M.; Lian, L. Y.; Redfield, C.; Topping, K. D., Measurement of hydrogen exchange rates using 2D NMR spectroscopy. *J. Magn. Reson.* **1986,** *69*, 201-209.

28. Hills, B. P.; Wright, K. M.; Belton, P. S., Proton N.M.R. studies of chemical and diffusive exchange in carbohydrate systems. *Mol. Phys.* **1989,** *67*, 1309-1326.

29. Jen, J., Chemical exchange and NMR T_2 relaxation. *Adv. Mol. Relax. Int. Pr.* **1974,** *6*, 171-183.

30. Carver, J. P.; Richards, R. E., A general two-site solution for the chemical exchange produced dependence of T_2 upon the Carr-Purcell pulse separation. *J. Magn. Reson.* **1972,** *6*, 89-105.

31. Cocivera, M., Nuclear spin relaxation in methanol. Effect of proton exchange. *J Chem. Phys.* **1967,** *47*, 1112-1116.

32. Fabri, D.; Williams, M. A. K.; Halstead, T. K., Water T_2 relaxation in sugar solutions. *Carbohyd. Res.* **2005,** *340*, 889-905.

33. Calucci, L.; Forte, C.; Ranucci, E., Water/polymer interactions in poly(amidoamine) hydrogels by ^{1}H nuclear magnetic resonance relaxation and magnetization transfer. *J. Chem. Phys.* **2008,** *129*, 064511-1 - 064511-8.

34. Rabenstein, D. L.; Fan, S.; Nakashima, T. T., Attenuation of the water resonance in fourier transform ^{1}H NMR spectra of aqueous solutions by spin-spin relaxation. *J Magn. Reson.* **1985,** *64*, 541-546.

35. Rabenstein, D. L.; Fan, S., Proton nuclear magnetic resonance spectroscopy of aqueous solutions: Complete elimination of the water resonance by spin-spin relaxation. *Anal. Chem.* **1986,** *58*, 3178-3184.

36. Carr, H. Y.; Purcell, E. M., Effects of diffusion on free precession in nuclear magnetic resonance experiments. *Phys. Rev.* **1954,** *94*, 630-638.

37. Meiboom, S.; Gill, D., Modified spin-echo method for measuring nuclear relaxation times. *Rev. Sci. Instrum.* **1958,** *29*, 688-691.

38. Mao, X.-a.; Guo, J.-x.; Ye, C.-h., Radiation damping effects of transverse relaxation time measurements. *Chem. Phys. Lett.* **1994,** *227*, 65-68.

39. Van Geet, A. L., Calibration of methanol and glycol nuclear magnetic resonance thermometers with a static thermistor probe. *Anal.Chem.* **1968,** *40*, 2227-2229.

40. Wolfram, S., *Mathematica: A System for Doing Mathematics by Computer*, 2nd ed.; Addison-Wesley Publishing Company: Reading, MA, **1991**.

41. Bain, A. D., Chemical exchange in NMR. *Prog. Nucl. Mag. Res. Sp.* **2003,** *43*, 63-103.

42. Chen, J. H.; Mao, X. A., Radiation damping transfer in nuclear magnetic resonance experiments via chemical exchange. *J. Chem. Phys.* **1997,** *107*, 7120-7126.

43. Tadimalla, S.; Momot, K. I., Effect of partial H_2O-D_2O replacement on the anisotropy of transverse proton spin relaxation in bovine articular cartilage. *PLoS ONE.* **2014,** *9*, e115288.

44. McIntosh, L. P., CPMG. In *Encyclopedia of Biophysics*, Roberts, G. K., Ed. Springer Berlin Heidelberg: 2013; pp 386-386.

45. Langeslay, D. J.; Beecher, C. N.; Naggi, A.; Guerrini, M.; Torri, G.; Larive, C. K., Characterizing the microstructure of heparin and heparan sulfate using *N*-sulfoglucosamine ^{1}H and ^{15}N NMR chemical shift analysis. *Anal. Chem.* **2013,** *85*, 1247-1255.

CHAPTER SEVEN

Conclusions and Future Directions

7.1 Conclusions

Heparin is an unbranched, highly anionic polysaccharide that is known to mediate a variety of biological processes by binding to over 400 different proteins.[1] Heparin's microheterogeneity is introduced during its biosynthesis. The work presented in this dissertation demonstrates chromatographic methods of isolating heparin oligosaccharides for structure elucidation as well as methods for secondary structure elucidation through investigation of hydrogen bonding in the exchangeable hydroxyl (OH) and amine (NH_3^+) protons. These experiments build on previous studies of the heparin sulfamate ($NHSO_3^-$) protons, which show the importance of the 3-*O*-sulfate group in the AT-III binding pentasaccharide for hydrogen bonding stabilization of secondary structure to prepare it for protein binding.

In Chapter 2 we presented a method to isolate 3-*O*-sulfated oligosaccharides from a heparin digestion without the need for affinity chromatography. By screening the tetra- and hexasaccharide SEC fractions of the low molecular weight heparin, enoxaparin, using [^{1}H, ^{15}N] HSQC NMR, we could identify those SEC fractions containing the important glucosamine 3-*O*-sulfate group. Interestingly, the 3-*O*-sulfated oligosaccharides eluted later in the SEC separation perhaps because its participation in a hydrogen bond to the adjacent sulfamate proton makes the oligosaccharides more compact. Rather than pooling the size-uniform SEC fractions prior to separation by

charge, we separated each tetrasaccharide SEC fraction individually to obtain less complex SAX-HPLC separations. By focusing on the SEC fractions that show evidence of 3-*O*-sulfation in their [^{1}H,^{15}N] HSQC spectra, we were able to isolate a unique 3-*O*-sulfated tetrasaccharide that originally co-eluted with a more abundant component in the pooled tetrasaccharide SAX separation. The hexasaccharides were also screened using [^{1}H, ^{15}N] HSQC NMR and separated by charge as individual SEC fractions, but due to the greater complexity of the hexasaccharides, it was difficult to resolve many oligosaccharides of interest in high purity. An additional separation method could be utilized for separations of larger oligosaccharides (section 7.2).

Chapter 3 presents, to our knowledge, the first experimental evidence of intramolecular hydrogen bonding involving the hydroxyl protons of the synthetic pentasaccharide, Arixtra. This study used temperature coefficients, $\Delta\delta$ values, and solvent exchange rates. This work was prompted by a study by Langeslay et al. in which MD simulations predicted hydrogen bonds involving both the Arixtra sulfamate protons and hydroxyl protons.[2] Experimental evidence presented in Chapter 3 suggested hydrogen bonds involving the GlcA(II)OH3 and IdoA2S(IV)OH3 hydroxyl protons in Arixtra. The error associated with the exchange rate measurements was also evaluated. It was found that CO_2 content could dramatically affect the relative exchange rates of hydroxyl protons within a sample and that care must be taken when comparing exchange rates between samples. We also address, for the first time, the issue of radiation damping in aqueous solutions in the calculations of hydroxyl proton solvent exchange rates.

In Chapter 4 the effects of structural heterogeneity on hydroxyl proton hydrogen bonding patterns was investigated using three isolated heparin oligosaccharides. Specifically, we focused on oligosaccharides that are structurally similar to Arixtra but that do not have the important 3-*O*-sulfate group. As in Chapter 3, temperature coefficients, $\Delta\delta$ measurements, and solvent exchange rates were used to evaluate intramolecular hydroxyl proton hydrogen bonding patterns. Without the adjacent glucosamine 3-*O*-sulfate group, the IdoA2S residue changes its conformation from majority $^{2}S_{O}$ to majority $^{1}C_{4}$,[3] which most likely moves the IdoA2SOH3 proton away from the sulfamate protons to which it is hydrogen bonded in Arixtra. Without the 3-*O*-sulfated glucosamine residue, the GlcAOH3 proton hydrogen bond appears to be weaker while the GlcNS6SOH3 proton appears to be in a stronger hydrogen bond. The results summarized in Chapters 3 and 4 illustrate the importance of elements of primary structure in determining heparin local secondary structure.

Chapter 5 presents, for the first time, the direct NMR detection of the amine protons in the heparan sulfate related monosaccharides D-glucosamine (GlcN) and 3-*O*-sulfated D-glucosamine (GlcN3S). Direct detection of the amine protons allows for characterization by [^{1}H, ^{15}N] HSQC NMR. Exchange of the amine protons was also investigated using temperature coefficients, energy barriers of chemical exchange ($\Delta G^{\ddagger}$), and solvent exchange rates. The possible existence of a salt bridge was investigated by measuring the pK_a values of the amine group through NMR pH titrations following the H2 proton chemical shifts. Although no evidence of a salt bridge was found for the

GlcN3S monosaccharide, the results of this experiment demonstrate the feasibility of probing for structurally important salt bridges in longer oligosaccharides.

In Chapter 6 hydroxyl proton transverse relaxation rates ($R_2 = 1/T_2$) were evaluated for their potential to reflect hydrogen bonding by comparing the hydroxyl proton R_2 values to solvent exchange rates measured using EXSY. The use of transverse relaxation rates to identify hydroxyl proton hydrogen bonds would be desirable due to shorter experiment times and because in EXSY noise and artifacts at the water frequency that can impact the volume integration of exchange cross peaks. GlcN and GlcN3S were initially used as test compounds because their hydroxyl protons can be detected in slightly acidic solution, reducing the extent of bicarbonate contamination, and because their amine groups act as a buffer stabilizing the solution pH. Although the R_2 values measured for the GlcN and GlcN3S hydroxyl protons correlated well with the solvent exchange rates, similar measurements for the Arixtra hydroxyl protons did not provide good agreement between the R_2 values and EXSY results. Investigation of hydroxyl proton transverse relation in Arixtra solutions with and without added bicarbonate revealed that bicarbonate affects the R_2 values in a non-uniform manner compared to the solvent exchange rates, which are primarily impacted by T_1 relaxation. Further investigation is required to evaluate whether bicarbonate affects the Arixtra conformation, however based on these initial studies we conclude that EXSY measurements are a more robust method of evaluating oligosaccharide hydroxyl protons solvent exchange.

7.2 Future directions

Complete resolution of the hexasaccharides by SAX-HPLC is more challenging than that of the tetrasaccharides due to the increased structural complexity of the mixture with many more isomeric oligosaccharides possible. One approach that can improve the resolution of the hexasaccharides involves a second separation of isolated SAX-HPLC peaks using histamine in the SAX running buffer. Histamine is known to bind heparin[4,5,6] at specific sites along the chain containing GlcNS and IdoA2S residues.[6] Dynamic interactions of the heparin oligosaccharides with the stationary phase and the mobile phase histamine and sodium chloride will produce a different SAX profile separating co-eluting oligosaccharides based on their different histamine binding affinities. Another plausible approach would be to re-separate the isolated SAX peaks using an analytical-scale SAX-HPLC column. The greater resolution provided by an analytical-scale column could be sufficient to isolate oligosaccharides with similar structures in sufficient quantities for NMR identification.

In Chapter 2, heparin SEC fractions were examined for the presence of 3-*O*-sulfated oligosaccharides using their unique sulfamate ^{1}H and ^{15}N chemical shifts. With the identification of experimental conditions for detection of saccharide amine protons by NMR (Chapter 5), it is now feasible to screen heparan sulfate SEC fractions using their [^{1}H, ^{15}N] HSQC spectra. As was done to correlate sulfamate NH chemical shifts with oligosaccharide structure,[7] a library of oligosaccharides with known structures would be needed to establish a database of glucosamine ^{1}H and ^{15}N chemical shifts. As a starting point, Arixtra can be *N*-desulfated through solvolysis[8] and used as a standard for the ^{1}H

and ^{15}N chemical shifts of amine protons adjacent to a 3-*O*-sulfate group as well as the reducing end glucosamine. The same *N*-desulfation procedure can be applied to isolated heparin oligosaccharides of known structure that do not contain a 3-*O*-sulfate group. Isolation and identification of depolymerized heparan sulfate would produce additional oligosaccharides containing glucosamine residues with free amine groups, allowing for the development of a complete chemical shift library of unique oligosaccharides.

The exchange properties of amine protons can also be explored using *N*-desulfated Arixtra and isolated heparan sulfate oligosaccharides using temperature coefficients, $\Delta\delta$ measurements, energy barriers for chemical exchange ($\Delta G^{\ddagger}$), and solvent exchange rates. These values can be compared to those of the amine protons of monosaccharides GlcN and GlcN3S (Chapters 5) to examine their potential participation in hydrogen bonds or salt bridges. Heparan sulfate secondary structure can also be evaluated though investigation of amine group acidity (pK_a). Although no salt bridge was discovered in the 3-*O*-sulfated glucosamine monosaccharide (Chapter 5), it is possible this is due to an interaction between the 3-*O*-sulfate group and the adjacent OH4 proton. This interaction would not be observed in the longer chains due to the $\beta(1\rightarrow4)$-*O*-linkage at the C4 position, increasing the likelihood of salt bridge formation in heparin sulfate oligosaccharides.

It was observed in Chapter 6 that the hydroxyl protons of GlcN and GlcN3S are detected by NMR at a more acidic pH than those of Arixtra and structurally related heparin oligosaccharides. Furthermore, Langeslay et al. observed that more highly negatively charged oligosaccharides required a more basic pH to slow the solvent

exchange of the sulfamate protons to allow NMR detection.[2] It was hypothesized that the negative charges on the sulfamate groups repelled the negative charged hydroxide ions (OH^-), reducing the hydroxide catalyzed exchange rate. We posit that the opposite is also true for our positively charged amine groups in Chapter 5. The correlation of structure and hydroxyl proton solvent exchange rates could be investigated in greater detail by exploring the hydroxyl proton exchange rates of positively charged, negatively charged, and neutral oligosaccharides. Studies of hydroxyl proton exchange in longer oligosaccharides with varying amounts of both positive and negative charges could provide insight into the role that both the NH_3^+ and OSO_3^- groups play in the solvent exchange reactions of heparin and heparin sulfate oligosaccharides.

A thorough examination of the effects of bicarbonate on hydroxyl proton exchange should be performed using heparin oligosaccharides. A bicarbonate titration using isolated heparin oligosaccharides of known structure could be performed to investigate the effects that minute structural changes have on the bicarbonate catalysis of hydroxyl proton solvent exchange. Because the IdoA2S(IV)OH3 proton in Arixtra is the most sensitive to bicarbonate catalyzed exchange, experiments with oligosaccharides containing an IdoA2S residue but no 3-*O*-sulfated glucosamine residue would provide insights into the effect of the 3-*O*-sulfo group on IdoA2SOH3 solvent accessibility. Furthermore, it was observed that the GlcA(II)OH2 and OH3 protons in Arixtra exchanged slower in the presence of bicarbonate, suggesting a bicarbonate titration of oligosaccharides containing a GlcA residue should also be conducted. Additionally, investigation of transverse relaxation rates should be repeated under an N_2 atmosphere

scrubbed of CO_2 to remove the potential effects of bicarbonate on these measurements. Finally, molecular dynamic (MD) simulations would provide more insight to confirm hydrogen bonds and predict possible hydrogen bond acceptors.

7.3 References

1. Peysselon, F.; Ricard-Blum, S., Heparin–protein interactions: From affinity and kinetics to biological roles. Application to an interaction network regulating angiogenesis. *Matrix Biol.* **2014,** *35*, 73-81.

2. Langeslay, D. J.; Young, R. P.; Beni, S.; Beecher, C. N.; Mueller, L. J.; Larive, C. K., Sulfamate proton solvent exchange in heparin oligosaccharides: Evidence for a persistent hydrogen bond in the antithrombin-binding pentasaccharide Arixtra. *Glycobiology* **2012,** *22*, 1173-1182.

3. Ferro, D. R.; Provasoli, A.; Ragazzi, M.; Torri, G.; Casu, B.; Gatti, G.; Jacquinet, J. C.; Sinay, P.; Petitou, M.; Choay, J., Evidence for conformational equilibrium of the sulfated L-isuronate residue in heparin and in synthetic heparin monosaccharides and oligosaccharides: NMR and force-field studies. *J. Am. Chem. Soc.* **1986,** *108*, 6773-6778.

4. Kobayashi, Y., Histamine binding by heparin. *Arch. Biochem. Biophys.* **1962,** *96*, 20-27.

5. Rabenstein, D. L.; Bratt, P.; Peng, J., Quantitative characterization of the binding of histamine by heparin. *Biochemistry* **1998,** *37*, 14121-14127.

6. Chuang, W.-L.; Christ, M. D.; Peng, J.; Rabenstein, D. L., An NMR and molecular modeling study of the site-specific binding of histamine by heparin, chemically modified heparin, and heparin-derived oligosaccharides. *Biochemistry* **2000,** *39*, 3542-3555.

7. Langeslay, D. J.; Beni, S.; Larive, C. K., Detection of the ^{1}H and ^{15}N NMR resonances of sulfamate groups in aqueous solution: A new tool for heparin and heparan sulfate characterization. *Analytical Chemistry* **2011,** *83*, 8006-8010.

8. Irimura, T.; Nakajima, M.; Nicolson, G. L., Chemically modified heparins as inhibitors of heparan sulfate specific endo-β-glucuronidase (heparanase) of metastatic melanoma cells. *Biochemistry* **1986,** *25*, 5322-5328.